The role of morphology in spider vibration sensing



Thomas Miller

St Anne's College

University of Oxford

A thesis submitted for the degree of

Doctor of Philosophy

Trinity 2024



Grammostola pulchra “Charlotte” in her enclosure at Wytham – the individual from which the laser vibrometry measurements were taken

Abstract

The transmission of vibrational waves through materials known as substrates is ubiquitous in the environment, and consequently is widely used as a source of sensory information by animals. Substrate-borne vibration sensing (hereafter “vibration sensing”) is a particularly important modality for arthropods, where it is ancestral to acoustic hearing. Arthropods such as spiders use substrate-borne vibrations to gather abiotic information about their environment, detect prey, avoid predators, and communicate with conspecifics. The mechanosensors involved in vibration sensing are embedded within the arthropod cuticle and thus measure the motion of the body in response to vibrational input. Due to this transmission stage from substrate through body to mechanosensor, I hypothesise that variation in body morphology may modulate vibration sensing – potentially through morphological computation, where information processing is outsourced from nervous system to morphology. Is morphology involved in mechanisms of source localisation before mechanotransduction, and what physical constraints does morphology impose on vibration sensing?

I use spiders as a model organism to test this hypothesis. I begin by introducing the framework upon which my research is based, decomposing the morphological traits into a series of biomechanical parameters. I then quantify these biomechanical parameters and the distribution of spider mechanosensors using SEM imaging and CT scanning. I perform dynamic tests on a live, untethered tarantula in its natural posture to measure the movement of the system in response to vibrational input and quantify the inherent body dynamics independent of substrate properties or input type (i.e. its natural modes). The relative motion of body/leg segments provides information about the stimulation of mechanosensors from joint bending before mechanotransduction. I then use these datasets to calibrate a simplified mathematical model of the spider and simulate its response to vibration sources as they might occur in a biological context. Through varying the source location and biomechanical parameters of the spider body, I investigate mechanisms of source location and the influence of morphological trait variation on substrate-borne vibration sensing.

By applying this interdisciplinary approach, combining experimental and simulated data, I demonstrate that amplitude ratios in vertical motion between leg segments on opposite sides of the body are likely the primary cue used by tarantulas for source localisation, and that the asymmetries in the dynamic response of the spider body allow estimation of source angle, but not source distance. Differences in frequency filtering and time delays between mechanosensor locations are unlikely to be relevant cues due to physical and physiological constraints. Since vibrational information is transmitted through the body with high efficacy, I conclude that whilst morphology is very important for vibration sensing, it is unlikely that the problem of information processing for source localisation is simplified using morphological computation.

Acknowledgements

This work was made possible through funding provided by a studentship on a Royal Society University Research Fellowship (URF\R1\191033). I also received funding from St Anne's College and Department of Biology at the University of Oxford, and Paul Scherrer Institut – I thank these institutions for supporting the research.

I would first like to thank my supervisor, Beth Mortimer, for being such a great mentor, not only in terms of the spider project but also setting a fantastic example in how to navigate the academic landscape. Our discussions are always so useful, and Beth has been instrumental in driving my enthusiasm for the research forward – I hope that we will continue to collaborate in the future. Likewise, I thank my co-supervisors, Graham Taylor and Alice Cicirello, for offering many key insights and ideas, particularly on the more mathematical side of the project.

I thank everyone in the Animal Vibration Lab and Flight Group at Wytham for providing such a welcoming research group atmosphere. I want to especially thank Jun Wu for his support and collaboration on the spider project – the modelling wouldn't been possible without him! Fritz Vollrath has also had many useful (and eclectic!) ideas for the project and spider setup at Wytham. My alter-ego in the lab, Tom Mulder (Miller) has provided endless entertainment and support both in Oxford and elsewhere; I was grateful to join him for a particularly memorable trip to Portugal to study fiddler crabs.

Similarly, Leonidas Romanos-Davranoglou at the OUMNH has been a fantastic collaborator, opening up some research opportunities in exciting new fields complementary to my DPhil project, and which culminated in two very interesting (and intense!) trips to Paul Scherrer Institut, Switzerland to carry out the experimental work. I would additionally like to thank Christian Schlepütz, and the other scientists at PSI, for facilitating this research, some of which has been included in Chapter 3.

The experimental work on the spiders would not have been possible without the staff at the John Krebs Field station, Wytham – particularly Helen Sanders and Dave Wilson, whose expertise as animal technicians has kept the spider population thriving. Similarly, I thank John Hogg for machining some of the bespoke components used during the experiments.

I want to thank all the people who have supported me personally over the past few years – friends, housemates, people who share my passions of ornithology, geology and road cycling. These include Joe Morford, James Kempton, Henry Grub, Lucienne Pullen, Bradley Sawyer, Victor Ajuwon, Clement Collins-Rice, Seb Dows-Miller, Jack Beckwith, Paris Jaggers, Mayur Prag, James Hammond, Alice Edney, Lewis Fisher-Reeves, Trina Siddiqi-Davies, Joe Wynn, Paddy Lewin, Adam Hartley, Ian Lewington, Ben Sheldon, Kameran Sabbaghi, Mark Varah, everyone in OUCC, and Ollie Padget (who also deserves special thanks for being my bird ringing trainer and enabling me to gain my license during the DPhil).

Finally, and most importantly, I thank my family – Mum, Dad and Henry.

Declaration and author contributions

This DPhil thesis was completed at the University of Oxford between October 2019 and April 2023 under the supervision of Dr Beth Mortimer, Professor Graham Taylor, and Dr Alice Cicirello. No part of this thesis has been previously submitted for another degree.

The work described in the thesis was primarily carried out by the author, except for Chapter 4, which has been published in Journal of the Royal Society Interface with Jun Wu as first author and me as co-author. For this paper, I was involved in conceptualization, data curation, investigation, writing—original draft, writing—review and editing. Author lists are included at the beginning of each chapter, whilst a full breakdown of the author and co-author contributions are listed in at the end of each chapter.

Author institutions

Indicated by superscript above each author

[1] Department of Biology, University of Oxford

[2] Oxford University Museum of Natural History

[3] Paul Scherrer Institut

[4] Department of Engineering, University of Cambridge

Table of contents

Introduction 1

Chapter 1 – Control vs. Constraint: understanding the mechanisms of vibration transmission during substrate-borne information transfer 13

Chapter 2 – Slit sense organ distribution on the legs of two species of orb-weaving spider (Araneae: Araneidae) 47

Chapter 3 – Mass distribution of the tarantula *Grammostola pulchra* measured through synchrotron-based micro-CT scanning 73

Chapter 4 – Spider dynamics under vertical vibration and its implications for biological vibration sensing 97

Chapter 5 – Frequency, time, and amplitude differences across the spider body and their role in substrate-borne vibration sensing 129

Conclusion 163

Bibliography 173

Appendix 1 183

Appendix 2 193

Appendix 3 195

Appendix 4 209

Introduction

1 General introduction

The mechanisms of animal sensing have long fascinated biological researchers. This is particularly true for sensory modalities which are unfamiliar to humans – such as the detection of magnetic fields, infrared radiation, or inaudible vibrations through the ground. It is vibration sensing which this thesis is centred on.

The use of inaudible vibrations by animals was first described in the literature by Frej Ossiannilsson, who monographed the Swedish Auchenorrhyncha. Previously, it was thought that most environmental substrates were not suitable for transmitting biologically useful vibrational information due to their material properties. Ossiannilsson noted that planthopper and leafhoppers had tymbals despite being seemingly inaudible – by pressing a test tube containing singing males into his ear, he was able to detect their songs (Hill and Wessel, 2016). His doctoral thesis was focused specifically on the vibration-producing organs of these insects. This work was continued by Hildegard Strübing, who showed that vibrational communication is used by planthoppers for courtship (Wessel, 2014).

Subsequent research into the biological use of vibrations has led to a plethora of terms being used in the literature, each with its own subtle definition: vibration sensing, substrate-borne/substrate-borne vibration detection, biotremology, seismic sensing, even “hearing” using “ears” (Hill et al., 2019, Hill and Wessel, 2016, Miller and Mortimer, 2020, Elias et al., 2003, O'Connell-Rodwell, 2007). Key to these ideas is the distinction between the detection of vibrations that propagate through a solid substrate and those that propagate as an airborne acoustic wave. Here, I consider a vibrational wave to be the oscillation of particles through a transmission medium. Where the transmission medium is air, vibrations propagate as acoustic pressure waves which are detected as

sounds – i.e. hearing (Göpfert and Hennig, 2016). Tympanal hearing mechanisms directly measure pressure differences across a membrane, whilst particle velocity hearing mechanisms such as mosquito antennae sense the vibrations of air molecules. Where the transmission medium is a solid substrate, vibrations are detected through direct contact with this substrate – commonly the ground, vegetation or structures built by animals such as webs. I will refer to vibration transmission in this latter context as substrate-borne, and by extension substrate-borne vibration sensing as the use of this information as a sensory modality by animals.

Whilst in principle hearing and substrate-borne vibration sensing appear to be quite disparate, at a mechanistic level they are not so easy to separate. Both involve the stimulation of organs called mechanosensors through the motion of a transmission medium, leading to sensory transduction. The mechanosensors themselves may be lever sensors, such as hair structures or antennae, cuticular strain sensors, or tympana (Barth, 2019). Some mechanosensor types are used for both vibration sensing and acoustic hearing – for instance sensory hairs, which in some contexts act as flow detectors to sense acoustic waves whilst in other contexts bridge the gap between leg segments to detect joint bending for proprioception (Seyfarth et al., 1990). Indeed, in some animals, the same sensors are used simultaneously for detection of substrate-borne vibrations and acoustic waves. In elephants, for instance, the inner ear is responsible for substrate-borne vibration sensing through direct bone conduction from the ground as well as acoustic hearing (Bouley et al., 2007). To give a human analogy, this is also the mechanism of bone-conducting headphones.

Perhaps the clearest way to separate these modalities mechanistically is through considering the transmission pathway through which information must flow. Ears used for acoustic hearing are peripheral sensors and hence most information flow is through the transmission medium (i.e. the air). Mechanosensors involved in substrate-borne vibration sensing typically measure the motion of a body part that is in contact with the transmission medium (i.e. a solid substrate), and are therefore embedded sensors.

Because of this, the sensors are typically simpler and more numerous than ears and are distributed widely across the animal's body.

I will first overview vibration sensing in arthropods, before focusing specifically on the research conducted on spiders. I will identify open questions in the literature and then outline the research arc of this thesis.

2 Arthropods

Substrate-borne vibration sensing is considered a basal modality in arthropods, in contrast to acoustic hearing, which is thought to have evolved multiple times in response to selection pressures such as airborne predation (Yager, 1999). Arthropods detect substrate-borne vibrations by measuring the motion of their body as vibrational waves travel through them (Miller and Mortimer, 2020). The types of embedded mechanosensor used for vibration sensing in insects, arachnids and crustacea are similar in their core function but differ in structure, number, and location (Figure 1).

Insect and crustacean strain sensors involved in substrate-borne vibration sensing include the subgenual organs and campaniform sensilla. Subgenual organs are found on the tibia of insects directly below the joint with the femur in all six legs (Strauss et al., 2021). They are chordotonal organs, which are composed of fundamental neuronal units called scolopidia (Yack, 2004). The organ is suspended within the haemolymph cavity and has a complex structure, with one end attached to the subgenual nerve and the other attached to the inner surface of the cuticle on the opposite site (Menzel and Tautz, 1994). Campaniform sensilla are much more numerous and are distributed widely across the legs and body of both insects and crustaceans (Barth, 1980, Pringle, 1938, Dinges et al., 2021). They contain a flexible cap that protrudes above a hole in the exoskeleton cuticle. This cap deforms in response to cuticular strain, which leads to an action potential being generated in the dendrite innervating the cap (Moran et al., 1971).

Arachnid mechanosensors evolved independently to insect and crustacean strain sensors. They consist of narrow gaps in the cuticle known as slit sensilla and have a similar mechanism to the campaniform sensilla in that cuticular strain leads to deformation of a membrane stretched across the gap. In spiders, the slit sensilla are grouped into discrete structures called lyriform organs, which possess a much higher sensitivity to cuticular strains than single slits (Pringle, 1955). Slit sensilla have been studied using light microscopy of dissected cuticle and SEM imaging (Miller et al., 2022, Vogel, 1923, Barth and Libera, 1970).

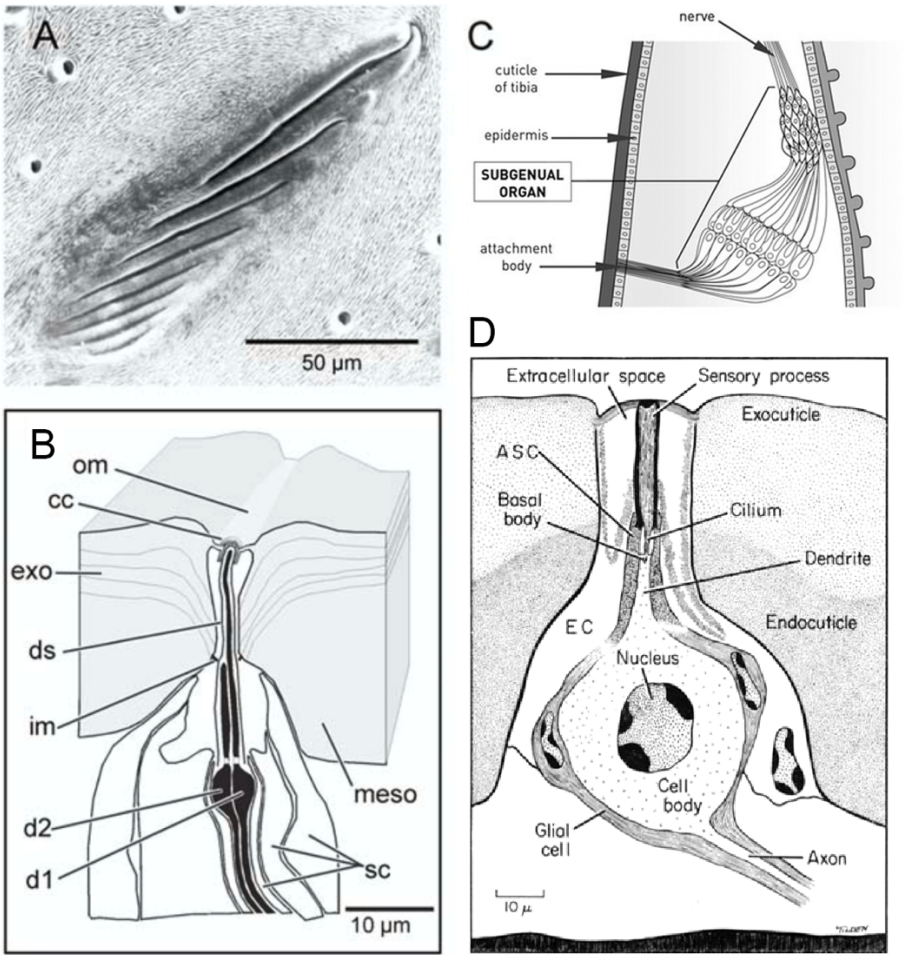


Figure 1. Comparison of arthropod mechanosensors. A, SEM image of the external structure of lyriform organ VS-3 on the leg of the spider *Cupiennius salei*. B, Diagram of internal structure of spider slit sense organ – om outer membrane, cc coupling cylinder, d1, d2 dendrites, ds dendritic sheath, exo exocuticle, im inner membrane, meso mesocuticle, sc glial sheath cells. C, diagram of internal structure of subgenual organ on the insect leg. D, diagram of internal structure of campaniform sensilla on the leg of the cockroach *Blaberus discoidalis*. A-B, adapted from French et al (French et al., 2002) with permission from Springer Nature Journals, license number 5751861264643 https://link.springer.com/journal/359. C, adapted from Hunt and Richard (Hunt and Richard, 2013) with permission from Springer Nature Journals, license number 5751871338979 https://link.springer.com/journal/40. D, adapted from Moran et al. (Moran et al., 1971). Originally published in Journal of Cell Biology, https://doi.org/10.1083/jcb.48.1.155.

3 Spiders

Substrate-borne vibration sensing is the primary sensory modality for many spider species, which make them ideal model organisms in this context. Both biotic and abiotic vibrations can theoretically be used by spiders as information sources. Biotic vibration sources include vibrations produced intentionally by other animals for communication (such as conspecific courtship) or unintentionally as a cue (such as the footsteps of a prey item, potentially revealing its location) (Elias et al., 2005, Elias et al., 2003, Schuch and Barth, 1990, Schuch and Barth, 1985, Masters, 1984b). Abiotic vibration sources include vibrations generated by wind and rain and hence are indicative of environmental conditions, although these vibrations tend to be low frequency and subject to high pass filtering by the spider (Masters, 1984b, Young et al., 2014). The relevant substrates include the ground, vegetation, or structures produced by the spider specifically for vibration transmission such as webs. The distances over which these vibrations are transmitted varies depending on a species' biological context but is typically on a scale of millimetres to metres and depends on how homogenous and connected the substrates along the transmission pathway are.

Much of what is known about the mechanisms of spider mechanosensation is the result of decades of research on *Cupiennius salei*, which has become a model species for studying vibration sensing (Barth, 2002a). Beginning in the late 1960s, Friedrich Barth and colleagues began investigating the structure and function of *Cupiennius* mechanosensors involved in substrate-borne vibration sensing, air flow sensors and proprioception. Using intracellular electrophysiological recording equipment, they quantified the threshold curves of the slit sensilla in response to a known vibrational input at the base of the leg (Figure 2) (Barth and Bohnenberger, 1978, Barth and Geethabali, 1982). In these experiments, the spider was fixed in an armature with the focal leg joint allowed to move freely. This work then expanded to include behavioural trials measuring the orientation and prey capture latency of the spiders before and after

the ablation of key lyriform organs on the legs of the spider (Seyfarth et al., 1982, Barth and Seyfarth, 1971, Seyfarth and Barth, 1972).

A particular focus in more recent work has been the modelling and measurement of cuticular strains. Understanding how cuticular deformation leads to mechanosensor stimulation is crucial for understanding the relationship between morphology and substrate-borne vibration sensing. Strain is challenging to measure experimentally because the device must be glued to the spider's exoskeleton – a method which inherently changes the biomechanical properties of the system (Blickhan, 1986, Blickhan et al., 2021). To some extent this can be accounted for, as the strain gauge has known stiffness and mass, but the problem is further complicated by the behavioural reaction of the spider to contact measurements. Physical and finite element modelling of the mechanosensors has been used to quantify the magnitude and direction of strains that result in the stimulation of lyriform organs with different slit arrangements (Hössl et al., 2007, Hössl et al., 2009, Barth et al., 1984).

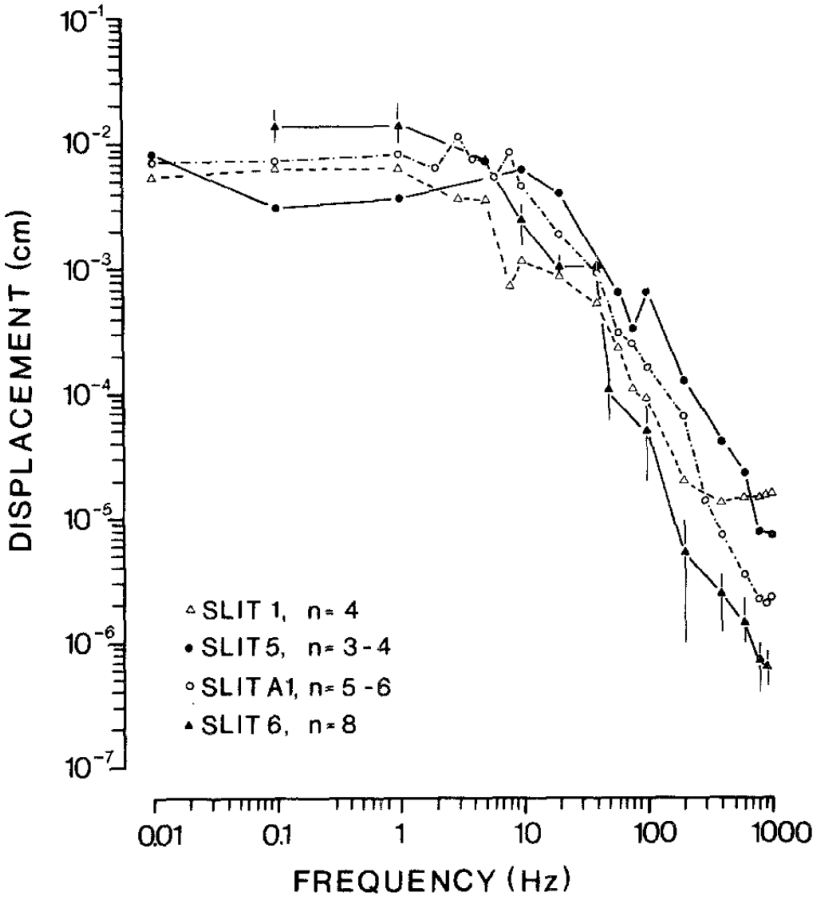


Figure 2. Threshold curves of slits in the metatarsal lyriform organ of *Cupiennius salei* under loose coupling to vibration input in the vertical axis. Adapted from Barth and Geethabali (1982) with permission from Springer Nature Journals, license number 5751880180926 https://link.springer.com/journal/359.

It is evident that strain sensors embedded in the cuticle are capable of detecting deformation resulting from not only the transmission of externally generated vibrations through the body, but also muscle contraction, changes in haemolymph pressure and the resultant forces from locomotion. Thus, they have the potential to function both as exteroceptors and proprioceptors (Barth, 2021). This poses interesting questions about how this multifunctionality is achieved. Mechanosensors are likely segregated between these functions based on their location, with exteroceptors positioned at joints where bending is generated primarily through substrate movement (for instance at the distal tips of the legs) in comparison to proprioceptors, which are typically located near muscle

attachment sites (Barth, 2021, Young et al., 2016). It is also possible that there is temporal separation, with proprioception taking precedence whilst the animal is moving. Many spiders, for instance, are sit and wait hunters, so vibration source localisation is likely computed whilst the animal is stationary.

4 Open questions

Despite the detailed work on the location and threshold curves of individual mechanosensors, our understanding of spider mechanosensation remains something of a black box – the relationship between the mechanical input and electrophysiological output has been experimentally quantified, but the dynamic response of the body as an intermediate stage remains understudied. Due to the embedded nature of mechanosensors involved in substrate-borne vibration sensing, morphology is likely to have a direct effect on information processing before sensory transduction (Miller and Mortimer, 2020), but empirical evidence supporting this idea is limited to the high-pass filtering properties of the cuticular pad adjacent to the HS10 lyriform organ (Erko et al., 2015).

This thesis aims to address this knowledge gap by quantifying the mechanics of the spider's body as vibrations are transmitted from substrate to mechanosensor. The dynamic response of the body is modulated by biomechanical parameters that covary with morphological traits. By breaking down the system into mass, springs/dampers, and geometry, I will be able to link biological variation in morphology with variation in the dynamic response and hence patterns of mechanosensor stimulation.

An open question concerns the mechanisms through which substrate-borne vibration sensing is robust to the morphological variation experienced by spiders (for example mass fluctuations due to feeding status in the short term and growth/development in the long term). This is important for understanding the biological context of the dynamic response – we might expect a high level of robustness given the need to maintain the efficacy of substrate-borne vibration sensing for biological functions. Another question is

whether spiders can actively change their dynamic response through behaviours such as posture, to influence the filtering of vibrational information through the body. This would implicate an adaptive role for morphological trait variation.

5 Research arc

In Chapter 1, I review the literature and set out the framework through which I consider vibration sensing in each subsequent chapter of the thesis. I identify biological traits that covary with biomechanical parameters which may influence vibration sensing. Variation in morphological traits is of particular relevance to the dynamics of the spider's body under vibrational input, as I am most interested in constraints and potential control mechanisms used by spiders for vibration sensing. This chapter has been published in Frontiers in Ecology and Evolution.

The data chapters of this thesis span Chapters 2, 3, 4 and 5. The first experimental aim of the thesis, covered in Chapters 2 and 3, is to collect data on mechanosensor location and biomechanical parameters (mass distribution, geometry) from potential spider study species. The distribution of mechanosensors across the spider body, particularly the legs, is critical for understanding the interaction between morphology and mechanosensation. The biomechanical parameters of the spider body are required to accurately simulate the dynamic response of the spider body and inform the minimum number of elements necessary to effectively model the system. The second experimental aim of the thesis, covered in Chapters 4 and 5, is to develop a method for quantifying and modelling the dynamical response of the spider system to vibrational input, in order to understand patterns of mechanosensor stimulation and reveal the influence of body dynamics on substrate-borne vibration sensing. I collect experimental data measuring the motion of the spider body, before using this data and the results in Chapters 2 and 3 to model and simulate the response of the spider body to vibrational input. Leg nomenclature follows a logical system but differs between data chapters – in Chapters 2 and 3, legs are numbered 1-4 anteriorly to posteriorly without reference to left/right sides of the body due to bilateral symmetry. In Chapters 4 and 5, when

mapping the experimental measurement points, legs are labelled A-H with each segment labelled 1-5, and in the mathematical model each leg is modelled as a single element labelled e.g. rf1 (right front 2), lr2 (left rear 2) as detailed in the figures.

In Chapter 2, I use scanning electron microscopy (SEM) to map the mechanosensors on the preserved legs of *Araneus diadematus* and *Trichonephila edulis*, two species of orb-weaving spider that differ in their morphology. In addition to distribution, I also categorise each mechanosensor based on the detailed morphology revealed in the images (e.g. lyriform organ, group of slit, large isolated slit, small isolated slit). The sensitivities and potential functions of these different mechanosensor types are established in the literature, so by linking this with their distribution I am able to determine which parts of the spider body have the highest densities of mechanosensors that are directly involved in detecting externally generated vibrations. This chapter has been published in Arthropod Structure and Development.

In Chapter 3, I use a whole-body CT scan of *Grammostola pulchra* to calculate the relative mass and mass moment of inertia of each body segment, and hence mass distribution across the body of the spider. I also investigate methods for approximating body segments as simple geometrical shapes for modelling and assess the accuracy of these methods in terms of mass distribution.

In Chapters 4 and 5 (which may be considered by the reader to be a “super-chapter”, with some details of methodology examined in more detail in Chapter 5), I perform a modal test on the spider to reveal the inherent dynamics of the body independent from substrate properties and source input, enabling me to make broad inferences about the role of body dynamics in different biological contexts. These dynamic properties include the natural frequencies of the system, which are important for understanding whether vibrational inputs in the biologically relevant frequency range are amplified by the biomechanical properties of the spider body.

The best available tool for measuring the freely vibrating system is laser vibrometry, as it is a non-contact measurement that does not influence the biomechanical properties of the spider system. For this approach, manipulation of the spider must be minimal – the animal should be alive, untethered, and stationary for the duration of the experiment. A limitation of this method is that the point measurements are not necessarily perfectly repeatable due to the need to aim the laser beam. The input type and vibration stage must be chosen such that the modal properties of the spider can be identified, whilst also avoiding any behavioural reaction from the spider that will cause the test to be terminated. Measurements are taken sequentially with a repeated input using two vibrometers. By focusing the laser at the mechanosensor locations identified in Chapter 2, particularly around the lyriform organs near the joints between leg segments, I am able to quantify the relative motion of the system at the areas which are most important for mechanosensor stimulation.

I use the results from this experiment in two ways. The vibrometry output is a direct measurement of the motion of the system under vibrational input and hence is informative in terms of quantifying the relative motion of each body segment – a parameter which is correlated with mechanosensor stimulation. In Chapter 4, I construct and calibrate a simple mathematical model of the spider, composed of mass-spring-damper elements using parameters obtained in Chapter 3. I then investigate the effect of parameters that are difficult to vary experimentally by simulating the response of the model to vibrational input. This chapter has been published in Proceedings of the Royal Society Interface. In Chapter 5, I investigate mechanisms of source localisation using the experimental and simulated data.

I conclude the thesis by synthesising the findings from the data chapters and addressing some of the questions which I have laid out in Chapter 1. I discuss how spider body dynamics are involved in the mechanisms of substrate-borne vibration sensing, especially in the context of source localisation. I assess the overall importance of morphology as a control mechanism for vibration sensing and suggest directions for future research in this area.

Chapter 1

Control vs. Constraint: understanding the mechanisms of vibration transmission during substrate-borne information transfer

Thomas E. Miller[1] and Beth Mortimer[1]

Adapted from:

Miller, T. E. and B. Mortimer (2020). "Control vs. Constraint: Understanding the Mechanisms of Vibration Transmission During Substrate-borne Information Transfer." Frontiers in Ecology and Evolution 8

Abstract

Substrate-borne vibrations are ubiquitous in the environment and are widely used as an information source by animals, whether they are generated by biotic or abiotic sources. The process of vibration information transfer is subject to a wide range of physical constraints, especially during the vibration transmission phase. This is because vibrations must travel through materials in the environment and body of the animal before reaching embedded mechanosensors. Morphology therefore plays a key and often overlooked role in shaping information flow. Web-building spiders are ideal organisms for studying vibration information transfer due to the level of control they have over morphological traits, both within the web (environment) and body, which can give insights for bioinspired design. Here we investigate the mechanisms governing vibration information transfer, including the relative roles of constraints and control mechanisms. We review the known and theoretical contributions of morphological and behavioural traits to vibration transmission in these spiders, and propose an interdisciplinary framework for considering the effects of these traits from a biomechanical perspective. Whereas morphological traits act as a series of springs, dampers and masses arranged in a specific geometry to influence vibration transmission, behavioural traits influence these morphologies often over small timescales in response to changing conditions. We then explore the relative roles of constraints and control mechanisms in shaping the variation of these traits at various taxonomic levels. This analysis reveals the importance of morphology modification to gain control over vibration transmission to mitigate constraints and essentially promote information transfer. In particular, we hypothesize that morphological computation is used by spiders during vibration information transfer to reduce the amount of processing required by the central nervous system (CNS); a hypothesis that can be tested experimentally in the future. We can take inspiration from how spiders control vibration transmission and apply these insights to bioinspired engineering. In particular, the role of morphological computation for vibration control could open up potential developments for soft robots, which could use multi-scale vibration sensory systems inspired by spiders to quickly and efficiently adapt to changing environments.

1 Introduction

Substrate-borne vibrations are an important sensory mode for many animals. These vibrations, which propagate through and along the surfaces of materials known as substrates, are ubiquitous in the environment and the study of the biological use of these vibrations is known as “biotremology” (Hill and Wessel, 2016). They can either be produced intentionally as a signal (e.g., in courtship) for communication, or as an unintentional cue (e.g., through the movement of a prey item) that can be used for information by receivers (Mortimer, 2017). Traditionally these vibrations have been overlooked as a potential source of biologically relevant information, with modern techniques unveiling the importance of this sensory modality. This is especially true for terrestrial arthropods, the context of this review, where substrate-borne vibration information transfer was likely used long before acoustic information transfer (or hearing) evolved (Cocroft and Rodríguez, 2005; Hill, 2009).

Like other sensory modalities, the biological use of substrate-borne vibrations for information transfer involves the generation, transmission and sensing (here used to refer to sensory transduction) of vibrations. This review focuses on the role of vibration transmission as an important, but relatively overlooked stage in this process, which is the stage encompassing everything between generating a vibration and transduction within sensory cells. This stage is interesting because although the theory of how vibrations propagate through materials is well developed, its application within this biological context is in its infancy and the role of natural selection in shaping or controlling this process is not well understood. In terrestrial arthropods, vibrations first propagate through the substrate before passing into the arthropod’s body where its leg couples with the substrate. Following coupling, vibrations propagate to mechanosensors that are typically embedded in the leg (Figure 1; Pringle, 1955). Mechanical transmission of vibrations therefore involves both propagation of the vibration within a material in the environment (or substrate) and within the animal’s body. Not covered here, at mechanosensors, mechanical stimuli (such as vibrations) lead to the generation of an action potential in the sensory neurons innervating the sensor, and the wave is

transformed into an electrical signal that travels along this neuron (Barth and Pickelmann, 1975). For detail and discussion on the effect of neuronal filtering and sensory transduction on the transformation of vibrational information, we refer readers to an alternative review (Barth, 2019).

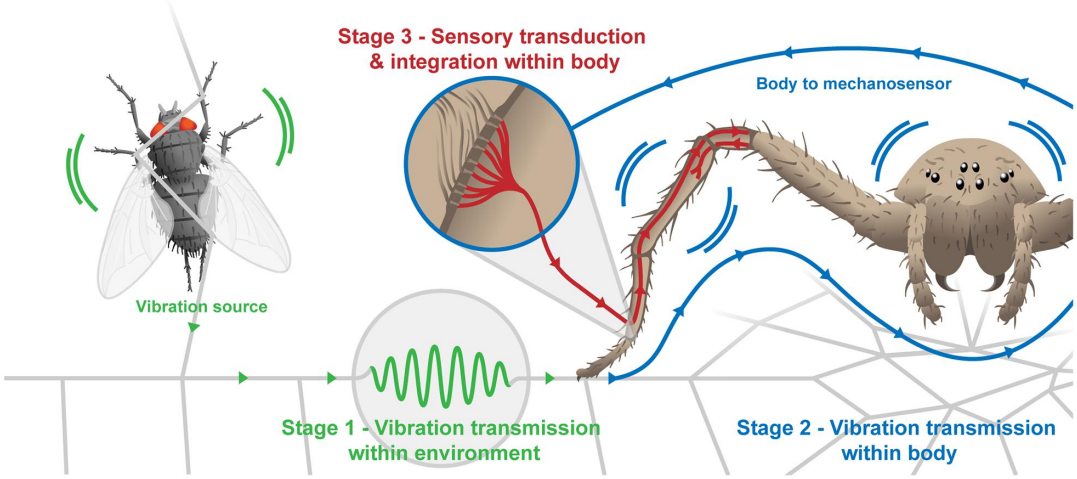


Figure 1. Diagrammatic representation of the stages in vibration sensing detailed in Table 1. Stage 1—transmission from source of vibration through environmental substrates (in this case the web) to the body. Stage 2—body transformation of input wave before it reaches the mechanosensor (lyriform organ shown in insert). Stage 3—sensory transduction of vibrational information, which feeds back to determine behaviour, in turn influencing Stages 1 and 2.

Vibration transmission is shaped by the interplay between natural selection, evolutionary, and physical constraints, yet the interactions between these processes in this context are not well understood. Both morphological and behavioural traits have been shaped by natural selection to influence vibration transmission (Table 1), which are under evolutionary constraints, e.g., trade-offs and developmental constraints. Each stage of transmission also varies in the degree to which physical constraints are acting. These physical constraints are imposed by their biomechanics and include damping (energy loss) and filtering of vibrational information (Mortimer, 2017). Control mechanisms can be used to mitigate these constraints (see section “Discussion”).

Table 1. The focus of this review is vibration transmission, which is in the physical realm and involves mechanical vibrations propagating through the environment (Stage 1) and body (Stage 2).

Stages in vibration information transfer	Traits under selection to promote vibration information transfer	Relevant physical constraints
1. Vibration transmission within environment.	If applicable, production and mechanics of own substrate (e.g., web); Choice of substrate; Sensing behaviors (e.g., positioning and freezing)	Damping, filtering and distortion; Vary with substrate and transmission distance
2. Vibration transmission within/along body.	Mechanics of body materials and joints (masses, springs, dampers); Body plan and geometry; Sensor placement and integration; Sensing behaviors (e.g., posture control)	Damping, filtering and distortion; Vary with coupling, body mechanics and sensor position
3. Sensory transduction and integration within body.	Mechanotransduction mechanism (e.g., ion channel type, number and position); Sensory thresholds (e.g., frequency, amplitude); Neuronal anatomy and sensory integration (e.g., positive/negative feedback); Sensorimotor feedback	Physiological constraints act; Vary with all aspects of neurophysiology

Vibration sensing, or sensory transduction, is in the physiological realm and involves mechanotransduction and integration of sensory information within cells (Stage 3). Both morphological and behavioural traits that are under selection to promote vibration transmission are given. Physical constraints vary to different extents within each stage.

In this review, we will use spiders as a case study to probe the mechanisms influencing vibration transmission during the process of vibration information transfer, building on previous reviews that discuss physical constraints acting during vibration transmission (Mortimer, 2017, 2019; Barth, 2019). This is the dominant sensory modality for many spiders (Barth, 2002a), and is used for communication with conspecifics during courtship (Schüch and Barth, 1985, 1990; Elias et al., 2003, 2005), as well as sensing prey and

predators (Klärner and Barth, 1982; Masters, 1984b; Landolfa and Barth, 1996). As such, mechanisms to influence vibration transmission apply to varied biological contexts with spiders, including prey capture, and conspecific communication. The mechanosensors involved in spider vibration sensing are slit sensilla—some of which are grouped into distinct structures known as lyriform organs (Barth, 2002a). In particular, the metatarsal lyriform organ has been intensively studied for its role in vibration sensing (Barth, 2002a). In addition to sensing externally generated vibrations, spiders use slit sensilla to sense internally generated vibrations, known as proprioception (Seyfarth, 1978).

Morphological and behavioural traits in spiders are extremely variable and the mechanisms causing this variation and the implications for information transfer, whether natural or engineered, have been largely unexplored. Web-building spiders are an excellent model species to study this due to the impressive control mechanisms that can influence vibration transmission both within the environment and body, which in theory allow them to mitigate physical constraints. For spiders, morphological traits include the structures and materials of both the body of the spider and the extended phenotype of the web, and behavioural traits act to influence morphology during vibration transmission (Table 1). This is exemplified by orb-weaving spiders that generate aerial orb webs that act as a snare for prey capture and a vibration transmission platform (Mortimer, 2019). Through modifying the extended phenotype of the web, these spiders are thought to influence vibration transmission outside the body (Mortimer et al., 2016). Most literature on orb weaver vibration transmission is on prey capture, although the web is also used to transmit vibrations during courtship (Wignall and Heberstein, 2013).

An aim of this review is to combine perspectives from across biology and the physical sciences to explore the mechanisms governing vibration transmission. One concept that we will come back to in the Discussion is the idea of morphological computation, which is a term more typically applied to artificial systems (such as robots). Morphological computation is where the body, rather than central nervous system (CNS), is used to control actions or information, thus reducing the total level of processing required by

the CNS. Recently, there has been increasing recognition of its role in biological systems—for example, animals rely heavily on the material properties of their leg muscles and tendons to walk/run, rather than these leg movements being closely controlled by the CNS (Mo et al., 2020). In sensory systems, morphological computation could be used to pre-process information before sensory transduction occurs, which in our context would be during the vibration transmission stage. This is thought to occur in the insect eye, where the arrangement of light-sensitive cells allows insects to accurately gauge distance without additional processing in the CNS (Franceschini et al., 1992). During vibration information transfer in terrestrial arthropods, since mechanosensors are embedded into the cuticle or leg (Yack, 2004), vibratory waves must travel through the body of the animal before they are sensed. This means vibration information transfer is more heavily influenced by morphology than other senses (whether acoustic vibration, olfaction or visual), and morphological computation is likely to play a role in this context.

Using orb weaving spiders as a case study, this review will overview the known and theoretical contributions of morphological and behavioural traits to the biomechanics of vibration transmission (sections “Influence of Morphological Traits” and “Influence of Behavioural Traits,” respectively). We deconstruct the effect that these traits have on three key parameters that can be used to model the system—mass/density, springs/dampers (energy storage/loss), and geometry. We explore the interactions and trade-offs between these three parameters, morphological and behavioural traits in the Discussion. Using this approach, we show that orb-weaving spiders possess a high level of control over morphological and behavioural traits during vibration transmission over multiple timescales. We follow with a discussion of how variation in these traits (within an individual, between individuals of the same species, and between species) can be explained by the action of control mechanisms and constraints (Discussion). We suggest that within a species, morphology is controlled flexibly via behaviour, which acts to mitigate against various constraints in variable contexts. We conclude that morphology likely plays a key role in transforming information before the vibrational wave reaches a mechanosensor, and hypothesize a role for morphological computation (section

"Discussion"). The review provides insights into the relative roles of natural selection, evolutionary and physical constraints in shaping vibration sensing in terrestrial arthropods, but also reveals the mechanisms that can be applied to bioinspired design of devices that use substrate-borne vibrations for information.

2 Influence of Morphological Traits

From a biomechanical perspective, morphological traits can be seen as systems with a series of masses, springs, and dampers arranged in a specific geometry that influences its motion over time, whether in the environment (here the web) or within/through the body (here the spider's body). These three parameters are not mutually exclusive and they interact with each other to influence vibration propagation. Yet thinking of vibrating systems, including animals, as these constituent parameters provides a framework to help us to understand the underlying biomechanics governing its motion and compare between biological systems that vary to different degrees to gain insights into its evolution. Within this section ("Influence of Morphological Traits"), each component will be discussed separately, with the aim that the importance of each component to vibration transmission can be outlined.

Mass is distributed both within the substrate and within the body and is particularly important due to physical constraints acting to dampen (or dissipate energy), filter, and distort vibrational information (i.e., influence the relationship between frequency components). Density is a measure of distributed mass, so is discussed within the section on Masses (section "Masses"). Whereas springs govern energy storage in the system when the springs are compressed or stretched, dampers govern the energy lost from the system, usually due to friction. In our orb-weaver spider context, springs/dampers are the silk threads, the cuticle that forms the exoskeleton of the spider and the spider's joints. Finally, these parameters come together into a specific geometrical arrangement (web shape, body plan, and mechanosensor structure) to govern vibration transmission and shape the information that can be extracted by the animal due to sensor placement. Here we discuss the known and theoretical

contributions of masses, springs, dampers, and geometry to vibration transmission, using this interdisciplinary framework in the context of orb-weaving spiders, where the behaviours that influence these factors are reviewed in section “Influence of Behavioural Traits.”

2.1 Masses

Vibration transmission through a material is influenced by mass distribution, including changes in density of a material through which a wave propagates. In our spider context, we will focus on masses in the web, as the spider’s engineered substrate, and in the body, through which vibrations need to propagate before reaching embedded mechanosensors (section “Web and Body Transmission”). Mass and density (in combination with material properties and geometry) govern the speed of vibration transmission, how it loses energy over distance and time, and how the wave is filtered (section “Mechanical Impedance and Resonance”) (Mortimer, 2017). Masses also interact with the other biomechanical parameters of springs and dampers (section “Springs and Dampers”), according to their geometry (section “Geometry”).

2.1.1 Web and Body Transmission

The influence that masses have on vibration transmission differs markedly between the web and the body. The mass of the silk threads comprising the web is negligible compared with the spider’s body and prey items in the web—therefore, the dynamics of vibration transmission are largely dependent on the masses suspended by the silk threads, rather than the web itself. All spider body plans consist of a fused head and body segment (cephalothorax) joined to an abdomen segment via the waist-like pedicel, and eight legs, all of which vary in their mass and geometry (Foelix, 1979). In particular, these masses modulate how vibrations are transmitted through the legs at different joint angles, where higher masses lead to greater forces exerted around the leg joints (via gravity), influencing their springs and dampers (see section “Springs and Dampers”).

The mass distribution of a spider and its web is stochastic, with the mass of objects caught in the web (such as prey and debris), as well as the mass of the spider's body, varying over time. The mass of the spider's cephalothorax will fluctuate due to factors such as starvation and dehydration, which will reduce the volume of internal fluid (haemolymph) in the abdomen, as well as the production of eggs by female spiders (Foelix, 1979). Similarly, the amount of silk protein stored in the silk glands will deplete when the spider spins a new web and will then gradually refill (Vollrath, 1999). This is variation that spiders have some control over, but largely cannot avoid, and thus mass fluctuation imposes a physical constraint. Mhatre et al. (2018) simulated the vibrational response of a female black widow spider to vibration, which showed that abdomen mass could vary from 20% to 150% of its in vivo value without a measurable effect on the vibrational response to stimuli between 5 and 200 Hz. Spiders likely possess mechanisms that enable them to account for wave transformation due to their own mass fluctuation, which may be "known" by the spider—this is a topic requiring further research.

2.1.2 Mechanical Impedance and Resonance

As a vibratory wave propagates through a system, the masses it encounters will resist changes in motion that will act to transform the vibratory wave. This tendency for a mass to resist changes in velocity as it is oscillated is known as mechanical impedance, which leads to energy loss and/or reflection of vibrations as a wave passes from a material of one density to another (e.g., from silk to cuticle) (Main, 1993). From a biological perspective, it may therefore be desirable to minimize changes in density and material properties (such as stiffness) throughout transmission, as energy loss will lead to reduction in signal amplitude and therefore make vibrations more difficult to detect. This is especially important in two contexts where waves are transmitted between disparate materials: within a heterogenous substrate (or multi-material substrate) (Elias and Mason, 2014); and at the coupling points between the substrate and the body.

Starting with the former, damping in heterogenous materials may be reduced through morphological adaptations such as impedance matching (O'Connell-Rodwell, 2007),

where materials with similar properties are used to minimize changes in mechanical impedance. The degree of sclerotization (cross-linking) in a spider's exoskeleton varies across different parts of the body and legs (Blickhan and Barth, 1985), therefore altering the material properties through which vibrational waves propagate. Gradients in material properties of the cuticle are often found [e.g., elastic modulus varying from 8.3 (±1.1) to 2.8 (±1.3) GPa across the cuticular pad] (Young et al., 2014; Erko et al., 2015), which would reduce mechanical impedance changes and so reduce damping and filtering of the vibration. Impedance matching mechanisms via gradients in material properties in terrestrial arthropods require further research.

Moving on to the effect of coupling, the energy loss caused by the coupling between silk and the spider claw (tarsus) is expected to differ between wave types, which is the type of vibrational wave propagating through the material. In the spider web, wave types vary in the direction of oscillation, where longitudinal waves oscillate within the axis of the fibre and transverse waves oscillate perpendicular to the fibre axis. Whilst only longitudinal wave transmission to the tarsus has been measured, the fact that transmission of longitudinal waves through the web shows less damping compared transverse (c. −2 dB on the same silk thread compared with c. −16 at 20 Hz) (Masters and Markl, 1981; Masters, 1984a), means that we can estimate the results for transmission to the tarsus. These differences are expected to become more pronounced above 100 Hz, after which transverse wave damping increases (down to c. −50 dB on the same silk thread) (Masters, 1984a; Landolfa and Barth, 1996). Since longitudinal vibrations are particularly important for initiating predatory behaviour in orb weavers (Klärner and Barth, 1982), these observations support the idea that coupling functions to preserve longitudinal wave transmission between the silk and tarsus.

Changes in mechanical impedance also affect vibration transmission when objects sit in the web, such as the spider, prey or debris. Evidence from modelling suggests that the presence of the spider itself at the web centre (hub) leads to significant damping compared with empty webs—c. −16/−36 dB for transverse/longitudinal waves, respectively (Mortimer et al., 2018). Often the presence of these objects cannot be

avoided and so present a constraint on vibration transmission. However, some spiders may be able to use the mechanical impedance of their body mass functionally in vibration information transfer. This is because a mass at the hub alters both the speeds and amplitudes of vibrations in the web (Mortimer et al., 2018), which provide information on the location of a vibration source (Mortimer et al., 2019). Mechanical impedance of prey items may also be used by orb weavers as a prey localization cue (Mortimer et al., 2019).

Vibrations often contain multiple frequencies at once. Resonance is where the frequency of an input vibration matches the natural frequency of the system through which it travels, resulting in these frequencies being amplified. The natural frequency of the system is governed by its masses and geometry (Balachandran and Magrab, 2008)—in this case it includes objects in the web and the silk threads comprising the web. At low frequencies (<30 Hz), in theory resonance may occur in the body of the spider itself, or other large objects (such as prey bundles) in the web (Frohlich and Buskirk, 1982). Frequencies in this range contain noise from environmental factors (such as wind) (Masters, 1984b; Wu and Elias, 2014), so resonance of objects in the web is therefore unlikely to be used functionally by the spider. However, spiders may be able to use resonance of silk threads [predicted to be in the hundreds to thousands of Hertz range (Frohlich and Buskirk, 1982)] to locate small objects, by “plucking” silk threads and detecting vibrational cues specific to the thread on which the object sits (Klärner and Barth, 1982). A hypothesized mechanism for this object localization method is the use of wave reflection off the object due to mechanical impedance changes that result in high frequency vibrations on these specific threads (Mortimer, 2019).

2.2 Springs and Dampers

The springs and dampers in a vibrating system govern the energy stored and lost during vibration transmission. This is determined by the material and structural properties of the material through which a vibrational wave travels. Most biological tissues contain biopolymers, meaning that they behave as viscoelastic materials (Vincent, 1990). Many

biological viscoelastic materials behave like springs at low deformations, meaning they have a linear relationship between force and displacement up to a certain displacement. In this range, they can store and return energy like a spring. Outside this deformation range, they no longer behave as springs, but the material deforms to dissipate energy from the system, which is viscous behaviour. This energy dissipation, or damping, depends on the time that the material has to deform (e.g., it can extend more over longer timescales) and the temperature (e.g., it can extend more at higher temperatures), as both influence the energy introduced to the biopolymer, which alters its structure beyond a transition point (the glass transition temperature of the biopolymer) (Guan et al., 2012). This makes energy dissipation time-, frequency-, and temperature-dependent. Viscoelastic materials therefore act as both springs and dampers, where this behaviour changes with both deformation range and frequency (Vincent, 1990).

In context, the most important viscoelastic materials for spiders are the silk threads that make up the web, and the spider's body tissues—especially the cuticle of the exoskeleton, in which the slit sensilla vibration sensors are embedded (Barth, 2019). The springs/dampers within the materials interact with mass to influence vibration transmission: the stiffness and density of these materials are linked to wavespeed and damping, which in turn are involved in frequency filtering and hence determine the shape of the vibrational wave that arrives at the sensor (Mortimer, 2017). These materials also make up structures such as joints that have their own springs and dampers as they move. The properties of the materials and structures therefore have a profound effect on the transmission of vibrational waves.

2.2.1 Vibration Transmission Within Web Environment

The spring-like behaviour of silk at low deformations governs the transmission of vibrations through the web. A key property of a spring is its stiffness, which is the gradient of the relationship between force and extension, which governs the tension or force on the silk when a displacement is applied (Vollrath, 2000). Spider dragline silk is

unique in the range of stiffness available, due to an unusual property called supercontraction, where high humidity [>70% relative humidity (RH)] dramatically alters the silk structure and reduces its stiffness (Liu et al., 2008). Here, we will briefly review the effects of silk tension, stiffness, and supercontraction on vibration transmission in webs, whilst the behaviours that are able to control these features are reviewed later (section “Influence of Behaviour”).

Silk tension both controls web geometry and is determined by it. This feedback system is vital for maintaining the mechanical integrity of the web, with mooring threads that attach to the environment being under the greatest tension (Wirth and Barth, 1992). Silk tension is particularly important for the transmission of transverse waves as it directly affects wavespeed and amplitude when interacting with mass per unit length and geometry (Mortimer et al., 2014, 2016). Conversely, longitudinal wave transmission is influenced by stiffness (Frohlich and Buskirk, 1982), which is of particular importance for predatory behaviour due to its low damping in the web (almost no damping, > −2 dB, from prey-capture region to hub along same silk thread in the biologically relevant range of 1–10,000 Hz) (Masters and Markl, 1981). Stiffness is influenced by supercontraction, which decreases the order of the protein structure and reduces stiffness (Liu et al., 2008; Guan et al., 2011). The degree of supercontraction is altered by the proportion of proline amino acid in the silk proteins—silks from different species of spider contain varying amounts of proline (ranging from as little as 0.6 to 14.3 mole%), and thus experience different degrees of supercontraction (Liu et al., 2008).

2.2.2 Vibration Transmission Within/Along Body

As slit sensilla are embedded sensors, the material properties of the cuticle directly influence vibrations before they reach the sensors, and also govern how the slit sensilla deform in response to vibrational waves. Since the cuticle behaves like a spring at low deformations, the slit sensilla are able to deform when extended and then return to their original state (Hössl et al., 2006). The exoskeleton covering the legs, where the largest concentrations of slit sensilla are found, is composed of stiff exocuticle. The

opisthosoma (posterior part of the abdomen), on the other hand, is covered by less stiff mesocuticle, and therefore the slit sensilla found here will undergo greater deformation in response to a vibrational wave compared with those surrounded by a stiffer material (Barth, 2002a).

A cuticular pad situated distally (toward the claw) to the metatarsal lyriform organ is involved in transmitting and filtering vibrations as they propagate from the tarsus to the metatarsus leg segments (McConney et al., 2007; Young et al., 2014; Erko et al., 2015). The viscoelasticity of the pad allows it to act as a high-pass filter, meaning it filters out low-frequency background noise (e.g., vibrations of c. < 10 Hz). At low frequencies, the pad behaves in a viscous manner, producing maximum damping properties. This means that large tarsal deflections (angular displacements c. 10° and above) are required to activate the slit sensilla, which also acts to prevent damage to the organ at high deflections (Young et al., 2014; Erko et al., 2015). At higher frequencies (>10 Hz), the pad transitions to a spring-like state, becoming stiffer and transmitting vibrations much more effectively. These properties are temperature-dependent, with the pad damping vibrations at higher temperatures (>21°C at 10 Hz) (McConney et al., 2007; Young et al., 2014).

In addition to the cuticle, the joints between leg segments themselves act as springs and dampers. For some joint motions (loading along the leg axis), joints behave as springs (Blickhan, 1986). For other joint motions (dorsoventral and lateral deflections), increased joint deflection stretches the articular membrane, which is thought to increase the alignment within the material, increasing stiffness (Blickhan, 1986). This results in energy being lost as the joint is loaded and unloaded, so the joint acts as a damper under certain conditions (Blickhan, 1986). As the lyriform organs are typically embedded near the leg joints, their mechanical sensitivity (here taken as the ratio of input force to cuticle deformation, i.e., the strain) is influenced by the strains and changes in stiffness in the cuticle that is generated by joint movement. When the legs are loaded axially, the deformation in the cuticle is negligible around 170° (between c. −0.1 and 0.1 με/mN), but the deformation, and presumably lyriform organ sensitivity,

increases above/below this joint angle as the cuticle is put under tension/compression, respectively (Blickhan and Barth, 1985). There are some exceptions to this (e.g., VS-5 lyriform organ), where organs are compressed (and therefore stimulated) during leg extension (Blickhan and Barth, 1985).

2.3 Geometry

The vibrational motion of a system made of masses, springs, and dampers is determined by its overall geometrical structure. Diversity in web shapes and body plans influences vibration transmission through these materials. Variation in the geometry of morphological traits between species can be explained by the evolution of divergent hunting strategies, shaped in part by various constraints. In addition, mechanosensor geometry and placement varies within an individual, both spatially over different areas of the body, and temporally due to development and regeneration.

2.3.1 Vibration Transmission Within Web and Body

Web geometry is highly variable both within and between individuals. Individual variation in web geometry usually arises due to external and internal factors that change over time. For example, orb webs built at 20% relative humidity have c. 80% the capture area of webs built at 70% relative humidity (Vollrath et al., 1997). Starvation has also been shown to affect the variability of web geometry—when sufficiently fed, spiders use web modifications (such as increased capture area) to reduce variability in web geometry, which is thought to produce a more optimal phenotype for prey capture effectiveness (Vollrath and Samu, 1997). Whilst this variation has been well quantified, the trade-offs between mechanical functions vs. vibration transmission when geometry is modified have largely not been investigated, and future experiments should aim to quantify both mechanical and vibration transmission properties as web geometry changes and their implications for prey capture.

Web geometry due to the spider's resting location on the orb web alters vibration transmission, where some individuals sit in a retreat at the edge of their web rather than being positioned at the hub (center). Some spider species are more likely to employ this strategy than others, such as *Zygiella x-notata*, which senses web vibrations using a signal thread that joins the retreat to the hub, passing through a sector devoid of crossing threads (Klärner and Barth, 1982; Mortimer et al., 2018). Thus, they initially forgo the ability to localize prey on the web in favor of being less conspicuous at the retreat to avoid predation (Pasquet et al., 2007). After sensing prey struggling in the web, *Z. x-notata* moves along the signal thread to the hub, where it is able to orient toward the source vibration, making prey capture take longer (Klärner and Barth, 1982). The change in resting position does not impose any biologically relevant time cost due to vibration propagation through the web, but signals arriving at the retreat will be more damped than those at the hub (−1.37 ± 0.91 dB on the signal thread relative to the hub) (Mortimer et al., 2018).

There is high interspecific variation in web geometry (Foelix, 1979), and different web types are characteristic of separate taxonomic groups—these include orb webs, funnel webs, tubular webs, sheet webs, and tangle webs. Whilst most studies have focused on orb webs as their regular structure makes them easier to model, other web geometries are a promising area for future research, as each has their own unique transmission properties. For example, whilst the transmission efficiencies of transverse and longitudinal waves through orb webs differ greatly (especially with masses in the web as described previously) (Masters, 1984a; Landolfa and Barth, 1996; Mortimer et al., 2016), in other web geometries, such as sheet and tangle webs, they may propagate equally well (Naftilan, 1999; Vibert et al., 2016). In these web types, there are a large number of points where threads come into contact with each other, and unlike in orb webs, the angles between threads tend to be quite variable (Vibert et al., 2016). This irregular web architecture means that there is a lot of variation in what frequencies are transmitted best within and between webs, suggesting that frequency may not be the most important factor for discriminating between vibratory sources for these spiders. Modelling suggests that resonance of the silk threads may be useful in enhancing the

amplitude of prey generated vibrations in funnel/sheet webs, with amplification occurring within some of the frequency range that prey struggles at (2–200 Hz) (Naftilan, 1999).

The influence that the overall body plan of the spider has on vibration transmission is a largely unexplored area, yet is likely to prove vital in our understanding of how evolution and constraints have shaped vibration information transfer. A useful approach will be to model diverse spider body plans as mass-spring-dampers systems to investigate the physical relationships underlying vibration transmission. From a mass-spring-damper perspective, overall body plan matters because it determines the dynamics of the vibrating system (including torques and resonances). We can consider two extremes of spider morphology and compare the body plan of the Pholcidae (cellar spiders) with the Theraphosidae (tarantulas) (Figure 2; Foelix, 1979). In Pholcidae, a pendulous abdomen is connected to a small cephalothorax, which is in turn supported by very long, thin legs. In Theraphosidae, the legs are much shorter and thicker, comprising a larger proportion of the spider's overall mass. These families have evolved disparate hunting strategies, with the Pholcidae employing a web to trap prey, and Theraphosidae being ambush predators. Therefore, their difference in morphology is also correlated with a difference in substrate through which they sense vibrations (ground/tree vs. the web), and a difference in the vibrations of prey. The leg and body shapes can be assumed to be adaptive for their respective hunting strategies, shaped by evolutionary and physical constraints including trade-offs; for example the strong, muscular legs in Theraphosidae have to be able to overpower prey as well as sense vibrations. Whether the shapes of the legs and body are adaptive in vibration transmission remains to be seen, but in theory these differences will influence vibration transmission.

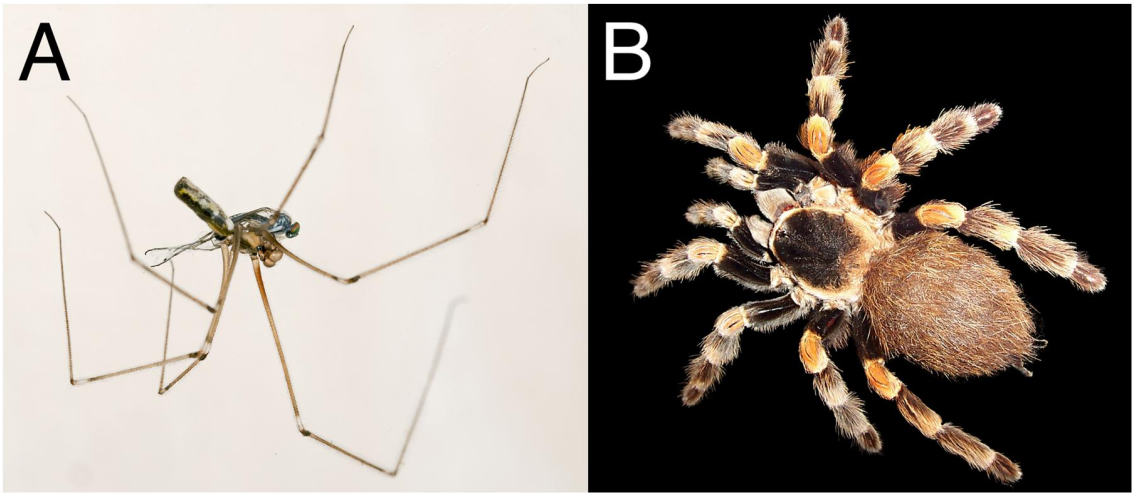


Figure 2. Comparison of the body geometries of *Pholcus phalangioides* (A) and *Brachypelma smithi* (B). Open source images: A—Filename "Pholcus phalangiodes MHNT male. jpg," courtesy of Didier Descouens, License CC BY-SA 4.0, B—Filename "Brachypelma edit. jpg," courtesy of user "Fir0002," License CC BY-SA 3.0.

2.3.2 Mechanosensor Geometry and Placement

Sensor geometry and placement is key to how mechanosensors respond to deformations in the exoskeleton, from the position of individual slits, through to the geometry and position of the sensors on the body. The spatial and temporal variation in slit sensilla geometry across individual spiders has been extensively studied in a single species—*Cupiennius salei* (Barth, 2019). Understanding interspecific variation in sensor geometry is currently limited, but further research would reveal how spiders in different contexts solve the problems of sensor placement to promote vibrational information transfer. More research is needed on the distributions of slit sensilla across all parts of the spiders' bodies on a range of spider species other than the well-studied *Cupiennius salei*.

We can first consider the shape and structure of individual slits. Variation in slit length (5–200 µm) affects the sensitivity of the organ, as a larger slit will deform more than a smaller slit. This induces a greater deflection in the covering membrane that spans the slit and which sensory cells are attached to, which in turn makes vibrations easier to

sense and decode (Barth, 1972; Barth and Pickelmann, 1975). The base curvature of the covering membrane also varies, with some forming a deeper trough within the slit than others—again, this affects sensitivity as greater curvature will mean that the membrane deflects more as the slit deforms (Barth and Bohnenberger, 1978). This is linked to the position of the neurons that innervate the membrane, with most dendrites connecting near the middle, where the greatest deformation occurs (Molina et al., 2009).

The arrangement of slits within the lyriform organs also has implications for vibration sensing. Slit arrangements and overall organ shape differ between lyriform organs located on different areas of the leg, which give each organ subtly different sensing capabilities (Figure 3A; Barth et al., 1984; Hössl et al., 2007, 2009). Heart-shaped arrangements found on the trochanter (leg segment), for example, are particularly sensitive to load direction (Barth et al., 1984), whilst slightly asymmetrical triangular arrangements can be used for measuring different response ranges (Hössl et al., 2009). The orientation of these slits relative to the leg axis is also important for vibration sensing, as the greatest deformation will be induced when the long axis is perpendicular to the direction of the input force. Because of this, most slit sensilla, including those in the lyriform organs, are oriented parallel to the long axis of the legs—which is the direction of vibrational wave transmission. However, not all of them are, and the reasons for this variation are currently unclear. This could be investigated by comparing slit orientation in different species and correlating this with morphological/life strategy differences.

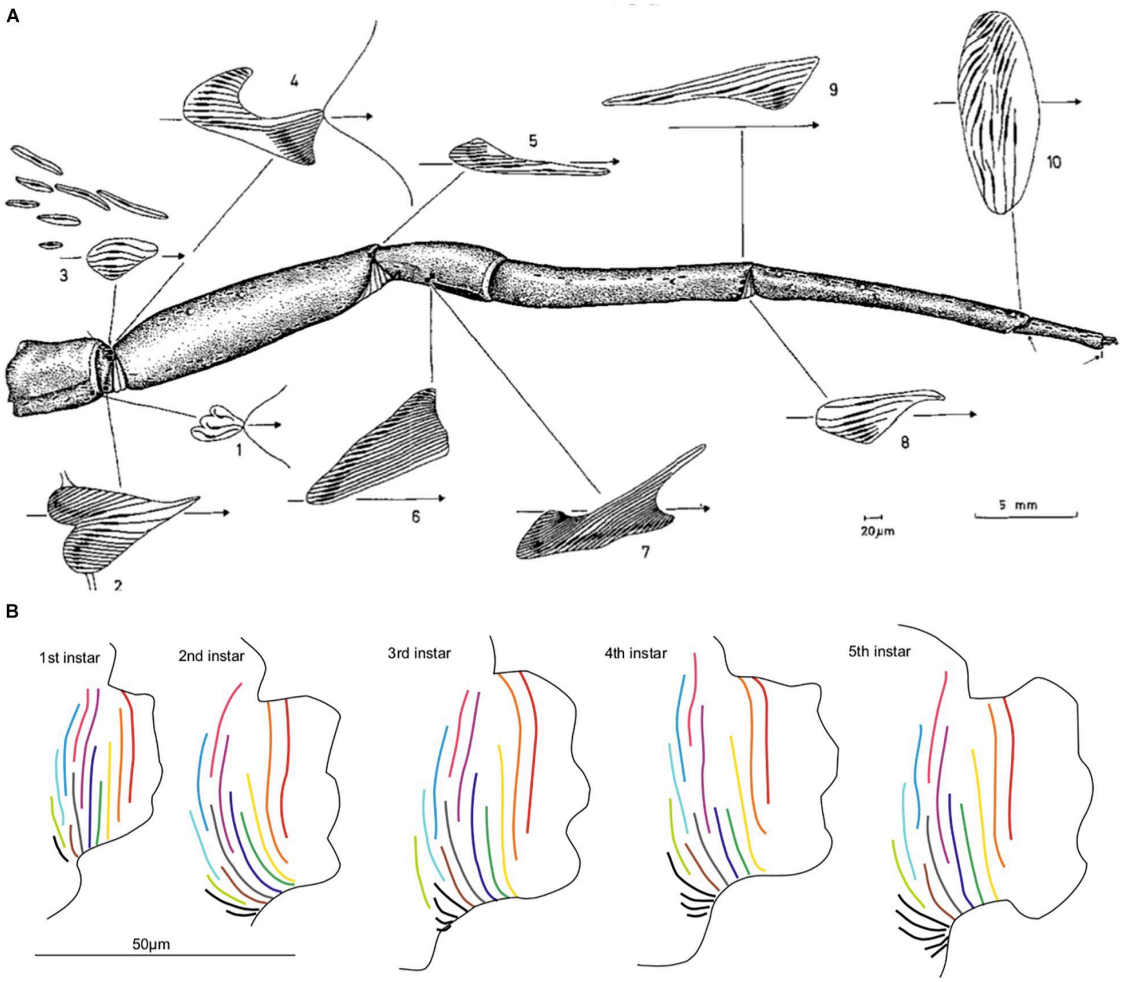


Figure 3. A—spatial variation in lyriform organ geometry on the posterior of the first leg of *Cupiennius salei*, including heart-shaped, triangular, oval and irregular arrangements of slits. B—temporal variation in the HS10 lyriform organ on xthe first leg over the first 5 juvenile instars of *Latrodectus hesperus*, demonstrating changes in shape as well as increase in overall number of slits through growth. A—Reprinted by permission from Springer Nature Copyright Clearance Centre: Springer Nature, Zoomorphologie (Slit sense-organs of arachnids - Comparative-study of their topography on walking legs (Chelicerata. Arachnida), Barth, F. G. and Stagl, J.) [Copyright], (1976). B—Reprinted by permission from Springer Nature Copyright Clearance Centre: Springer Nature, Zoomorphology (Developmental morphology of a lyriform organ in the Western black widow (*Latrodectus hesperus*), Morley, E. L., et al.) [Copyright], (2016).

Lyriform organ geometry changes over development, where the lyriform organs and metatarsal pads grow at different rates (Figure 3B; Morley et al., 2016). The pad shows isometric scaling (proportional) relative to metatarsal length, as the pad grows at the same rate as the rest of the leg. However, the lyriform organ starts out relatively large and grows slowly using hypoallometric scaling in order to preserve function (Morley et al., 2016). This results in these two components being mismatched during early moult stages due to developmental constraints and trade-offs, with the small pad meaning that juveniles are less able to filter low-frequency environmental noise (<40 Hz) (Morley et al., 2016). Whether the effect of this mismatch is compensated for by the nervous system, handled by morphology or mitigated through behaviour, remains an open question.

Both slit length and lyriform organ geometry are also affected by limb regeneration. Some spiders lose limbs and regrow them during successive moults. However, it can take several moults before the limb regains normal morphology, where the regenerated leg from the first moult may be only half the length of the others, yet appears to function normally (Vollrath, 1995). Crucially, the shape of the lyriform organs on regenerated legs differs from normal legs—the triangular organ, for example, has a lower apex whilst legs are regenerating (Speck-Hergenröder and Barth, 1988). Further research is needed to determine whether differences in the shape of the lyriform organ are adaptive, whether due to regeneration, development, and interspecific differences. Using modelling, evidence could be provided that this variation is adaptive by demonstrating that changes in lyriform organ morphology produce a compensatory transformation in the input wave.

Finally, the location of the slit sensilla on the body determines how they respond to forces and may be linked to their function (Barth and Stagl, 1976). Slit sensilla are distributed throughout the spider's body and are extremely numerous, with around 3,500 in *Cupiennius salei* (Barth, 2002b). In general, the highest concentrations of slits (both single slits, loose groups, and lyriform organs) are found in the proximal segments of the legs (closer to body), which is correlated with increased musculature in this

region. Lyriform organs are typically located at or near the leg joints (Barth, 2019), where the forces through the cuticle are likely to be highest. Single slit sensilla, on the other hand, are often found well away from the joints in the middle of the leg segments. They are, however, frequently located near where the muscle attaches to the cuticle, which supports the idea that these organs function in proprioception, through the sensing of internally generated strains from muscular contraction (Seyfarth et al., 1985). Other organs are located toward the distal ends of the legs, such as the metatarsal lyriform organ and the tarsal slits (Barth, 2002a). These organs respond to external vibrations (Barth and Bohnenberger, 1978; Speck and Barth, 1982), which makes sense given they are located closer to the coupling point with the substrate. However, vibrations will continue to propagate up through the leg and body after reaching the metatarsal lyriform organ and hence more proximally located organs are likely to be involved as well, which is supported by evidence that spiders still orient toward vibration sources (albeit with reduced accuracy) when the metatarsal lyriform organs are ablated (Seyfarth and Barth, 1972; Seyfarth et al., 1982; Bleckmann and Barth, 1984).

3 Influence of Behavioural Traits

Behaviour is a key mechanism influencing vibration transmission as it acts to influence morphology in different biological contexts. This includes altering mass distribution, the parameters of springs and dampers through stiffness and tension, and changing overall geometry—both in the extended phenotype of the web and in the spider's body.

3.1 Vibration Transmission Within Web

The extended phenotype of the spider web is an excellent example of using behaviour to control an individual's vibratory environment. Different elements of the web can be modified to alter different aspects of vibration transmission, whilst maintaining other functions such as prey capture ability. We have already discussed how masses, springs, dampers, and geometry within the web may influence vibration transmission, and here

we discuss the degree of behavioural control spiders have over these factors, and link these with the biological contexts that drive spiders to make these changes.

Starting with the effect of masses, some spiders will actively remove foreign objects from their web (Cloudsley-Thompson, 1995; Pasquet et al., 2007). Whilst these tidying behaviours may be driven by a number of different selection pressures [e.g., avoiding damage to the web, hygienic reasons (Straus and Avilés, 2018)], they will also affect vibration transmission by modifying mechanical impedance on the web. Orb weavers have been shown to locate these objects using a "plucking" behaviour (Klärner and Barth, 1982). The presence of some masses in the web (such as stored prey items) is, however, unavoidable, despite their impact on vibration transmission. Behaviours such as caching prey (storing food e.g., in *Nephila*) are used to cope with a variable food supply (de Crespigny et al., 2001) and also attract more insects into the web (Henaut et al., 2010). However, caching prey only within a small area may mitigate the impact of stored food on vibration transmission as their effect on vibration transmission would be location specific.

Orb weaving spiders have behavioural mechanisms to control the springs and dampers of the web, via changing tension, stiffness, and supercontraction. Spiders may adjust silk tension in order to deliberately modulate the transmission of vibrations through the web in response to a change in conditions (Watanabe, 2000). As well as controlling silk tension, spiders are also able to modulate silk stiffness. Orb weavers can adjust silk stiffness during web construction [by spinning silk more quickly (Vollrath et al., 2001)] and after the web is complete (by applying a force to a thread). Both of these processes result in increased ordering of the protein structure and hence increase stiffness (Guan et al., 2012). Spiders can modulate supercontraction to a certain degree by changing silk tension, as threads will not supercontract at high tensions (>140 MPa) (Boutry and Blackledge, 2010; Guan et al., 2011). Therefore, leaving threads slack will lead to increased supercontraction. Threads may also end up being unintentionally slack due to web damage, where supercontraction could act to increase thread tension in these areas. Spiders can also stretch out supercontracted threads to increase stiffness

following supercontraction (Guinea et al., 2005). Spiders may therefore modify stiffness using these mechanisms to modulate trade-offs, for example increasing silk stiffness to prioritize mechanical function at the expense of prey sensing ability, as increased stiffness reduces longitudinal wave amplitude (Mortimer et al., 2016). Although these are mechanisms in theory, whether orb weavers actually apply their ability to modulate stiffness to control web properties and vibration transmission is currently unclear. Experiments would be needed to link sensory cues with spider control mechanisms and the resulting mechanical and vibrational properties of the web would need to be quantified.

Individual spiders will modify the geometry of their webs to influence trade-offs in response to environmental variables (Vollrath et al., 1997). When it is windy, garden cross spiders will produce a smaller, rounder orb; with fewer and more widely spaced capture spiral threads (40,686 mm2 total area and 14,545 mm spiral length in still conditions vs. 35,235 mm2 total area and 13,039 mm spiral length in windy conditions) (Vollrath and Samu, 1997)—this geometry is less likely to catch the wind like a sail and get damaged (Zaera et al., 2014). We hypothesize that in these situations, spiders prioritize the mechanical integrity of their web over vibration transmission, as fewer capture spirals reduce transverse wave amplitude (Mortimer et al., 2016). However, there are other relevant trade-offs at play here—these same modifications are also likely to reduce the prey-capture effectiveness of the web.

Orb weavers can also alter the transmission properties of their web in response to their energetic state (Watanabe, 2000). Starved spiders are more likely to target smaller prey items that would usually be ignored when satiated (Herberstein et al., 1998). Some orb weavers (e.g., *Octonoba sybotides)* modify web geometry when starved by forming webs with spiral rather than linear stabilimenta (web decorations). This is thought to increase radial thread tension (Eberhard, 1972), which makes low amplitude transverse vibrations produced by small prey easier to detect (Mortimer et al., 2016). In turn, this allows starved spiders to respond to small prey more quickly (Watanabe, 2000).

Using all of these mechanisms, orb-weaving spiders in theory are able to adjust the vibration transmission properties of their web at multiple temporal levels, possibly even specifically targeting certain wave types (longitudinal or transverse waves). This high level of control enables them to effectively respond to changes in environment, web damage, fluctuations in body mass, and climatic factors—variation which might otherwise impair vibration information transfer.

3.2 Vibration Transmission Within/Along Body

The dynamics of vibration transmission in a spider's body is strongly influenced by posture, which spiders actively control. We have already discussed how leg angle influences the springs and dampers of the joints, as well as the sensitivity of the lyriform organs, and here we examine how spiders use behaviour to control this.

Spiders in theory can use postural changes to alter mass distribution, springs/dampers and geometry in response to different behavioural contexts. For example, the crouching posture tends to be adopted more frequently when a spider is starved (Mhatre et al., 2018). Empirical evidence for the effect of posture is currently limited to the role of springs/dampers at individual leg joints (Blickhan, 1986). Whilst evidence from modelling indicates that full-body geometry and mass distribution is also important for vibration dynamics (Mhatre et al., 2018), this is an area that is yet to be fully investigated. We do know that different postures are correlated with the sensitivity of the lyriform organs, as different joint angles influence the extension and stiffness of the cuticle surrounding the joint (Blickhan, 1986). Spiders adopt different resting postures when sitting at the hub or retreat of their webs, such that their legs are in contact with the relevant silk threads for vibration sensing (Klärner and Barth, 1982). Resting positions are typically used when the spider is sensing externally generated vibrations—in this configuration, the tibia-metatarsus angle is small (<120°), and the sensitivity of the organs is maximized. When the spider is walking, the legs are extended through much of the stepping cycle, reducing the sensitivity of the lyriform organs (Blickhan and Barth, 1985). Therefore, the spider maximizes lyriform organ sensitivity in contexts

where they are most likely to show predatory behaviour in response to vibrations. During locomotion, other functions are prioritized, where lyriform organs may serve more of a proprioceptive function (Barth, 2002a).

4 Discussion

So far, this review has covered the mechanisms governing vibration transmission using orb-weaving spiders as examples of animals that influence transmission both within the environment and the body. We have demonstrated that a wide range of morphological and behavioural traits influence vibration transmission via their effects on masses, springs, dampers, and geometry, which interact together to govern vibrational motion. We have also shown that these traits have considerable variation at different levels. How can we understand this variation to uncover the constraints acting on this sensory mode and the evolutionary drivers? Here we discuss the roles that constraints and control have in shaping this trait variation across different time scales and taxonomic levels, and the implications for vibration sensing. Through this discussion, we hypothesize a role for morphological computation in shaping vibration transmission, which can be tested for in future studies and applied within bioinspired engineering.

Firstly, we see that constraints of different types are acting on the morphological traits. The first type is physical constraints—the action of damping, filtering or distortion caused by the physics underlying the dynamics of vibration transmission. Physical constraints are governed by the geometry and properties of masses, springs, and dampers, and act to filter and dampen vibrational information, exemplified by the effects of the spider's body properties and geometry on vibration transmission both in the web and through the body. These physical constraints ultimately influence propagation distance, the transmission quality of different frequencies, and the ability of the spider to filter information from noise (Mortimer, 2017). The second type is evolutionary trade-offs, given that the web and spider bodies are multifunctional, their morphologies are important not only for vibration transmission, but also other biological functions. For example, web geometry, tension, stiffness, and supercontraction affect

both the function of the orb web to capture prey, as well as vibration transmission (Mortimer et al., 2016). Also, the spring and damper properties of spider leg joints are important for locomotion, as well as vibration sensing (Blickhan and Barth, 1985). The third type of constraint is developmental constraints, where the development of the spider's morphological traits determines their geometry and properties, such as the effects of spider age or leg regeneration. For example, vibration transmission through the body and sensory transduction are affected over the course of development by the different growing rates of the metatarsal lyriform organs and associated metatarsal pads (Morley et al., 2016). These constraints do not act equally on morphological traits; some are more prone to one type of constraint than another.

The constraints do not solely act to limit or fix variation in morphological traits; we found examples of the constraints leading to non-functional variation and even constraints being harnessed for functional uses. For example, some morphological features such as leg length affect vibration transmission, but are relatively fixed within an individual due to development constraints (except over development and regeneration). In terms of non-functional variation, some morphological features will vary, but their variation may not be functionally useful for vibration sensing, such as masses in the web. As we have seen, masses have significant effects on vibration transmission due to the strong influence of mechanical impedance, a physical constraint. There are also a few examples of where apparent physical constraints cause variation that may be harnessed for functional uses in the web. For example, although the spider body mass affects vibration transmission via mechanical impedance, this accentuates orientation cues in the web, which spiders may use to locate prey (Mortimer et al., 2019). As a final thought, few of the morphological traits we have reviewed appear to be free from any form of constraint, with the possible exception of mechanosensor placement. The sheer number of sensors and their wide distribution across spider bodies suggests that evolution was able to come up with this solution repeatedly for functional uses, resulting in apparent redundancy in the system. Investigation of sensor placement differences and functionality across different species that differ in their ecology will be able to solve this mystery.

Even where constraints may be acting on morphology, there are different control mechanisms that can mitigate constraints to maintain functionality for vibration sensing. We can infer a control mechanism is in place when a trait shows variation that is functionally useful, but species comparisons and behavioural studies would provide direct evidence. Control mechanisms can be at the individual level due to plasticity that acts at small time scales to shape trait variation. However, they can also be due to evolution acting over longer timescales driving species differences through niche adaptation. We see that individual spiders are unable to directly control leg and body morphology to mitigate constraints, as these are generally fixed following development. This means that an individual's vibration transmission system must be robust to variation, which may explain the number of sensors and redundancy in the system. However, spiders can directly control web morphological traits as they have silks with an impressive range of properties, which is functionally useful to the spider. Silk property variation can control the spring and dampers of their extended phenotype at short timescales in response to changing conditions (Mortimer et al., 2014). We also see evidence for control of constraints via niche adaptation in different spider species as certain morphological traits correlate with particular hunting strategies. However, data on the functionality of specific differences between species in body morphology for vibration sensing is lacking. How different species morphologies influence inherent trade-offs, as well as physical and developmental constraints, requires further study. An interdisciplinary approach utilizing modelling (informed through experimental determination of relevant biomechanical parameters) and behavioural trials would be a promising line of research. In combination, we note that spider morphology does not vary as much between species as other terrestrial arthropods, where morphological diversity is more common in silk-use than overall body plan (Vollrath, 1999).

Behaviour is an important mechanism controlling morphology. The constraints and control mechanisms above do not apply in the same way to behavioural traits, which in its nature can be more variable, with plasticity at the individual level and niche adaptation at the species level. At the individual level, we see examples of using

behaviour to mitigate physical constraints by removing masses on the web (Cloudsley-Thompson, 1995), controlling web properties and geometry (Watanabe, 2000; Mortimer et al., 2016), as well as dictating spider position and posture on the web (Mhatre et al., 2018; Mortimer et al., 2018). We also see evidence of using behaviour to shape trade-offs between different functions, for example adjusting web geometry in response to changing environmental conditions to shape mechanical verses sensory functions (Vollrath et al., 1997). These behavioural control mechanisms are extremely useful as they effectively harness the multifunctionality of morphological traits that underlie the trade-off, to enable the spider to deal with variable conditions by changing a multifunctional trait (Vollrath, 1999). Whether behaviour can be used to mitigate developmental constraints (such as lyriform organ/pad mismatch) is a current research gap, but could be explored by investigating behaviours that juvenile spiders might use to avoid the problem of filtering low-frequency environmental noise.

The high level of involvement that morphology has in vibration transmission suggests a role for morphological computation, where morphology acts to perform useful tasks within a system (Muller and Hoffmann, 2017). Morphological computation is uniquely applicable to our spider context as vibrational information propagates through both the web and body morphology before reaching embedded mechanosensors. In this context, you can see how morphology, or behaviour via its action on morphology, could act on vibrational information during propagation to filter and transform vibrational waves, which could be used in theory to promote information transfer. Using morphological computation, the filtering of information from noise is not handled solely by the nervous system, but by the masses, springs/dampers, and geometry of the web/body morphology, with each of these parameters potentially being tuned to transform the input wave differently under varying conditions. We might expect morphological computation to be selected for in terrestrial arthropods as it is in theory an efficient way, in terms of computational cost and potentially energetic cost, to promote information transfer. This is because complex computational tasks that would usually be performed by the CNS are replaced with relatively simple and potentially passive responses that are governed by a system's morphology (Muller and Hoffmann, 2017).

This reduces computational cost as the animal, in theory, can compute more quickly, as CNS processing takes time, but it also reduces the complexity and number of connections required in the nervous system (Pfeifer and Bongard, 2006). It can potentially increase energetic efficiency as the computational tasks could involve passive responses of morphology rather than active metabolic processes in the CNS (Muller and Hoffmann, 2017).

Since morphological computation would be influenced by both morphological and behavioural traits, control of these traits can be selected for in vibration-sensing animals to influence vibration transmission via filtering input waves. Individual plasticity in these traits is likely to influence vibration information transfer through morphological computation. Whether morphology is controlled by an individual to functionally influence vibration transmission through the body warrants further research, but we can make predictions for how control via morphological computation would work in natural contexts. Possible examples of plasticity in spider morphological traits include the shape of the lyriform organs throughout development and after regeneration. If morphological variation here is functional for vibration information transfer, we would predict lyriform organ shape to transform input waves to compensate for leg length changes before sensory transduction occurs, thus avoiding the need for extra processing in the CNS. In this example, both leg length and lyriform organ shape are morphological traits influencing vibration transmission, as these traits alter the mass and material property distribution of the spider's leg (aspects of mass, springs/dampers, and geometry). Spider behavioural traits potentially involved in morphological computation include posture changes and modifying web geometry, which could be used to functionally influence vibration transmission. If the web uses morphological computation, we would predict that spiders use behaviour to modify web properties in response to environmental factors to alter the vibrational information that arrives at the spider, thus avoiding the need for extra processing in the CNS as environment changes. In this example, spider web building is a behavioural trait influencing web geometry as a morphological trait. The geometry of the web in turn influences vibration transmission, as this governs mass and material property distribution of the spider's web (aspects of mass,

springs/dampers, and geometry). Web-building spiders are special in this case; since they control their vibratory environment, they can mitigate the physical constraints faced by many other organisms that are limited by the transmission properties of the substrate upon which they live. This again highlights how web-building spiders are an ideal model organism for studying vibration information transfer, since they have control over morphology in both their vibration transmission platform and their body.

Using spiders as inspiration, these control mechanisms could have direct applications for developing new, bioinspired technologies that use substrate-borne vibrations for information (Lipson, 2014; Barth, 2019)—for example soft robots for search-and-rescue applications (Hawkes et al., 2017). Designing robots to cope with unknown environments in real-time is a challenge for engineers, as environmental variability can pose problems for artificial systems (Hauser et al., 2011). Sensing here is key, where substrate-borne vibrations can be used to monitor the internal and external environment to respond appropriately in real-time to environmental variability to maintain functionality. Morphological computation is an efficient way to solve these problems for artificial systems as computational tasks can be outsourced to the system's morphology, which reduces power requirements. If the insights of how animals, such as spiders, achieve this can be applied to robotic design, it can open up new applications for robots that are adaptable to changing environments. A spider-inspired soft robot would use morphological computation to increase not only efficiency and adaptability, but also damage tolerance, for example using "smart" structures to detect and compensate for damage to part of its body (Hauser et al., 2014). To reach this stage, it is necessary to fill the current research gap in our fundamental understanding of how an eight-legged spider-shaped morphology transmits vibrations. What are the most important biomechanical parameters influencing wave transmission? Is there any evidence for morphological computation significantly reducing processing cost in the CNS? Is the system robust enough for morphological computation to still be effective in the face of variation in morphology over time, and could an individual spider exploit this? How does this process vary in different species, with different life strategies and

different morphologies? Mathematical modelling of the whole-body system, combined with experimental manipulations of the animal systems, may provide the answer.

Further research is likely to show that morphological computation in nature is far more widespread than has previously been recognized. We suggest that evolution has produced an array of sensory solutions to problems faced by engineers, and that continued research into understanding the mechanisms that natural systems use to promote information transfer will lead to new types of technologies for varied applications.

Author Contributions

T.E.M.: conceptualization, investigation, methodology, writing – original draft, writing – review and editing. B.M.: conceptualization, funding acquisition, methodology, project administration, supervision, writing – review and editing.

All authors contributed to the article and approved the submitted version.

Conflict of Interest

The authors declare that the research was conducted in the absence of any commercial or financial relationships that could be construed as a potential conflict of interest.

Funding

This work was supported by the Royal Society University Research Fellowship to BM (URF\R1\191033).

Acknowledgments

We thank the Royal Society for funding. We thank Tom Mulder for discussions on spider biotremology and also for his comments on the manuscript.

Chapter 2

Slit sense organ distribution on the legs of two species of orb-weaving spider (Araneae: Araneidae)

Thomas E. Miller[1], Graham K. Taylor[1] and Beth Mortimer[1]

Adapted from:

Miller, T. E., et al. (2022). "Slit sense organ distribution on the legs of two species of orb-weaving spider (Araneae: Araneidae)." Arthropod Structure & Development 67.

Abstract

Biotic and abiotic mechanical stimuli are ubiquitous in the environment, and are a widely used source of sensory information in arthropods. Spiders sense mechanical stimuli using hundreds of slit sense organs (small isolated slits, large isolated slits, groups of slits and lyriform organs) distributed across their bodies and appendages. These slit sense organs are embedded in the exoskeleton and detect cuticular strain. Therefore, the spatial pattern of these sensors can give clues into how mechanical stimuli from different sources might be processed and filtered as they are transmitted through the body. Here, we map the distribution of slit sense organs on the legs in two species of orb-weaving spider, *Araneus diadematus* and *Trichonephila edulis*, in which slit sense organ distribution has not previously been investigated. We image the spiders' legs using scanning electron microscopy, and trace the position and orientation of slits on these images to describe the distribution and external morphology of the slit sense organs. We show that both species have a similar distribution of slit sense organs, with small isolated slits occurring in consistent lines parallel to the long axis of the legs, whilst large isolated slits, groups of slits and lyriform organs appear in fixed positions near the leg joints. Our findings support what has been described in the literature for several other species of spider, which indicates that slit organ arrangement is conserved across spiders in different evolutionary lineages and with disparate hunting strategies. The dispersed distribution of small isolated slits along the whole length of the leg may be used to detect large-scale strain of the leg segment as a result of muscle activity or internal changes in haemolymph pressure.

1 Introduction

Arthropods possess a wide range of internal and external sensory structures that enable them to detect biotic and abiotic sources of information in their environment. Mechanosensation in arthropods often involves detecting cuticular strains caused by internally or externally applied forces. The resulting strains range in type from transient slow strains, to high frequency vibrational waves. The latter are key for spiders, which are an excellent model system for studying vibration sensing (Barth, 2002; Mortimer, 2019). Spiders sense vibrations through materials such as silk, the surface of water, plant stems, soil and rocks, and in many species this is the dominant sensory modality (Hebets, 2008). They use substrate-borne vibrations as an information source for prey and predator detection (Klärner and Barth, 1982; Masters, 1984; Landolfa and Barth, 1996; Mortimer et al., 2018) and courtship (Schüch and Barth, 1985, 1990; Elias et al., 2003, 2005). Mechanical stimuli are also used for proprioception (Seyfarth, 1978; Seyfarth et al., 1985).

The sensory structures that are involved in mechanosensing in spiders include mechanosensory setae (hairs attached to the cuticle) and slit sense organs (Pringle, 1955). Slit sense organs, the focus of this study, are embedded sensors that consist of a slit in the cuticle surrounded by a smooth raised border (Figure 1). Each slit is innervated by two dendrites – one ending at the outer slit membrane and a second close to the inner membrane (Molina et al., 2009). An action potential is generated as a result of cuticle strain, typically compression perpendicular to the long axis of the slit, which bends the membrane (Barth, 1972a, b). The mechanical sensitivity of the slits is high, with compression of only 2.5 nm sufficient to generate an action potential in *Cupiennius salei* (Barth and Geethabali, 1982). Cuticle strain can be induced both by externally generated vibrations that are transmitted from an environmental substrate into the body of the spider, or can be internally generated by muscle contraction and changes in haemolymph pressure (Seyfarth et al., 1985; Blickhan and Barth, 1985).

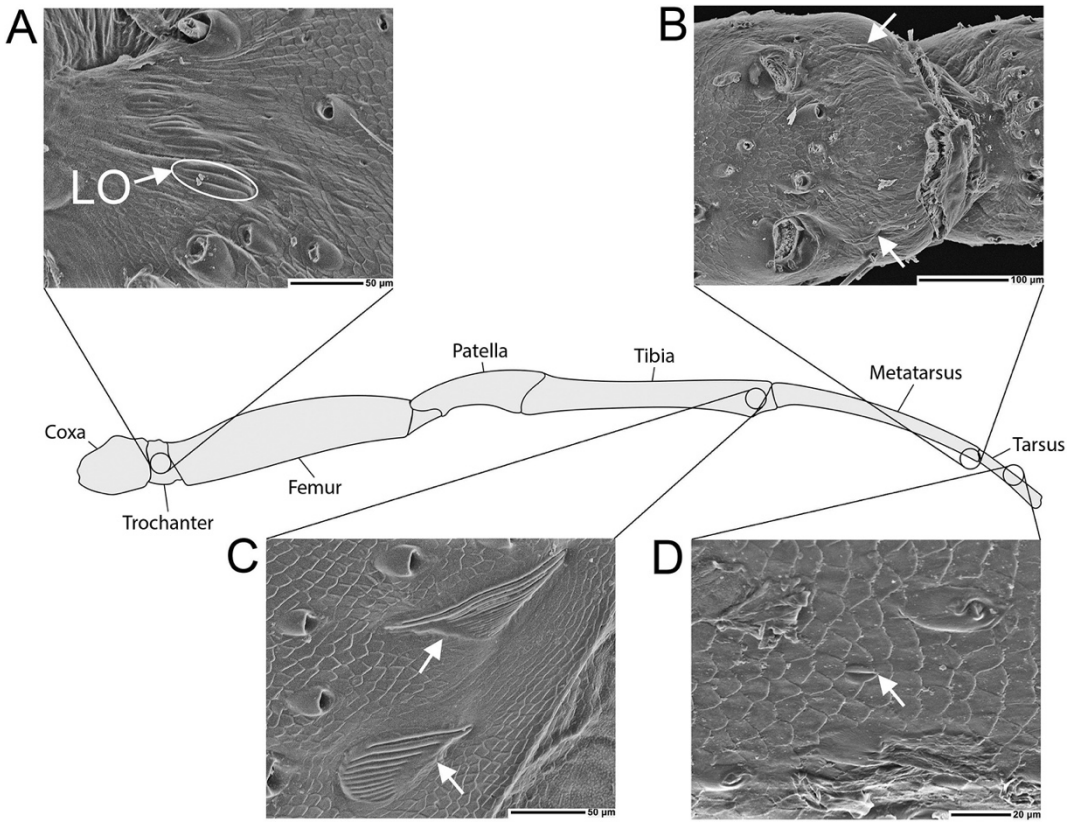


Figure 1. Types of slit sense organ found on spider walking legs, illustrated on leg 1 of *Araneus diadematus.* A – group of slits (on the posterior side of the trochanter, also containing a lyriform organ (LO) consisting of two slits in the middle). B – two large isolated slits (>30 µm; on the ventral side of the distal end of metatarsus, arrows). C – two lyriform organs (on the lateral side of the distal end of the tibia, arrows). D – small isolated slit (<30 µm; on dorsal side of the tarsus, arrow).

Slit sense organs are widely distributed on the walking legs, pedipalps, chelicerae, prosoma, opisthosoma and spinnerets, indicating that cuticle strain is an important source of information across the whole body of the spider. Slits can be arranged singly, in loose groups, or as discrete arrays of two or more slits known as lyriform organs. Lyriform organs are up to two orders of magnitude more sensitive than the single slits (Speck and Barth, 1982) and are thought to be particularly important for the detection of externally generated vibrations. The HS10 lyriform organ, defined by its location at the distal end of the metatarsus, is thought to be particularly involved in vibration sensing, because it detects dorsal-ventral movement of the tarsus via a pad at the joint

which acts as a high-pass filter (McConney et al., 2007; Schaber et al., 2012; Morley et al., 2016). It has been identified in most species of spiders previously described in the literature (see 4. Discussion). Isolated slits are extremely numerous in some species (around 1500 in *C. salei*) and are found on all body segments (Barth and Libera, 1970; Barth, 2002). Lyriform organs, on the other hand, tend to be located in fixed positions close to the joints of the walking legs, chelicerae and spinnerets (Patil et al., 2006; Barth, 2019; Seo et al., 2020). Cuticular strain is predicted to be higher in these areas, leading to maximal slit strain and hence detectability of motion (Blickhan and Barth, 1985). Strain is influenced by the mass distribution, body and leg geometry, and cuticle stiffness of the spider (Miller and Mortimer, 2020). These different aspects of morphology vary between and within species, and could therefore be expected to result in interspecific differences in slit sense organ distribution across the legs and body of the spider.

Most research has focused on the structure and morphology of individual slit sense organs in model species such as *C. salei* (Barth, 2019), but as the whole body of the spider is used as a transmission platform for vibrational information, and as different frequencies of vibration are represented more strongly at different points on the body (Mhatre et al., 2018), their overall distribution along this transmission pathway is likely to be key for vibration sensing as well as sensing other mechanical stimuli (Miller and Mortimer, 2020). It is therefore surprising that relatively few spider species have had the distribution of their slit sense organs mapped – these species are *C. salei* (Barth and Libera, 1970), *Argiope bruennichi* (Ganske and Uhl, 2018), *Larinioides sclopetarius* (Vogel, 1923), *Trichonephila clavata* (Seo et al., 2020) and *Comaroma simonii* (Kropf, 1998). In these select species, most of the single slits are arranged along lines parallel to the long axis of the leg, with the exception of the dwarf species *C. simonii*, which has a reduced number of rather sporadically distributed slits (Kropf, 1998). Aside from these studies, most other research has focused solely on the lyriform organs rather than including the single slits (Seo et al., 2020). However, single slits may still be important in sensing externally generated vibrations, as spiders are still able to orient towards a vibration source (albeit with reduced accuracy) after ablation of the lyriform organs (Seyfarth, 1978; Seyfarth et al., 1982). The wealth of other slit sense organs found across

the spider is therefore a comparatively overlooked, and potentially important, method to sense mechanosensory information for the animal.

The types of mechanosensory inputs relevant for different spider taxa likely depend on their hunting strategy and mode of life. Orb-weavers, for instance, utilise silk webs to snare their prey rather than hunting on leaves like *C. salei*, and hence differ in the substrate materials through which vibrations are transmitted. Because of this, orb-weavers and sit-and-wait hunters experience different cues from prey (e.g. flying insects struggling on a web versus footsteps on leaves and branches) and internally generated cuticular strains (e.g. because of differences in posture and activity levels). But is this reflected in the distribution of their slit sense organs, or are arrangements conserved despite these ecological and behavioural differences? It is difficult to probe these questions currently, owing to the low number of species examined to date, so mapping the distribution of slit sense organs in species other than the well-studied *C. salei* is of value in enabling further comparative study.

In this paper, we examine the number, distribution, external structure, and intraspecific variation of single slits, groups of slits, and lyriform organs on the walking legs of the females of two species of orb-weaving spider, *Araneus diadematus* and *Trichonephila edulis*. Both species are in the family Araneidae (comprising orb-weaving spiders) but are placed in two different subfamilies (Scharff et al., 2020), with Nephilinae being a more basal clade. Therefore, comparison between A*. diadematus* and *T. edulis* is of value as it allows comparison across these two lineages within Araneidae.

As well as their divergent evolutionary history, *A. diadematus* and T*. edulis* differ in their web structure and body morphology. Both *Araneus* and *Trichonephila* produce a planar web with an oval capture spiral to snare flying insects, and sense vibrations from struggling prey by resting their walking legs on the radial threads. However, members of Nephilinae, including *Trichonephila*, retain the non-sticky spiral scaffold in their completed webs, in contrast to *A. diadematus* (Hormiga et al., 1995). In addition, T. edulis webs differ from *A. diadematus* in containing debris lines, often being constructed

at oblique angles and frequently connected to webs built by smaller individuals. In terms of body morphology, *Trichonephila* is larger than *Araneus* and has a significantly different body plan, with much longer and proportionally thinner legs (Figure 2). These factors combined indicate that the type of mechanical stimuli experienced by A*. diadematus* and T*. edulis* on their webs may well differ, despite sharing the same basic hunting strategy.

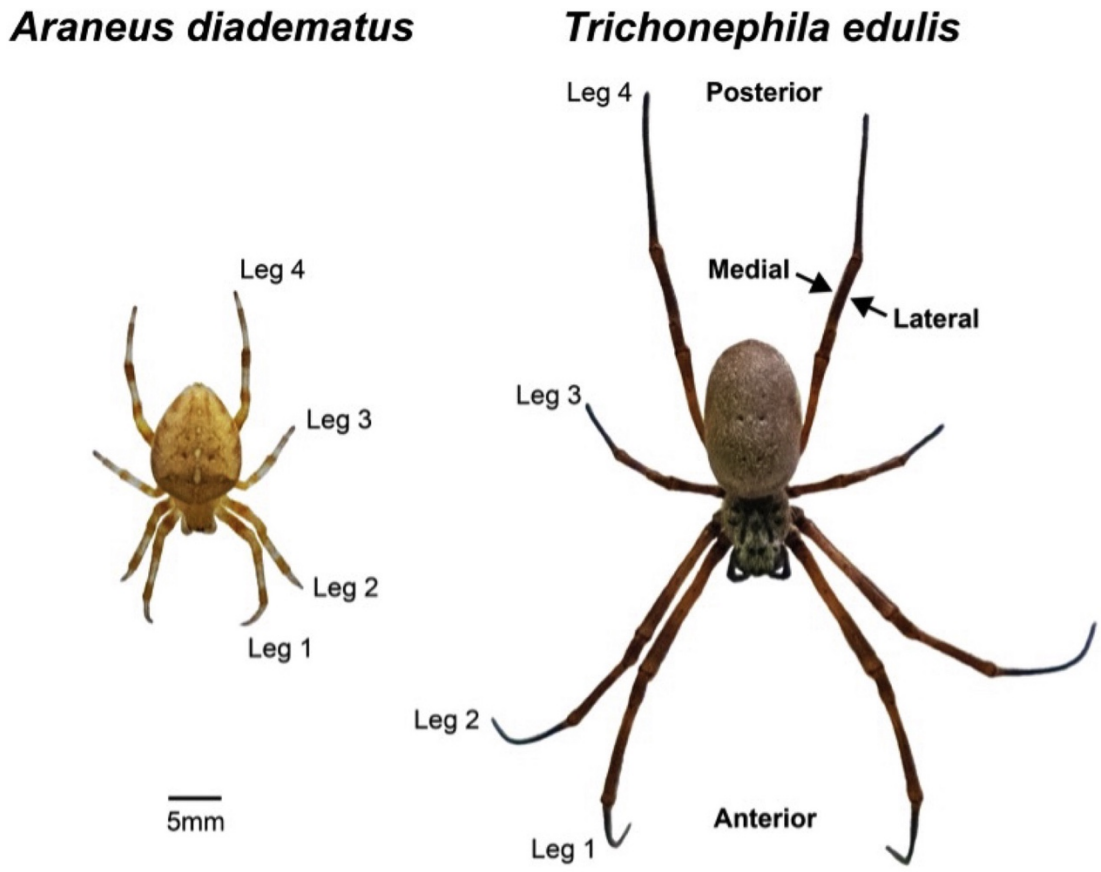


Figure 2. Comparison of the morphology of adult female *Araneus diadematus* and *Trichonephila edulis*, with an explanation of positional terms used in Section 3 Results.

We produce comprehensive slit organ distribution maps and describe the external morphology of the individual slit organs in both species. Females were chosen for the comparison as in both species they exclusively construct orb webs, whereas males tend to wander or, in the case of *Trichonephila*, occupy the orb webs of females in order to steal prey (Liebsch et al., 2020).

2 Methods

2.1 Studied species

A. diadematus were collected from the wild in Oxfordshire, UK in 2020, kept in Perspex frames measuring 30 cm × 30 cm × 5 cm and separated by greased Perspex sheets to prevent webs being attached to the sides. The spiders were fed with live *Drosophila melanogaster* and *Calliphora vomitoria* and sprayed with water twice per week. *T. edulis* were taken from a captive population that is maintained in a temperature-controlled room (20 °C ± 5 °C) with an accompanying fly population. The spiders were sprayed with water twice per week and allowed to feed ad libitum on *D. melanogaster* and *C. vomitoria*.

2.2 Specimen preparation

Adult female specimens of both species were anaesthetised using ethyl acetate vapours. Specimens were then preserved in 70% ethanol solution before being transferred to a 95% ethanol solution to further dehydrate them.

The right-hand side legs were removed from the specimens and air dried before being shaved of all setae and trichobothria using a mounted pin and scalpels under a stereomicroscope, in order to prevent these structures from obscuring the slit sense organs beneath them. The legs were divided into 3 or 4 sections in *Araneus* and 4 or 7 sections in *Trichonephila* using scalpels. Where possible the legs were divided at the natural split between segments – if this was not possible, a single incision was made in the middle of the segment. It is possible, although unlikely, that these incisions may have led to the loss of a very low number of small isolated slits which happened to coincide with the incision pathway. The sections were then mounted along their long axis by gluing the ends of the leg sections onto a pin using cyanoacrylate. The specimens were sputter coated with gold-palladium for 150 s at 18 mA using an Emitech SC7620 sputter coater. The pins were mounted on a rotating specimen holder using conductive

tape, such that the long axis of the leg segment was oriented perpendicularly to the imaging beam. Each leg segment was imaged using a scanning electron microscope (SEM; Neoscope JCM-5000) at 0, 90, 180 and 270° angles of rotation around the long axis of the leg, in order to image the dorsal, medial, ventral and lateral sides of the leg segment. This enabled us to image the entire surface of each leg specimen, which would have been impossible using a conventional stub-mounted setup.

2.3 Image mapping

The SEM images were combined using Adobe Photoshop and digitally traced to mark out the position of the slit sense organs. Visual inspection of slit length revealed a bimodal distribution and hence we follow Barth and Libera (1970) and Barth and Stagl (1976) in classifying the isolated slits into small isolated slits and large isolated slits, which also have subtly different morphologies.

Slit sense organ categories, adapted from Barth and Stagl (1976). Examples of each of these categories are shown in (Figure 1):

1. Small isolated slits (Figure 1:D).
2. Large isolated slits, with diffuse border (Figure 1:B).
3. Groups of slits comprising 2 or more slits less than 100 µm away from each other (Figure 1:A).
4. Lyriform organs consisting of 2 or more slits in an approximately parallel arrangement with a distinct border (Figure 1:C).

A full map of the right-hand legs was produced for a single individual of *Araneus* and *Trichonephila*. We manually counted the number of each category of slit sense organ on each leg. Using a method where incisions were made in the centre of some leg segments could have led to a slight underestimation of the total number of slits (see above), but would not have affected the distribution of slits elsewhere on the legs. We did not duplicate the count of any slits that appeared on more than one map from different

angles. On the maps in Figures 3-6 and Appendix 1 – Supplementary figures 1-10, individual slits will be shown from more than one angle and hence appear on more than one map. In Figures 3-6 and Appendix 1 – Supplementary figures 1-10, individual slit sense organs are shown in their accurate positions, traced from the SEM images, but are enlarged so that they are visible on a figure of the whole leg. The outlines of the legs correspond to the shape of the leg segments on the SEM images that the figures were traced from.

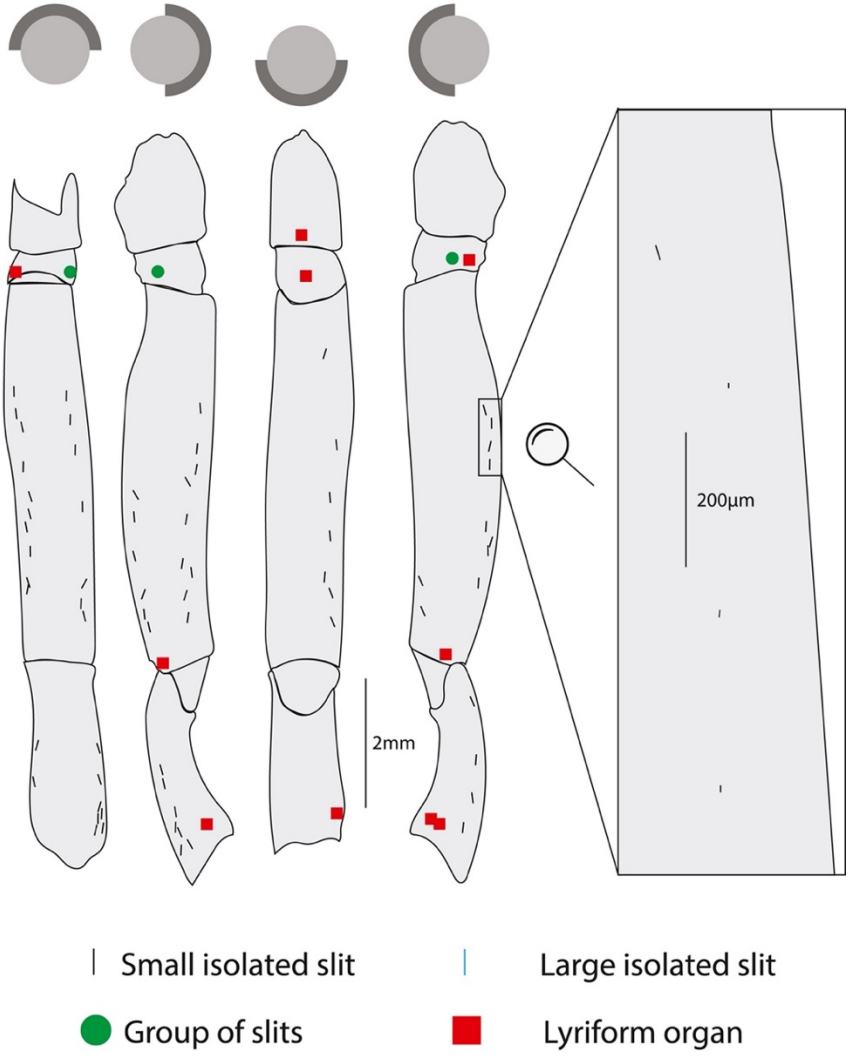


Figure 3. Schematic map of upper portion of Leg 1 of *Araneus diadematus*. From left to right – dorsal, prolateral, ventral and retrolateral view. The small isolated slits are enlarged to increase legibility and show orientation – an indication closer to their true

size is given in the magnified view on the right (with small inaccuracies due to pixel sizes on SEM images).

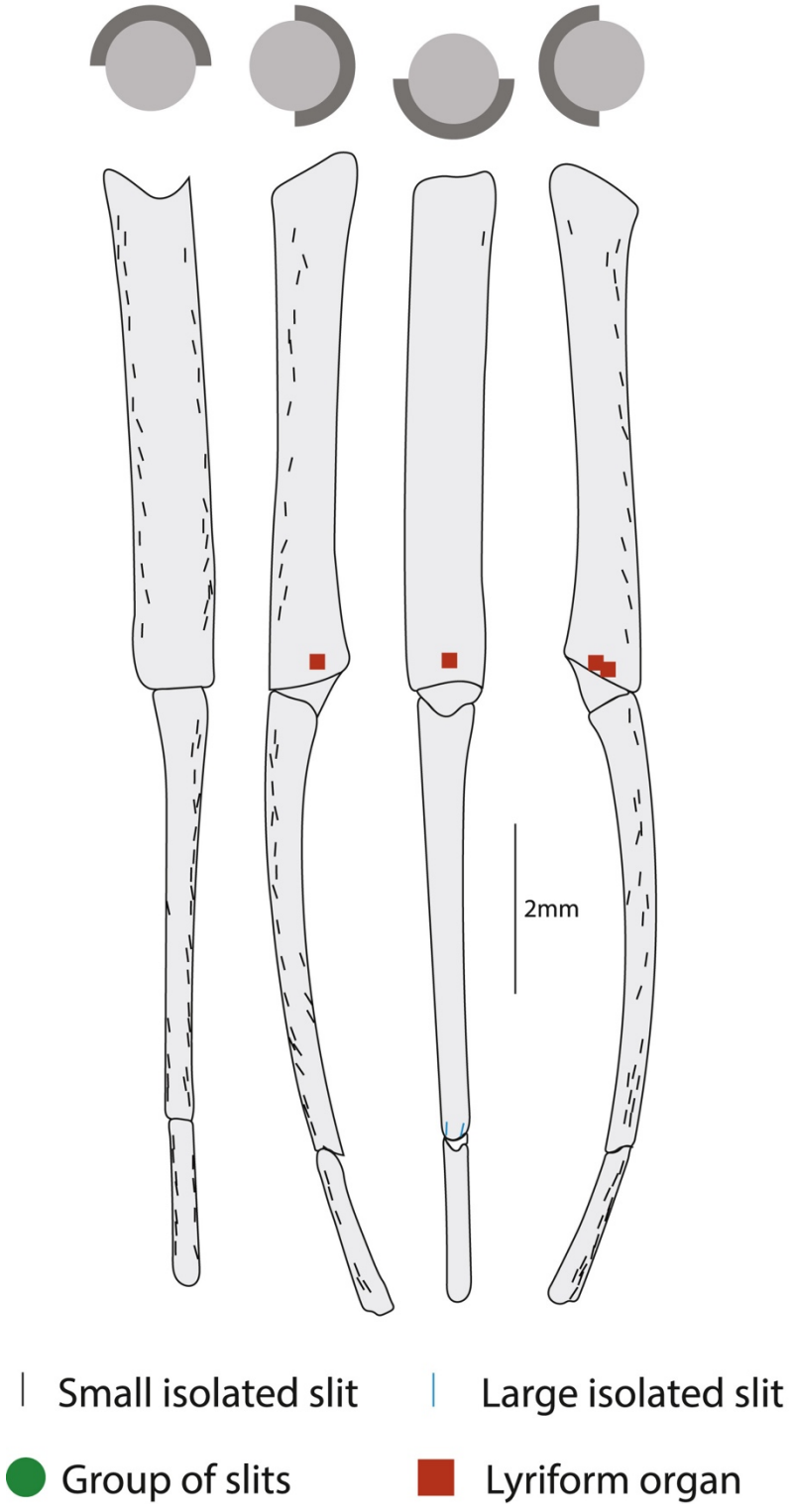


Figure 4. Schematic map of lower portion of Leg 1 of *Araneus diadematus*. From left to right – dorsal, prolateral, ventral and retrolateral view.

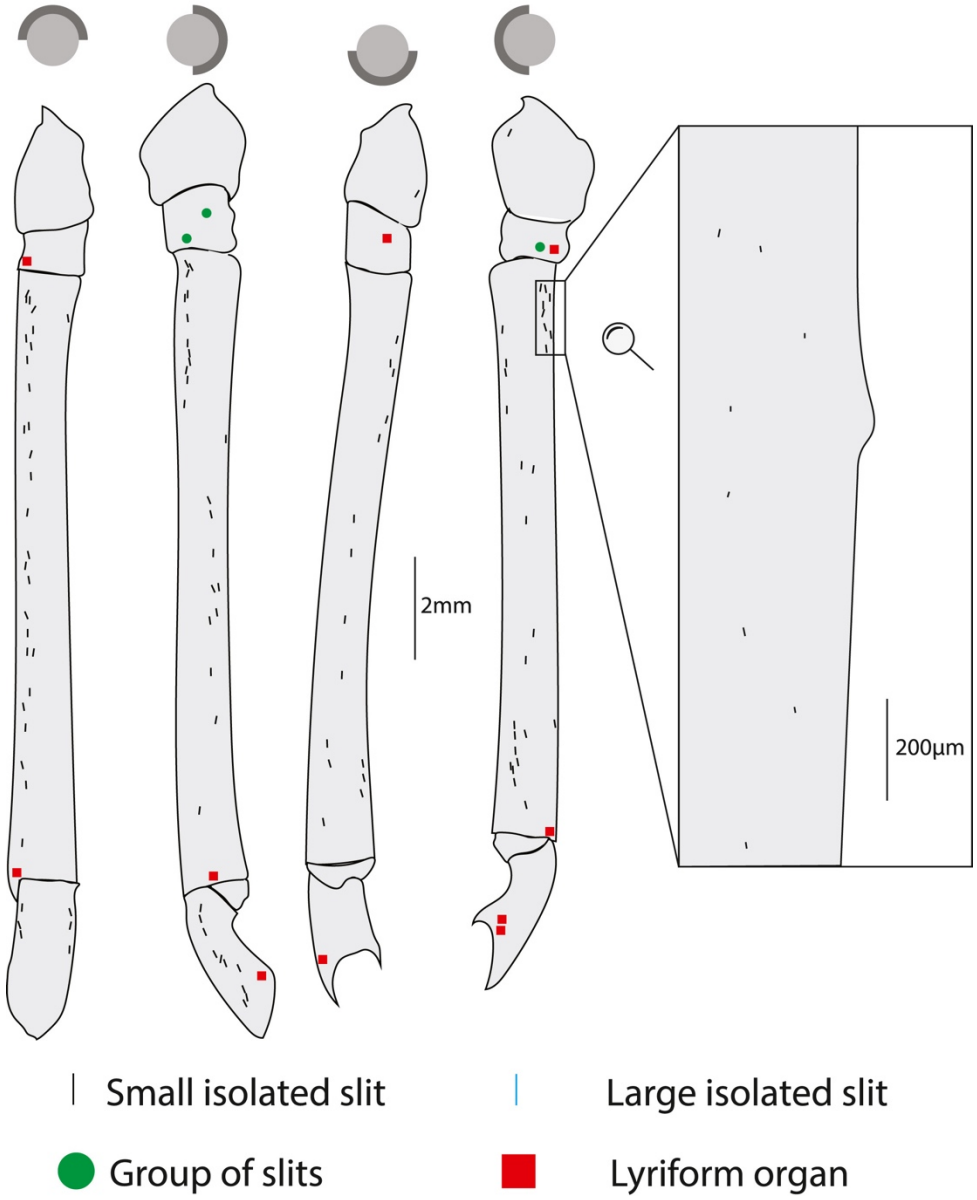


Figure 5. Schematic map of upper portion of Leg 1 of *Trichonephila edulis*. From left to right – dorsal, prolateral, ventral and retrolateral view. The small isolated slits are enlarged to increase legibility and show orientation – an indication closer to their true size is given in the magnified view on the right (with small inaccuracies due to pixel sizes on SEM images).

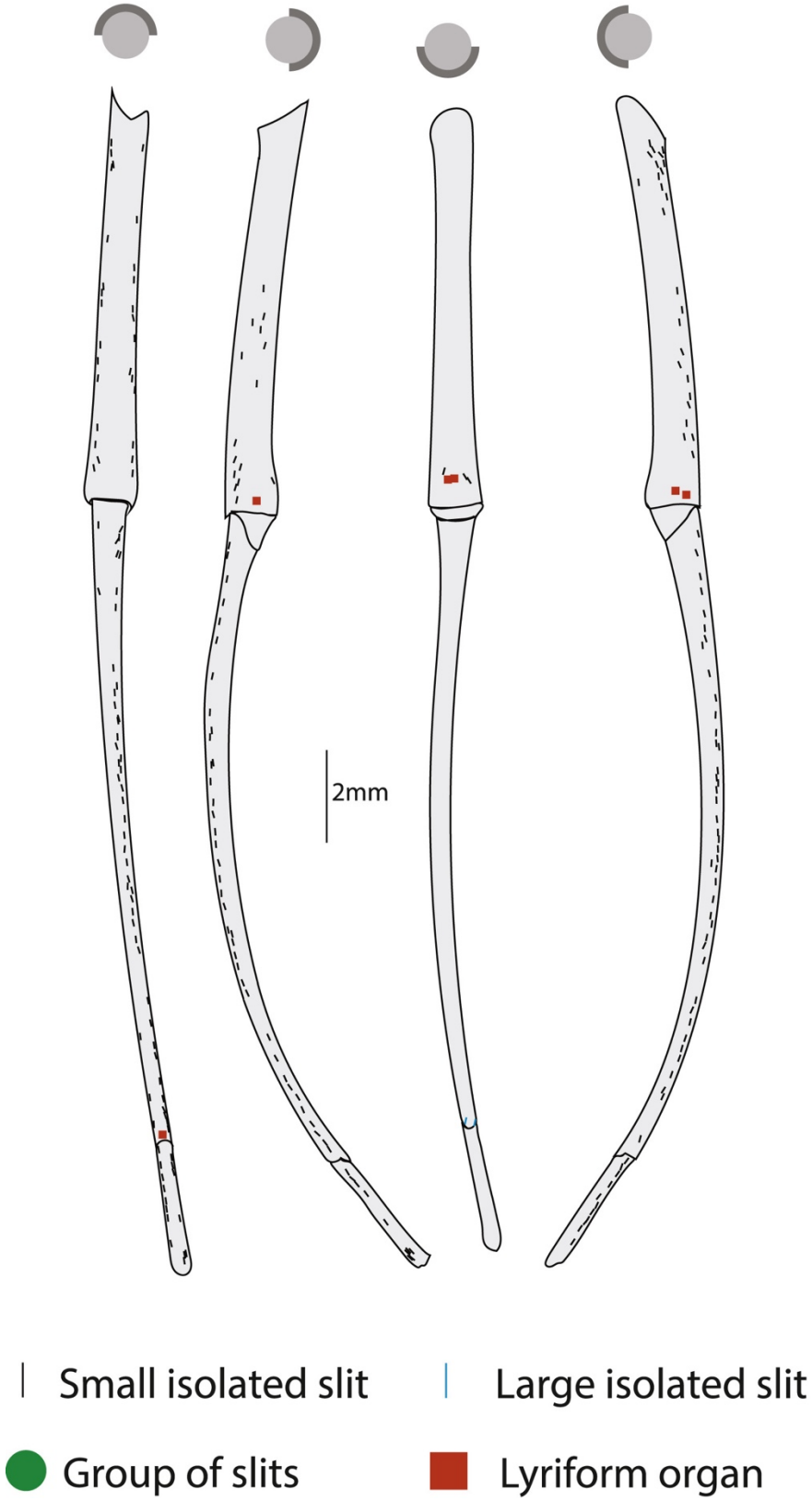

2mm
Small isolated slit
Large isolated slit
Group of slits
Lyriform organ

Figure 6. Schematic map of lower portion of Leg 1 of *Trichonephila edulis*. From left to right – dorsal, prolateral, ventral and retrolateral view.

Visual comparison with two other specimens of each species was used to verify that the overall arrangement of slit sense organs (in terms of lines of single slits, and position of large slits, groups of slits and lyriform organs) was the same between individuals. To quantify the extent of intra-specific variation, we used full maps for a single leg segment (the metatarsus) of the third leg on the other two individuals of each species to provide the number of small isolated slits (in each of the medial and lateral lines), large isolated slits, groups of slits, extra slits and lyriform organs described in Table 2.

Cephalothorax width was measured by placing the spiders on a grid. Leg length was measured by summing the length of each leg segment from Figure 3, Figure 4, Figure 5, Figure 6 and Appendix 1 – Supplementary figures 1-10 with reference to the SEM scale bars in order to obtain the total leg length when fully straightened.

3 Results

3.1 Small isolated slits

3.1.1 Morphology of small isolated slits

The external morphologies of the small isolated slits in *A. diadematus* and *T. edulis* are similar, consisting of a slit in the cuticle bordered by a raised “lip” on either side (Figure 1). Nevertheless, whereas slit morphology is quite uniform in *A. diadematus*, there is more variation in *T. edulis*, with morphologies ranging from long thin slits to sensilla with concave depressions around the slits.

Table 1. Total number of small isolated slits on the walking legs of *Araneus diadematus* and *Trichonephila edulis*.

Leg	*Araneus diadematus*		*Trichonephila edulis*	
	Leg length (mm)	Number of slits	Leg length (mm)	Number of slits
1	24.2	147	46.0	255
2	21.4	145	50.4	225
3	14.6	91	24.6	113
4	20.4	137	40.8	170
Total		520		763

3.1.2. Number of small isolated slits

The total number of small isolated slits recorded in our full map of one *A. diadematus* specimen is 520 compared with 763 in our map of T*. edulis* (Table 1), which corresponds with the larger body size of *T. edulis*. The numbers of slits on each leg ranks with the leg length for *A. diadematus*, whilst in *T. edulis* leg 2 has fewer slits despite being longer than leg 1. In particular, the short third leg of both species has far fewer slit organs (Table 1).

Table 2. Number and distribution of small isolated slits (medial line, lateral line and extra slits situated away from the main lines of slits), large isolated slits, groups of slits and lyriform organs on the metatarsus of the third leg of three specimens of *Araneus diadematus* and *Trichonephila edulis*.

Species	No.	Cephalothorax width (mm)	Medial line	Lateral line	Extra slits	Large slits	Groups of slits	Lyriform organs
A. diadematus	1	5	10	7	2	2	0	1
	2	4.3	9	4	0	2	0	1
	3	4.6	13	8	0	2	0	1
T. edulis	1	5.8	12	16	0	2	0	1
	2	6.2	24	22	0	2	0	1
	3	7.4	24	33	2	2	0	1

3.1.3 Distribution of small isolated slits

Small isolated slits are widely distributed across the leg segments of both *A. diadematus* and *T. edulis* with the exception of the coxa, which only has a few sparse slits in both species. Most of the small isolated slits are arranged in lines parallel to the long axis of the leg. On the tarsus, metatarsus, tibia and patella, the slits are arranged in two lines on the dorso-medial and dorso-lateral sides of the leg segment. The femur of both species has a different arrangement to the rest of the leg. In *A. diadematus*, there are 4 lines of slit sensilla in legs 1–3 and 3 lines on leg 4. In *T. edulis*, there are 4 lines of slit sensilla on the femur in all 4 legs (Figure 3, Figure 4, Figure 5, Figure 6 and Appendix 1 – Supplementary figures 1–10).

There are also a few slits located away from the main lines, which are referred to in Table 2 as “Extra slits”. We were unable to identify any consistent pattern in the location of these slits and they were low in number.

3.1.4 Intraspecific variation in distribution of small isolated slits

Individuals of both species vary in the number and exact position of the small isolated slits (Table 2) although the overall distribution (in terms of the number and position of the lines of slits and discrete groups) is the same in all individuals (Figure 3, Figure 4, Figure 5, Figure 6 and Appendix 1 – Supplementary figures 1-10). Individuals vary in the number of slits per line and also the number of random extra slits situated away from the main lines. The total number of slits per line correlates approximately with body size, here approximated using cephalothorax width, e.g. after Olive (1980).

3.2 Large isolated slits

In contrast to the small isolated slits, the large isolated slits are far fewer in number and occur in fixed positions that do not vary between individuals. Two large slits, one anterior, one posterior, are present on the underside of the distal end of the metatarsus, opposite the HS10 lyriform organs. The anterior slit is located slightly closer to the prosoma than the posterior slit. There are also large slits on the coxa of legs 2 and 3 in *A. diadematus*, but not *T. edulis*.

3.3 Groups of slits

Groups of slits are located in fixed positions on the medial and lateral sides of the trochanter extending towards the body from a protrusion of cuticle. Each group consists of up to 10 slits less than 100 µm apart. The whole group is typically no more than 200 µm across. Most of the individual slits making up the group would be classed as “large”, being similar in size to the large isolated slits, although there are a few smaller ones.

3.4 Lyriform organs

The final category of slit sense organs, the lyriform organs, also occur in fixed positions on the leg (Figure 3, Figure 4, Figure 5, Figure 6 and Appendix 1 – Supplementary figures 1–10). There are 110 lyriform organs across all eight walking legs of *A. diadematus* and 108 in *T. edulis* (Tables 3 and 4). Both species have either 12 or 13 lyriform organs per leg. The position of lyriform organs in *T. edulis* is almost identical across all 4 walking legs, but legs 1 and 2 have an extra lyriform organ on the ventral side of the tibia (Table 3).

Table 3. Number of lyriform organs on each walking leg in *Araneus diadematus*.

Segment	Leg 1	Leg 2	Leg 3	Leg 4	Total
Tarsus	0	0	0	0	0
Metatarsus	1	1	1	1	4
Tibia	4	4	4	4	16
Patella	3	3	3	3	12
Femur	2	2	3	2	9
Trochanter	3	3	3	3	12
Coxa	1	0	0	1	2
Total	14	13	14	13	55

Table 4. Number of lyriform organs on each walking leg in *Trichonephila edulis*.

Segment	Leg 1	Leg 2	Leg 3	Leg 4	Total
Tarsus	0	0	0	0	0
Metatarsus	1	1	1	1	4
Tibia	5	5	4	4	18
Patella	3	3	3	3	12
Femur	2	2	2	2	8
Trochanter	3	3	3	3	12
Coxa	0	0	0	0	0
Total	14	14	13	13	54

In both *A. diadematus* and *T. edulis*, there is a lyriform organ embedded within the group of slits on the posterior side of the trochanter (Figure 1:A). This whole structure could be considered intermediate between groups of slits and lyriform organs – the organ itself is very simple, consisting only of two slits, and is surrounded by tightly packed single slits forming the rest of the group. In some cases, it is difficult to actually identify the organ. Although difficult to define, we have followed Barth and Libera (1970) in considering this structure as a lyriform organ embedded within a group of slits.

In *A. diadematus*, there is an extra lyriform organ (consisting of two slits, similar to those on the trochanter) on the ventral side of the coxa on legs 1 and 4, whilst on legs 2 and 3 this organ is replaced by a single large slit. There is also an extra lyriform organ on the femur of leg 3, but aside from that, the arrangement of lyriform organs is identical between legs (Table 4).

In both species, the tibia was the leg segment most richly supplied with lyriform organs, followed by the patella (Tables 3 and 4). This is in contrast to the distribution of single slits and other slit sense organs, which were concentrated proximally.

4 Discussion

4.1 Comparison with other spiders

The main objective of the present study was to map the overall distribution of slit sense organs (defined into categories of: single isolated slits, large isolated slits, groups of slits and lyriform organs) on the walking legs of two species of mature female orb-weavers. In order to enable future research that aims to explain patterns in the distribution of slit sense organs across large areas of the body (i.e. entire legs), we particularly focused on the distribution of the understudied small isolated slits, which are organised in lines along each leg segment – very different to the local measurements taken by lyriform organs at specific sites. Our maps record the exact position and orientation of each small isolated slit, which could be used as the basis for future comparative study.

Putting these findings in context, we find that the distribution of slit sense organs on the walking legs of both *A. diadematus* and T*. edulis* supports what has been found for other species described in the literature. Lyriform organs, large isolated slits and groups of slits are located consistently near joints, whilst small isolated slits are distributed in lines along the length of the leg. This suggests that slit sense organ distribution on the legs is tightly controlled by physical or evolutionary constraints, which are heavily linked with morphology and body plan. We compare our findings to a few species where distribution maps have previously been produced for at least one leg, listed above in Section 1 Introduction. McIndoo (1911) produced a comprehensive survey of slit sense organ distribution in 39 different species, which provides some useful context for this work. However, it is difficult to use his study as a comparative tool, as McIndoo did not identify many of the spiders to species level (and many of the genera have now been renamed and taxonomically split), did not produce distribution maps, and defined the

slit sense organs in a different way to what is currently used in the literature (for instance, it is not clear whether his category of “simple lyriform organ” also includes loose groups of slits).

Our study found that intraspecific variation in slit sense organ distribution was low, which suggests that slit sense organ distribution is either functionally useful or constrained through development/body plan. The overall pattern of small isolated slits was the same in all individuals measured, as were the location of specific groups of slits and individual large slits – this supports what has been previously described in the literature (Barth and Libera, 1970; Barth and Stagl, 1976).

4.1.1 Small isolated slits

The external morphology of the small isolated slits is variable between species – they universally consist of a slit surrounded by a smooth protrusion, which in *A. diadematus*, *T. edulis* and *A. bruennichi* tend to be “lips” or flat C-shaped areas either side of the slit (Ganske and Uhl, 2018). In *C. salei*, the morphology is slightly different, with the slit being bordered by two elevated bulges (Barth and Libera, 1970).

The overall distribution patterns of small isolated slits we described, consisting of two lines of slits on the dorsomedial and dorsolateral sides of the tarsus, metatarsus, tibia and patella; multiple lines on the femur; and the proximal concentration of single isolated slits, are also found in other species of spider, such as the orb-weavers *A. bruennichi* (Ganske and Uhl, 2018) and *L. sclopetarius* (Vogel, 1923), and the sit-and-wait hunter *C. salei* (Barth and Libera, 1970). In terms of explaining these conserved patterns, Barth and Stagl (1976) suggested that the proximal concentration might be due to the increased number of muscles in this area, where the main back-and-forth movement of the leg is generated when walking. It is also possible that the lines of small isolated slits correlate with the position of haemolymph channels. We therefore hypothesise that single slits are coordinated in lines to effectively detect strains over a large area, such as

the entire length of the leg segment, rather than localised information at a point of interest such as a lyriform organ.

In contrast to these findings, the dwarf spider *C. simonii* does not possess such a regular and consistent distribution of small isolated slits – instead of discrete lines, they are grouped rather sporadically on the walking legs (Kropf, 1998). This is also combined with a low number of single slits (around 250) compared with the other species discussed above. These differences may be linked to its much smaller body size – shorter legs may mean that detection of large-scale strains is not as important as in larger spiders, whilst the magnitude of internal forces acting on the legs will also be reduced due to low body mass.

Within the lines of small isolated slits, the exact location, size and orientation of a specific slit are highly variable between individuals, as is the number of slits in each line and the number of random slits away from the lines. We were unable to correlate these differences with any variation in morphology, although it is probable that larger individuals have more slits.

4.1.2 Other slit sense organs

Two large slits are present on the underside of the distal end of the metatarsus, directly opposite the HS10 lyriform organ, in both *A. diadematus* and *T. edulis*. These slits have also been reported in *L. sclopetarius* (Vogel, 1923), an orb-weaver which is closely related *to A. diadematus*. They were not observed in any of the other species of spider to our knowledge.

Groups of slits on the medial and lateral sides of the trochanter seem to be consistently present in *A. diadematus*, *T. edulis*, C*. s*alei (Barth and Libera, 1970) and *L. sclopetarius* (Vogel, 1923). In *C. salei,* there is also a single lyriform organ in the middle of this group (Barth and Libera, 1970), whilst in *A. bruennichi* these groups of slits are replaced on legs 2–4 with lyriform organs (Ganske and Uhl, 2018).

The distribution in T. edulis is similar but not identical in the closely related *T. clavata* – interestingly, *T. clavata* seems unusual in missing the HS10 metatarsal lyriform organ on leg 4 (Seo et al., 2020). *C. salei* has 15 lyriform organs in total on the leg, again in a similar arrangement, but with an extra two lyriform organs on the trochanter (Barth and Libera, 1970).

The location of the lyriform organs within individuals of the same species appears essentially fixed. Previous research has shown that the morphology of each individual lyriform organ (such as the number, length and orientation of the component slits and the overall shape of the organ), changes between successive moults throughout an individual's development (Morley et al., 2016) and varies depending on whether a leg has been regenerated (Vollrath, 1995). For mature adults of the same sex on legs that have not been regrown, it has been reported that variation in lyriform organ morphology is very low (Barth and Stagl, 1976; Morley et al., 2016).

4.2 Comparison with other arachnids

All arachnids utilise slit sense organs as their mechanoreceptors for sensing cuticular strain. Spiders are exceptional in the number of lyriform organs present on the legs, possibly due to increased reliance on sensing externally generated vibrations for hunting and courtship. Instead, these other arachnid groups tend to have more groups of slits and large isolated slits. Small single slits are more sparsely distributed in the other arachnid groups – the whip spider most closely resembles spiders in having a line of slits on the dorsomedial side of the leg (Barth and Stagl, 1976), but the others mainly have only loose groupings, or in the case of the scorpion just a profusion of slits covering the cuticle (Barth and Wadepuhl, 1975). The fact that the overall, large scale distribution of the slit sense organs in spiders is quite tightly organised (e.g. the long lines of small isolated slits along the legs) suggests that the function of these organs is particularly crucial for spiders, especially when compared with the somewhat sporadic and sparse distribution of these organs in other arachnids.

4.3. Comparison with other arthropods

The sort of questions that pertain to the distribution of arachnid slit sensilla apply equally to other arthropods, in terms of the way in which the biomechanics of the animal's body influence cuticular strains and the dynamics of mechanosensing – and by extension the distribution of embedded mechanosensors across the animal's body. Insects detect strains in their cuticle using campaniform sensilla, which are analogous to the slit sensilla of arachnids (Pringle, 1955). They consist of a flexible cap innervated by a dendrite that responds to cuticular strain (Pringle, 1938). Several studies have produced maps of insect campaniform sensilla, most notably on the cockroach *Periplaneta americana* (Pringle, 1938), but also on the fruit fly model species *D. melanogaster* (Dinges et al., 2020) and the blowfly *Calliphora vicina* (Gnatzy et al., 1987). In all of these insects, the campaniform sensilla tend to be distributed in fields (groups of slits) near the leg joints in a similar way to lyriform organs, although there are also sparse single sensilla away from these main groups. As is the case with body size in spiders, very small insects, such as the aphid *Mindarus*, possess a reduced number of campaniform sensilla (Montagano and Favret, 2016). In addition, the observed concentration of slit sense organs proximally on the leg in spiders is also apparent in the distribution of campaniform sensilla in insects, suggesting that increased musculature in the proximal leg segments influences slit sense organ distribution in both insects and arachnids (Pringle, 1938).

Therefore, it can be seen that some elements of the overall distribution of slit sense organs in insects are broadly similar to spiders, although the organisation of small isolated slits in long lines appears to be a spider-specific trait.

4.4 Further research/conclusion

Our study found that there are only minor differences in the slit organ distributions on the legs of T*. edulis* and *A. diadematus*. Furthermore, we add these two species to a

growing list of spiders that seem to be remarkably similar in their arrangement of slit organs, despite different morphologies, hunting strategies and evolutionary histories.

The stand out feature of the observed slit organ distributions is that the single isolated slits are almost always arranged in four lines along the leg. As the slit sense organs are sensitive to compression perpendicular to the long axis of the slit, and most of the slits are orientated roughly parallel to the long axis of the leg, this indicates that these lines function to detect expansion/contraction of the cuticle or torsional forces in the leg around the central axis of the leg. Whether the distribution is developmentally conserved, or constrained by underlying leg musculature or 8-legged body plan shared by all spiders, remains to be investigated. Understanding the functional arrangement of this slit organ arrangement, as well as its developmental pathway, are the first steps to potentially providing insights into whether mechanosensing in spiders is modulated by evolutionary or physical constraints.

Previous research has focused mainly on the function of the lyriform organs, and our understanding of the function of the other slit sense organ types is limited. This question could be investigated through targeted ablation experiments, neurophysiological recordings or describing the ultra-structural characteristics of the organs – e.g. dendrite morphology and receptor cell number.

The overall distribution of slit sense organs (particularly the small isolated slits) may be particularly useful in understanding how mechanosensing works on a whole–body scale for morphological computation. Morphological computation is where the body is used to process information before sensory transduction, thus reducing the total level of processing required in the central nervous system (Miller and Mortimer, 2020). As the body of the spider acts as a transmission platform for vibrational information, we might expect that the frequency content of a signal changes as it propagates through the body. Frequency segregation certainly seems to occur in the legs of the spider, with frequencies above 30 Hz attenuating significantly from the distal to the proximal leg segments, and evidence from modelling suggests that this changes depending on

posture (Mhatre et al., 2018). It is possible that the slit sense organs are arranged tonotopically to reflect this – i.e. their frequency sensitivity may vary along the length of the leg. Assessing overall distribution may therefore be crucial in the context of morphological computation. Further research is needed to uncover potential factors that might explain the functional significance of the observed slit organ distribution. This could be investigated through finite element modelling of the legs of the spider, which would enable areas of strain concentration to be identified. It is unclear what factors, internal or external, explain and control this distribution, making this a promising area for future research into arthropod proprioception and haptic sensing.

Author contributions

T.E.M.: conceptualization, investigation, methodology, writing – original draft, writing – review and editing. G.K.T. conceptualization, methodology, project administration, supervision, writing – review and editing. B.M.: conceptualization, funding acquisition, methodology, project administration, supervision, writing – review and editing.

All authors contributed to the article and approved the submitted version.

Funding

This work was supported by the Royal Society University Research Fellowship to BM (URF\R1\191033) and the US Air Force Office of Scientific Research (FA9550-09-1-0111).

Acknowledgments

We thank the Royal Society and US Air Force Office of Scientific Research for funding. We thank Tom Mulder and Michael Reinwald for discussions on slit sense organ distribution and Tom Mulder also for his comments on the manuscript. We thank Fritz Vollrath for allowing us to use the SEM and sputter coater.

Chapter 3

Mass distribution of the tarantula *Grammostola pulchra* measured through synchrotron-based micro-CT scanning

Thomas E. Miller[1], Jun Wu[1], Leonidas Romanos-Davranoglou[2], Christian Schlepütz[3], Alice Cicirello[4], Graham K. Taylor[1] and Beth Mortimer[1]

Abstract

Substrate-borne vibration sensing is a sensory modality that is uniquely intertwined with body morphology. In spiders, embedded mechanosensors measure the dynamic response of the body to vibrational input. Mass is an important biomechanical parameter that influences vibration sensing. Understanding how mass is distributed within the spider body is crucial for modelling the system and investigating how variation in biological traits modulate mass distribution and hence the dynamic response of the body. Here, we measure mass distribution in the tarantula *Grammostola pulchra* using CT scanning, a powerful tool for volumetric analysis of biological specimens. We calculate the mass, centre of mass and mass moments of inertia for each body segment in the scan and assess the utility of these results for modelling the spider body. We suggest methods for generalising these findings to other individuals of the same species by approximating each segment as a geometrical body.

1 Introduction

Body morphology is one of the most important determinants of an animal's biological function. Large-scale body morphology, such as the structure of leg joints, is important when considering animal biomechanics and locomotion (Dallmann et al., 2016, Blickhan et al., 2021). In the context of sensory ecology, the morphological structures of individual sensory organs have been intensively studied (Barth, 2019).

Body morphology is particularly relevant to animals which sense substrate-borne vibrations, such as arthropods (Hill and Wessel, 2016). Spiders are excellent model animals in which to study this modality due to the high sensitivity of many species to vibrations and reliance on substrate-borne vibrations as their primary information source (Barth, 2002a). The mechanosensors involved in substrate-borne vibration sensing (the slit sensilla) typically detect the motion of the spider's body as a vibrational input is transmitted through the system (Pringle, 1955), and hence are referred to as embedded sensors (Barth, 2019). This means that variation in morphology that influences the biomechanical parameters involved in vibration transmission may have a corresponding effect on the sensing of these vibrations (Miller and Mortimer, 2020, Wu et al., 2023).

In this study, we focus specifically on mass distribution as a body morphology parameter in the context of substrate-borne vibration sensing in spiders. Mass distribution refers to the spatial variation in mass throughout a solid body. The centre of mass is the point within an object where the mass weighted position vectors sum to zero, and thus a force applied at this point will result in linear acceleration of the object without corresponding angular acceleration (Batlle and Comdomines, 2022). Spider bodies typically have a non-uniform structure and therefore centre of mass can be difficult to estimate from first principles as one would for homogenous, regular objects. This also means that the spatial distribution of density is important when considering mass distribution in spiders.

Mass distribution is one of the key biomechanical parameters governing vibrational dynamics of the spider system, along with stiffness/damping and geometry (Miller and Mortimer, 2020). Mass distribution modulates the speed of vibration transmission through the system as well as attenuation of the wave through mechanical impedance (Mortimer, 2017). Understanding mass distribution is therefore important for understanding how variation in mass influences the dynamic response of the spider body to vibrational input and hence vibration sensing in different biological contexts.

Over long timescales, mass distribution varies throughout growth and development of the spider (Barth, 2002b). This variation is discrete with each successive moult and covaries with changes in body size and geometry. Over much shorter timescales, mass distribution varies on a day-to-day basis due to feeding status and reproduction (e.g. egg development) (Foellmer and Moya-Larano, 2007). This variation is continuous and does not covary much with the overall size and geometry of the spider's body – except for expansion of the isolated abdomen segment, which is the body part that typically experiences the most variation in mass over shorter timescales and hence has been used as an indicator of physiological condition (Fernandez-Montraveta and Moya-Larano, 2007). Both mass and density of the abdomen covary with these biological traits, leading to a relatively poor correlation between overall body mass and abdomen volume (after controlling for body size using cephalothorax width) (Moya-Larano et al., 2008).

Mass distribution may also vary due to injury changing the gross morphology of the animal. Leg loss is a typical occurrence in spiders, often during moulting or in response to predator attack (Brown et al., 2018). Asymmetric leg loss may cause large changes in the mass distribution of the spider if the mass of the legs is non-negligible when compared with the mass of the cephalothorax/abdomen. In some species, these changes may be reversed over medium-term timescales through regrowth of the lost leg over successive moults (Vollrath, 1995).

The relevant parameters for studying the effect of mass distribution on the vibratory dynamics of the spider body are the mass of each body segment, the centre of mass of

each segment and the whole body, and the mass moment of inertia (the resistance of body to angular acceleration around its rotational axis) (Batlle and Comdomines, 2022). X-ray CT scanning (hereafter referred to as CT scanning) is the preferred technique for measuring these parameters as a highly detailed 3D reconstruction can be generated without dissection of the specimen. These parameters can then be used in mass-spring-damper models and simulate the response of the spider to vibrational input. This type of model is widely used in mathematical modelling of vibration dynamics and is especially suited to biological systems such as the spider body due to the viscoelastic materials involved (such as cuticle), as well as the potential for non-linear responses (Wu et al., 2023, McConney et al., 2007).

Here, we measure mass distribution in the tarantula *Grammostola pulchra* using CT scanning. This species is a terrestrial hunter native to Southern Brazil (Pittella et al., 2023). The morphology of tarantulas and other ground-dwelling spiders differs substantially from web-building spiders, with much bulkier legs comprising a larger proportion of overall body mass. For an orb-weaver in its web, it may be a valid assumption to model the combined spider/orb web system as a single mass-spring-damper element, as the mass of the web is negligible compared to the mass of the spider body (Mortimer, 2019, Mortimer et al., 2019). For tarantulas, the dynamics of vibration transmission through the body are likely to be significantly more complex than this (Miller and Mortimer, 2020).

We use the CT scan data to calculate the mass, centre of mass, and mass moments of inertia of each body segment and validate methods of approximating these parameters using cylinder and ellipsoid models for a simple multi-body model. We discuss the implications of these results in the context of modelling the dynamic response of the spider body and assess the extent to which they can be generalised to different sized individuals of *Grammostola pulchra*.

2 Methods

We collected data from a specimen of *Grammostola pulchra* Mello-Leitão, 1921 kept in our captive lab population. The specimen was euthanised by freezing and placed in ethanol immediately prior to imaging using synchrotron radiation microcomputed tomography (SR-µCT) at the TOMCAT beamline, Swiss Light Source (SLS), Paul Scherrer Institute, Switzerland. The specimen was transferred to an Eppendorf tube and scanned at a beam energy of 21keV, exposure time of 4.5ms and a magnification of 4x.

Due to the large size of the specimen and the requirement for high resolution imaging, the scan was divided into 40 individual 360° scans, each covering a different part of the specimen with slight overlap between volumes. Tomographic reconstruction was performed using the GridRec software, resulting in a voxel size of 11µm. The resulting tomograms were then stitched together and visualised in three dimensions using AMIRA 6.1 software (Mercury Systems, Andover, MA, USA). This tomographic data will be made freely available through Morphosource.

We removed the cross-section of the tube containing the spider and any exterior voxels via segmentation in AMIRA 6.1. Using the same technique, we then isolated each body segment for analysis as a labels file. We assumed bilateral symmetry so only segmented the legs and pedipalp on the left-hand side of the specimen. We refer to the front left leg as leg 1, the second front left leg as leg 2, and the second rear left leg as leg 3. Due to damage to the spider specimen in preparation, we were not able to collect data from the rearmost leg (leg 4) and therefore this leg is omitted from the results and implications for modelling.

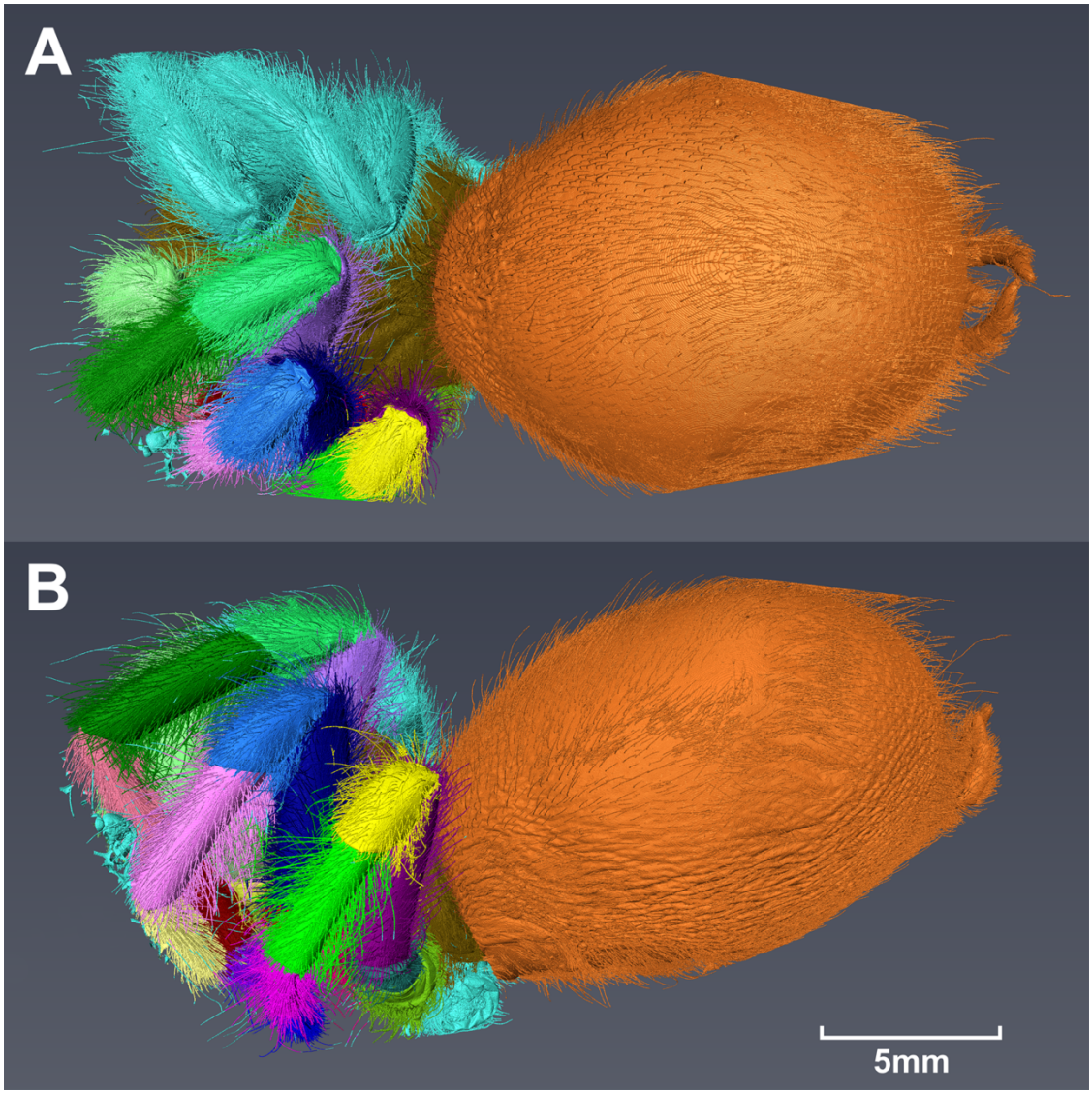


Figure 1. Segmented CT scan of *Grammostola pulchra* in (a) dorsal and (b) lateral view in AMIRA 6.1, with each segmented body part labelled in a different colour. Light blue indicates the unsegmented right-hand side of the spider body.

We exported the labels file as a TIFF stack and binarised each label segment in ImageJ. We then used the BoneJ plugin in ImageJ to calculate the mass, centre of mass and mass moments of inertia around each of the principal axes of each segment. For these calculations, we assumed that all of the cuticle, muscle and haemolymph within the labelled region had a uniform density of 1060kg/m^3, which is the measured density of cuticle in the closely related Chilean rose tarantula (*Grammostola rosea*) (Zentner, 2013) – for muscle and haemolymph, the assumed density is approximately the density of

water. Each image stack was also centred and rotated such that the principal axes of the segment were aligned with the x, y, and z axes of the image stack. For each segment, the z axis is in the length direction, whilst the x and y axes are the radial direction.

We measured the maximum dimensions of each segment along each of the three principal axes using ImageJ (Figure 2). These values were used to approximate each segment as a cylinder or ellipsoid, in order to validate simple analytical methods using the CT data. Whilst the detailed 3D reconstruction produced from the CT data could be used as a basis for a finite element model that exactly replicates the shape of the spider, a multi-body model using simple geometric bodies confers advantages in terms of easier manipulation of body geometry, and hence we focus on the application of our data to this technique. We used cylinder approximations for the leg segments and ellipsoid approximations for the abdomen and cephalothorax as these geometric bodies are closest to the shapes of the real segments. For cylinder approximations, the x and y measurements were averaged to produce a single value used as the diameter of the cylinder, with the z measurement used for the height. The volume of the cylinder was then calculated using the formula $v = \pi r^2 h$. We calculated the parallel and perpendicular mass moments of inertia of these cylinders using the formulae $I \parallel = \frac{mr^2}{2}$ and $I \perp = \frac{1}{12} m(h^2 + 3r^2)$, where m is the mass of the cylinder, r is the radius and h is the height.

For ellipsoid approximations, the volume was calculated using the formula $v = \frac{4}{3}\pi abc$, where a, b and c are the semiaxes of the ellipsoid (equated to half of the maximum dimension of the segment along its principal axes. We calculated the mass moments of inertia around these axes using the formulae $I_a = \frac{1}{5} m(b^2 + c^2)$, $I_b = \frac{1}{5} m(a^2 + c^2)$ and $I_c = \frac{1}{5} m(a^2 + b^2)$, where m is the mass of the ellipsoid.

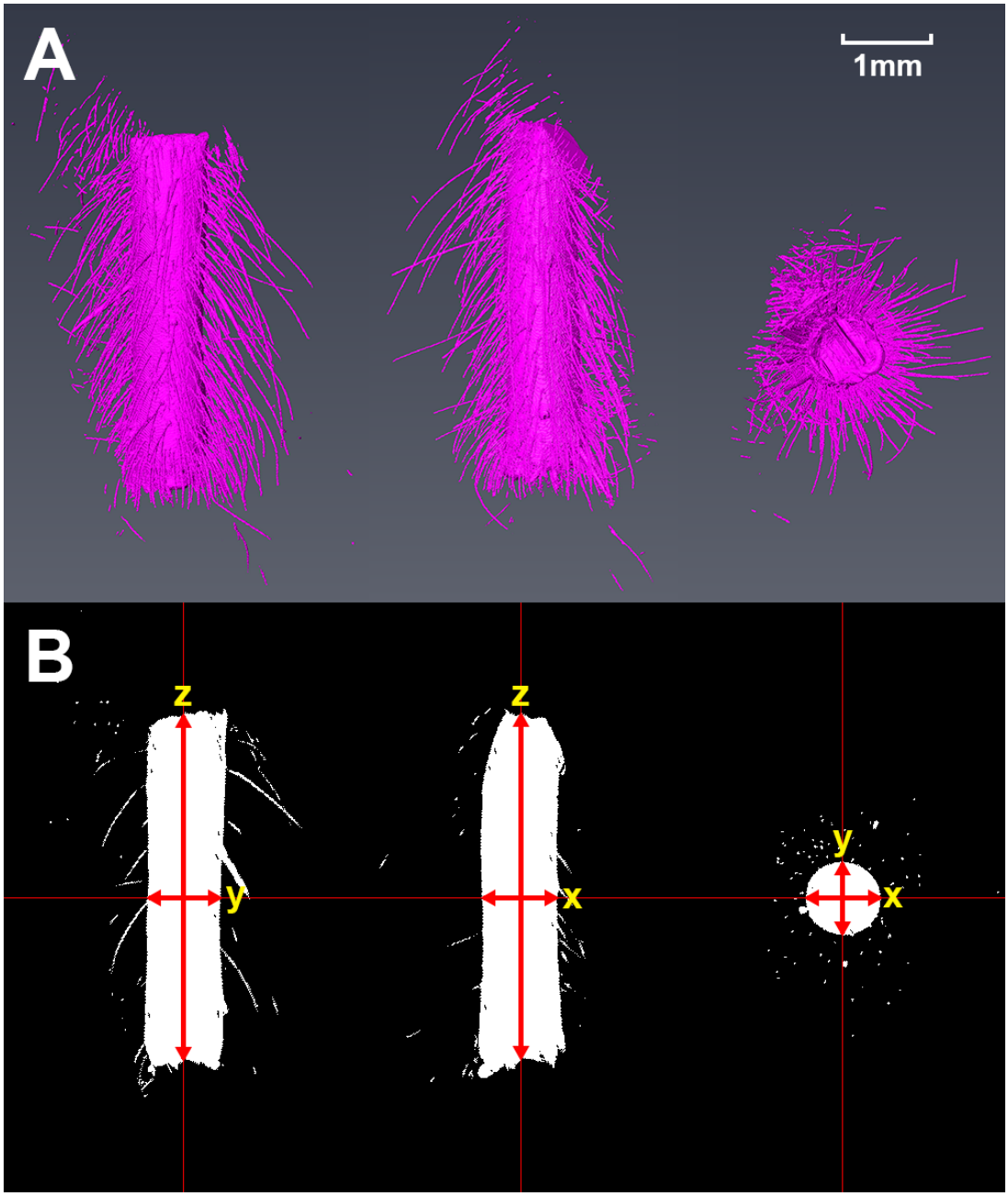


Figure 2. Metatarsus of leg 3 (a) segment label viewed in AMIRA 6.1 and (b) TIFF stack of labels file aligned and measured along principal axes x, y and z in ImageJ.

3 Results

3.1 Mass and mass moments of inertia

The calculated masses and mass moments of inertia for each segment isolated in the CT scan are given in Table 1. The centre of mass of the aligned stacks and the maximum dimensions of each segment along the principal axes are given in Appendix 2 – Supplementary table 1.

Table 1. Mass distribution parameters from calculated labelled CT scan data using BoneJ. Mass: mass of segment, from pixel values and density calibration coefficients, Icxx: moment around x axis passing through centre of mass, Icyy: moment around y axis passing through centre of mass, Iczz: moment around z axis passing through centre of mass.

Segment	Mass (g)	Icxx (kg.m^2)	Icyy (kg.m^2)	Iczz (kg.m^2)
Leg 1 coxa	0.00915	0.00912	0.00971	0.00414
Leg 1 femur	0.0117	0.0311	0.0305	0.00415
Leg 1 metatarsus	0.0026	0.0026	0.00259	0.000351
Leg 1 patella	0.00466	0.00383	0.00401	0.00124
Leg 1 tarsus	0.00219	0.00175	0.00176	0.000268
Leg 1 tibia	0.00651	0.0127	0.0126	0.00156
Leg 1 trochanter	0.0032	0.00119	0.000948	0.00129
Leg 2 coxa	0.00732	0.00544	0.00597	0.00323
Leg 2 femur	0.00912	0.019	0.0187	0.0028
Leg 2 metatarsus	0.00215	0.00196	0.00196	0.000249
Leg 2 patella	0.00374	0.00268	0.00254	0.000907
Leg 2 tarsus	0.00191	0.00149	0.00149	0.000205
Leg 2 tibia	0.00469	0.00748	0.00739	0.000938
Leg 2 trochanter	0.00241	0.000701	0.000778	0.000611
Leg 3 coxa	0.00753	0.00619	0.00553	0.00347
Leg 3 femur	0.00814	0.0154	0.0153	0.00228
Leg 3 metatarsus	0.0024	0.00313	0.00311	0.000303
Leg 3 patella	0.00251	0.00135	0.000535	0.0012
Leg 3 tarsus	0.00169	0.00129	0.00128	0.000168
Leg 3 tibia	0.00384	0.00539	0.00532	0.000705
Leg 3 trochanter	0.00222	0.000514	0.000716	0.000663
Abdomen	0.971	17.5	16.8	11.2
Cephalothorax	0.189	1.89	1.82	0.648
Pedipalp	0.0264	0.167	0.148	0.0384

3.2 Modelling the segment as cylinders using the x, y, z measurements from the CT scan

Next, we investigated the accuracy of approximating the leg segments as cylinders from the x, y and z measurements of each segment stack (subsequently referred to as Method 1). We calculated the percentage error between model and real segment and have indicated over-estimated values using green and under-estimated values using red in Tables 2-6.

The total mass estimates for the cylinders are poor. In general, the model overestimates the mass, in some cases by as much as 57.9%. This is despite the model not considering the mass of the hairs, as the dimensions along the principal axes were measured to the edge of the main exoskeleton segment only. The segments with highest percentage error are those which are the most irregular in shape, such as the trochanter, coxa, and patella.

The corresponding mass moments of inertia for these cylinder models is given in Table 3. The modelled cylinder is axisymmetric around the z axis passing through the centre of mass and thus a single value is given for the perpendicular mass moment of inertia. We calculated the percentage errors between this value and lcxx and lcyy, which correspond to the perpendicular mass moments of inertia in the real segment. Because the mass estimates are poor, many of the modelled leg segments show a very high percentage error in the estimated mass moments of inertia when compared with the real segments.

Table 2. Comparison of calculated mass of leg segment from labelled CT scan data using BoneJ and corresponding cylinder model.

Segment	Mass (g)	Model mass (g)	% error
Leg 1 coxa	0.00915	0.0124	35.5
Leg 1 femur	0.0117	0.0136	16.3
Leg 1 metatarsus	0.0026	0.00261	0.574
Leg 1 patella	0.00466	0.00574	23.2
Leg 1 tarsus	0.00219	0.00222	1.22
Leg 1 tibia	0.00651	0.00643	-1.28
Leg 1 trochanter	0.0032	0.00503	57.3
Leg 2 coxa	0.00732	0.00988	34.9
Leg 2 femur	0.00912	0.00967	6.06
Leg 2 metatarsus	0.00215	0.00198	-7.76
Leg 2 patella	0.00374	0.00471	26
Leg 2 tarsus	0.00191	0.00223	16.8
Leg 2 tibia	0.00469	0.00468	-0.296
Leg 2 trochanter	0.00241	0.0038	57.9
Leg 3 coxa	0.00753	0.00965	28.1
Leg 3 femur	0.00814	0.00902	10.8
Leg 3 metatarsus	0.0024	0.00219	-8.86
Leg 3 patella	0.00251	0.00382	52.5
Leg 3 tarsus	0.00169	0.00196	15.7
Leg 3 tibia	0.00384	0.00345	-10.3
Leg 3 trochanter	0.00222	0.00339	52.4

Table 3. Comparison of perpendicular and parallel mass moments of inertia of real segments and cylinder model. The cylinder is axisymmetric around Icxx and Icyy and hence a single value for the perpendicular mass moment of inertia is given.

	$I_{\perp}$ real		$I_{\perp}$ model			$I_{\parallel}$ real	$I_{\parallel}$ model	
Segment	Icxx (kg.m^2)	Icyy (kg.m^2)		% error to Icxx	% error to Icyy	Iczz (kg.m^2)		% error to Iczz
Leg 1 coxa	0.00912	0.00971	0.0163	78.7	67.9	0.00414	0.00648	56.5
Leg 1 femur	0.0311	0.0305	0.044	41.5	44.3	0.00415	0.00456	9.88
Leg 1 metatarsus	0.0026	0.00259	0.00276	6.15	6.56	0.000351	0.000296	-15.7
Leg 1 patella	0.00383	0.00401	0.00608	58.7	51.6	0.00124	0.00148	19.4
Leg 1 tarsus	0.00175	0.00176	0.0015	-14.3	-14.8	0.000268	0.000272	1.49
Leg 1 tibia	0.0127	0.0126	0.0123	-3.15	-2.38	0.00156	0.00133	-14.7
Leg 1 trochanter	0.00119	0.000948	0.00228	91.6	141	0.00129	0.00232	79.8
Leg 2 coxa	0.00544	0.00597	0.00938	72.4	57.1	0.00323	0.00509	57.6
Leg 2 femur	0.019	0.0187	0.02	5.26	6.95	0.0028	0.00293	4.64
Leg 2 metatarsus	0.00196	0.00196	0.00182	-7.14	-7.14	0.000249	0.000182	-26.9
Leg 2 patella	0.00268	0.00254	0.00411	53.4	61.8	0.000907	0.0011	21.3
Leg 2 tarsus	0.00149	0.00149	0.00188	26.2	26.2	0.000205	0.000244	19
Leg 2 tibia	0.00748	0.00739	0.0077	2.94	4.19	0.000938	0.000758	-19.2
Leg 2 trochanter	0.000701	0.000778	0.00174	148	124	0.000611	0.00113	84.9
Leg 3 coxa	0.00619	0.00553	0.00902	45.7	63.1	0.00347	0.00489	40.9
Leg 3 femur	0.0154	0.0153	0.0189	22.7	23.5	0.00228	0.00252	10.5
Leg 3 metatarsus	0.00313	0.00311	0.00273	-12.8	-12.2	0.000303	0.000188	-38
Leg 3 patella	0.00135	0.000535	0.0014	3.7	162	0.0012	0.00158	31.7
Leg 3 tarsus	0.00129	0.00128	0.00172	33.3	34.4	0.000168	0.000183	8.93
Leg 3 tibia	0.00539	0.00532	0.00438	-18.7	-17.7	0.000705	0.000471	-33.2
Leg 3 trochanter	0.000514	0.000716	0.00122	137	70.4	0.000663	0.00114	71.9

3.3 Modelling the leg segments as cylinders using the z measurement and mass from CT scan

An alternative way of modelling the segments as cylinders is to measure the length and volume of the segment from the CT scan, and then inversely calculate the radius using the formula for cylinder volume (subsequently referred to as Method 2). When applying this method to other individuals, we would estimate the volume as mass divided by the assumed density, in order to avoid the need for CT scanning multiple individuals.

The centre of mass of these cylinders is identical to Method 1 as varying the radius will not change the centre of mass coordinates. The percentage error associated with the mass moments of inertia is given in Table 4.

The estimated mass moments of inertia using this modelling method are much more accurate than Method 1 (Table 3), although for the trochanter, coxa, and patella there is still a high percentage error to the mass moments of inertia of the real segments (maximum error 45.1%). The perpendicular mass moments of inertia are mostly overestimated in the model, whilst the parallel mass moments of inertia are all underestimated.

Table 4. Comparison of perpendicular and parallel mass moments of inertia of real segments and cylinder model. The cylinder is axisymmetric around Icxx and Icyy and hence a single value for the perpendicular mass moment of inertia is given.

	$I_{\perp}$ real		$I_{\perp}$ model			$I_{\parallel}$ real	$I_{\parallel}$ model	
Segment	Icxx (kg.m^2)	Icyy (kg.m^2)		% error to Icxx	% error to Icyy	Iczz (kg.m^2)		% error to Iczz
Leg 1 coxa	0.00912	0.00971	0.0114	25	17.4	0.00414	0.00354	-14.5
Leg 1 femur	0.0311	0.0305	0.0376	20.9	23.3	0.00415	0.00338	-18.6
Leg 1 metatarsus	0.0026	0.00259	0.00274	5.38	5.79	0.000351	0.000292	-16.8
Leg 1 patella	0.00383	0.00401	0.00483	26.1	20.4	0.00124	0.000975	-21.4
Leg 1 tarsus	0.00175	0.00176	0.00148	-15.4	-15.9	0.000268	0.000266	-0.746
Leg 1 tibia	0.0127	0.0126	0.0125	-1.57	-0.794	0.00156	0.00137	-12.2
Leg 1 trochanter	0.00119	0.000948	0.00118	-0.84	24.5	0.00129	0.000937	-27.4
Leg 2 coxa	0.00544	0.00597	0.00646	18.7	8.21	0.00323	0.00279	-13.6
Leg 2 femur	0.019	0.0187	0.0188	-1.05	0.535	0.0028	0.0026	-7.14
Leg 2 metatarsus	0.00196	0.00196	0.00198	1.02	1.02	0.000249	0.000214	-14.1
Leg 2 patella	0.00268	0.00254	0.00318	18.7	25.2	0.000907	0.000696	-23.3
Leg 2 tarsus	0.00149	0.00149	0.00159	6.71	6.71	0.000205	0.000178	-13.2
Leg 2 tibia	0.00748	0.00739	0.00773	3.34	4.6	0.000938	0.000763	-18.7
Leg 2 trochanter	0.000701	0.000778	0.000969	38.2	24.6	0.000611	0.000452	-26
Leg 3 coxa	0.00619	0.00553	0.00663	7.11	19.9	0.00347	0.00298	-14.1
Leg 3 femur	0.0154	0.0153	0.0169	9.74	10.5	0.00228	0.00206	-9.65
Leg 3 metatarsus	0.00313	0.00311	0.00301	-3.83	-3.22	0.000303	0.000228	-24.8
Leg 3 patella	0.00135	0.000535	0.000741	-45.1	38.5	0.0012	0.00068	-43.3
Leg 3 tarsus	0.00129	0.00128	0.00147	14	14.8	0.000168	0.000136	-19
Leg 3 tibia	0.00539	0.00532	0.00491	-8.91	-7.71	0.000705	0.000585	-17
Leg 3 trochanter	0.000514	0.000716	0.000672	30.7	-6.15	0.000663	0.00049	-26.1

3.4 Modelling the cephalothorax and abdomen

We modelled the cephalothorax and abdomen as ellipsoids as this is the regular geometric body that most closely approximates their structure. The modelled mass values are quite accurate to the real segments (maximum error 5.93%). Correspondingly, the estimated mass moments of inertia are also acceptable, although mostly underestimated.

Table 5. Comparison of calculated mass of leg segment from labelled CT scan data using BoneJ and corresponding ellipsoid model.

Segment	Mass (g)	Model mass (g)	% error
Abdomen	0.971	0.965	-0.629
Cephalothorax	0.189	0.189	0.00683

Table 6. Comparison of mass moments of inertia of real segments and ellipsoid models.

Segment	Icxx	I_a	% error	Icyy	I_b	% error	Iczz	I_c	% error
Abdomen	17.5	17.0	-2.86	16.8	15.8	-5.95	11.2	11.3	0.893
Cephalothorax	1.89	1.50	-20.6	1.82	1.53	-15.9	0.648	0.564	-13.0

4 Discussion

4.1 Implications for a simple mass-spring-damper model

The dynamic response of the spider body to vibrational input can be usefully modelled by a simple mass-spring-damper model with 11 degrees of freedom, calibrated using experimental laser vibrometry data and measured biomechanical and geometrical parameters (Wu et al., 2023). Here, each leg of the spider body is modelled as a single mass. We can use our results to calculate the mass of complete legs 1-3 relative to the

abdomen/cephalothorax. Therefore, it enables accurate setting of the mass parameter for these model elements.

4.2 Implications for a multi-body model

A promising area of research is simulating the dynamic response of the spider body to vibrational input using multi-body models, where each body segment is modelled as a rigid element with 6 degrees-of-freedom (DOFs), including 3 translational DOFs and 3 rotational DOFs (Wu et al., 2022a, Wu et al., 2022b). The model needs the mass and moment of inertia of each segment as model parameters, which are exactly the data derived from this study (Shabana, 2020). Multi-body models typically have high degrees of freedom and may provide more resolution than simple models, enabling us to examine the motions of each segment in more directions and more complicated motion of the spider which may involve bending of the legs, etc. In the simple model described by (Wu et al., 2023), investigating these questions is not possible as only vertical motion is considered and each leg is modelled as a lumped mass.

A multi-body model requires calibration of many parameters in order to accurately simulate the dynamic response of the real spider. In the same way as with a simple model, our results enable us to quantify the relative mass of each body segment and hence accurately set this parameter for each multi-body model element.

We have also shown that the mass moments of inertia for most body segments can be approximated using either cylinders scaled from the CT scan z dimensions and masses (leg segments – Method 2), or ellipsoids scaled from the CT scan x, y and z dimensions (abdomen and cephalothorax). Our results therefore indicate that cylinders and ellipsoids can be used as the geometric bodies for each model element in the multi-body model. Where the mass moments of inertia have been consistently over/under-estimated, calibration may be possible to reduce the error associated with these values.

For the leg segments specifically, Method 2 matches the length of the model cylinder to the real segment and scales the radius such that the total mass is the same. Given that the estimates of the segment mass are relatively poor when modelling cylinders using x, y and z dimensions only (Method 1), Method 2 is advantageous so long as an accurate measurement of mass can be obtained, or the assumed density is accurately estimated. Segment radius is often inconsistent due to variation in the cross-sectional shape along the length of the segment, so in this respect length is a much more reliable measure. The implication for a multi-body model using the parameters derived from Method 2 is that the overall geometry of the leg will be the same as the real spider apart from the diameter of each leg segment. The parallel moment of inertia has the greatest effect on the simulated dynamic response, and this parameter is not affected much by the diameter of the leg.

There is a clear limitation in terms of modelling the trochanter, coxa, and patella due to their irregular geometries. We were not able to accurately approximate these leg segments using either of our cylinder models (Methods 1 and 2) and hence it is unlikely that their dynamics will be simulated accurately by a multi-body model that models each segment as a simple shape. One potential solution could be to simplify the cephalothorax/femur joint by subsuming the trochanter and coxa into either the femur or cephalothorax and hence modelling the whole area as only two elements. This would require combining the relevant label fields in ImageJ and re-analysing these segments using BoneJ. Since it has been shown that overall body dynamics can be reasonably well-modelled using a model with only 11 degrees of freedom (Wu et al., 2023), it is likely that reducing the number of elements in a multi-body model to eliminate the trochanter and coxa would have a negligible effect on the simulated response.

It is also possible to approximate the leg segments as cylinders using only the mass and mass moments of inertia from the CT scan – here, the cylinder height and radius could be inversely calculated from the formulae for parallel and perpendicular mass moments of inertia and cylinder volume. This model will be accurate in terms of the mass and mass moment of inertia, but the overall geometry of the spider will be affected as the

length of each segment will have a degree of error. These errors will be cumulative over the length of a whole leg, potentially resulting in a spider model with an inaccurate leg span or leg joint angles. This has implications for analyses related to posture and amplitude/time differences between specific mechanosensor locations, where distance from the source location is important (Chapter 5). Whether this method is better for modelling the dynamic response of the spider body to vibrational input compared with a model where the geometry is accurate, but the mass moments of inertia have a degree of error, will require further study, and may well depend on the research questions that the model is used for.

We did not attempt to model the pedipalp segment as a regular geometric body due to its complex structure. If this segment is included as a separate element in a multi-body model, and not simply modelled as part of the cephalothorax (which may be a valid assumption as it is only connected to the cephalothorax does not come into contact with the substrate), future research will be needed to find the best approximation for this segment in terms of the mass, centre of mass and mass moments of inertia.

4.3 Implications for obtaining parameters from multiple animals

Producing and analysing a CT scan of a spider specimen is a time-consuming process and requires killing the animal. If many experimental animals are required, for instance in a behavioural study, CT scanning each specimen to obtain the relevant parameters may not be possible or time effective. Thus, one of our central aims was to assess the feasibility of using a single CT scan to extrapolate these parameters between spiders of the same species, either through direct scaling or by modelling each segment as geometric bodies.

Given that the volume of each segment is known from the CT scan, we can express the volume of each segment as a proportion of the overall volume and hence obtain their relative volumes. If we assume isometric scaling between different individuals (i.e. a proportional increase in the size of each body segment with an increase in overall size,

thus consistent geometry), we can use the square-cube law to scale the relative volumes of individuals at different sizes: $V_2 = V_1 \left(\frac{\ell_2}{\ell_1}\right)^3$, where V_1 is the original volume, V_2 is the scaled volume, and ℓ_1, ℓ_2 are the dimensions of the two individuals. Dimensions used to compare the size of different individuals, such as cephalothorax width or total body length, can be easily measured from photographs (Moya-Larano et al., 2008).

Our results indicate that the measured x, y, and z dimensions alone are insufficient to effectively model the leg segments and estimate their mass moments of inertia. Directly obtaining the mass of each segment is undesirable as it would require destructive sampling of the animal and may be inaccurate due to haemolymph leaking from the segments during dissection. However, since the relative volumes of each segment can be scaled between individuals, we can calculate the mass of each segment from the total mass measured by weighing the animal. This simply requires multiplying the total mass by the relative volume of each segment. This is not possible for our dataset due to the missing fourth leg (as the total mass of our specimen cannot be compared to the total mass of a whole animal without a degree of uncertainty) but it would be achievable if a CT scan of a complete animal were obtained and analysed in the same way.

Method 2 could then be used to model multiple individuals using the calculated masses and lengths obtained through non-destructive sampling. It is worth noting, however, that the sources and effects of error will differ when measuring volume using the CT scan of a specimen and calculating mass using an assumed density, compared with measuring total mass of the animal, and calculating relative volumes and hence radii of each model segment using the assumed density.

One way to avoid this potential source of error is to directly generalise the mass moments of inertia from the CT scan to other individuals by calculating their ratio with respect to the reference moment of inertia, $I_r = mL^2$, where m is the total mass of the spider and L is the longest dimension of the body. Given that the relative mass of each segment is known, this means that the mass moments of inertia of a different sized

individual can be calculated simply by weighing the animal and measuring its overall length. Again, a CT scan of a complete animal would be required to employ this method.

5 Conclusion

In this study, we used a CT scan to quantify the mass distribution of *Grammostola pulchra*. The calculated mass, centre of mass and mass moment of inertia have direct applications as biomechanical parameters for modelling the spider body as a simple or multi-body model. We have proposed a method that can be applied to multiple individuals of *Grammostola pulchra* using the results from a CT scan of a single specimen. Using these techniques, we can estimate the biomechanical parameters of an experimental individual from relatively simple measurements (such as body mass and dimensions) without needing to do a CT scan every time. Further research using CT scans of different species could focus on the biological implications of mass distribution resulting from interspecific variation in morphology.

Author contributions

T.E.M. conceptualization, data curation, formal analysis, investigation, methodology, software, validation, visualization, writing—original draft, writing—review and editing. L.R.D. conceptualization, resources, data curation54, investigation, methodology, funding acquisition, methodology, project administration, supervision, writing—review and editing. C.M.S. project administration, resources, methodology, software. B.M. conceptualization, funding acquisition, methodology, project administration, supervision, writing—review and editing. G.K.T. conceptualization, funding acquisition, methodology, project administration, supervision, writing—review and editing.

All authors contributed to the article and approved the submitted version.

Funding

This work was supported by the Royal Society University Research Fellowship to BM (URF\R1\191033) and a Paul Scherrer Institut beamtime grant to LRD.

Acknowledgments

We thank Oxford University Museum of Natural History for access to the AMIRA 6.1 software and the staff at Paul Scherrer Institut for facilitating this research. We thank the animal technicians at John Krebs Field Station for their valued contributions to spider husbandry.

Chapter 4

Spider dynamics under vertical vibration and its implications for biological vibration sensing

Jun Wu[1], Thomas E. Miller[1], Alice Cicirello[2], and Beth Mortimer[1]

Adapted from:

Wu, J., et al. (2023). "Spider dynamics under vertical vibration and its implications for biological vibration sensing." Journal of the Royal Society Interface 20(206).

Abstract

Often overlooked, vibration transmission through the entire body of an animal is an important factor in understanding vibration sensing in animals. To investigate the role of dynamic properties and vibration transmission through the body, we used a modal test and lumped parameter modelling for a spider. The modal test used laser vibrometry data on a tarantula and revealed five modes of the spider in the frequency range of 20–200 Hz. Our developed and calibrated model took into account the bounce, pitch and roll of the spider body and bounce of all the eight legs. We then performed a parametric study using this calibrated model, varying factors such as mass, inertia, leg stiffness, damping, angle and span to study what effect they had on vibration transmission. The results support that some biomechanical parameters can act as physical constraints on vibration sensing. In addition, the spider may actively control some biomechanical parameters to change the signal intensity it can sense. Furthermore, our analysis shows that the parameter changes in front and back legs have a greater influence on whole system dynamics, so may be of particular importance for active control mechanisms to facilitate biological sensing functions.

1 Introduction

In engineering, vibration sensing is an important technology for localizing sources of interest and monitoring or detecting potential issues with equipment, which can avoid accidents or economical loss (Li et al., 2020, Valero et al., 2021). In biology, vast numbers of animals are adept at vibration sensing, which for arthropods is usually performed through sensors embedded in their numerous legs (Pringle, 1955, Yack, 2004). Among them, spiders are arguably the vibration sensing experts in the animal kingdom, which enables them to detect prey, find mates and avoid predators effectively (Mortimer, 2017, Mortimer, 2019). Understanding how spiders sense vibrations is helpful for developing innovative bioinspired technologies for use in engineering (Barth, 2019, Miller and Mortimer, 2020, Bosia et al., 2022).

The vibration receptors of spiders are highly sensitive, capable of sensing external vibrational stimuli with amplitudes down to tens of nanometres (Barth, 2008, Barth and Geethabali, 1982). Since spiders are found in diverse environments but have similar basic body plans, spiders are therefore good model organisms for studying vibration sensing (Miller and Mortimer, 2020, Barth, 2021). The organs involved in mechanosensation, whether vibration sensing from external or internal sources, include slit sensilla, which act as detectors of strain of the spider's exoskeleton (Blickhan et al., 2021). The slits, often parallel to the leg axis, have a membrane across them and mechanosensory cells attached beneath that send a nerve impulse when the slit is deformed perpendicular to the axis of slit (Blickhan et al., 2021, Molina et al., 2009). Slit sensilla are often co-located to form groups of slits and lyriform organs (Barth and Bohnenberger, 1978, Miller et al., 2022). Some are more sensitive to external vibrational stimuli than other slit sensilla. The metatarsal lyriform organs, located on the distal end of the spider metatarsus (towards the claw end of the spider leg), show high vibration sensitivity (Barth and Geethabali, 1982, Barth, 2012). Slits on the pretarsal claw are also vibration sensitive (Speck and Barth, 1982). However, other lyriform organs, generally situated close to leg joints, detect internally generated vibrations, for example being involved in kinaesthetic orientation (Seyfarth and Barth, 1972).

To be detected by the spider, external vibration stimuli have two mediums through which the vibration propagates before reaching the mechanosensors: the material in the environment (e.g. spider webs) and the spider body (Miller and Mortimer, 2020). For spiders that build webs, the webs play an important role in shaping vibrational information (Mortimer et al., 2016), whether for detection and localization of prey, objects or potential mates. The vibration transmission through different kinds of webs has been investigated in orb webs (Mortimer et al., 2016, Landolfa and Barth, 1996), sheet and tangle webs (Vibert et al., 2016). Other spiders detect vibrations along other substrates such as the ground or mixed media (Gordon and Uetz, 2011, Sun et al., 2021). Regardless of the substrate, the spider is able to discriminate between vibration sources and orientate/locate these sources (Landolfa and Barth, 1996).

Compared with effects of the substrate, particularly webs, the dynamics of the spider itself has been relatively overlooked. In fact, experimental studies of web vibration have often not included the spider, yet inertial effects of the added mass of the spider are important for vibrational motion of the whole system (Mortimer et al., 2018). By dynamics of the spider, we mean not only the motion of the spider legs, cephalothorax and abdomen combined, but also the interaction with the multiple points of contact with the vibrating surface that the spider is standing on. Previous studies have been focused on individual organs and leg segments in isolation (Barth and Geethabali, 1982, Barth and Bohnenberger, 1978, Bohnenberger, 1981). To our knowledge, little research related to whole-body dynamics of spiders has been published to date. The dynamic properties of the spider, including the natural frequencies, mode shapes and damping ratios, can have a significant influence on vibration transmission (Miller and Mortimer, 2020). We would also expect the influence of spider dynamics to change with substrate, as webs may in turn be influenced by the motion of the spider on it, whereas this is less likely for more dense substrates.

One key biological function of vibration sensing is to determine the source location, which spiders do through comparison of vibrational inputs from lyriform organs on all

eight legs (Hergenröder R., 1983, Seyfarth et al., 1982). This has been evidenced through ablation of the tibial and femoral lyriform organs, which reduces the directional accuracy of orientation (Barth and Seyfarth, 1971). Ground-dwelling spiders show a preference for certain substrate types to maximize transmission efficacy for communication (Sun et al., 2021, Gordon and Uetz, 2011). The chosen hunting substrates of spiders such as *Cupiennius salei*, which are sit-and-wait predators on the surface of large, broad-leaved, mechanically strong plants such as bromeliads, also possibly implicates a role for substrate preference in a hunting context (Barth, 2008). Web-building spiders possess even more control over the vibration transmission properties. Web-building spiders possess far more control over the vibration transmission properties of their substrate as they engineer it themselves, which means the degree of physical constraints may differ between orb weavers and terrestrially hunting spiders (Mortimer et al., 2019).

Source localization in spiders is dependent on the spider body–substrate combined vibrational dynamics. This means that variation in the biomechanical parameters of the spider body would be expected to affect the ability of the spider to accurately localize vibrational sources. Some of these parameters can theoretically be controlled by the spider through changes in leg mechanical properties via mechanisms such as hydrostatic pressure (Wilson, 1970) or muscle action (Blickhan, 1986) that vary leg joint stiffness and damping, and even changes in posture that vary leg span and angle (Mhatre, 2016). Other parameters will be dependent on physiological state or other constraints such as body mass, inertial or mass distribution, and body size and scaling that will vary with developmental stage and nutritional state (Foelix, 2010, Provencher and Riechert, 1991, Hesselberg, 2010). In the natural system, variation in a single biological trait can influence several of these biomechanical parameters at once, which can make it difficult to study their effects experimentally. Using a modelling approach we can examine the effects of biomechanical parameters in isolation, which can give insights into the physical constraints acting on vibration source localization.

To this end, the motivation of this paper is to study the dynamics of a freely vibrating, untethered live spider in its natural posture using laser vibrometry in order to develop

models of its vibration dynamics. We use the tarantula *Grammostola pulchra*, a terrestrial hunter which is ideally suited for vibrometry experiments (it retains a constant posture for extended periods). This species hunts on soily substrates of grasslands (Pittella et al., 2023). With these data, we perform a modal test and develop a corresponding mathematical model to describe the general biodynamics of the spider on a vibrating surface. Using the model, we study how changes in mechanical parameters (Table 1) including mass/inertia, stiffness, damping and leg length/angle influence its vibration transmission, including the interaction with vibration source location and substrate wave speed, and hence the overall effect on vibration source localization. Knowing how different parameters influence the vibration transmission through the spider body provides cues for how the spider may control its body to aid in vibration sensing or be limited by physical parameters outside of their control.

Table 1. Nomenclature

Symbols

$\mathrm{Im}(*)$ $\mathrm{Re}(*)$	imaginary part and real part of *, respectively
I_x, I_y	moments of inertia of the spider body in pitch (x) and roll (y) directions, respectively
j	imaginary unit j= −1
k_{ijn}, c_{ijn}	stiffness and damping coefficient of the connection between leg ijn (see §3.1) and the body
$k^g{}_{ijn}, c^g{}_{ijn}$	stiffness and damping coefficient of the contact between leg ijn (see §3.1) and the ground
m	total mass of the spider
m_b	mass of the spider body, including abdomen and cephalothorax
m_{ijn}	mass of leg ijn (see §3.1)
t	time
V	wave speed
ω_b	bounce of the spider body in the model
β	decay rate
φ_b, θ_b	pitch and roll of the spider body in the model, respectively
λ	wavelength

Abbreviations

DOF	degree of freedom
EoM	equation of motion
FRF	frequency response function
MAC	modal assurance criterion
WMAC	weighted modal assurance criterion

2 Experimental set-up

The modal test is a commonly used experimental method to derive the modal properties of a dynamic or biodynamic system, i.e. the inherent frequency-specific vibration characteristics (Wu et al., 2022a, Wu et al., 2022b). The modal properties of the spider (i.e. substrate independent) were investigated using the set-up shown in figure 1 and Appendix 3 – Supplementary Material, figure S1. We used immature specimens of *Grammostola pulchra* from our captive laboratory population. The spiders were kept in plastic terrariums with damp coir substrate and fed with crickets twice weekly, with water available in a dish. The animals were housed in a temperature-controlled room set at 20°C, on a 12/2 h day/night cycle. An untethered, live *G. pulchra* in its natural posture was put on an aluminium circular plate. The plate was connected to the top of a shaker (Modal Shop K2004E01) using a threaded bolt. The out-of-plane acceleration of the plate was measured by an accelerometer (PCB 352A21). The vertical velocity response of the spider was measured by a laser Doppler vibrometer (LDV) (Polytec VibroOne), whose advantage is it enables non-contact measurement as opposed to other measurement methods, e.g. strain gauge and accelerometer. The distance between the vibrometer and the spider was adjusted to maximize the signal-to-noise ratio. A circular tube with no contact with the plate was used to enclose the plate during the test to avoid the spider escaping.

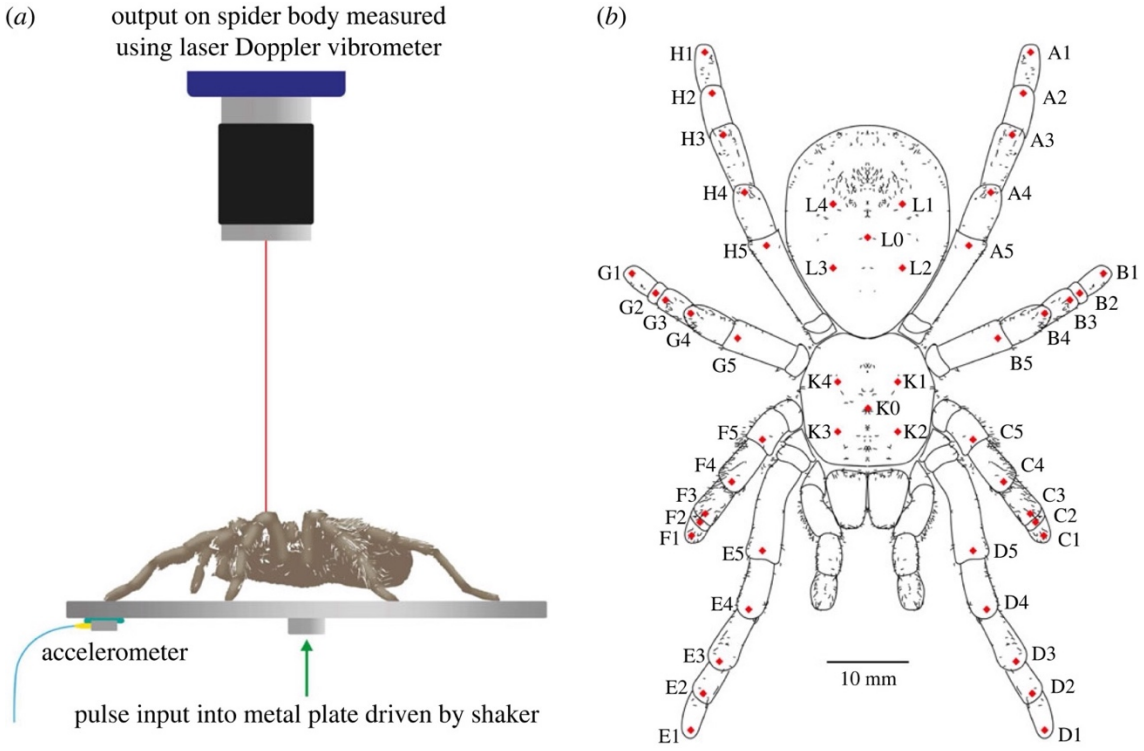


Figure 1. Experiment: (a) set-up; (b) measurement points on the spider. This figure is used for illustration of all the measurement points, given by the red dots in (b). Note the posture shown here is not the same as the test. During experiments, spiders were not anaesthetized or tethered but a tube was used to enclose the spider.

During the test, a pulse with a duration of 1.28 s and pulse width of 0.2 ms was used as the excitation and was generated by the shaker. Before the formal test, the response on the plate without the spider was measured under the pulse excitation, which was to ensure no resonances of the plate in the frequency range up to 500 Hz would affect the response. During the formal test, the spider had a constant posture (where any movement detected by visual inspection would terminate the test). The modal test followed the single-input multiple-output (SIMO) method (Ewins, 2000). The pulse excitation was repeated while each time the responses on the spider were measured by focusing the laser beam at one of the 50 different locations, including 5 points per leg, 5 points on the abdomen and 5 points on the cephalothorax, as shown in figure 1b. At each point, the measurement was repeated three times. Each point on the leg is named using a letter (standing for the leg) followed by a number (standing for its position on

the leg). The legs are named using the letters A–H from the left posterior leg to the right posterior leg in the clockwise direction, whilst the 5 points on each leg are named using the numbers 1–5 from the distal joints to the proximal joints. Each point on the abdomen and cephalothorax is named using the letter L and K respectively, followed by a number 0–4 for its position. All the data were acquired by the Polytec system with a sampling frequency of 25 600 Hz. The frequency response functions (FRFs), i.e. the ratio between the response (output) and excitation (input) expressed as a function of the excitation frequency, were calculated from the acceleration measured on the plate to the accelerations on the spider that are transformed from the velocity measured by the LDV. The FRFs are used to quantify the responses of the spider to the excitation. In this paper, the FRFs are calculated between two vibration quantities with the same unit, so they are also transmissibilities.

3 Modelling and analysis methods

3.1 Model description

Generally speaking, the modelling of the spider is very similar to the full car model (Esmailzadeh and Fahimi, 1997, Elbeheiry et al., 1996) in vehicle engineering, meaning that approaches from engineering can be applied to this novel context of exploring the biodynamics of the spider. The low model complexity brings about several advantages, including (1) it enables us to focus on the most critical aspects of the spider dynamics and simplify the representation while being sufficient to fulfil our objectives; (2) it is computationally less demanding; (3) it is more interpretable and easier to understand; (4) it is more robust and less prone to overfitting. Here we describe the components and parameters of the model, including relative locations, where the details of how the parameters are determined are given in Appendix 3 – Supplementary Material, S2. As shown in figure 2, the model includes the spider body and eight legs with a total of 11 degrees of freedom (DOF). To characterize the global vertical dynamics of the spider and focus on the most critical aspects of the spider dynamics while simplifying the representation, only the vertical vibration and the rigid-body motion of the spider body

and legs are considered. The spider body (including abdomen and cephalothorax) is modelled as a rigid body with 3 DOF, i.e. bounce ω_b, pitch φ_b and roll θ_b. Each of the 8 legs of the spider is modelled as a rigid body with bounce DOF g_{ijn} $(i = l, r;\ j = f, r;\ n = 1,2)$. The subscript denotes the leg name, in which the first letter *l* or *r* stands for the left or right leg, and the second letter for *r* stands for the anterior or posterior leg, and the final number 1 or 2 for the first or second leg (figure 2b). Each leg has a mass of m_{ijn}. The coordinates of the locations where each leg is in connection with the spider body are defined as (x_{ijn}, y_{jn}), and where the claw of each leg is in contact with the ground are defined as $({x^g}_{ijn}, {y^g}_{jn})$. Due to the symmetry about the mid-sagittal plane, it is satisfied that $m_{ljn} = m_{rjn}$, and $x_{ljn} = -x_{rjn}$, ${x^g}_{ljn} = -{x^g}_{rjn}$ as left and right sides are identical. The connection between the spider body (modelled here as combined cephalothorax and abdomen) and each leg is modelled as Kelvin–Voigt model by a spring–damper element with stiffness of k_{ijn} and damping coefficient of c_{ijn} (Karato, 2010). The contact between each leg and the ground is also modelled as Kelvin–Voigt model by a spring–damper element with stiffness of ${k^g}_{ijn}$ and damping coefficient of ${c^g}_{ijn}$. There is a vertical excitation z_{ijn} for leg *ijn*, whose coordinate is $({x^g}_{ijn}, {y^g}_{jn})$.

In terms of model inputs, the model uses either an equal input into each leg corresponding to the modal test, or a point vibration source excitation for parametric study. In the latter case, the source location is defined by the distance from the centre of mass (the origin) of the spider (R) and an angle α (positive if anti-clockwise) with respect to −y axis, as shown in figure 2b.

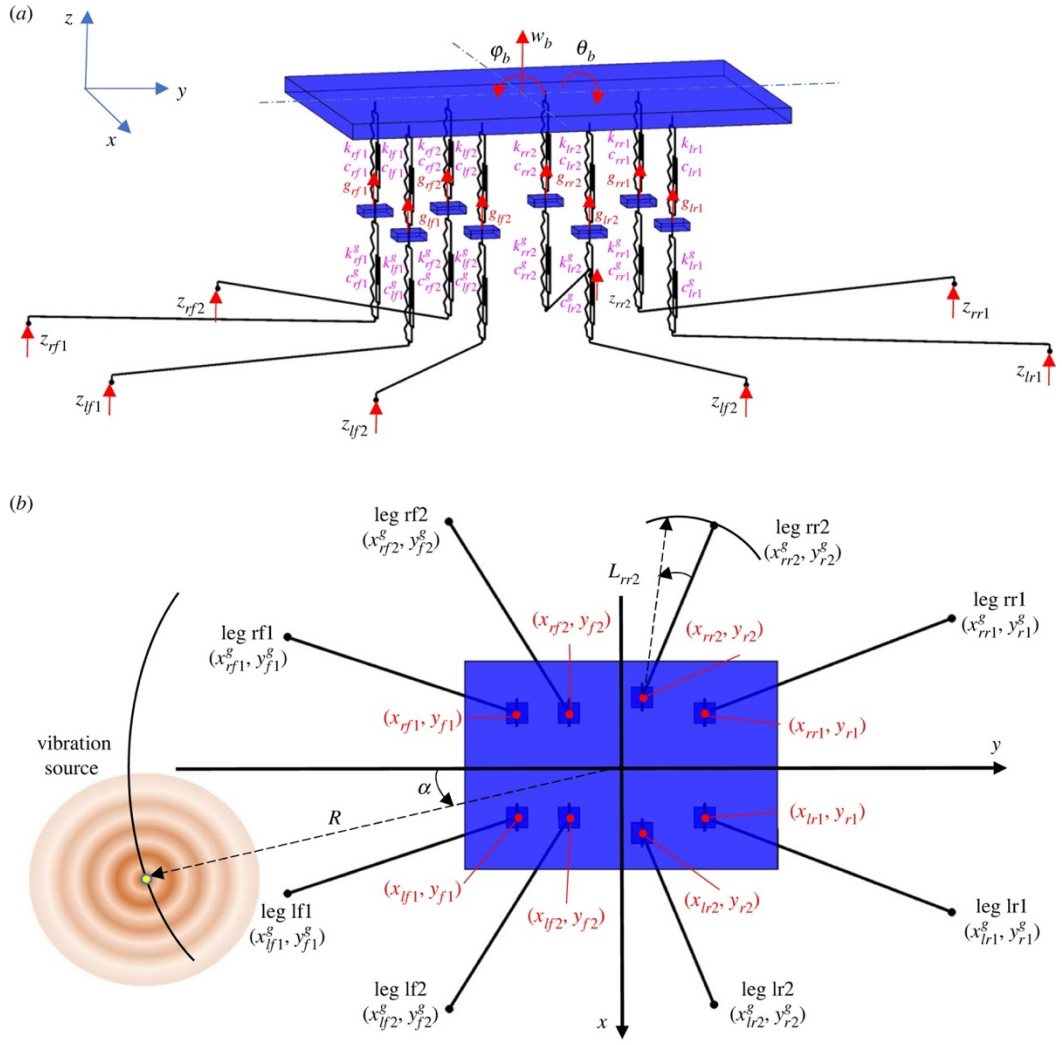


Figure 2. The lumped parameter model of a spider: (a) schematic diagram; (b) top view. The black horizontal lines are massless and artificial, only for distinguishing the leg input locations from leg–body connection locations. All parameters are explained in §3.1.

3.2 Equations of motion and model calibration

The equations of motion (EoM) of the spider model are derived according to Newton's second law (Appendix 3 – Supplementary Material, S1.1). Based on the EoM, modal analysis is carried out (Appendix 3 – Supplementary Material, S1.2), from which the modal frequencies, damping ratios and mode shapes of the model can be obtained. The FRFs are calculated (Appendix 3 – Supplementary Material, S1.3) based on the model

under equal inputs for all eight legs corresponding to the modal test or under a point vibration source excitation for parametric study.

To make the model have a good consistency with the experiment, model calibration is carried out considering four objectives (Appendix 3 – Supplementary Material, S2). Objective 1 is to minimize the difference of the natural frequencies between the model and experiment. Objective 2 is to minimize the difference of the damping ratios between the model and experiment. Objective 3 is to maximize the resemblance of the mode shapes between the model and experiment, while objective 4 is to minimize the difference of the FRFs between the model and experiment under equal leg inputs. The natural frequencies, damping ratios and mode shapes (considered in the first three objectives) are the inherent properties of the spider, independent of excitation. They are the same under equal input and under point vibration source input, so the model calibrated using the equal input can be applicable to the following parametric studies under point vibration source input. The fourth objective is complementary and optional, which is used to ensure the vibration transmission under equal input is accurate. The four objectives can be balanced by setting suitable weighting factors in electronic Appendix 3 – Supplementary Material, equation (S18). The obtained parameters are listed in Appendix 3 – Supplementary Material, table S1. Then sensitivity analysis is carried out to determine the confidence we have in the accuracy of the parameters (Appendix 3 – Supplementary Material, S3).

4 Results and discussion

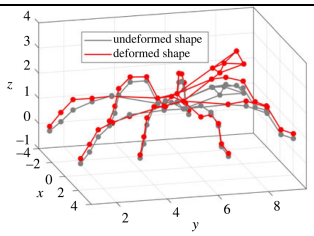
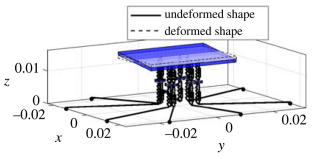
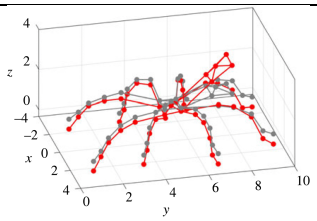
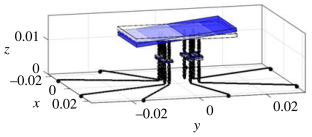
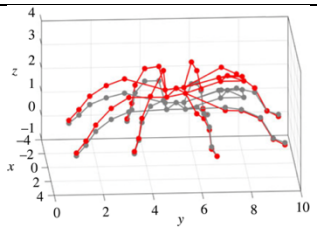
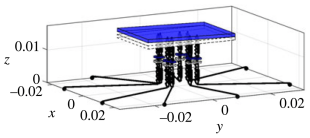
Our aim in this paper was to investigate the dynamics of an untethered spider on a vibrating surface and its implications for spider vibration sensing. Using a modal test based on laser vibrometry data, we reveal the modal properties of the spider and then develop and validate a mathematical model of the spider to simulate its dynamics (§4.1). We then use a parametric study approach on the calibrated model to investigate the influence of different selected parameters on the dynamic response of the spider–vibrating surface system (§4.2). This provides insights into the relative influence of

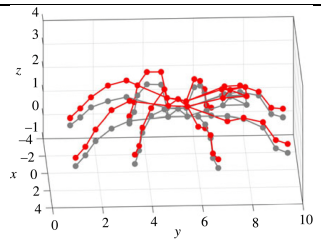
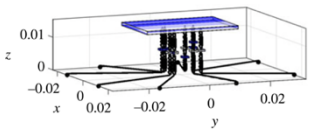
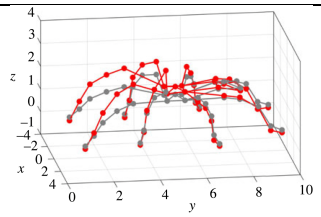
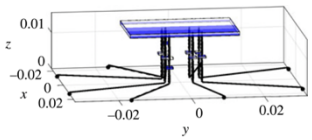
different mechanical parameters on spider dynamics. Furthermore, it reveals which parameters act as physical constraints or which can be actively controlled by the spider to influence vibration sensing, with a focus on the influence of parameters on source localization.

4.1 Modal properties and model validation

The modal identification was performed using the PolyMAX method (Peeters et al., 2004), and the results are shown in Electronic Supplementary Material, S4. The frequency above 200 Hz is not considered because the FRFs above 200 Hz have low amplitude and no obvious resonance frequencies while the pulse excitation can theoretically excite up to 5 kHz. In the modal test, five modes are identified in the frequency range of 20–200 Hz, as shown in Table 2. The first two modes are dominated by combined bounce and pitch motions. The mode shape of the first mode features the in-phase upward bounce and forward pitch (Electronic Supplementary Material, video S1) while the mode shape of the second features the out-of-phase upward bounce and forward pitch (Electronic Supplementary Material, video S2). The third mode is a whole-body upward bounce mode in phase with slight forward pitch of the cephalothorax (Electronic Supplementary Material, video S3). The fourth mode shape is very similar to the third, which features whole-body upward bounce out of phase with slight forward pitch of the cephalothorax (Electronic Supplementary Material, video S4). The fifth mode is dominated by the bounce of cephalothorax and all the legs with minor vibration of the abdomen (Electronic Supplementary Material, video S5).

Table 2. The comparison of the modal properties between the model and experiment. The coordinates of the points in the experimental mode shapes are measured from the spider under test. ‘WMAC’ (weighted modal assurance criterion) only applies to mode shape, and ‘error’ only applies to frequency and damping ratio. See Figure 1b for a full description of experimental laser vibrometry locations on the spider. See also Electronic Supplementary Material, videos S1–S7, that show mode shapes.

Mode	Property	Experiment	Model	WMAC	Error
1	Mode shape			<0.01	—
	Description	In-phase upward bounce and forward pitch	—	—	—
	Frequency (Hz)	31.75	31.83	—	<1%
	Damping ratio	0.227	0.228	—	<1%
2	Mode shape			0.59	—
	Description	Out-of-phase upward bounce and forward pitch	Pitch of the spider body	—	—
	Frequency (Hz)	37.65	36.79	—	2.3%
	Damping ratio	0.175	0.070	—	60%
3	Mode shape			0.83	—
	Description	Whole-body upward bounce in phase with slight forward cephalothorax pitch	Bounce of the spider body and all legs with slight body pitch	—	—
	Frequency (Hz)	74.15	70.12	—	5.4%
	Damping ratio	0.092	0.229	—	148.9%

4	Mode shape			0.016	—
	Description	Whole-body upward bounce out of phase with slight forward cephalothorax pitch	—	—	—
	Frequency (Hz)	108.43	109.51	—	<1%
	Damping ratio	0.076	0.090	—	18.4%
5	Mode shape			<0.01	—
	Description	Bounce of cephalothorax and all the legs with minor abdomen vibration.	—	—	—
	Frequency (Hz)	137.41	137.17	—	<1%
	Damping ratio	0.103	0.116	—	12.6%

On the one hand, it is well known that the signal energy generated by insects is dominated by frequencies in the range less than 1000 Hz (Mortimer, 2019). The resonances of the spider body lie within this range (below 200 Hz; note theoretical spider–web coupled systems are also in this range less than 20 Hz (Frohlich and Buskirk, 1982)), opening the possibility that changing body dynamics can enable higher amplitude sensing of the vibration signal. On the other hand, the spider dynamics makes it act like a low-pass filter when transmitting vibration to the slit sensilla. To sense all vibration frequencies equally below 1000 Hz, the slit sensilla need to be more sensitive to higher frequencies than lower frequencies, which is consistent with the tuning curves of slit sensilla (Mortimer, 2019).

The model parameters after calibration (which include masses, moments of inertia, stiffness, damping and coordinates of connection between legs and body) and the weighting factors are listed in Appendix 3 – Supplementary Material, Table S1. The frequencies of the model are in good agreement with the experiment with all errors less than 6% (Table 2). The damping ratios of 1st, 4th and 5th modes in the model are relatively consistent with the experiment (error less than 19%), while the damping ratios for the other two modes (2nd and 3rd) are not satisfactory (error greater than 60%). The 2nd and 3rd mode shapes of the model are generally in agreement with the experiment, while the other mode shapes are not. The 2nd mode shape in the model is dominated by the pitch of the spider body (Electronic Supplementary Material, video S6), while the 3rd mode shape is dominated by the bounce of the spider body and all legs with slight body pitch (Electronic Supplementary Material, video S7). It should be noted that the 2nd and 3rd modes should be more important than the others under equal leg inputs since their peaks are more prominent in the experimental FRFs (Appendix 3 – Supplementary Material, figures S2 and S3). Overall, the mode shapes of the spider tend to combine bounce motions of the whole body with pitch of the cephalothorax and abdomen, either in or out of phase. It should be noted that the FRFs in Appendix 3 – Supplementary Material, figures S2 and S3, are not perfectly symmetrical, and the potential reasons for bilateral asymmetry include: (1) the cumulative effect of small differences in leg joint angles between the left and right sides of the spider's body (Appendix 3 – Supplementary Material, figure S1); (2) larger variation in biomechanical parameters, such as muscle contraction and haemolymph pressure differences between left and right sides of the body. However, for simplicity and reducing model parameters, bilateral symmetry is assumed in the modelling.

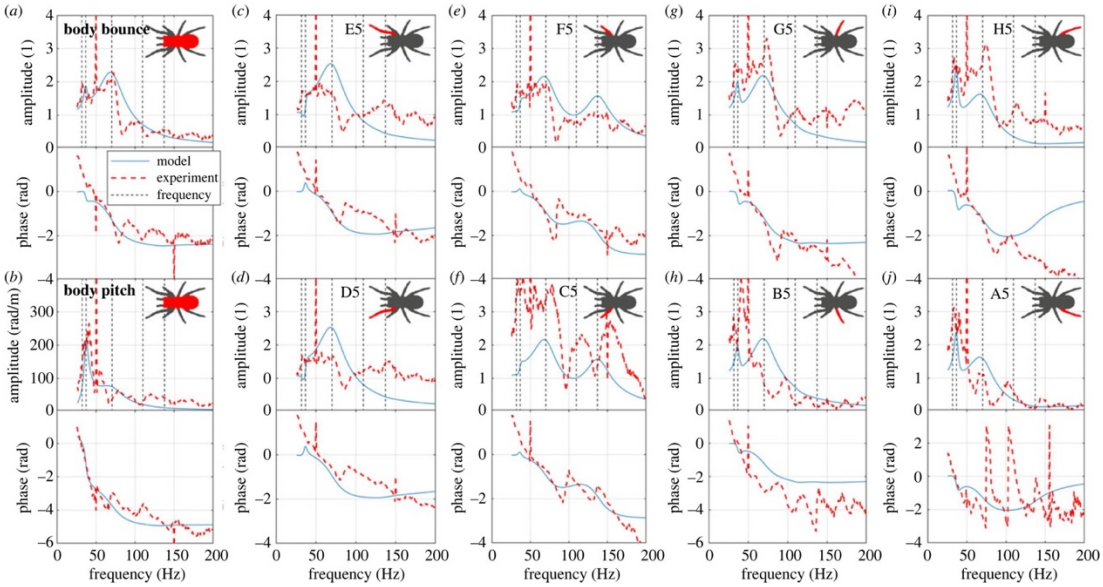


Figure 3. The comparison of the amplitudes and phases of FRFs between the model and experiment for (a) body bounce; (b) body pitch; (c) E5; (d) D5; (e) F5; (f) C5; (g) G5; (h) B5; (i) H5; (j) A5. Vertical dashed lines represent the natural frequencies of the model.

The comparison of the FRFs (including the amplitude and phase) between the model and experiment is shown in figure 3. The FRFs of the model show satisfactory agreement with the experimental FRFs, although the experimental FRFs are quite noisy, especially for the body bounce, body pitch, A5, F5, G5 and H5. This means, despite its simplicity and relatively few parameters and DOFs, the model can be adequately used to quantify the dynamics and vibration transmission of the spider.

In terms of the limitations of the model, due to the simplicity of the model the mode shapes of the spider cannot be reproduced perfectly, especially for the modes with complicated bending of the legs, or with different motions for the abdomen and cephalothorax. Furthermore, only vertical vibration is considered here under transverse wave excitation. However, in the natural context, substrate vibrations propagate not only as transverse waves, but also as other wave types such as longitudinal waves (Masters and Markl, 1981). In terms of the limitation of the modal test, with our approach using an equal vertical excitation into each leg, the roll vibration may not be excited due to the approximate symmetric property of the spider about the mid-sagittal

plane. Thus, it cannot be ruled out that there may be modes dominated by the roll motion of the spider body in the natural context in the considered frequency range. For example, in the real system, it is possible that roll plays a more significant role when inputs into all eight legs are asymmetrical or when asymmetrical postures are adopted by the spider. Future modal analyses should consider more of the three-dimensional motions of the spider system under different excitation regimes.

4.2 Vibration transmission

To investigate the implications of spider dynamics on spider vibration sensing, we moved to a more realistic environment where there is a point vibration source which propagates through a substrate and the coupled spider system. Using our calibrated mathematical model of the spider, this allows us to start to investigate the inter-leg differences between the legs in vibration transmission (§4.2.1). We then used the model to conduct a parametric study when there is a point vibration source, where parameters are varied systematically to determine their effect on spider dynamics, especially differences between the legs. The vibration source is assumed to be in a sinusoidal form. The parameters for the vibration source are listed in Table 3, in which the speed V and decay rate β of the vibration source are obtained from (Aicher and Tautz, 1990) on wet sand, which is within the right order of magnitude for wet soily substrate of tarantulas (Pittella et al., 2023).

The parameters we investigated include factors relating to the spider, including mass and inertia (§4.2.2), leg stiffness and damping (§4.2.3) and leg span and angle (§4.2.4), but also factors relating to the environment, such as wave speed (§4.2.5). All the parameters are kept the same as the reference parameters in Appendix 3 – Supplementary Material, Table S1, except the varying ones. We are focusing on the influence of parameter changes on the vibration transmissions to the spider body and all legs, which are quantified by FRFs.

Table 3. The parameters of the vibration source. The superscript 1 means the parameters were obtained from the literature (Aicher and Tautz, 1990) and superscript 2 means arbitrarily chosen for a point vibration source scenario.

Parameters	**Values**	**Parameters**	**Values**
V^1	80 m s-1	R^2	20cm
β^1	6.977 m-1	α^2	10°

4.2.1 Inter-leg difference

We start with how the vibration transmissions from different leg inputs differ when there is only one leg input at a time (Appendix 3 – Supplementary Material, equation (S7)). This simplified vibration input scenario allows us to investigate the relative contribution of different legs to spider vibration transmission. Figure 4 gives the FRFs from different single leg inputs to the bounce of leg lf1 (the output). It shows how the FRFs from different leg inputs differ, due to the difference in the vibration transmission through different legs.

This shows that inputs from the front and back leg inputs are easily transmitted to the other legs, while the transmissions from the middle four leg inputs are quite low except the within-leg transmission. This inter-leg difference is independent of the vibration source as it is a function of the model properties. Since the response of each leg or body is the summation of the vibration transmissions from all eight leg inputs, it can be expected that the parameter changes in the front and back legs have a greater influence on other legs, while the changes in each of the middle four legs may only affect that specific leg. This can generally be applied to the parameters investigated in the subsequent sections. The spider leg responses are therefore more robust to changes in biomechanical parameters in the middle four legs, while variation in the parameters in the front and back four legs will have a much greater influence on the spider leg responses.

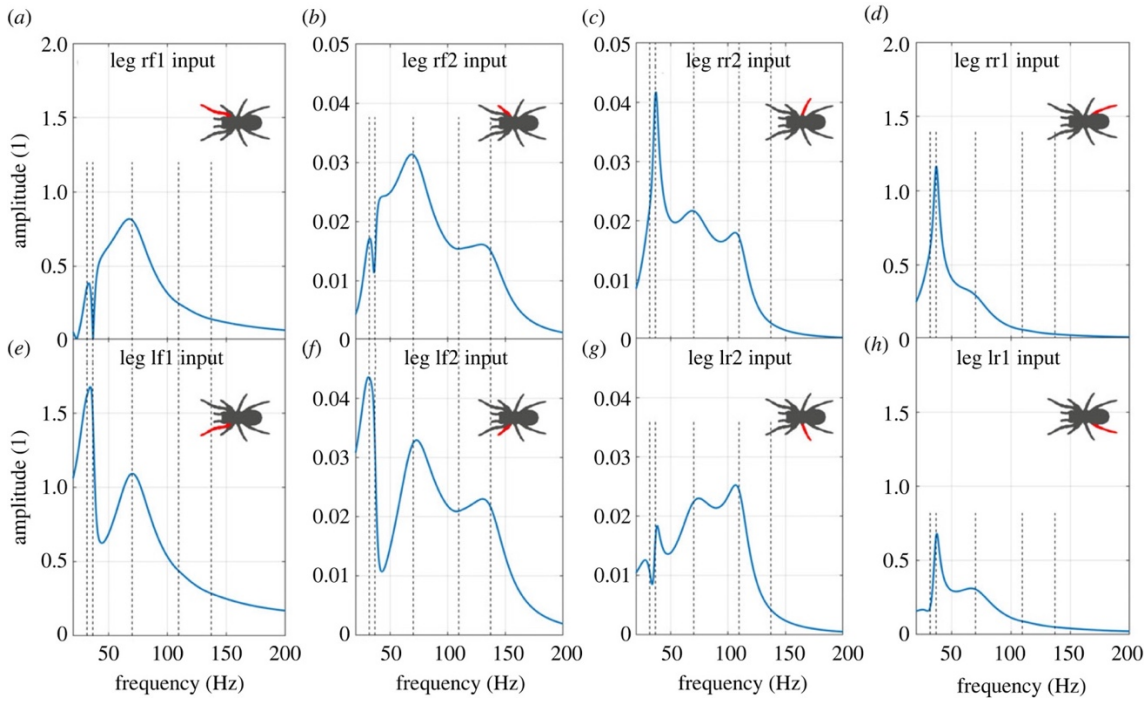


Figure 4. The FRFs to the bounce of leg lf1 from (a) leg rf1 single leg input, (b) leg rf2, (c) leg rr2, (d) leg rr1, (e) leg lf1, (f) leg lf2, (g) leg lr2, (h) leg lr1 single leg input. Note the different axes for (b), (c), (f) and (g). The vertical dashed lines represent the natural frequencies of the original system.

4.2.2 Influence of body mass and inertia

The influence of the body mass on the FRFs is plotted in figure 5. The FRFs in all subsequent subsections are calculated from leg lf1 input to all DOFs according to Appendix 3 – Supplementary Material, equation (S11). The FRFs show significant decrease of the third resonance frequency and its amplitude with the increasing body mass, which is because the increase of the body mass can increase the modal mass of the third mode that is dominated by the body bounce (Table 2), and the increase of the modal mass reduces the resonance frequency and the FRF amplitude according to single DOF system (Meirovitch, 2010). The effect is not equal between all four legs, with variation in mass having a greater influence on the middle four legs (lr2 and rr2 in particular).

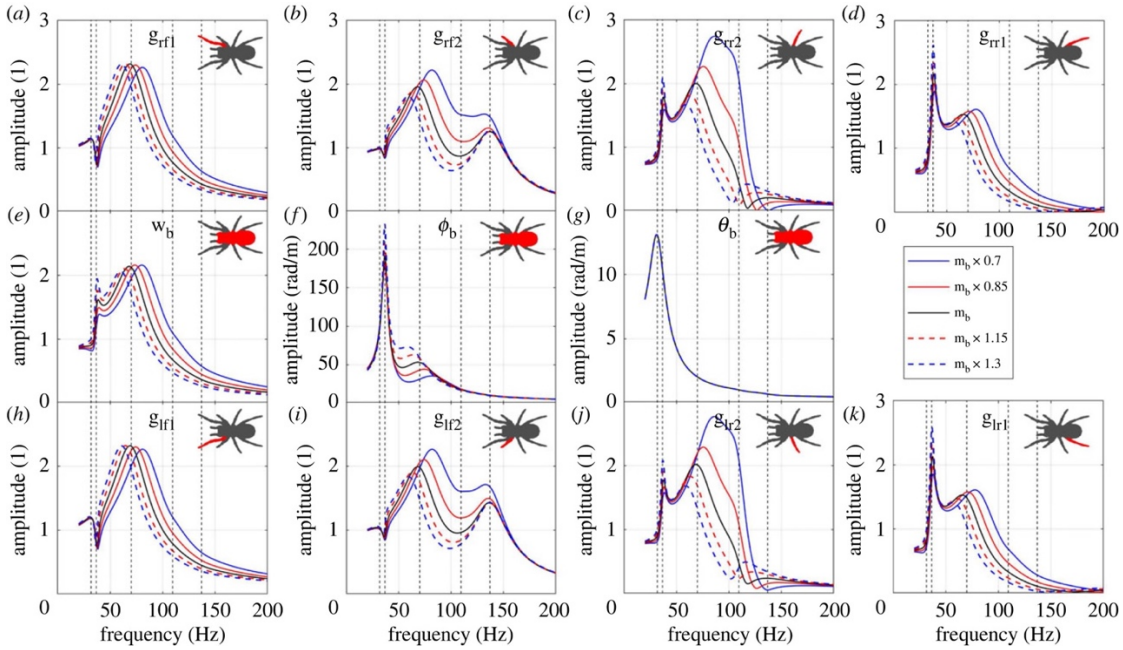


Figure 5. The influence of body mass m_b on the FRFs to (a) leg rf1 bounce; (b) leg rf2 bounce; (c) leg rr2 bounce; (d) leg rr1 bounce; (e) body bounce; (f) body pitch; (g) body roll; (h) leg lf1 bounce; (i) leg lf2 bounce; (j) leg lr2 bounce; (k) leg lr1 bounce. The vertical dashed lines represent the natural frequencies of the original system.

The change of the body mass leads to the change of the moment of inertia. The influence of the moment of inertia in pitch direction I_x on the FRFs is plotted in Appendix 3 – Supplementary Material, figure S4. The FRFs show significant decrease of the second resonance frequency and its amplitude with the increasing moment of inertia. This is because the increase of moment of inertia increases the modal mass of the second mode that is dominated by the body pitch (Table 2).

Overall, changes in mass, and linked moment of inertia, have effects on the frequency and amplitude of two major spider vibration modes. Short-term mass variation is influenced by several biological factors, including feeding status, hydration and reproduction, which may have some impact on the spider dynamics and so vibration sensing in the frequency range under 200 Hz.

4.2.3 Influence of stiffness and damping

To illustrate how the leg stiffness can influence the vibration transmission, as an example, the influence of the leg–body connection stiffness of the leg lr2 (k_{lr2}) is plotted in figure 6. The vibration transmission to leg lr2 is influenced by changing its stiffness, while the vibration transmissions to other legs remain the same. This is consistent with our point in §4.2.1 (figure 4) that the parameter changes in one of the middle four legs only influences itself. It can be expected that if stiffness of the front or back legs is changed, the vibration transmissions to all the legs will be changed. To be specific, the amplitude of the second resonance (corresponding to mode 2) is increased while the amplitude of the third one (corresponding to mode 3) is reduced with the increasing stiffness. Only slight shift of the resonance frequencies is observed with changing leg stiffness.

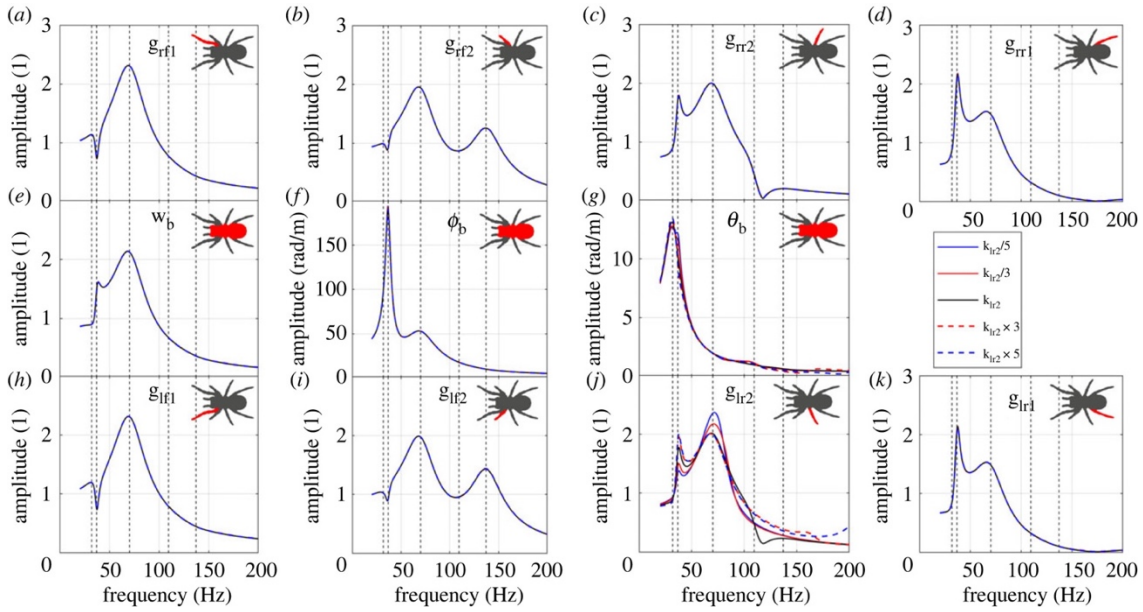


Figure 6. The influence of k_{lr2} on the FRFs to (a) leg rf1 bounce; (b) leg rf2 bounce; (c) leg rr2 bounce; (d) leg rr1 bounce; (e) body bounce; (f) body pitch; (g) body roll; (h) leg lf1 bounce; (i) leg lf2 bounce; (j) leg lr2 bounce; (k) leg lr1 bounce. The vertical dashed lines represent the natural frequencies of the original system.

To illustrate how the leg damping can influence the vibration transmission, as an example, the influence of the leg–body connection damping of the leg lf2 (c_{lf2}) is plotted in figure 7. The vibration transmission to leg lf2 is changed when its leg damping is changed, while the vibration transmissions to other legs remain the same (also consistent with §4.2.1). To be specific, the amplitude of the third resonance (corresponding to mode 3) is increased, while the amplitude of the fifth resonance (corresponding to mode 5) is suppressed significantly with the increasing damping coefficient. Only a slight shift of the resonance frequencies is observed with changing leg damping.

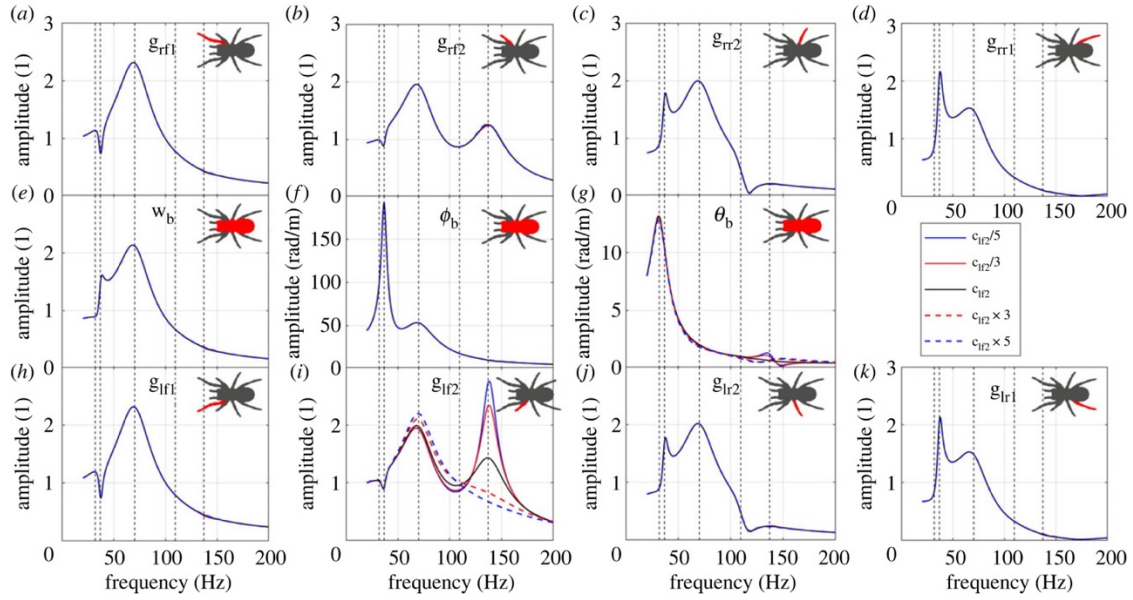


Figure 7. The influence of c_{lf2} on the FRFs to (a) leg rf1 bounce; (b) leg rf2 bounce; (c) leg rr2 bounce; (d) leg rr1 bounce; (e) body bounce; (f) body pitch; (g) body roll; (h) leg lf1 bounce; (i) leg lf2 bounce; (j) leg lr2 bounce; (k) leg lr1 bounce. The vertical dashed lines represent the natural frequencies of the original system.

Leg stiffness and damping are influenced by several biological factors including hardening of the cuticle after moulting (Politi et al., 2021), leg angle, as well as active muscle action (Blickhan, 1986) and hydrostatic pressure (Wilson, 1970). They can also be affected by the viscoelastic cuticle material structure, where specific temperature/humidity/strain rate (i.e. excitation frequency) combinations can alter

material structure–property links via glass transition effects (McConney et al., 2007, Klocke and Schmitz, 2011). These parameters could be seen as a constraint set by the mechanical properties of the spider, but equally the spider has some degree of control over these—for instance, increasing joint angle stretches the articular membrane, increasing alignment in the material and hence stiffness (Blickhan, 1986). Consistent with our findings here, leg joint viscoelasticity is dependent on the vibration direction, which may be used by the spider to control the signal amplitude transmitted to the mechanoreceptors (Blickhan, 1986). Therefore, it is possible that leg stiffness and damping could be used by the spider to actively control its vibration sensing, which will require further study to investigate.

4.2.4 Influence of leg span and angle

The vibrational input that goes into the spider is influenced by the leg–ground contact locations. In turn these are influenced firstly by leg span and the leg angle, as shown in figure 2b, but also properties of the substrate such as wave speed (§4.2.5).

The influence of the angle of a single leg (rf2) is shown in figure 8. Changing this angle has a significant influence on the FRF to leg rf2, while has no obvious influence on the FRFs to other legs (§4.2.1). In this case, a positive/anti-clockwise change of leg angle increases the FRF amplitude to leg rf2 above 100 Hz, dominated by the fifth mode. This is because the change of the angle of leg rf2 is almost along the line connecting the vibration source and leg–ground contact position (figure 9). In addition, there is no obvious shift of the resonance frequencies, which is because the change of the leg–ground contact position does not affect the natural frequencies of the spider.

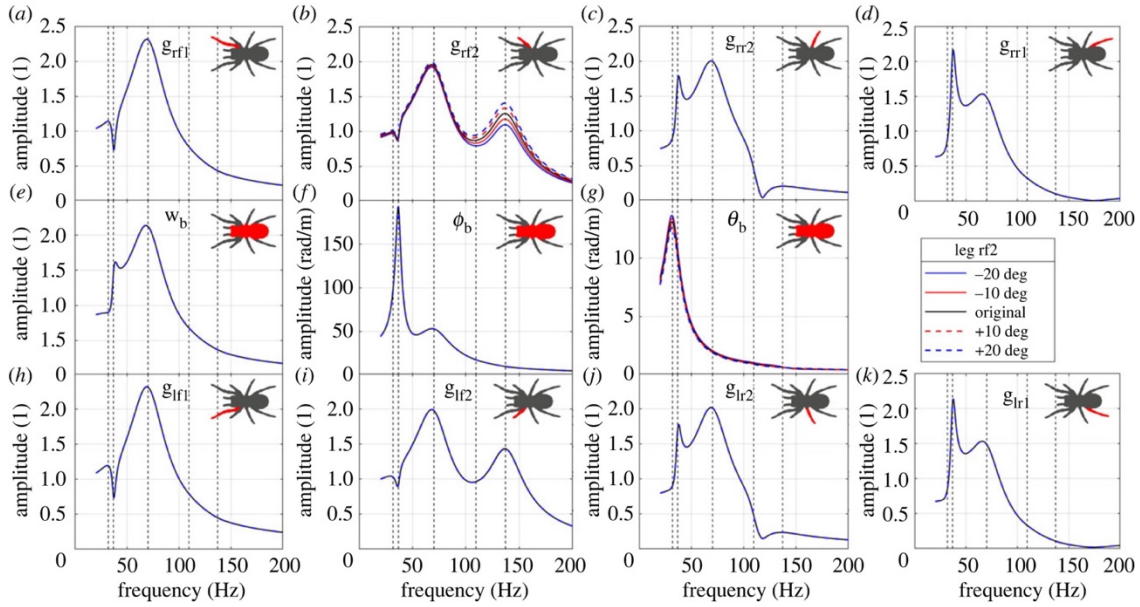


Figure 8. The influence of the angle of leg rf2 on the FRFs to (a) leg rf1 bounce; (b) leg rf2 bounce; (c) leg rr2 bounce; (d) leg rr1 bounce; (e) body bounce; (f) body pitch; (g) body roll; (h) leg lf1 bounce; (i) leg lf2 bounce; (j) leg lr2 bounce; (k) leg lr1 bounce. The vertical dashed lines represent the natural frequencies of the original system. The change of leg angle is positive if anti-clockwise (Figure 2b).

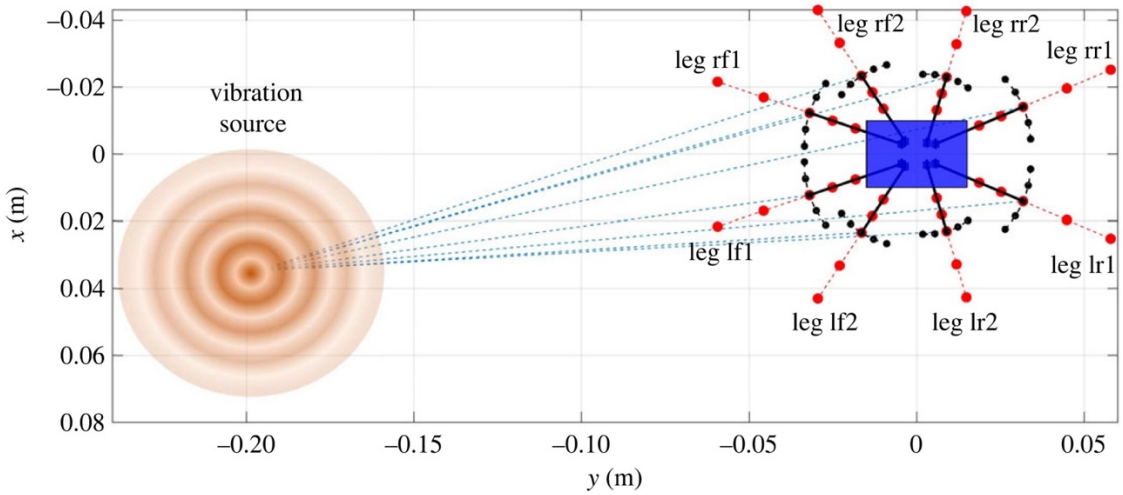


Figure 9. Schematic diagram showing the change of leg angle and span. The black dots stand for the 5 positions in the case of changing the leg angle, while the red dots for the 5 positions in the case of changing the leg span.

The influence of leg lf2 span is shown in figure 10. The change of the span has a significant influence on the FRF to leg lf2, while it has no obvious influence on the FRFs to other legs. In this case, an extension of the leg forward increases the FRF amplitude to leg lf2 above 100 Hz, dominated by the fifth mode. This is because the change of the span of leg lf2 is far from perpendicular to the line connecting the vibration source and leg–ground contact position (figure 9). In addition, there is still no obvious shift of the resonance frequencies.

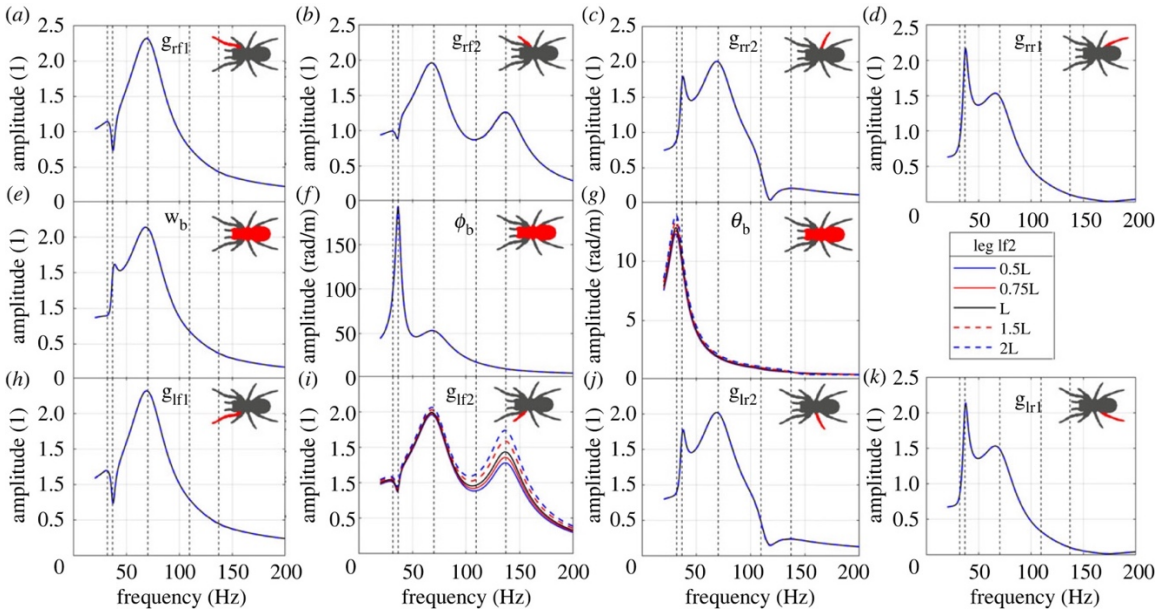


Figure 10. The influence of leg lf2 span on the FRFs to (a) leg rf1 bounce; (b) leg rf2 bounce; (c) leg rr2 bounce; (d) leg rr1 bounce; (e) body bounce; (f) body pitch; (g) body roll; (h) leg lf1 bounce; (i) leg lf2 bounce; (j) leg lr2 bounce; (k) leg lr1 bounce. The vertical dashed lines represent the natural frequencies of the original system.

By sensing different vibration intensities through varying the leg span and angle, the spider may be able to determine the direction of the vibration source relative to the leg orientation, which may be used as a directionality cue for the spider to localize the vibration source. Essentially, whether a change in leg span or angle makes a difference on the FRFs comes down to the leg–ground contact point distance from the vibration source (figure 9). Any change of the span/angle of one leg will only make a significant difference if the distance to the vibration source is altered. In terms of what this could

mean biologically, spiders in theory could adjust position of single legs to determine if changes are in line with the vibration source (where in line would result in higher difference in FRF). The magnitude of this effect will also be changed by the degree of attenuation and wave speed of the vibration through the substrate, as this governs how much the vibration alters with distance from the source (Mortimer, 2017) (in terms of amplitude and phase respectively). The effect of the wave speed is therefore investigated next.

4.2.5 Influence of wave speed

The wave speed is mainly dependent on the material properties of the substrate, and sometimes also on the loading (Mortimer et al., 2016). The influence of the wave speed on the FRFs is shown in figure 11. When the speed is greater than 60 m s^{-1}, the FRFs do not show significant difference with the increasing speed. This is because higher wave speed results in longer wavelength, and when the size of the spider is significantly smaller than the wavelength, the inputs into each leg are approximately equal if the decay rate is zero. So the FRFs will converge with the increase of the wave speed. For example, when the speed is 60 m s^{-1}, for a wave frequency between 20 and 200 Hz, the wavelength is between 0.3 and 3 m, which is much larger than the spider size. For speeds less than 60 m s^{-1} at this frequency range, the wavelength is comparable to the spider size, so there are significant differences between the leg inputs, and the FRFs vary significantly with the changing speed.

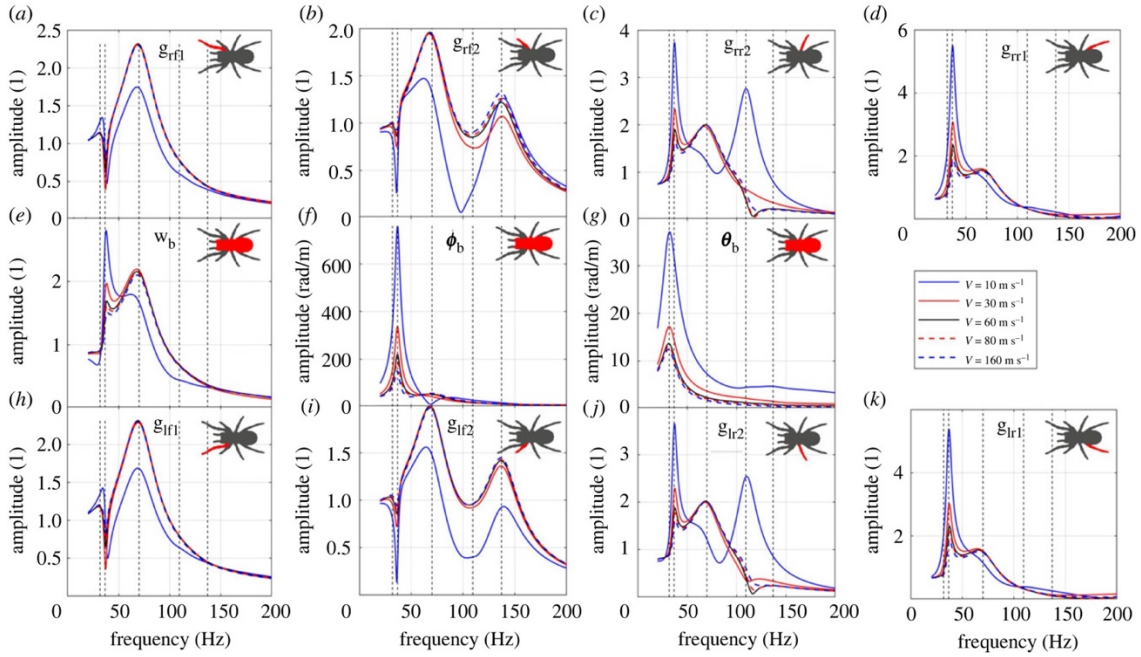


Figure 11. The influence of wave speed on the FRFs to (a) leg rf1 bounce; (b) leg rf2 bounce; (c) leg rr2 bounce; (d) leg rr1 bounce; (e) body bounce; (f) body pitch; (g) body roll; (h) leg lf1 bounce; (i) leg lf2 bounce; (j) leg lr2 bounce; (k) leg lr1 bounce. The vertical dashed lines represent the natural frequencies of the original system.

The wave speed does not change the dynamic properties of the spider, so it influences the FRFs globally. Thus, it can be expected that the wave speed will not affect how different parameters (i.e. body mass, leg stiffness, damping, leg span and angle) influence the FRFs. However, it will affect what vibration inputs go into each leg, thus it will affect the mechanism of localization (Mortimer, 2017).

5 Synthesis and conclusion

Here we investigated the vibration transmission through the spider body, which is an important factor in vibration sensing, yet has been understudied compared to vibration propagation through the environment (e.g. orb webs). To investigate the dynamic properties and vibration transmission through the body, a modal test and lumped parameter modelling for the spider (parametric study) were carried out, respectively.

For the modal test, modelling and experimental data were compared for calibration and validation, which showed five modes of the spider in the frequency range of 20–200 Hz, but no significant vibration above 200 Hz. For broadband prey-generated vibrations less than 1000 Hz, spider body resonance is therefore unlikely to play a role in amplifying biologically relevant vibrations greater than 200 Hz.

For the parametric study, the results showed that the vibration transmissions from different leg inputs caused substantial differences in overall spider dynamics, including what is sensed at each leg. This interaction within the whole spider system means that whole body spider dynamics need to be taken into account when understanding vibration sensing at any one part or leg. This supports the idea that changing morphology, whether geometry or properties, will influence vibration sensing inputs into the nervous system, as a type of morphological computation (Miller and Mortimer, 2020). In particular, our results suggest that the changes of biomechanical parameters in front and back legs can influence the leg responses more heavily compared to the middle legs. This effect could be used to help spiders localize vibration sources. More generally, it also means that to understand how vibration sources may be localized in any animal sensing vibrations through their legs, we need to understand how vibration dynamics of the whole system interact with the vibration surface. This applies to vast numbers of arthropods from spiders, to crabs, to insects.

The effects of biomechanical parameters investigated in the parametric study are influenced by multiple interacting biological processes within a single individual, from hunger and dehydration, through developmental stage (moult, growth, reproduction) (Foelix, 2010, Provencher and Riechert, 1991, Hesselberg, 2010, Politi et al., 2021). Therefore, we expect physical constraints to act on vibration sensing, as these biological processes will affect mass, inertia, stiffness and damping of biological materials outside of spiders' control. However, some parameters in theory can be actively controlled by the spider, including changing leg stiffness and damping, leg span and angle via muscle action and/or hydrostatic pressure to alter the vibration intensity and spectrum detected (Wilson, 1970, Blickhan, 1986). Of these, we propose that changing posture is

the most likely mechanism used to make small changes to spider biomechanics to influence vibration sensing over small timescales, as it will have influences on leg geometry and properties, as well as mass distribution. Outside of intra-individual variation, it is also possible that different individuals within a population or species have different strategies for how they mitigate the effect of physical constraints on vibration sensing.

Future research should focus on more advanced dynamical modelling of the spider and more complicated excitations. We would also encourage studies that collect empirical data on how spiders are influenced by and respond to biological processes that influence their biomechanics, whether development, malnutrition or leg loss and how this varies between species in different environments.

Ethics

This work did not require ethical approval from a human subject or animal welfare committee.

Data accessibility

The datasets and code supporting this article have been provided as part of the Electronic Supplementary Material (Wu et al., 2023).

Declaration of AI use

We have not used AI-assisted technologies in creating this article.

Authors' contributions

J.W.: conceptualization, data curation, formal analysis, investigation, methodology, software, validation, visualization, writing—original draft, writing—review and editing.

T.E.M.: conceptualization, data curation, investigation, writing—original draft, writing—review and editing. A.C.: conceptualization, funding acquisition, methodology, project administration, writing—review and editing. B.M.: conceptualization, funding acquisition, methodology, project administration, supervision, writing—review and editing.

All authors gave final approval for publication and agreed to be held accountable for the work performed therein.

Conflict of interest declaration

We declare we have no competing interests.

Funding

This work was supported by the Royal Society University Research Fellowship (grant no. URF\R1\191033).

Acknowledgements

We thank the animal technicians for their valued contributions to spider husbandry. For help with experimental set-ups, we thank John Hogg. For valuable discussions of the work, we thank Fritz Vollrath and Graham Taylor.

Footnotes

Electronic Supplementary Material is available online at https://doi.org/10.6084/m9.figshare.c.6823914.

Chapter 5

Frequency, time, and amplitude differences across the spider body and their role in substrate-borne vibration sensing

Thomas E. Miller[1], Jun Wu[1], Alice Cicirello[2], Graham K. Taylor[1] and Beth Mortimer[1]

Abstract

Substrate-borne vibration sensing is an important sensory modality in spiders. Due to the distributed and embedded nature of spider mechanosensors, vibration sensing is subject to mechanical filtering by the spider's legs and body. The dynamic properties of spider morphology must therefore play an important role in modulating information flow for vibration sensing. A key task utilising vibration sensing is the localisation of biologically relevant vibration sources, for example prey or conspecifics. Behavioural trials involving mechanosensor ablation have demonstrated that these organs are important for vibration source localisation, but the mechanisms of source localisation remain unknown. Here, we apply what is known about the sensitivity of spider mechanosensors to a laser vibrometry dataset quantifying the spider's mechanical response to vibrational input at 50 sampling points across its legs and body. We investigate whether frequency, time and amplitude comparisons between different mechanosensor locations could be used for source localisation by combining these empirical results with simulations from a calibrated mathematical model of the tarantula. We show that the spider is unlikely to use the observed frequency and time differences owing to physiological constraints on mechanosensor sensitivity, but that comparison of joint bending amplitude and potentially strain direction between segments may be sufficient for source localisation.

1 Introduction

Substrate-borne vibrations are ubiquitous in the environment and are an important information source for animals – particularly arthropods, in which substrate-borne vibration sensing is an ancient and basal modality (Hill et al., 2019, Cocroft and Rodríguez, 2005). Within arthropods, spiders are excellent model organisms for studying vibration sensing (Barth, 2021). They are highly sensitive to vibrations and for most species this is their primary sensory modality, using vibrations to detect prey (Klarner and Barth, 1982, Landolfa and Barth, 1996, Masters, 1984b), to assess environmental variables (Masters, 1984b), and for conspecific communication during courtship (Schuch and Barth, 1985, Schuch and Barth, 1990, Elias et al., 2005, Elias et al., 2003). These vibrations are detected as cuticular strains by mechanosensors embedded within the exoskeleton (Blickhan et al., 2021).

Despite being found in a diverse range of habitats, and employing many different hunting strategies, all spiders share the same basic body plan and underlying mechanosensory apparatus. Their mechanosensors, called slit sensilla, consist of a slit in the cuticle spanned by a flexible outer and inner membrane innervated by sensory neurons that are stimulated by transverse compression of the slit (Barth et al., 1984). Slit sensilla are distributed widely across the spider's legs and body, but their locations are broadly conserved, except in very small species (Miller et al., 2022, Barth and Libera, 1970, Ganske and Uhl, 2018, Kropf, 1998, Seo et al., 2020, Vogel, 1923). As well as single slits, slit sensilla can be found in loose groups and discrete structures called lyriform organs, which are typically located close to the joints between leg segments. Lyriform organs are highly sensitive to cuticular strains, with threshold displacements at the nanometre level. The metatarsal lyriform organ, HS10, is thought to be particularly important for detecting externally generated vibrations and is stimulated by deflections in both a lateral and dorsoventral direction (Barth and Geethabali, 1982). Other lyriform organs, such as HS8, have been implicated in proprioception and kinaesthetic orientation (Seyfarth and Barth, 1972, Barth and Bohnenberger, 1978, Bohnenberger, 1981).

The sensitivity and threshold curves of these mechanosensors have been heavily studied in the wandering spider *Cupiennius salei* (Barth and Bohnenberger, 1978, Barth and Geethabali, 1982, Gingl et al., 2006, Speck and Barth, 1982, Barth, 2021). Whilst there is some evidence for crude frequency filtering at the central nervous system level (Speckhergenroder and Barth, 1987), most processing takes place before mechanotransduction through mechanical filtering. The lyriform organs of *Cupiennius* are more sensitive to high-frequency vibrations above 40Hz, but other than this high-pass property they show no tuning to any narrow frequency range (Barth and Geethabali, 1982, Bohnenberger, 1981). A cuticular pad is responsible for transmitting deflections across the tarsus/metatarsus joint and filtering out low-frequency vibrations before they reach the metatarsal lyriform organ (McConney et al., 2007). Whilst the tuning curve of individual slits within an organ can vary, this tends to be at very low frequencies (<10Hz) (Barth and Geethabali, 1982). The single slits show a similar broad threshold curve, although the threshold displacements can be two orders of magnitude higher than the lyriform organs – thus, they possess a lower sensitivity (Speck and Barth, 1982). The similarity of these threshold curves to the few other species of spider for which intracellular electrophysiological recordings have been made (including *Zygiella*, despite this orb-weaver having a completely different hunting strategy and substrate) indicates that the properties of the mechanosensors may be broadly conserved across spiders (Barth and Geethabali, 1982, Liesenfeld, 1961).

The displacement detected at the mechanosensor is a reflection both of exteroception and body dynamics, as the biomechanical parameters of the spider's body (for example mass, stiffness/damping of joint segments, and overall geometry – and by extension variation in biological traits that affect these parameters), have the potential to influence vibration transmission through the body (Miller and Mortimer, 2020, Wu et al., 2023). For example, joint stiffness directly contributes to the high-pass properties of lyriform organs in *Cupiennius* and tarantulas (Blickhan, 1986). Therefore, it is important to consider the natural frequencies and the mode shapes of the spider body in response to vibrational input. The natural frequencies are the frequencies at which a system

resonates, and the corresponding mode shape at each natural frequency is the relative displacement of each element in a system representing the deformed shape as it resonates.

In theory, comparison of the frequency content between different body segments could provide information about the location of the source relative to the body. This phenomenon, where different frequencies are spatially mapped onto different mechanosensor locations, is known as tonotopy, and has been implicated in sensory systems involved in acoustic hearing such as the katydid ear (Montealegre-Z et al., 2012). In this system, dispersive wave propagation leads to the segregation of different frequencies across the basilar membrane in the inner ear. In a similar way, mechanical filtering either at the mechanosensor level or the whole-body level could fraction the frequency content of a given input signal to allow comparison of the frequencies detected at different mechanosensor locations for source localisation.

Another potential mechanism of source localisation is comparison of amplitude differences between measurement points, which are modulated by the rate of energy loss of the source wave as it passes through both environmental substrates and the spider body. Amplitude differences in the vertical displacement of different body segments are encoded in mechanosensors by the magnitude of joint bending, the mechanism through which is well-understood in *Cupiennius*. The lyriform organs are composed of multiple slits of varying length, which differ in mechanical sensitivity. As the entire organ is subjected to increasing cuticular deformation, the widest/longest slits are compressed and stimulated first, followed successively by the smaller slits. This implies that there is fractionation of the mechanical sensitivity of the whole organ, with the most sensitive slits responding to very small displacements and the least sensitive slits only stimulated by large displacements (Schaber et al., 2012).

Time delays between the motion of different body segments (particularly on opposite sides of the body) can also theoretically provide information about source angle, distance and wavespeed (Barth, 1993). Interaural delays are important for acoustic

hearing in many arthropods but have been comparatively understudied in the context of mechanosensor position in vibration sensing (Hartbauer and Römer, 2014). The most important factors here are wavespeed, which largely depends on the material properties of the spider's chosen substrate, and the distance between mechanosensors, which is constrained by the size of the animal. A facet that has been overlooked in previous studies focusing only on behaviour or individual mechanosensor response is that motion of each body segment is dependent not only on external excitation, but also the natural frequencies and mode shapes of the spider body. Therefore, the assumption that spiders can use a time of arrival difference in mechanosensor stimulation for source localisation may only be valid for the distal leg tips in direct contact with the substrate (Barth, 1993). In addition, real animals are constrained by the physiological limits of their nervous system when these delays are very small. In *Cupiennius*, behavioural trials have shown that the physiological limit to detection is a delay of around 4ms between the left and right sides of the body (Hergenroder and Barth, 1983, Barth, 1993, Wirth, 1984). For the tarantula *Grammostola pulchra*, any time delays across the distal tips of the legs are probably at the limit of what is physiologically detectable (a 3.5ms difference at the tarsus with a 7cm leg span, assuming a wavespeed of 20m/s).

Most previous research has focused on the preceding stage of vibration transmission through substrates, in particular spider webs. The sensitivity and threshold curves of individual mechanosensors is also well-understood. The effect that the dynamics of the spider body has on the important stage of transmission between substrate and mechanosensor, however, is relatively unknown – and the dynamics of an untethered spider may differ substantially from spiders mounted for measurements. It is also unknown how the spider uses the dynamic response of its body to vibrational input for computing source location, and which parameters are most important when making comparisons between mechanosensor measurements at different locations across the body.

The role of the spider body in vibration sensing is also implicitly linked with the concept of morphological computation, where information processing may be outsourced to

morphology instead of the central nervous system (CNS). Mechanical filtering, for example by the cuticular pad, can be considered morphological computation if it reduces the level of potential energy expenditure in the CNS. In the context of vibration sensing, evidence for morphological computation is mostly limited to discrete morphological structures, but there is increasing recognition of the role of the whole body as a vibration transmission platform, and the potential for spiders to control transmission dynamics actively through behaviour such as changing posture (Miller and Mortimer, 2020).

It is clear, therefore, that a more detailed investigation of the dynamics of vibration transmission through spiders in a natural posture is crucial for understanding the underlying mechanisms of vibration source localisation. The aim of this study is to investigate different dynamic scenarios using experimental measurements and modelling, to make broad inferences about the relative importance of parameters involved in spider vibration sensing. Wu et al (Wu et al., 2023) measured velocities across the complete legs and body of an untethered tarantula spider (*Grammostola pulchra*) in its natural posture using non-contact laser vibrometry, and used these measurements to estimate the mode shapes of the body and conduct parametric tests using a simplified mass-spring-damper model. Here, we use an extended version of this dataset to investigate whether frequency, time or amplitude differences between body segments can be used for vibration source localisation and combine these results with simulations from a calibrated model of the spider to investigate the most relevant cues for source localisation. Little data exists that specifically deals with the threshold curves and sensitivity of tarantula slit sensilla – but we can apply what is known about other spiders such as *Cupiennius* (also a sit and wait terrestrial hunter) to the tarantula system due to the broadly conserved properties of spider mechanosensors (Barth, 2002b). By measuring the motion of the entire system under vibrational input, we can compare the relative motion of each measurement point and therefore infer the overall pattern of mechanosensor stimulation across the body of the spider.

2 Methods

2.1 Experimental setup

We used a specimen of *Grammostola pulchra* Mello-Leitão, 1921 from our captive lab population. The spiders were kept in plastic terrariums with a coir substrate and fed with crickets twice weekly, in a temperature-controlled room set at 20°C with a 12-hour day/night cycle. *G. pulchra* is native to Southern Brazil and is ground-dwelling. They have a calm temperament which made them convenient for use in these experiments. We measured the mass of the spider using an Ohaus Pioneer mass balance and photographed the spider on the day of the experiment. Photos from three angles were used to produce a 3D skeleton of the spider's body, which was later used for animation of the mode shapes (Wu et al., 2023).

The vibration stage consisted of a circular aluminium plate attached directly to the shaker (Modal Shop K2004E01) using a threaded bolt. We measured the motion of this plate using an accelerometer (PCB 352A21) attached to the bottom of the aluminium plate. The dimensions of the plate were chosen to avoid resonances at lower frequencies which would influence the response of the spider body, and this was verified by measuring the response of the plate without the spider present.

The aluminium plate was driven by a square wave input in the vertical axis generated with a signal generator (Polytec Scanning Vibrometer Software 8.51 Manual). This pulse/impact input was chosen for three reasons – the regular occurrence of this signal type in a biological context, the broadband excitation of frequencies in the biologically relevant range (up to 1000Hz), and the fact that it did not elicit a behavioural response in the spider.

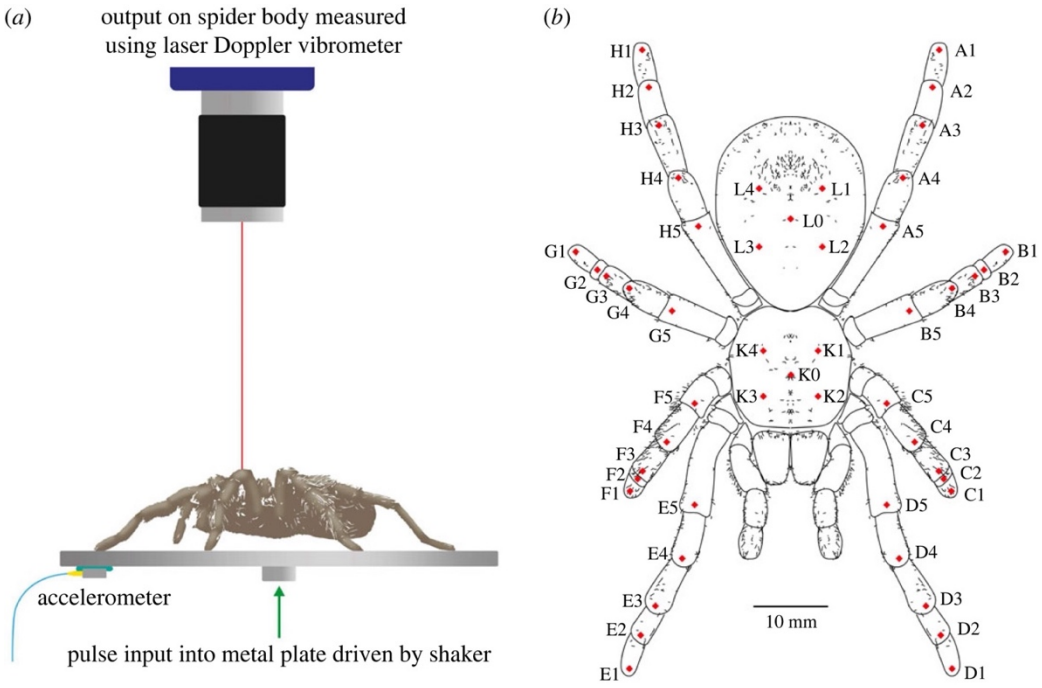


Figure 1. Experiment: (a) set-up; (b) vertical measurement points on the spider. This figure is used for illustration of all the measurement points, given by the red dots in (b). Note the posture shown here is not the same as the test. During experiments, spiders were not anaesthetized or tethered but a tube was used to enclose the spider and prevent escape from the arena. Reproduced from Wu et al (Wu et al., 2023) under CC BY 4.0 License for open access publications in Journal of the Royal Society Interface.

The spider was guided towards the centre of the aluminium plate using forceps and left to acclimatise. The spider was not tethered or restrained in any way. If the spider moved, it was encouraged back to the centre using the forceps. After the spider had assumed a relaxed posture for around 10 minutes, the test was performed. During the dynamic test, the spider's posture was approximately bilaterally symmetrical, but from front to back legs there were differences in posture – in particular, the front legs were more retracted during the test. If the spider moved, the experiment was restarted, until a full set of measurements could be taken since the spider needed to remain still for the entirety of data collection.

A laser Doppler vibrometer (Polytec VibroOne) was used to measure the velocity of the spider's body in the vertical axis in response to vibrational input. Recordings were taken in the time domain with a total length of 1.28s. Our sampling frequency was 25.6kHz. We focused the laser on 50 pre-determined vertical points on the spider's body, which are illustrated in Figure 1. Measurements were not taken from the trochanter and coxa as these were obscured when the spider was in its natural posture. The laser was focused directly onto the cuticle of the spider without any reflective material attached to the body. The motion measured by the laser vibrometer is the vertical motion of the measurement point relative to the device. Since the measurement point was not fixed relative to the spider body, we consider it a floating reference frame. This technique adequately captures the dynamics of the spider body in the vertical axis, but there is the potential for measurement error caused by motion of body segments in the horizontal axis. We assume that these displacements are minor relative to motion in the vertical axis due to the pulse input being confined to the vertical axis.

We generated the pulse input three times after focusing the laser on each measurement point, taking a new recording each time. After three repeats were taken for each measurement point, we moved the laser vibrometer to the next point and repeated the process until data was collected from all 50 points.

The coherence between two signals is a real-valued function that is obtained from the ratio of the magnitude squared of the cross-spectral density between the two signals, and the product of auto-spectral density of each signal. In an ideal linear time invariant (i.e. with constant parameters) system with a single input and single output, the coherence would be close to 1, therefore enabling us to accurately capture the complete system dynamics. The coherence is equal to zero when the input and output are completely unrelated. Values of coherence between 0 and 1 could be caused by: inherent presence of measurement noise; the presence of other unmeasured inputs producing the output; nonlinearities in the relationships between input and output. Moreover, it is expected that in the presence of anti-resonances there will be a low coherence value. Therefore, recordings with low coherence were discarded. It was

verified that the coherence of the retained measurements was mostly above 0.9 in the frequency range of interest, although a few leg segments, and the abdomen showed slightly lower coherence – these segments are however retained in the graphs for comparison. See Appendix 4 – Supplementary figure 1 for coherence graphs of each repeat.

2.2 Data analysis and modelling

We used the vibrometer measurement of the spider's body as our output response. We used the accelerometer measurement of the aluminium plate as our input data due to the difficulty of mounting a second vibrometer in the vertical axis. A Tukey window with a cosine taper of 10% was applied to the input and output data in the time domain, to smooth the start and end of the recording to zero whilst preserving the amplitude of the signal for the duration of the input pulse. The data was then converted to the frequency domain using a discrete Fourier transform (DFT). A frequency response function (FRF), expressing the magnitude and phase of the output DFT relative to the input DFT, was calculated for each point on the spider using the modalfrf function in Matlab. We then took the mean of the FRFs of each of the three repeats for each point to calculate a single average FRF. While time averaging improves the signal-to-noise ratio, frequency domain averaging only reduces the variance of the estimates. Averaging is performed in the frequency domain because in this particular application, it is difficult to create identical impulses in time domain. For 3 out of the 50 measurement points, the input accelerometer measurement in one of the repeats was unusable due to equipment error, resulting in a very low coherence, so the average FRF was calculated by taking the mean of the other two repeats.

The disadvantage of a pulse input in terms of FRF analysis is that all frequencies are excited simultaneously, so the measured response of the spider body at a particular frequency is the response to that frequency and any superimposed harmonics associated with lower frequencies. This means that, harmonic content which might arise from nonlinearity would not be discernible. However, given the coherence values

achieved and the low amplitude of the pulse it is reasonable to assume that the relationship between input and output is linear over the frequency range considered and any nonlinear effects caused by time-variation in the spider model parameters (e.g. variation in leg rigidity caused by muscle contraction) will be negligible.

An important property that is also displayed in some symmetrical nonlinear systems is reciprocity (Worden and Tomlinson, 2001). This means that we could assume that the reciprocity property would hold (i.e. the input at the degree of freedom (DoF) **p** produces a output at the DoF **q**, that is the same as the output at DoF **p** caused by the same input applied at DoF **q**). If reciprocity holds, by definition the stiffness matrix of the system will be symmetric, and also the FRF matrix will be symmetric. During the experiment, we judged the spider's posture to be approximately bilaterally symmetrical, so we assumed that the average FRFs obtained for measurement points on symmetrical leg segment pairs would retain bilaterally symmetrical properties. As a result of this assumption, the FRFs obtained for symmetrical leg segment pairs could be exploited to highlight inherent differences in response that would enable the spider to locate the vibration source.

To quantify differences in the frequency response between measurement points, we calculated the mean squared error (MSE) of the average FRFs obtained at each bilateral pair of legs (e.g. lr1/rr1), between the tarsus of each leg and all other segments, between the cephalothorax and all other segments in each leg, and between adjacent segments in each leg (Supplementary table 1). With this global metric, the lower the MSE, the greater the degree of similarity between the FRFs. We reproduce the full MSE values in the Supplementary Material (Appendix 4 – Supplementary table 1).

Wu et al (Wu et al., 2023) used a version of this dataset consisting of only one repeat (without taking an average) of a transfer function between the voltage input and the vibrometer output to calibrate a simple 11 DOF mass-spring-damper model of the spider body, in order to probe variables influencing vibration sensing through parametric tests (Figure 2). The model was constructed in Matlab using Simulink. Full details of this

method are given in that study, but in brief – a PolyMAX algorithm was first used to identify the natural frequencies of the entire spider system from our 50 measured points across the body. In total, five natural frequencies were identified – at 31.75Hz, 37.65Hz, 74.15Hz, 108.43Hz and 137.41Hz. Then, the natural frequencies and damping ratios of the model were calibrated to the real system, whilst also attempting to ensure that the mode shapes and FRFs showed a satisfactory match. A limitation of our method is that we were not able to apply a sinusoidal input closer or exactly at these calculated natural frequencies to the real spider to validate them, because persistent stimuli invoked a behavioural response.

Here, we use the same model (Wu et al., 2023) to investigate frequency, amplitude and time differences between body and legs, particularly on opposite sides of the animal. This cannot be probed using the vibrometry experimental data as the input into all eight legs was equal. In a natural setting, a point vibration source will lead to asymmetries in the response across the body, depending on the location of the input relative to the spider. We therefore applied a pulse input at five angles to the model (0°, 45°, 90°, 135° and 180°, at a distance of 0.2m, on the left side of the body only due to bilateral symmetry). A wavespeed of 20m/s was chosen as this is a good approximation of the wavespeed through typical substrates that the spider might use, such as vegetation or dry soil (Barth, 1993). Since the model has only 11 degrees of freedom, with each leg modelled as a single mass-spring-damper element, we were unable to use the model to probe differences between leg segments within the same leg. We examined the response of each model element in the time domain and frequency domain. To calculate amplitude ratios across opposite sides of the body, we used a peak finding algorithm to identify the maximum amplitude of the simulated response of each leg in the time domain.

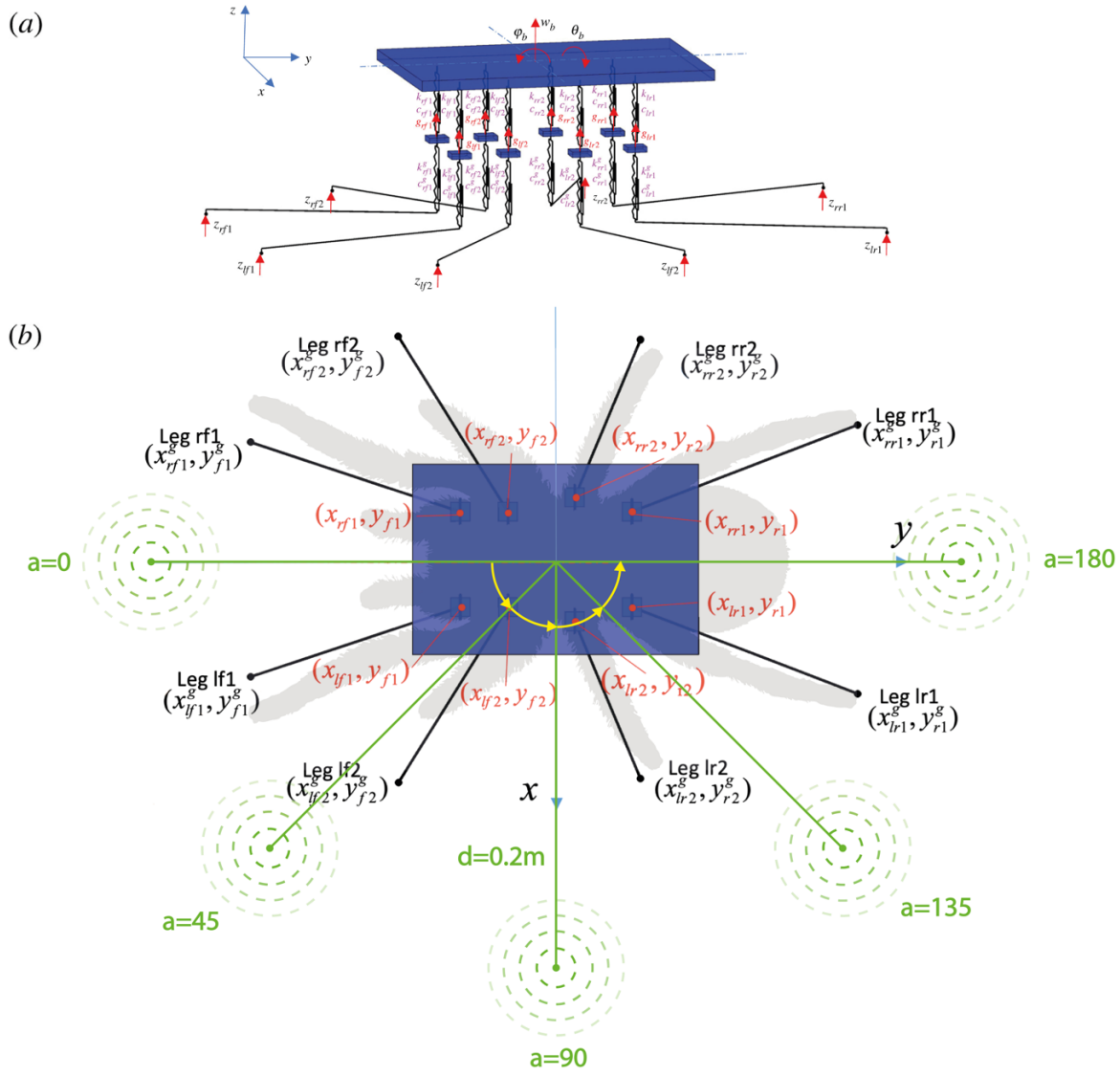


Figure 2. The lumped parameter spider model (a) schematic view; (b) top view of the model with pulse vibration source locations, angle to y-axis 0, 45, 90, 135 and 180 degrees. Distance from source to body 0.2m – diagram not to scale. Adapted from Wu et al (Wu et al., 2023) under CC BY 4.0 License for open access publications in Journal of the Royal Society Interface.

3 Results

3.1 Experimental response

In terms of assessing the motion of the cephalothorax relative to the leg segments, the results show that the characteristics of the FRFs at different frequency ranges are similar for all legs (Figure 3). Below 20Hz, the FRFs for all segments are dominated by noise and are therefore not considered. Between 20Hz and 80Hz, the magnitude of the response of most leg segments is similar. There is probably limited joint bending taking place as the relative motion between leg segments is low. In this range, the magnitude of the FRFs for the cephalothorax, abdomen and proximal leg segments is greater than the distal leg segments.

In contrast, above 80Hz there is a sudden decline in the magnitude of the response in the proximal leg segments, cephalothorax and abdomen, with the response falling below the magnitude of the distal leg segments – the opposite of the pattern observed in the 20-80Hz range. This drop-off is associated with the third mode of the spider body (Wu et al., 2023). Due to some asymmetry in the rearmost legs, the tibia, patella and femur of lr1 and lr2 do not follow this pattern, with their motion being more similar to the abdomen in that there is a decline after the peak associated with the first/second mode.

The FRFs indicate that the proximal leg segments (patella, femur), cephalothorax and abdomen are vibrating at a much lower amplitude than the distal leg segments at the same frequencies. In addition, the phase of the abdomen and cephalothorax decreases above 80 Hz, indicating that at these higher frequencies, the motion of these segments is out of phase with the distal leg segments (figure 4). This will lead to increased joint bending above this range, particularly in the proximal leg segments near the attachment to the cephalothorax.

By calculating the Mean Standard Error (MSE), we quantified the expected variation in FRFs between symmetrical leg segment pairs (based on the a priori assumption that if the spider's posture and each measurement point was perfectly symmetrical, then the MSE would be 0), enabling us to highlight inherent differences in response due to biomechanical parameters that are outside this expected level of variation.

The MSE results indicate that we are limited to comparison of the relative motion of the cephalothorax/abdomen and the rest of the leg as a whole unit, which is reflected in our decision to model the legs of the spider body as a single mass-spring-damper element. For all legs, the MSE between most of the adjacent leg segments is in the same range or even lower than the left/right comparison (except for the asymmetries in the rear leg pairs as described previously). This indicates that the expected variation is greater than any inherent differences in the FRFs between adjacent segments.

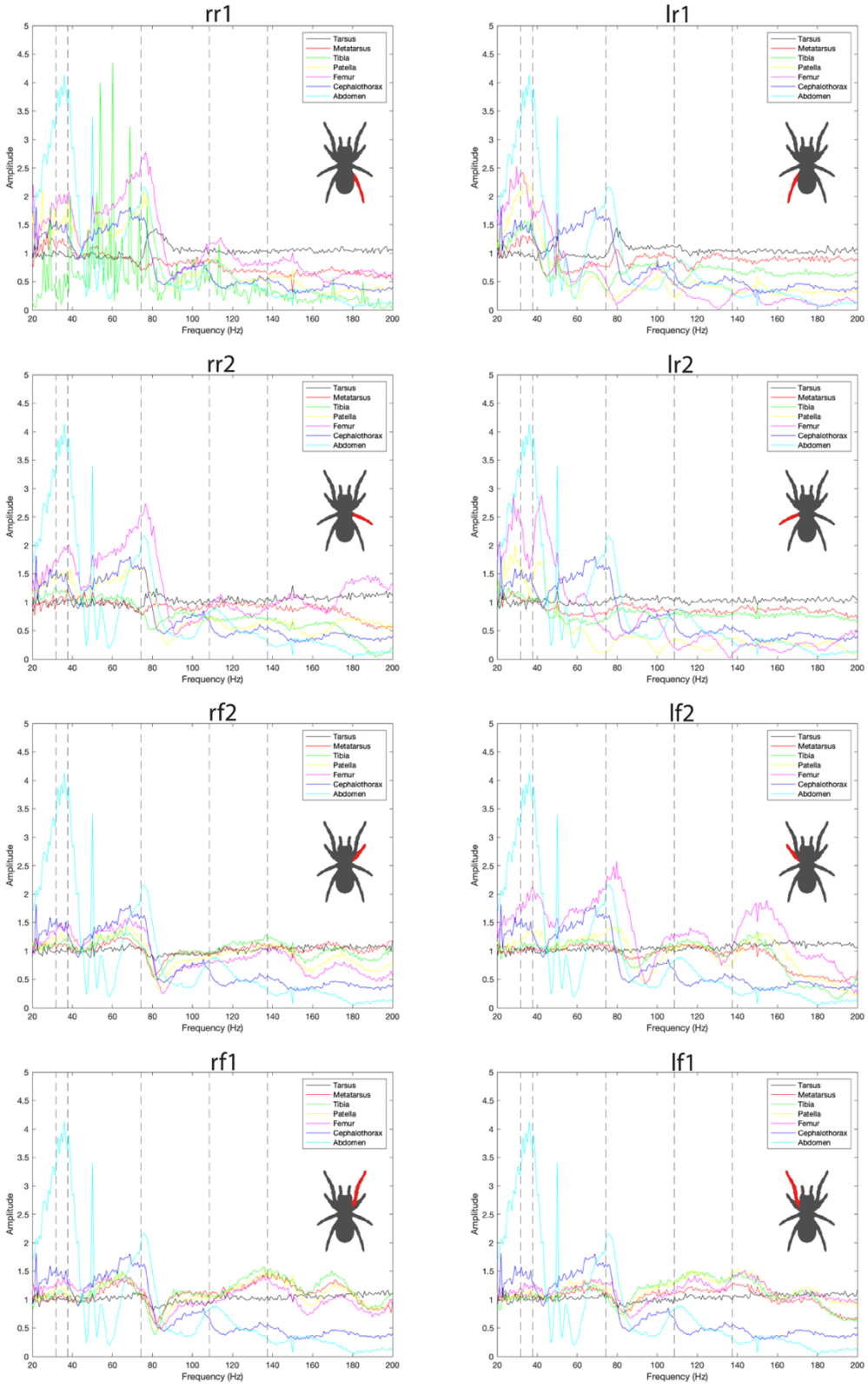


Figure 3. Magnitude of average FRFs for legs rr1, rr2, rf2, rf1, lr1, lr2, lf2 and lf1 calculated from the modal test in the range 20-200 Hz. Cephalothorax and abdomen plotted over each graph. Vertical dashed lines indicate the five modes of the spider body.

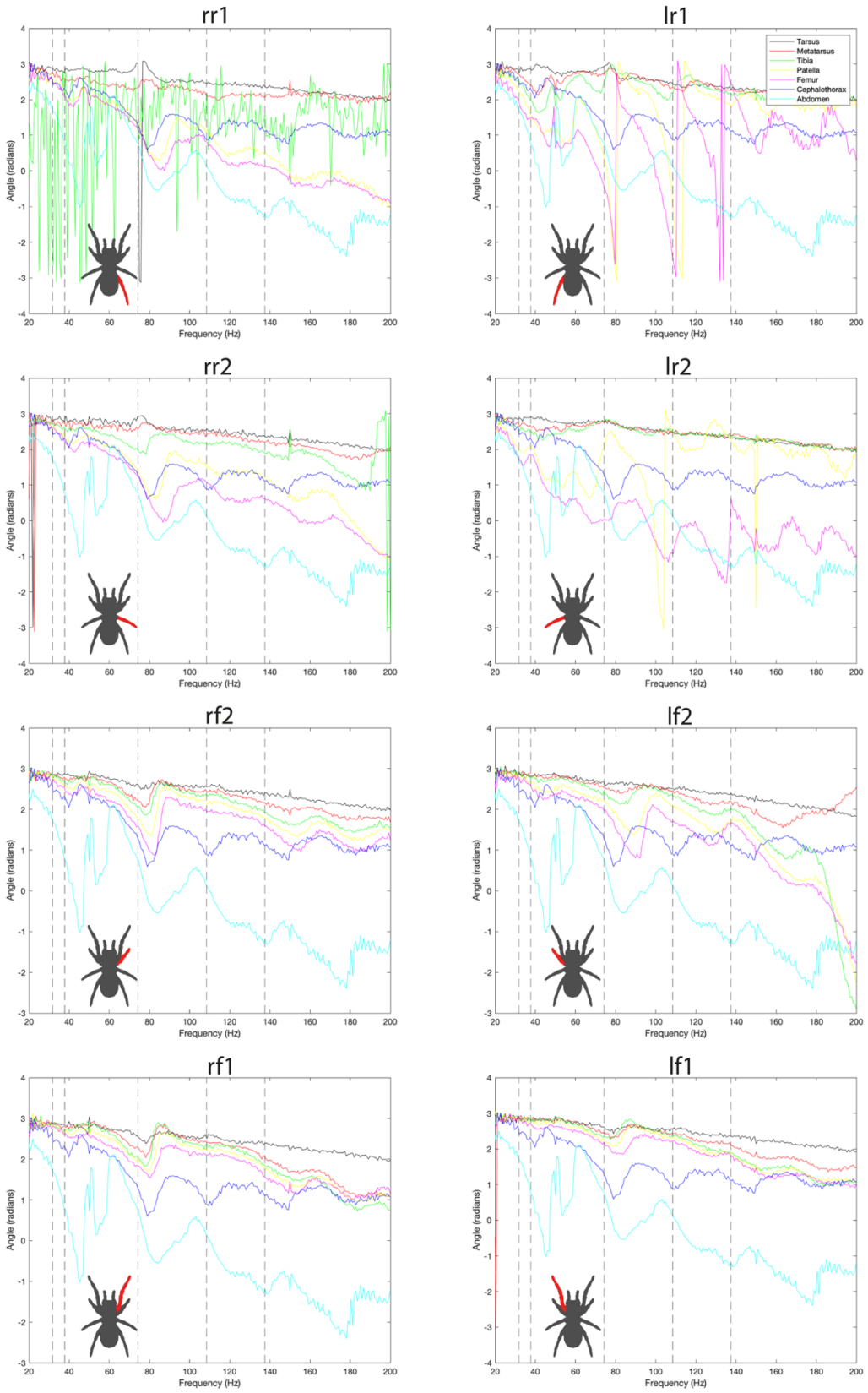


Figure 4. Phase of average FRFs for legs rr1, rr2, rf2, rf1, lr1, lr2, lf2 and lf1 calculated from the modal test in the range 20-200 Hz. Cephalothorax and abdomen plotted over each graph. Vertical dashed lines indicate the five modes of the spider body.

As expected, there is more of a difference in the FRFs between the cephalothorax/abdomen and distal leg segments than there is in symmetrical left/right leg segment pairs. For the front two pairs of legs (lf1/rf1 and lf2/rf2), the MSE between equivalent left/right leg segments is consistently an order of magnitude lower than between the cephalothorax and all the leg segments apart from an asymmetry in the FRFs of the femur. For the rear two leg pairs (lr2/rr2 and lr1/rr1) there is a much greater degree of bilateral asymmetry across most leg segments, meaning that we are less confident in assessing differences in the FRFs for these legs. Overall, however, the MSE between the cephalothorax and the distal leg segments (tarsus/metatarsus) for the rearmost two leg pairs is still higher than the left/right comparison for these same segments, indicating that we can still usefully interpret differences in the FRFs. A possible reason for these asymmetries could be poor coherence (<0.6) at some measurement points, indicating more noise and/or nonlinearity between the input and the output, e.g. in the tibia of rr1, and possibly the patella and femur in lr1. A different reason for this asymmetry could be low repeatability of the measurement point caused by the floating measurement point in the laser vibrometry technique.

3.2 Simulated response

The MSE results justify the decision to model each leg as a single element, as we lack the resolution required to probe small differences in the FRFs between adjacent leg segments and use this to calibrate the model.

To test whether frequency segregation is a method that spiders use for source localisation, we first investigated the simulated response in the frequency domain. The simulated FRFs reveal the natural frequencies and mode shapes of the spider body predominantly excited for each source angle. The results indicate that the magnitude of the response of each body segment varies with source angle, particularly in the extent to which different natural frequencies are excited. When the source angle is at 0°, the FRFs of legs rf1 and lf1 are dominated by the third mode, whilst the amplitude of the first/second modes is greatly reduced. When the angle is at 180°, the opposite is

observed, with the FRFs being dominated by the first/second modes. At 45°, 90°, and 135°, where the input angle is off to one side, a roll motion is excited, and the response is bilaterally asymmetrical. This is most apparent in the middle legs rf2, lf2, rr2 and lr2, where the amplitude of the fourth and fifth modes are dominant on the left side of the body (the same side as the source).

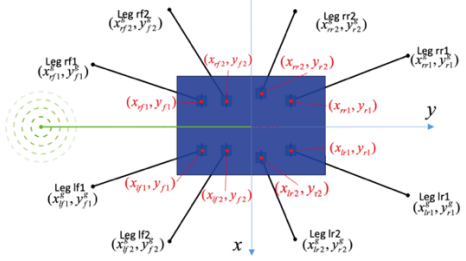
The influence of source angle on the frequency response can be explained by considering the mode shape of each natural frequency. The first/second modes are dominated by forward pitching of the cephalothorax, which can either be in or out of phase with the legs. The third mode is dominated by whole-body upward bounce. The fourth/fifth modes are dominated by leg bounce with reduced cephalothorax movement. When the source is in front of the spider (angle=0°) any forward pitching motion is counteracted by the direction of the input vibration, instead leading to whole-body bounce. When the source is directly behind (angle=180°), forward pitching is accentuated. The bilateral asymmetries in the middle legs at angles 45°, 90°, and 135° lead to increased excitation of the fourth/fifth modes due to the roll motion of the body having more of an influence on the motion of these legs when compared to the outer four legs. This shows that source angle is important for modulating the dynamic response of the spider and hence patterns of joint bending across the body.

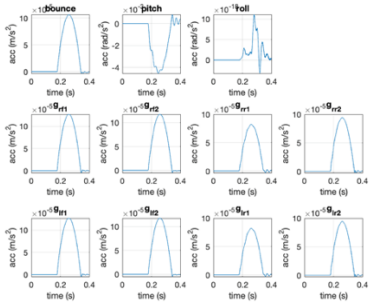
Figure 5. Expanded results of our simulation in the time domain and frequency domain. Each model element is shown in a separate graph, along with the pitch, roll and bounce of the central cephalothorax element.

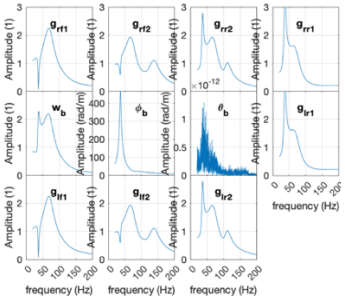
Time domain

FRF

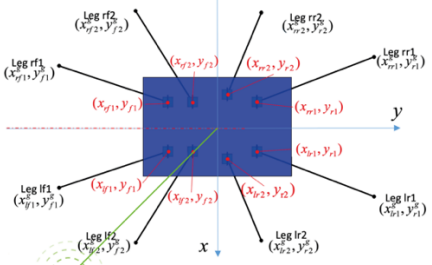
a=0

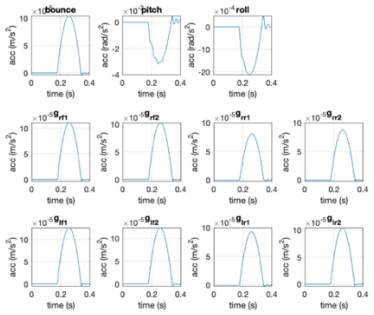


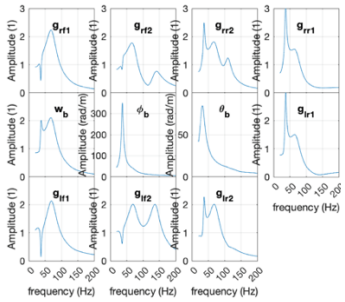




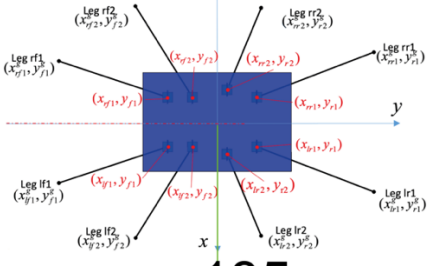
a=45

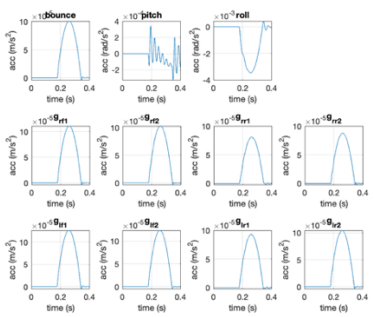


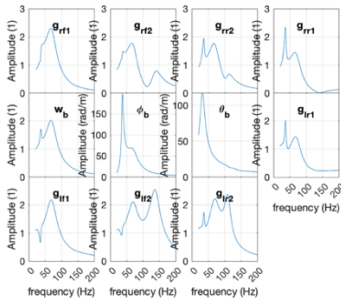




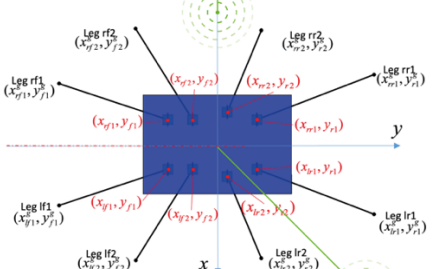
a=90

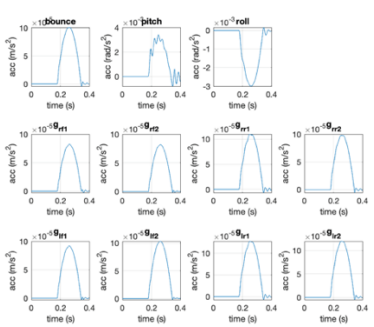


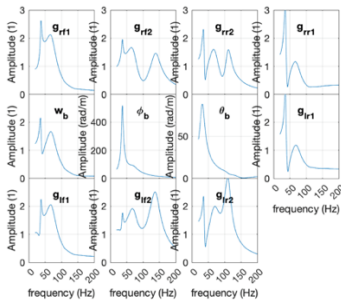




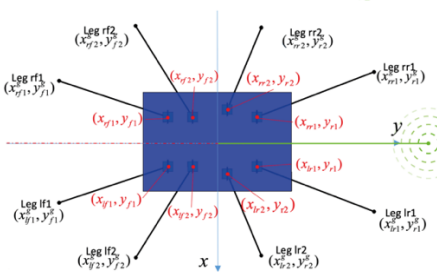
a=135

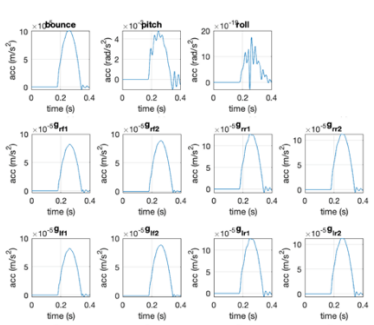


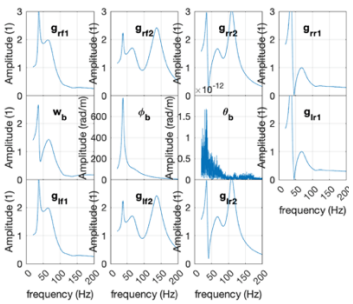




a=180







Varying source angle does not generate substantial time delays in the response between legs or body at a wavespeed of 20m/s (figure 5, 6). The curve of the vertical displacement of each model segment is almost exactly in phase throughout the duration of motion, and the associated time delays are too small to be physiologically detectable (<3ms). The vertical bounce of the legs is out of phase with the pitch/roll of the cephalothorax depending on the source location, which could indicate that there is more joint bending at the distal segments of the leg (trochanter/coxa) at certain input angles (figure 5).

Amplitude ratios differ between legs on opposite sides of the spider body relative to the source location. When varying source angle, the responses of the legs closest to the source always have a higher amplitude than those on the opposite side of the body (figure 5, 6; table 2). Correspondingly, the amplitude ratios between leg pairs parallel to the source direction are significantly higher than leg pairs perpendicular to the source direction for all source angles simulated (Table 2). For example, when a=90°, the central left legs (lf2 and lr2) are closest to the source. The maximum amplitude ratio between these legs and the opposite legs on the right side of the body is 1.3335 (for leg pair lf2/rf2). In contrast, the maximum amplitude ratios within leg pairs on the left and right side of the spider body are 1.0655 and 1.0553 respectively.

The amplitude ratios of the substrate motion at the substrate-leg coupling point are also given in Table 2. Comparing these to the amplitude ratios of the leg response, in most cases the amplitude ratio of the legs is slightly lower (marked in red) except for four leg pairs where it is slightly higher (marked in green). Overall, the amplitude ratios are similar between substrate and legs.

We then tested whether amplitude ratio differs when varying source distance. Our simulations showed that at biologically relevant spatial scales for vibration sensing (up to 1m distance from source to spider model), amplitude ratio does not significantly change with source distance. This is true for all simulated source angles (Table 3).

We have assumed here that increased vertical displacement of each leg element in our simulation is correlated with an increase in the relative motion of individual segments, leading to higher joint bending magnitude and hence mechanosensor stimulation in the real spider. This is a level of detail which is not captured in our simple model but is supported by evidence from the experimental FRFs of each leg segment.

Table 2. Peak amplitude rations of leg and substrate motion between selected leg pairs at different source angles.

	Source angle (degrees)				
Leg pair	**0°**	**45°**	**90°**	**135°**	**180°**
Opposite sides of body to source angle	 **lf1/lr1 rf1/rr1** *Leg* 1.5394 *Substrate* 1.5553	 **lf1/rr1** *Leg* 1.5563 *Substrate* 1.5531	 **lf2/rf2** *Leg* 1.3335 *Substrate* 1.3820	 **lr1/rf1** *Leg* 1.5499 *Substrate* 1.5552	 **lr1/lf1 rr1/rf1** *Leg* 1.5491 *Substrate* 1.5527
	 **lf2/lr2 rf2/rr2** *Leg* 1.2475 *Substrate* 1.1907	 **lf2/rr2** *Leg* 1.4045 *Substrate* 1.4235	 **lr2/rr2** *Leg* 1.3028 *Substrate* 1.3754	 **lr2/rf2** *Leg* 1.4664 *Substrate* 1.4200	 **lr2/lf2 rr2/rf2** *Leg* 1.2651 *Substrate* 1.1918

Perpendicular to source angle	1 (bilateral symmetry)	 **rf1/lr1** *Leg* 1.1823 *Substrate* 1.1994	 **rf1/rf2** *Leg* 1.0553 *Substrate* 1.0669	 **rr1/lf1** *Leg* 1.1934 *Substrate* 1.1967	1 (bilateral symmetry)
		 **lr2/rf2** *Leg* 1.0211 *Substrate* 1.1130	 **lf2/lf1** *Leg* 1.0655 *Substrate* 1.0945	 **lf2/rr2** *Leg* 1.0530 *Substrate* 1.1023	

Table 3. Simulated peak amplitude ratios between legs on opposite sides of the body varying source angle and distance. Legs used to calculate amplitude ratios were lf1/lr1 for a=0°, lf1/rr1 for a=45°, lr2/rr2 for a=90°, lr1/rf1 for a=135°, and lr1/lf1 for a=180°.

	Source angle (degrees)				
Source distance (m)	**0°**	**45°**	**90°**	**135°**	**180°**
0.05	1.51	1.53	1.28	1.52	1.51
0.1	1.54	1.55	1.30	1.54	1.54
0.15	1.54	1.56	1.30	1.55	1.55
0.2	1.54	1.56	1.30	1.55	1.55
0.25	1.54	1.56	1.30	1.55	1.55
0.3	1.54	1.56	1.30	1.55	1.55
0.35	1.54	1.56	1.30	1.55	1.55
0.4	1.54	1.55	1.30	1.55	1.55
0.45	1.54	1.56	1.31	1.56	1.55
0.5	1.54	1.56	1.30	1.55	1.55
1	1.54	1.56	1.30	1.55	1.55

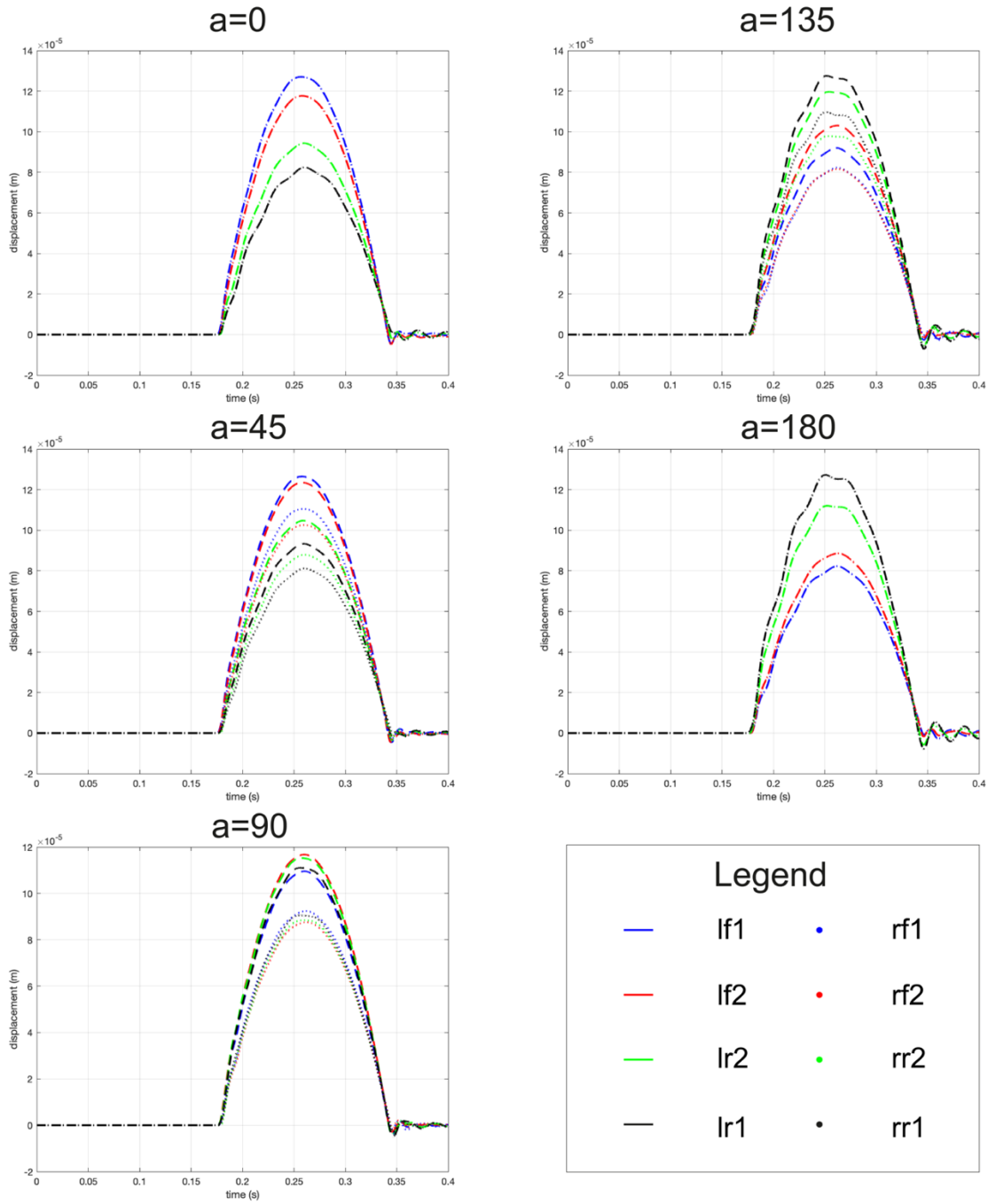


Figure 6. Time domain simulation of spider model legs in response to pulse input at source angle=0°,45°,90°,135° and 180° (collapsed version of figure 5). Legs on the left side of the body are plotted using a dashed line, legs on the right side of the body are plotted using a dotted line. Bilaterally symmetrical leg pairs on opposite sides of the body are plotted in the same colour. A combined dashed/dotted line indicates overlap of leg motion due to bilateral symmetry.

4 Discussion

Spiders such as tarantulas rely heavily on detection of substrate-borne vibrations for prey capture, predator avoidance and courtship. Therefore, vibration source localisation is one of the most important tasks that a spider's sensory system must accomplish. The embedded nature of spider mechanosensors means that the dynamics of the body in response to vibrational input are an intrinsic part of the mechanisms underlying source localisation. Our experiment isolated the effect of body dynamics from substrate dynamics on vibration sensing, enabling us to investigate fundamental questions about the role of morphology for source localisation. The frequency, amplitude and phase of the dynamic response are all parameters that could be potentially used by the spider to estimate source angle and distance, but our simulated results indicate that only comparison of amplitude differences across legs is likely to be used for localisation. The biological context in which each of these three parameters is used for source localisation and the implications for spider vibration sensing is discussed below (sections 4.1 and 4.2 respectively).

4.1 Biological relevance of frequency, amplitude and time delays

4.1.1 Frequency

Our results show that the frequency range that is least affected by intrinsic body dynamics in *Grammostola pulchra* is above 20Hz. Above 200Hz, the response is dominated by noise, which poses a discrimination issue for spiders sensing vibrations even though the mechanosensors possess a high sensitivity in this range. The absence of distinguishable resonant frequencies (i.e. high modal overlap) in this range means that it is unlikely that spiders can use mechanical resonance to amplify biologically relevant signals above 200Hz and aid detection of these signals. These results are comparable to those reported previously in the literature, which indicate limited mechanosensor sensitivity for frequencies below ~30Hz in *Cupiennius salei* (Barth and Geethabali, 1982), and body modes present at relatively low frequencies in *Latrodectus hesperus* (Mhatre,

2016). Whilst spider mechanosensors are theoretically capable of detecting very low frequencies (Bohnenberger, 1981, Barth and Geethabali, 1982), frequencies in this range are mainly generated by environmental noise such as wind, so may have less biological importance. This may explain, in an adaptive sense, why low frequencies are subjected to high-pass mechanical filtering by the cuticular pad (McConney et al., 2007).

The relative role of substrate dynamics and body dynamics on the frequency response varies at different frequency ranges. In the 20-80Hz range, the vertical bounce of the legs and cephalothorax are approximately in phase with the input. Above 80Hz, the cephalothorax bounce has a greater effect on overall body dynamics as it lags behind the legs and travels a shorter distance in the vertical axis, resulting in a different pattern of inter-segment motion and presumably stimulation of the lyriform organs. These are fundamental properties of the system and are therefore independent of variation in vibration input type and substrate dynamics, enabling these conclusions to be applied to a variety of biological contexts when *Grammostola* senses substrate-borne vibrations.

In terms of using frequency for source localisation, the simulated FRFs for each model element show that the magnitude of the peaks varies with source angle, so we conclude that the extent to which different modes are being excited is at least partially modulated by source angle. Whether the real spider can actually use frequency differences for source localisation is an open question. Previous research has shown that most spider mechanosensors are broadly tuned within the frequency range of interest (Barth and Geethabali, 1982, Bohnenberger, 1981, Speck and Barth, 1982). Therefore, we might expect that the mechanosensors will be stimulated by any cuticle strain in the frequency range of interest, regardless of whether the amplitude is greatest at the second mode or fourth mode for example. In contrast to Mhatre et al (Mhatre, 2016), we find no evidence in the tarantula body dynamics for mechanical tuning of the joints that might limit the frequencies detected by mechanosensors at each leg segment.

Previous studies using modelling have indicated that the lyriform organs are sensitive to the direction of strain (Hössl et al., 2006, Hössl et al., 2009), which would support the

argument that it is not frequency content per se that matters for source localisation, but rather the type of cuticle strain generated by the differing frequency response of each body segment, especially at the articulations between body and leg segments. We conclude that that the direction of strains, modulated by the excitation of different modes at different source angles, could potentially be used by the spider to estimate source angle, but that frequency segregation or tuning of individual body segments is unlikely to play a significant role.

4.1.2 Amplitude

In the time domain, the simulated vertical displacement of each model element shows that body dynamics are involved in generating an amplitude difference across the legs of the spider on opposite sides of the body. The amplitude ratios across opposite leg pairs vary with the angle of the source relative to the spider body, indicating that this parameter could be used by the spider to estimate source angle (Table 2).

The influence of the body versus substrate dynamics in generating this amplitude difference is shown in Table 2. The decay rate of the wave through the substrate is largely responsible for the observed amplitude ratios, as the amplitude ratios of the substrate at the leg/substrate coupling point are very similar (mostly slightly higher) to the amplitude ratios of the equivalent leg pairs. This indicates that the body dynamics do not dampen the substrate wave very much, but rather act to effectively transmit the input through the body to the mechanosensors. In some leg pairs the amplitude ratio of the leg motion is slightly higher than that of the substrate, indicating that in certain directions the body dynamics are responsible for amplifying the amplitude asymmetry in the substrate motion. This could be explained by the fact that the dynamic response of a single leg is a summation of the input into all the other legs, and each leg varies in the extent to which it influences the motion of the other model elements (Wu et al., 2023).

Varying source distance does not significantly change the simulated amplitude ratio between legs on opposite sides of the body. The absolute amplitude does vary with

source distance, but since the amplitude of the input source is not known by the spider, a small amplitude source cannot be differentiated from a more distant large amplitude source. Thus, we conclude that it is unlikely that spiders can use amplitude differences in vertical displacement to estimate source distance. It is possible that constraints on the distance through which substrate-borne vibration sensing operates in biological contexts (such as the heterogeneity of natural substrates and the small amplitude of source vibrations relative to noise) means that estimation of source distance is not important for successful prey capture in *Grammostola*.

4.1.3 Time delays

We found that the time delays between the vertical response of different body segments are likely too small to be physiologically detectable (<4ms) and thus the effect of body dynamics on this parameter is of limited use to the spider for source localisation. For time delays to enter the physiologically detectable range, wavespeeds would have to be low (below 10m/s) – since wavespeed is a parameter that is largely governed by the chosen substrate, we would not expect *G. pulchra* to be able to use this in a natural setting. Similarly, in a tarantula of this size, time of arrival differences at the distal tips of the legs are at the limit of what is physiologically detectable (a 3.5ms difference at the tarsus with a 7cm leg span, assuming a wavespeed of 20m/s). Comparison between mechanosensors closer to the cephalothorax will depend on the modal dynamics of the spider body rather than simply a time of arrival difference in the transmission of the vibrational wave.

Our model is limited in that it considers vertical motion only (due to the dynamic test measuring vertical motion) – however, transverse motion of the leg segments has also been shown to stimulate the mechanosensors (Barth and Geethabali, 1982). Therefore, it is possible that x, y, and z differences in non-vertical directions could be used for source localisation, but we argue that this is unlikely given how small the measured time delays are. Further research modelling motion in all three axes is likely needed to investigate this fully.

4.2 Implications for spider vibration sensing

Overall, our experimental and simulated results indicate that body dynamics in the vertical axis, modulated by morphological traits, play an important role in transmitting an asymmetrical response relative to the source that can therefore be used by the spider for source localisation. The results suggest that the magnitude and direction of strains detected by the mechanosensors, rather than time delays, are likely to be the most important cues used by tarantulas for vibration source localisation. Specifically, we found that these cues could potentially be used to estimate source angle. Interestingly, we were unable to identify any parameter that could be used to estimate source distance. This indicates that prey capture is only triggered when the source amplitude is over a certain threshold – i.e. within a couple body lengths of the spider, when the ambush is most likely to be successful. This coincides with what we know about tarantula predatory behaviour (Foelix, 2010, Pittella et al., 2023). Therefore, the most crucial stage is probably estimation of source angle and orientation towards the target before the tarantula begins moving towards the prey – which will usually be almost immediately encountered. Thus estimation of distances at a scale of many body lengths may simply not be relevant to the tarantula.

An interesting comparison can be made to web-building spiders, with an engineered substrate of the silk web that offers a degree of control over physical constraints. Since the capture area of the structure may be large relative to the body length of the spider (up to c. 30 body lengths in *Trichonephila*), source localisation becomes much more important to ensure timely and successful prey capture. The level of control provided by the web substrate means that vibration source localisation is a much more predictable task for web-building spiders when compared with terrestrial hunting spiders. In addition, web-building spiders may have more information at their disposal for source localisation than the tarantula does. The flexible web structure facilitates vibration transmission from struggling prey as longitudinal, transverse and lateral waves along threads, whilst typical prey signals generated from animals walking on the ground are

the equivalent of propagating lateral waves, with motion primarily perpendicular to the substrate plane as we have simulated here. Modelling has indicated that source distance estimation within orb-webs can be achieved through comparison of transverse wave amplitude between legs, whilst angle can be estimated through comparison of longitudinal and lateral waves (Mortimer et al., 2019). Here, the interaction between substrate and body dynamics is important for modulating these parameters, as the mass of the spider body on the web generates a "shadowing" effect as the waves travel across the web, increasing attenuation and thus amplitude differences used for source localisation.

Evidence from modelling suggests that in some spiders, individual leg segments are mechanically tuned, despite the mechanosensors being sensitive to a broad range of frequencies – a form of morphological computation (Mhatre, 2016). We argue that in tarantulas, morphological computation in the spider system is more likely to be used to make the system more robust to variation in biomechanical parameters that have the potential to influence body dynamics and hence vibration sensing. This is supported by parametric tests using our calibrated model, where inherent inter-leg variation in transmissibility means that changes in body mass have a reduced effect on the dynamics of the whole system (Wu et al., 2023).

As well as insights into the biology of vibration sensing in tarantulas, our findings can be applied to engineered systems of mechanosensors. We have suggested that spiders are capable of vibration source localisation using the magnitude and direction of strains, without comparison of frequency content or time delays between body segments. Crucially, it is not necessary for sensors to be tuned to specific frequencies, which reduces the complexity of each individual unit. The implication for engineered systems is that a network of many simple strain sensors is sufficient for vibration source localisation, and that the distribution of sensors and shape of the overall structure are the most important parameters. One possible application of a system of strain sensors is in the detection of defects in mechanical systems (Valeev, 2023).

Future research should focus on quantifying the relationship between joint bending and mechanosensor stimulation by directly measuring cuticular strains, rather than simply inferring joint bending from relative motion as we have done here. Similarly, more advanced modelling, including multibody modelling of the spider body and finite element modelling of the exoskeleton at mechanosensor locations, will provide complementary evidence using variation in excitations and biomechanical parameters that is impossible in an experimental context.

Author contributions

T.E.M.: conceptualization, data curation, formal analysis, investigation, methodology, software, validation, visualization, writing—original draft, writing—review and editing. J.W.: conceptualization, data curation, methodology, software, investigation, writing—review and editing. A.C.: conceptualization, funding acquisition, methodology, project administration, writing—review and editing. G.K.T.: conceptualization, funding acquisition, methodology, project administration, supervision, writing—review and editing. B.M.: conceptualization, funding acquisition, methodology, project administration, supervision, writing—review and editing.

All authors contributed to the article and approved the submitted version.

Funding

This work was supported by the Royal Society University Research Fellowship (grant no. URF\R1\191033).

Acknowledgements

We thank the animal technicians for their valued contributions to spider husbandry. For help with experimental set-ups, we thank John Hogg.

Conclusion

1 Thesis summary

The primary aim of this thesis is to explore questions relating to the role of spider body morphology in substrate-borne vibration sensing. I first set out the research arc in the Introduction, before framing the problem for the first time in terms of biomechanical constraints and the control mechanisms potentially used to mitigate these in my literature review (Chapter 1). I then employed a variety of techniques including SEM imaging and CT scanning to investigate and quantify the morphologies of three species of spiders, revealing broadly conserved patterns of mechanosensor location (Chapter 2) and quantifying fundamental biomechanical parameters (Chapter 3). I conducted for the first time a full dynamic test on a live, untethered spider using laser vibrometry, and combined these results with the findings in Chapters 2 and 3 to construct and calibrate a mathematical model of the spider (Chapter 4). I was able to use the experimental response and simulated response to make broad inferences about the role of various biomechanical parameters in substrate-borne vibration sensing, and how variation in morphology might affect this modality (Chapter 5).

I isolated the effect of body dynamics from substrate, showing that morphology is of fundamental importance to substrate-borne vibration sensing (Wu et al., 2023). My experimental results have quantified the motion of an untethered, freely vibrating spider body in response to vibrational input, including the inherent properties of the system such as the natural frequencies (Peeters et al., 2004, Ewins, 2000). The natural frequencies of the tarantula spider's body are low (<140Hz), overlapping with the frequency of biologically-relevant source vibrations (Masters, 1984b, Schuch and Barth, 1990, Barth et al., 1988) – indicating that the spider can potentially use this phenomenon to amplify these signals. The relative motion of different body segments in the vertical axis, where the majority of biological useful information exists, is used as a proxy for joint bending, enabling us to infer patterns of mechanosensor stimulation at

different frequencies (Blickhan et al., 2021). The vertical modal shapes of the spider provide further evidence showing how the amplitude and phase of the legs and cephalothorax vary depending on the frequency range. Overall, the experimental results indicate that the dynamic response of the spider body facilitates the transmission of vibrations from the substrate to the mechanosensors, rather than losing biologically relevant source information through damping or distorting the input signal.

A surprising finding was how simply the inherent vertical motion of the spider body (independent of substrate properties and excitation type) could be modelled. The frequency response of all eight legs is similar and there are limited detectable differences between leg segments within the same leg. This supported the decision to model each leg and the cephalothorax/abdomen as single mass-spring damper elements, resulting in a model with only 11 degrees of freedom. In contrast to finite element modelling, the parameters required to calibrate the model can be obtained relatively easily from a dynamic test using laser vibrometry, and the measurement of other morphological parameters such as mass and geometry dimensions (Wu et al., 2023), without the need for full CT scans. Therefore, the simple model could theoretically be applied to other spider species once these parameters are obtained, which would need to be validated – demonstrating the potential utility of this technique for future research.

2 Synthesis

2.1 Functions of substrate-borne vibration sensing

The transmission of vibrations through the body of the spider is used for two main functions – providing information about an externally-generated vibration source (exteroception) (Barth and Geethabali, 1982), and proprioception resulting from joint bending generated by the spider's own body movements (Barth and Bohnenberger, 1978, Pringle, 1955).

The first function involves vibration detection above noise, followed by source localisation (the position of the source relative to the spider) and identification of the type of signal (biotic vs. abiotic, prey vs. conspecific), in order to inform the appropriate behavioural response (Seyfarth et al., 1982, Landolfa and Barth, 1996). Source localisation can theoretically be achieved through comparison of the input detected at multiple mechanosensors located in different positions across the spider body (Hergenröder R., 1983). I have shown that the amplitude ratio between legs on opposite sides of the body is correlated with source angle and hence could be used by the tarantula for localisation. This asymmetry in input is largely generated by the decay rate of the source wave through the substrate but is transmitted to the mechanosensors with high fidelity by the dynamics of the spider body. The inherent body dynamics also mean that the vertical modal shapes excited at different source angles could also provide information about source angle, in terms of the type and direction of joint bending – a function potentially facilitated by high spatial resolution of the mechanosensors, which cover most areas of the spider body (Miller et al., 2022, Barth and Libera, 1970, Ganske and Uhl, 2018, Kropf, 1998, Seo et al., 2020, Vogel, 1923). In contrast, frequency filtering or time delays are unlikely to be used for source angle estimation as the response of these parameters at different mechanosensor locations cannot be correlated with source angle. Similarly, convergence of amplitude ratios and time delays means that far-field distance estimation is probably not possible. Our conclusions from these simulations are consistent with the biological context in which tarantulas hunt (Foelix, 2010, Pittella et al., 2023) and provide strong evidence that the vibrational mechanisms used by the real spider for source localisation involve comparison of the magnitude of the dynamic response at different mechanosensor locations – a mechanism which is facilitated by the biomechanical parameters that govern morphology.

I have already shown that the frequency, amplitude, and phase of the time domain input are transmitted to the distributed mechanosensor locations with high efficacy, enabling discrimination between different source signals. Using simulations, I have expanded on this by suggesting that there is a degree of robustness in the system due to inherent

differences in the extent to which variation within each leg influences global body dynamics (Wu et al., 2023). Specifically, variation in the properties of the middle four legs have less of an influence on dynamics than the outer four legs. This potentially allows for consistent source localisation by mitigating the effect of physical constraints such as whole-body changes in mass and geometry due to feeding, reproduction or injury. Therefore, I suggest that the variation in the global effect of each leg is functionally useful, and hence could be used as a control mechanism in the context of substrate-borne vibration sensing (Miller and Mortimer, 2020).

Whether the spider can actively use behaviour to add a further level of control is an open question. Whilst theoretically spiders may be able to use behaviour to mitigate physical constraints (such as variation in morphological traits that influence biomechanical parameters), or adapt to changing external conditions (such as background noise level or substrate properties) (Mhatre, 2016, Blickhan, 1986), I have not shown whether spiders employ these mechanisms adaptively in biological contexts, although my results indicate that varying parameters such as leg angle induces a corresponding change in the simulated response of the spider body. Understanding the output of the system in terms of behaviour is crucial for determining whether morphological computation has a role either as an active and passive control mechanism, which should be a focus of future research.

Similarly, the role of morphology in facilitating the proprioceptive sense remains to be investigated beyond the function of individual mechanosensors. Both the experimental and simulated response involved a static spider with an external input, and therefore cannot be extrapolated to the dynamic response generated by movement patterns. Future research in this area may focus on measuring cuticular strain in walking spiders (Blickhan et al., 2021).

2.2 The role of morphology

The pathway through which information flows in substrate-borne vibration sensing involves vibration transmission through environmental substrates, transmission through the body of the animal, and mechanotransduction in the nervous system (Miller and Mortimer, 2020). Each of these three stages has a different set of relevant biological traits under selection and corresponding physical and physiological constraints, where intra- and inter-specific variation would be expected. I have primarily focused on the transmission stage through the body of the spider as this is where variation in morphological parameters, in theory, has the greatest influence on substrate-borne vibration sensing.

Despite this transmission stage being relatively understudied, my results have shown that morphology has an inherent and wide effect on substrate-borne vibration sensing. This is especially relevant for non-web building spiders that have a low level of control over the transmission stage through the substrate – most terrestrial hunters, for instance, have far less behavioural flexibility in choosing the transmission properties of their substrate when compared with web-building spiders (Sun et al., 2021). I did not investigate the role of mechanotransduction, but applied previous neurophysiological research on slit sensilla tuning curves on other species (primarily *Cupiennius salei*) to the tarantula system (Barth and Bohnenberger, 1978, Barth and Geethabali, 1982, Gingl et al., 2006, Speck and Barth, 1982, Barth, 2021). Morphology and mechanotransduction are integrated elegantly in spider vibration sensing. It is the interaction between morphology and substrate which generates the asymmetries in the dynamic response to a vibration source that is sensed and used for source localisation, whilst the mechanosensors themselves are broadly tuned to a wide range of biologically relevant frequencies (Barth and Geethabali, 1982, Bohnenberger, 1981). In the tarantula, morphology transmits the information content from the substrate and therefore facilitates the key functions in substrate-borne vibration sensing.

Morphological computation, where processing of information is outsourced to morphology in order to reduce computational cost in the nervous system (Müller and Hoffmann, 2017), has been hypothesised to be involved in substrate-borne vibration sensing (Miller and Mortimer, 2020). At the mechanosensor scale, previous research has shown that the morphology of mechanosensors involved in vibration sensing (such as lyriform organs), and acoustic hearing more generally, are responsible for frequency segregation and processing of information before mechanotransduction (Hössl et al., 2009, Hössl et al., 2007, Montealegre-Z et al., 2012). Morphological structures auxiliary to the mechanosensors, such as the cuticular pad, are also involved in the filtering of vibrations (Erko et al., 2015, Young et al., 2014). I would therefore consider these processes (here referred to in this context as filtering and distorting information) to be examples of morphological computation in substrate-borne vibration sensing.

At the whole-body scale, however, the picture is less clear. In theory, the dynamic response of the body (here referring to the relative motion of entire segments around joints) could be used in addition to mechanosensor-scale processes to filter and distort vibrational information adaptively for vibration sensing. An implication of this is that global changes in posture (and other morphological traits covarying with biomechanical parameters) may influence the processing of vibrational information, opening the possibility that spiders can actively use behaviour to modulate vibration sensing (Miller and Mortimer, 2020, Mhatre, 2016).

As discussed above, vibration source localisation is one of the primary functions in which these mechanisms could be applied. My results show that amplitude ratios in vertical motion on opposite sides of the body can be used to estimate source angle, and in terms of this parameter, morphology does not play a major role in processing and filtering information along the transmission pathway from source to mechanosensor. Instead, since the dynamic response of the body shows low levels of damping and noise in the relevant frequency range, this indicates that source information is transmitted to the mechanosensors with high efficacy. I argue that since amplitude ratios on opposite sides of the body are very similar to amplitude ratios in equivalent positions through the

substrate, it is largely substrate dynamics that facilitate source angle estimation. Therefore, this mechanism is probably not an example of morphological computation as information is transmitted through the body to the mechanosensors with high efficacy, rather than morphology playing a major role in filtering and distorting vibrational information usefully in this system. For parameters other than amplitude ratios in the vertical axis, I have not found any evidence for morphological computation, as the inherent body dynamics do not generate time delays that are physiologically detectable.

A counter to this is that at certain input angles, my simulations indicate that the asymmetry in vertical motion of the substrate is slightly amplified by the body, which would implicate a role for morphological computation as substrate dynamics are not solely responsible for the amplitude ratio asymmetries detected at the mechanosensors. An explanation for this could be the excitation of different vertical modal shapes at different source angles, which are inherent properties of the system modulated by morphology. It is not clear, however, the extent to which this information can be usefully applied for source localisation, and further research is needed to demonstrate whether this mechanism is adaptive in terms of outsourcing functions from the central nervous system and hence an example of morphological computation.

Another function which could be considered morphological computation is the mitigation of physical constraints that may influence vibration sensing via control mechanisms that make the dynamic response of the system robust. As discussed above, the dynamic properties of the middle four legs potentially reduce the global effect of variation in certain biomechanical parameters on the dynamic response of the whole body. This is particularly relevant as changes in body mass (a physical constraint) have the most effect on the middle four legs, possibly due to the centre of mass of the spider being located over these legs. Since these are inherent properties of body dynamics that passively reduce the need for subsequent nervous system compensation, I would consider this hypothesised mechanism to be morphological computation. Further research is needed, however, to establish an explicit link between mass variation, the dynamic response and a consistent output in terms of behaviour in the tarantula system,

despite some supporting experimental evidence for this effect in a web-building spider (Mhatre, 2016).

Overall, my thesis indicates that the body acts as a platform that transmits information from substrate to mechanosensors with high efficacy for use in functions such as source localisation. Morphological computation at the whole-body scale is likely not involved in source localisation for substrate-borne vibration sensing. I hypothesise that the inherent properties of the body may be involved in making the system robust to variation that might reduce the effectiveness of vibration sensing, but more research is needed to demonstrate that this mechanism is an example of morphological computation. Equally, the embedded nature of the mechanosensors in substrate-borne vibration sensing means that partially due to semantics, the term morphological computation may be applied to mechanosensor-scale processes immediately prior to mechanotransduction.

Despite the low number of species studied, the results of my thesis are relevant to other spiders and arthropods more generally. I have suggested possible mechanisms contributing to source localisation in biological systems, expanding on theoretical predictions made in the literature such as the comparison of time of arrival differences between legs (Barth, 1993). The experimental techniques that I have developed to test these predictions can be universally applied to subjects of a similar scale to the tarantula and thus my results facilitate future research into the body dynamics of a range of different species. This will reveal whether source localisation mechanisms are broadly conserved across arthropods, or if there is a strong influence of phylogeny, morphology, or life strategy on variation in these mechanisms.

The influence of growth and development on mechanisms of source localisation is also relevant here – time delays in the dynamic response, for instance, are likely to be larger in animals with wider leg spans, potentially meaning that time delays as well as amplitude could be used in source localisation (Hartbauer and Römer, 2014). This opens the question of whether mechanisms of source localisation stay consistent throughout an animal's growth and development. The discrete stages of growth in arthropods due to moulting, also involving replacement of the cuticular mechanosensors at each instar,

may mean that they are uniquely suited to tuning the morphology/mechanosensor interface through development (Vollrath, 1995). A combination of dynamic tests using laser vibrometry and modelling at different spatial scales could be employed in the future to test these hypotheses.

3 Applications

The results from my thesis could also be applied to engineered systems, which are increasingly turning to biological solutions for inspiration on how to solve universal problems. It can be challenging to develop engineered systems that are able to cope with environmental variability in real time (Hauser et al., 2011), yet evolution has equipped animals with sensory systems that facilitate these functions. I have demonstrated that a network of relatively simple, non-directional sensors distributed across a multi-legged body is sufficient to estimate source angle. Future research might approach the question from a bio-inspired perspective, for instance by focusing on the minimum number of sensors, or sensor locations, that are sufficient for source localisation – which may potentially reduce the complexity, cost and size of artificial vibration sensors.

Moving forward, I believe that a combination of dynamic testing in all three planes and more complex mathematical modelling, perhaps using multibody simulations, will allow investigation of deeper questions concerning the role of morphology in substrate-borne vibration sensing.

Bibliography

AICHER, B. & TAUTZ, J. 1990. Vibrational communication in the fiddler crab, *Uca pugilator*. 1. signal transmission through the substratum. *Journal of Comparative Physiology a-Sensory Neural and Behavioral Physiology,* 166**,** 345-353.

BALACHANDRAN, B. & MAGRAB, E. B. 2008. *Vibrations,* Toronto, CL Engineering.

BARTH, F. G. 1972a. The physiology of slit sense organs I. Model experiments on the role of the cuticular slit in stimulus conduction | Die Physiologie der Spaltsinnesorgane I. Modellversuche zur Rolle des cuticularen Spaltes beim Reiztransport. *J. Comp. Physiol.,* 78**,** 315-336.

BARTH, F. G. 1972b. The physiology of slit sense organs II. Functional morphology of a mechanoreceptor | Die Physiologie der Spaltsinnesorgane II. Funktionelle Morpologie eines Mechanoreceptors. *J. Comp. Physiol.,* 81**,** 159-186.

BARTH, F. G. 1980. Campaniform sensilla - another vibration receptor in the crab leg. *Naturwissenschaften,* 67**,** 201-202.

BARTH, F. G. 1993. Sensory guidance in spider pre-copulatory behavior. *Comparative Biochemistry and Physiology a-Molecular & Integrative Physiology,* 104**,** 717-733.

BARTH, F. G. 2002a. Spider senses - technical perfection and biology. *Zoology,* 105**,** 271-285.

BARTH, F. G. 2002b. *A spider's world: Senses and behavior.* Book.

BARTH, F. G. 2008. *Cupiennius* (Araneae, Ctenidae): biology and sensory ecology of a model spider. *Stapfia,* 88**,** 211-224.

BARTH, F. G. 2012. *Spider strain detection.*

BARTH, F. G. 2019. Mechanics to pre-process information for the fine tuning of mechanoreceptors. *Journal of Comparative Physiology a-Neuroethology Sensory Neural and Behavioral Physiology,* 205**,** 661-686.

BARTH, F. G. 2021. A spider in motion: facets of sensory guidance. *Journal of Comparative Physiology a-Neuroethology Sensory Neural and Behavioral Physiology,* 207**,** 239-255.

BARTH, F. G., BLECKMANN, H., BOHNENBERGER, J. & SEYFARTH, E. A. 1988. Spiders of the genus *Cupiennius* Simon 1891 (Araneae, Ctenidae) .2. On the vibratory environment of a wandering spider. *Oecologia,* 77**,** 194-201.

BARTH, F. G. & BOHNENBERGER, J. 1978. Lyriform slit sense organ - thresholds and stimulus amplitude ranges in a multi-unit mechanoreceptor. *Journal of Comparative Physiology,* 125**,** 37-43.

BARTH, F. G., FICKER, E. & FEDERLE, H. U. 1984. Model studies on the mechanical significance of grouping in compound spider slit sensilla (Chelicerata, Araneida). *Zoomorphology,* 104**,** 204-215.

BARTH, F. G. & GEETHABALI 1982. Spider Vibration Receptors - Threshold Curves of Individual Slits in the Metatarsal Lyriform Organ. *Journal of Comparative Physiology,* 148**,** 175-185.

BARTH, F. G. & LIBERA, W. 1970. Illustrated catalogue of a spider's slit sense organs (*Cupiennius salei* Keys). *Zeitschrift Fur Morphologie Der Tiere,* 68**,** 343-&.

BARTH, F. G. & PICKELMANN, P. 1975. Lyriform slit sense-organs - Modeling an arthropod mechanoreceptor. *J. Comp. Physiol.,* 103**,** 39–54.

BARTH, F. G. & SEYFARTH, E. A. 1971. Slit sense organs and kinesthetic orientation. *Zeitschrift Fur Vergleichende Physiologie,* 74**,** 326-&.

BARTH, F. G. & STAGL, J. 1976. Slit sense-organs of arachnids - Comparative-study of their topography on walking legs (Chelicerata. Arachnida). *Zoomorphologie,* 86**,** 1–23.

BARTH, F. G. & WADEPUHL, M. 1975. Slit sense organs on the scorpion leg (*Androctonus australis* L., Buthidae). *J. Morphol.,* 145**,** 209227.

BATLLE, J. A. & COMDOMINES, A. B. 2022. *Rigid Body Dynamics,* Cambridge, Cambridge University Press.

BLECKMANN, H. & BARTH, F. G. 1984. Sensory ecology of a semi-aquatic spider (*Dolomedes triton*) 2. the release of predatory behaviour by water-surface waves. *Behav. Ecol. Sociobiol.,* 14**,** 303–312.

BLICKHAN, R. 1986. Stiffness of an arthropod leg joint. *Journal of Biomechanics,* 19**,** 375-384.

BLICKHAN, R. & BARTH, F. G. 1985. Strains in the exoskeleton of spiders. *J. Comp. Physiol. A,* 157**,** 115–147.

BLICKHAN, R., WEIHMANN, T. & BARTH, F. G. 2021. Measuring strain in the exoskeleton of spiders-virtues and caveats. *Journal of Comparative Physiology a-Neuroethology Sensory Neural and Behavioral Physiology,* 207**,** 191-204.

BOHNENBERGER, J. 1981. Matched transfer characteristics of single units in a compound slit sense organ. *Journal of Comparative Physiology,* 142**,** 391-402.

BOSIA, F., POGGETTO, V. F. D., GLIOZZI, A. S., GRECO, G., LOTT, M., MINIACI, M., ONGARO, F., ONORATO, M., SEYYEDIZADEH, S. F., TORTELLO, M. & PUGNO, N. M. 2022. Optimized structures for vibration attenuation and sound control in nature: A review. *Matter,* 5**,** 3311-3340.

BOULEY, D. M., ALARCÓN, C. N., HILDEBRANDT, T. & O'CONNELL-RODWELL, C. E. 2007. The distribution, density and three-dimensional histomorphology of Pacinian corpuscles in the foot of the Asian elephant (*Elephas maximus*) and their potential role in seismic communication. *Journal of Anatomy,* 211**,** 428-435.

BOUTRY, C. & BLACKLEDGE, T. A. 2010. Evolution of supercontraction in spider silk: structure-function relationship from tarantulas to orb-weavers. *Journal of Experimental Biology,* 213**,** 3505-3514.

BROWN, C. A., AMAYA, C. C. & FORMANOWICZ, D. R., JR. 2018. The frequency of leg autotomy and its influence on survival in natural populations of the wolf spider *Pardosa valens*. *Canadian Journal of Zoology,* 96**,** 973-979.

CLOUDSLEY-THOMPSON, J. L. 1995. A review of the anti-predator devices of spiders. *Bull. Br. Arachnol. Soc.,* 10**,** 81-96.

COCROFT, R. B. & RODRÍGUEZ, R. L. 2005. The behavioral ecology of insect vibrational communication. *Bioscience,* 55**,** 323-334.

DALLMANN, C. J., DUERR, V. & SCHMITZ, J. 2016. Joint torques in a freely walking insect reveal distinct functions of leg joints in propulsion and posture control. *Proceedings of the Royal Society B-Biological Sciences,* 283.

DE CRESPIGNY, F. E. C., HERBERSTEIN, M. E. & ELGAR, M. A. 2001. Food caching in orb-web spiders (Araneae: Araneoidea). *Naturwissenschaften,* 88**,** 42-45.

DINGES, G. F., CHOCKLEY, A. S., BOCKEMÜHL, T., ITO, K., BLANKE, A. & BÜSCHGES, A. 2021. Location and arrangement of campaniform sensilla in *Drosophila melanogaster*. *Journal of Comparative Neurology,* 529**,** 905-925.

EBERHARD, W. G. 1972. The web of *Uloborus diversus* Araneae Uloboridae. *J. Zool.,* 166**,** 417-465.

ELBEHEIRY, E. M., KARNOPP, D. C., ELARABY, M. E. & ABDELRAAOUF, A. M. 1996. Suboptimal control design of active and passive suspensions based on a full car model. *Vehicle System Dynamics,* 26**,** 197-222.

ELIAS, D. O., HEBETS, E. A., HOY, R. R. & MASON, A. C. 2005. Seismic signals are crucial for male mating success in a visual specialist jumping spider (Araneae: Salticidae). *Animal Behaviour,* 69**,** 931-938.

ELIAS, D. O. & MASON, A. C. 2014. The role of wave and substrate heterogeneity in vibratory communication: practical issues in studying the effect of vibratory environments in communication. *In:* COCROFT, R. B., GOGALA, M., HILL, P. S. M. & WESSEL, A. (eds.) *Studying Vibrational Communication.* New York: Springer.

ELIAS, D. O., MASON, A. C., MADDISON, W. P. & HOY, R. R. 2003. Seismic signals in a courting male jumping spider (Araneae: Salticidae). *Journal of Experimental Biology,* 206**,** 4029-4039.

ERKO, M., YOUNES-METZLER, O., RACK, A., ZASLANSKY, P., YOUNG, S. L., MILLIRON, G., CHYASNAVICHYUS, M., BARTH, F. G., FRATZL, P., TSUKRUK, V., ZLOTNIKOV, I. & POLITI, Y. 2015. Micro- and nano-structural details of a spider's filter for substrate vibrations: relevance for low-frequency signal transmission. *Journal of the Royal Society Interface,* 12.

ESMAILZADEH, E. & FAHIMI, F. 1997. Optimal adaptive active suspensions for a full car model. *Vehicle System Dynamics,* 27**,** 89-107.

EWINS, D. J. 2000. *Modal testing: theory, practice, and application.,* Baldock, UK, Research Studies Press.

FERNANDEZ-MONTRAVETA, C. & MOYA-LARANO, J. 2007. Sex-specific plasticity of growth and maturation size in a spider:: implications for sexual size dimorphism. *Journal of Evolutionary Biology,* 20**,** 1689-1699.

FOELIX, R. 1979. *Biology of Spiders,* New York, NY, Oxford University Press.

FOELIX, R. 2010. *Biology of Spiders*, Oxford University Press, USA.

FOELLMER, M. W. & MOYA-LARANO, J. 2007. *Sexual dimorphism in spiders: patterns and processes.* Book chapter; Meeting paper.

FRANCESCHINI, N., PICHON, J. M. & BLANES, C. 1992. From insect vision to robot vision. *Phil. Trans. R. Soc. Lond. B,* 337**,** 283–294.

FRENCH, A. S., TORKKELI, P. H. & SEYFARTH, E. A. 2002. From stress and strain to spikes: mechanotransduction in spider slit sensilla. *Journal of Comparative Physiology a-Neuroethology Sensory Neural and Behavioral Physiology,* 188**,** 739-752.

FROHLICH, C. & BUSKIRK, R. E. 1982. Transmission and attenuation of vibration in orb spider webs. *Journal of Theoretical Biology,* 95**,** 13-36.

GANSKE, A. S. & UHL, G. 2018. The sensory equipment of a spider - A morphological survey of different types of sensillum in both sexes of *Argiope bruennichi* (Araneae, Araneidae). *Arthropod Structure & Development,* 47**,** 144-161.

GINGL, E., BURGER, A. M. & BARTH, F. G. 2006. Intracellular recording from a spider vibration receptor. *Journal of Comparative Physiology a-Neuroethology Sensory Neural and Behavioral Physiology,* 192**,** 551-558.

GNATZY, W., GRÜNERT, U. & BENDER, M. 1987. Campaniform sensilla of Calliphora vicina (Insecta, Diptera). *Zoomorphology,* 106**,** 312-319.

GÖPFERT, M. C. & HENNIG, R. M. 2016. Hearing in Insects. *Annual Review of Entomology*, 61, 257-276

GORDON, S. D. & UETZ, G. W. 2011. Multimodal communication of wolf spiders on different substrates: evidence for behavioural plasticity. *Animal Behaviour,* 81**,** 367-375.

GUAN, J., PORTER, D. & VOLLRATH, F. 2012. Silks cope with stress by tuning their mechanical properties under load. *Polymer,* 53**,** 2717-2726.

GUAN, J., VOLLRATH, F. & PORTER, D. 2011. Two Mechanisms for Supercontraction in *Nephila* Spider Dragline Silk. *Biomacromolecules,* 12**,** 4030-4035.

GUINEA, G. V., ELICES, M., PÉREZ-RIGUEIRO, J. & PLAZA, G. R. 2005. Stretching of supercontracted fibers:: a link between spinning and the variability of spider silk. *Journal of Experimental Biology,* 208**,** 25-30.

HARTBAUER, M. & RÖMER, H. 2014. From microseconds to seconds and minutes-time computation in insect hearing. *Frontiers in Physiology,* 5.

HAUSER, H., IJSPEERT, A. J., FÜCHSLIN, R. M., PFEIFER, R. & MAASS, W. 2011. Towards a theoretical foundation for morphological computation with compliant bodies. *Biological Cybernetics,* 105**,** 355-370.

HAUSER, H., NAKAJIMA, K. & FÜCHSLIN, R. M. 2014. Morphological computation - The body as a computational resource. *In:* HAUSER, H., FÜCHSLIN, R. M. & PFEIFER, R. (eds.) *Opinions and Outlooks on Morphological Computation.* (e-book).

HAWKES, E. W., BLUMENSCHEIN, L. H., GREER, J. D. & OKAMURA, A. M. 2017. A soft robot that navigates its environment through growth. *Science Robotics,* 2.

HEBETS, E. A. 2008. Seismic signal dominance in the multimodal courtship display of the wolf spider *Schizocosa stridulans* Stratton 1991. *Behavioral Ecology,* 19**,** 1250-1257.

HENAUT, Y., MACHKOUR-M'RABET, S., WINTERTON, P. & CALMÉ, S. 2010. Insect attraction by webs of *Nephila clavipes* (Araneae: Nephilidae). *J. Arachnol.,* 38.

HERBERSTEIN, M. E., ABERNETHY, K. E., BACKHOUSE, K., BRADFORD, H., DE CRESPIGNY, F. E. C. & LUCKOCK, P. R. The effect of feeding history on prey capture behaviour in the orbweb spider *Argiope keyserlingi* Karsch (Araneae: Araneidae). *Ethology,* 104**,** 565–571.

HERGENRODER, R. & BARTH, F. G. 1983. The release of attack and escape behavior by vibratory stimuli in a wandering spider (*Cupiennius salei* Keys). *Journal of Comparative Physiology,* 152**,** 347-358.

HERGENRÖDER R., B. F. G. 1983. Vibratory signals and spider behavior: how do the sensory inputs from the eight legs interact in orientation? *J. Comp. Physiol.,* 152**,** 361-371.

HESSELBERG, T. 2010. Ontogenetic Changes in Web Design in Two Orb-Web Spiders. *Ethology,* 116**,** 535-545.

HILL, P. S. M. 2009. How do animals use substrate-borne vibrations as an information source? *Naturwissenschaften,* 96**,** 1355-1371.

HILL, P. S. M., VIRANT-DOBERLET, M. & WESSEL, A. 2019. What Is Biotremology? *In:* HILL, P. S. M., LAKESHARLAN, R., MAZZONI, V., NARINS, P. M., VIRANT-DOBERLET, M. & WESSEL, A. (eds.) *Biotremology: Studying Vibrational Behavior.*

HILL, P. S. M. & WESSEL, A. 2016. Biotremology. *Current Biology,* 26**,** R187-R191.

HORMIGA, G., EBERHARD, W. G. & CODDINGTON, J. A. 1995. Web-construction behavior in Australian Phonognatha and the phylogeny of Nephiline and Tetragnathid spiders (Araneae, Tetragnathidae). *Australian Journal of Zoology,* 43**,** 313-364.

HÖSSL, B., BÖHM, H. J., RAMMERSTORFER, F. G. & BARTH, F. G. 2007. Finite element modeling of arachnid slit sensilla- : I. : The mechanical significance of different slit arrays. *Journal of Comparative Physiology a-Neuroethology Sensory Neural and Behavioral Physiology,* 193**,** 445-459.

HÖSSL, B., BÖHM, H. J., RAMMERSTORFER, F. G., MÜLLAN, R. & BARTH, F. G. 2006. Studying the deformation of arachnid slit sensilla by a fracture mechanical approach. *Journal of Biomechanics,* 39**,** 1761-1768.

HÖSSL, B., BÖHM, H. J., SCHABER, C. F., RAMMERSTORFER, F. G. & BARTH, F. G. 2009. Finite element modeling of arachnid slit sensilla: II. Actual lyriform organs and the face deformations of the individual slits. *Journal of Comparative Physiology a-Neuroethology Sensory Neural and Behavioral Physiology,* 195**,** 881-894.

HUNT, J. H. & RICHARD, F. J. 2013. Intracolony vibroacoustic communication in social insects. *Insectes Sociaux,* 60**,** 403-417.

KARATO, S. 2010. Rheology of the Earth's mantle: A historical review. *Gondwana Research,* 18**,** 17-45.

KLARNER, D. & BARTH, F. G. 1982. Vibratory signals and prey capture in orb-weaving spiders (*Zygiella x-notata*, *Nephila clavipes*, Araneidae). *Journal of Comparative Physiology,* 148**,** 445-455.

KLOCKE, D. & SCHMITZ, H. 2011. Water as a major modulator of the mechanical properties of insect cuticle. *Acta Biomaterialia,* 7**,** 2935-2942.

KROPF, C. 1998. Slit sense organs of *Comaroma simonii* Bertkau: a morphological atlas (Araneae, Anapidae). *Proceedings of the 17th European colloquium of arachnology,* Edinburgh 1997 (1998)**,** 151-159.

LANDOLFA, M. A. & BARTH, F. G. 1996. Vibrations in the orb web of the spider Nephila clavipes: Cues for discrimination and orientation. *Journal of Comparative Physiology a-Sensory Neural and Behavioral Physiology,* 179**,** 493-508.

LI, T. L., GUO, J. X., TAN, Y. G. & ZHOU, Z. D. 2020. Recent Advances and Tendency in Fiber Bragg Grating-Based Vibration Sensor: A Review. *Ieee Sensors Journal,* 20**,** 12074-12087.

LIEBSCH, C., FLIESS, M., KUHBIER, J. W., VOGT, P. M. & STRAUSS, S. 2020. *Nephila edulis* - breeding and care under laboratory conditions. *Development Genes and Evolution,* 230**,** 203-211.

LIESENFELD, F. J. 1961. Über Leistung und Sitz des Erschütterungssinnes von Netzspinnen. *Biol. Zbl,* 80**,** 466-475.

LIPSON, H. 2014. Challenges and Opportunities for Design, Simulation, and Fabrication of Soft Robots. *Soft Robotics,* 1**,** 21-27.

LIU, Y., SPONNER, A., PORTER, D. & VOLLRATH, F. 2008. Proline and processing of spider silks. *Biomacromolecules,* 9**,** 116-121.

MAIN, I. G. 1993. *Vibrations and Waves in Physics,* Cambridge, Cambridge University Press.

MASTERS, W. M. 1984a. Vibrations in the orbwebs of *Nuctenea sclopetaria* (Araneidae) .1. Transmission through the web. *Behavioral Ecology and Sociobiology,* 15**,** 207-215.

MASTERS, W. M. 1984b. Vibrations in the orbwebs of *Nuctenea sclopetaria* (Araneidae). 2. Prey and wind signals and the spider's response threshold. *Behavioral Ecology and Sociobiology,* 15**,** 217-223.

MASTERS, W. M. & MARKL, H. 1981. Vibration signal transmission in spider orb webs. *Science,* 213**,** 363-365.

MCCONNEY, M. E., SCHABER, C. F., JULIAN, M. D., BARTH, F. G. & TSUKRUK, V. V. 2007. Viscoelastic nanoscale properties of cuticle contribute to the high-pass properties of spider vibration receptor (*Cupiennius salei* Keys). *Journal of the Royal Society Interface,* 4**,** 1135-1143.

MCINDOO, N. E. 1911. The lyriform organs and tactile hairs of araneids. *Proc. Acad. Nat. Sci. Phila. 63.*

MEIROVITCH, L. 2010. *Fundamentals of vibrations.,* Long Grove, IL, Waveland Press.

MENZEL, J. G. & TAUTZ, J. 1994. Functional-morphology of the subgenual organ of the carpenter ant. *Tissue & Cell,* 26**,** 735-746.

MHATRE, N., SIVALINGHEM, S., MASON, A. C. 2016. Posture controls mechanical tuning in the black widow spider mechanosensory system. *bioRxiv*.

MILLER, T. E. & MORTIMER, B. 2020. Control vs. Constraint: Understanding the Mechanisms of Vibration Transmission During Material-Bound Information Transfer. *Frontiers in Ecology and Evolution,* 8.

MILLER, T. E., TAYLOR, G. K. & MORTIMER, B. 2022. Slit sense organ distribution on the legs of two species of orb-weaving spider (Araneae: Araneidae). *Arthropod Structure & Development,* 67.

MO, A., IZZI, F., HAEUFLE, D. F. B. & BADRI-SPRÖWITZ, A. 2020. Effective Viscous Damping Enables Morphological Computation in Legged Locomotion. *Frontiers in Robotics and Ai,* 7.

MOLINA, J., SCHABER, C. F. & BARTH, F. G. 2009. In search of differences between the two types of sensory cells innervating spider slit sensilla (*Cupiennius salei* Keys.). *Journal of Comparative Physiology a-Neuroethology Sensory Neural and Behavioral Physiology,* 195**,** 1031-1041.

MONTAGANO, L. & FAVRET, C. 2016. The distribution of campaniform sensilla on the appendages of *Mindarus* species (Hemiptera: Aphididae). *Entomol. News,* 126**,** 196-203.

MONTEALEGRE-Z, F., JONSSON, T., ROBSON-BROWN, K. A., POSTLES, M. & ROBERT, D. 2012. Convergent Evolution Between Insect and Mammalian Audition. *Science,* 338**,** 968-971.

MORAN, D. T., CHAPMAN, K. M. & ELLIS, R. A. 1971. Fine structure of cockroach campaniform sensilla. *Journal of Cell Biology,* 48**,** 155-&.

MORLEY, E. L., SIVALINGHEM, S. & MASON, A. C. 2016. Developmental morphology of a lyriform organ in the Western black widow (*Latrodectus hesperus*). *Zoomorphology,* 135**,** 433-440.

MORTIMER, B. 2017. Biotremology: Do physical constraints limit the propagation of vibrational information? *Animal Behaviour,* 130**,** 165-174.

MORTIMER, B. 2019. A Spider's Vibration Landscape: Adaptations to Promote Vibrational Information Transfer in Orb Webs. *Integrative and Comparative Biology,* 59**,** 1636-1645.

MORTIMER, B., GORDON, S. D., HOLLAND, C., SIVIOUR, C. R., VOLLRATH, F. & WINDMILL, J. F. C. 2014. The Speed of Sound in Silk: Linking Material Performance to Biological Function. *Advanced Materials,* 26**,** 5179-5183.

MORTIMER, B., SOLER, A., SIVIOUR, C. R. & VOLLRATH, F. 2018. Remote monitoring of vibrational information in spider webs. *Science of Nature,* 105.

MORTIMER, B., SOLER, A., SIVIOUR, C. R., ZAERA, R. & VOLLRATH, F. 2016. Tuning the instrument: sonic properties in the spider's web. *Journal of the Royal Society Interface,* 13.

MORTIMER, B., SOLER, A., WILKINS, L. & VOLLRATH, F. 2019. Decoding the locational information in the orb web vibrations of *Araneus diadematus* and *Zygiella x-notata*. *Journal of the Royal Society Interface,* 16.

MOYA-LARANO, J., MACIAS-ORDONEZ, R., BLANCKENHORN, W. U. & FERNANDEZ-MONTRAVETA, C. 2008. Analysing body condition: mass, volume or density? *Journal of Animal Ecology,* 77**,** 1099-1108.

MÜLLER, V. C. & HOFFMANN, M. 2017. What Is Morphological Computation? On How the Body Contributes to Cognition and Control. *Artificial Life,* 23**,** 1-24.

NAFTILAN, S. A. 1999. Transmission of vibrations in funnel and sheet spider webs. *International Journal of Biological Macromolecules,* 24**,** 289-293.

O'CONNELL-RODWELL, C. E. 2007. Keeping an "Ear" to the ground: Seismic communication in elephants. *Physiology,* 22**,** 287-294.

OLIVE, C. W. 1980. Foraging specializations in orb-weaving spiders. *Ecology,* 61**,** 1133-1144.

PASQUET, A., CARDOT, J. & LEBORGNE, R. 2007. Wasp attacks and spider defence in the orb weaving species *Zygiella x-notata*. *Journal of Insect Behavior,* 20**,** 553-564.

PATIL, B., PRABHU, S. & RAJASHEKHAR, K. P. 2006. Lyriform slit sense organs on the pedipalps and spinnerets of spiders. *Journal of Biosciences,* 31**,** 75-84.

PEETERS, B., VAN DER AUWERAER, H., GUILLAUME, P. & LEURIDAN, J. 2004. The PolyMAX frequency-domain method: a new standard for modal parameter estimation? *Shock and Vibration,* 11**,** 395-409.

PFEIFER, R. & BONGARD, J. 2006. *How the Body Shapes the Way we Think: A New View of Intelligence.,* Cambridge, MA, MIT Press.

PITTELLA, R. S., BASSA, P. G., ZEFA, E. & BIANCHI, F. M. 2023. Using the Integrative Approach to Update a Gap of One Century: Redescription and New Distribution Records of the South American Tarantulas *Grammostola pulchra* (Araneae: Mygalomorphae: Theraphosidae). *Zoological Studies,* 62.

POLITI, Y., BERTINETTI, L., FRATZL, P. & BARTH, F. G. 2021. The spider cuticle: a remarkable material toolbox for functional diversity. *Philosophical Transactions of the Royal Society a-Mathematical Physical and Engineering Sciences,* 379.

PRINGLE, J. W. S. 1938. Proprioception in insects II. The action of the campaniform sensilla on the legs. *Journal of Experimental Biology,* 15**,** 114-131.

PRINGLE, J. W. S. 1955. The Function of the Lyriform Organs of Arachnids. *Journal of Experimental Biology,* 32**,** 270-278.

PROVENCHER, L. & RIECHERT, S. E. 1991. Short-term effects of hunger conditioning on spider behavior, predation, and gain of weight. *Oikos,* 62**,** 160-166.

SCHABER, C. F., GORB, S. N. & BARTH, F. G. 2012. Force transformation in spider strain sensors: white light interferometry. *Journal of the Royal Society Interface,* 9**,** 1254-1264.

SCHARFF, N., CODDINGTON, J. A., BLACKLEDGE, T. A., AGNARSSON, I., FRAMENAU, V. W., SZUTS, T., HAYASHI, C. Y. & DIMITROV, D. 2020. Phylogeny of the orb-weaving spider family Araneidae (Araneae: Araneoidea). *Cladistics,* 36**,** 1-21.

SCHUCH, W. & BARTH, F. G. 1985. Temporal patterns in the vibratory courtship signals of the wandering spider *Cupiennius salei* Keys. *Behavioral Ecology and Sociobiology,* 16**,** 263-271.

SCHUCH, W. & BARTH, F. G. 1990. Vibratory communication in a spider - female responses to synthetic male vibrations. *Journal of Comparative Physiology a-Neuroethology Sensory Neural and Behavioral Physiology,* 166**,** 817-826.

SEO, J. H., KIM, K. J., KIM, H. & MOON, M. J. 2020. Lyriform vibration receptors in the web-building spider, *Nephila clavata* (Araneidae: Araneae: Arachnida). *Entomological Research,* 50**,** 586-593.

SEYFARTH, E. A. 1978. Lyriform slit sense-organs and muscle reflexes in spider leg. *J. Comp. Physiol.,* 125**,** 45–57.

SEYFARTH, E. A. & BARTH, F. G. 1972. Compound slit sense organs on spider leg - mechanoreceptors involved in kinesthetic orientation. *Journal of Comparative Physiology,* 78**,** 176-&.

SEYFARTH, E. A., ECKWEILER, W. & HAMMER, K. 1985. Proprioceptors and sensory nerves in the legs of a spider. *Cupiennius salei* (Arachnida, Araneida). *Zoomorphology,* 105**,** 190-196.

SEYFARTH, E. A., GNATZY, W. & HAMMER, K. 1990. Coxal hair plates in spiders - physiology, fine-structure, and specific central projections. *Journal of Comparative Physiology a-Sensory Neural and Behavioral Physiology,* 166**,** 633-642.

SEYFARTH, E. A., HERGENRODER, R., EBBES, H. & BARTH, F. G. 1982. Idiothetic orientation of a wandering spider - compensation of detours and estimates of goal distance. *Behavioral Ecology and Sociobiology,* 11**,** 139-148.

SHABANA, A. A. 2020. *Dynamics of multibody systems.,* Cambridge, Cambridge University Press.

SPECK, J. & BARTH, F. G. 1982. Vibration sensitivity of pretarsal slit sensilla in the spider leg. *Journal of Comparative Physiology,* 148**,** 187-194.

SPECK-HERGENRÖDER, J. & BARTH, F. G. 1988. Vibration sensitive hairs on the spider leg. *Experientia,* 44**,** 13-14.

SPECKHERGENRODER, J. & BARTH, F. G. 1987. Tuning of vibration sensitive neurons in the central nervous system of a wandering spider, *Cupiennius salei* Keys. *Journal of Comparative Physiology a-Sensory Neural and Behavioral Physiology,* 160**,** 467-475.

STRAUS, S. & AVILÉS, L. 2018. Effects of host colony size and hygiene behaviours on social spider kleptoparasite loads along an elevation gradient. *Functional Ecology,* 32**,** 2707-2716.

STRAUSS, J., MORITZ, L. & RÜHR, P. T. 2021. The Subgenual Organ Complex in Stick Insects: Functional Morphology and Mechanical Coupling of a Complex Mechanosensory Organ. *Frontiers in Ecology and Evolution,* 9.

SUN, Y. H., BRANDT, E. E., ELIAS, D. O., ROSENTHAL, M. & KAMATH, A. 2021. Jumping Spiders (*Habronattus clypeatus*) Exhibit Substrate Preferences that Partially Maximize Vibration Transmission Efficiency. *Journal of Insect Behavior,* 34**,** 151-161.

VALEEV, A. 2023. Condition monitoring based on locating defects via strain gauge analysis. *Mechanical Systems and Signal Processing,* 182.

VALERO, M., LI, F. Y., ZHAO, L., ZHANG, C., GARRIDO, J. & HAN, Z. 2021. Vibration sensing-based human and infrastructure safety/health monitoring: A survey. *Digital Signal Processing,* 114.

VIBERT, S., SCOTT, C. & GRIES, G. 2016. Vibration transmission through sheet webs of hobo spiders (*Eratigena agrestis*) and tangle webs of western black widow spiders (*Latrodectus hesperus*). *Journal of Comparative Physiology a-Neuroethology Sensory Neural and Behavioral Physiology,* 202**,** 749-758.

VINCENT, J. 1990. *Structural Biomaterials Revised Edition.,* New Jersey, Princeton University Press.

VOGEL, H. 1923. Über die Spaltsinneorgane der Radnetzspinnen. *Jena. Z. Naturw,* 59**,** 171-208.

VOLLRATH, F. 1995. Lyriform organs on regenerated spider legs. *Bull. Br. Arachnol. Soc,* 10**,** 115-188.

VOLLRATH, F. 1999. Biology of spider silk. *International Journal of Biological Macromolecules,* 24**,** 81-88.

VOLLRATH, F. 2000. Strength and structure of spiders' silks. *J. Biotechnol.,* 74**,** 67-83.

VOLLRATH, F., DOWNES, M. & KRACKOW, S. 1997. Design variability in web geometry of an orb-weaving spider. *Physiology & Behavior,* 62**,** 735-743.

VOLLRATH, F., MADSEN, B. & SHAO, Z. Z. 2001. The effect of spinning conditions on the mechanics of a spider's dragline silk. *Proceedings of the Royal Society B-Biological Sciences,* 268**,** 2339-2346.

VOLLRATH, F. & SAMU, F. 1997. The effect of starvation on web geometry in an orb-weaving spider. *Bull. Br. Arachnol. Soc,* 10**,** 295-298.

WATANABE, T. 2000. The effect of starvation on web geometry in an orb-weaving spider. *Proc. R. Soc. B,* 267**,** 565–569.

WESSEL, A. 2014. Hildegard Strübing: A Pioneer in Vibrational Communication Research. *In:* COCROFT, R. B., GOGALA, M., HILL, P. S. M. & WESSEL, A. (eds.) *Studying Vibrational Communication.* Berlin, Heidelberg: Springer Berlin Heidelberg.

WIGNALL, A. E. & HERBERSTEIN, M. E. 2013. The Influence of Vibratory Courtship on Female Mating Behaviour in Orb-Web Spiders (*Argiope keyserlingi*, Karsch 1878). *Plos One,* 8.

WILSON, R. S. 1970. Some comments on the hydrostatic system of spiders (Chelicerata, Araneae). *Zeitschrift für Morphologie der Tiere,* 68**,** 308-322.

WIRTH, E. 1984. *Die Bedeutung von Zeit- und Amplitude- nunterschieden fur die Orientierung nach vibratorischen Signalen bei Spinnen.*, Diplomarbeit, Fachbereich Biolo- gie der Universitit Frankfurt.

WIRTH, E. & BARTH, F. G. 1992. Forces in the spider orb web. *J. Comp. Physiol. A,* 171**,** 359–371.

WORDEN, K. & TOMLINSON, G. R. 2001. *Nonlinearity in Structural Dynamics: Detection, Identification and Modelling,* Boca Raton, CRC Press.

WU, C. H. & ELIAS, D. O. 2014. Vibratory noise in anthropogenic habitats and its effect on prey detection in a web-building spider. *Animal Behaviour,* 90**,** 47-56.

WU, J., MILLER, T. E., CICIRELLO, A. & MORTIMER, B. 2023. Spider dynamics under vertical vibration and its implications for biological vibration sensing. *Journal of the Royal Society Interface,* 20.

WU, J., ONDRA, V., LUEBKER, J., KALOW, S., RIEMENSCHNEIDER, J. & TITURUS, B. 2022a. Experimental modal analysis of a rotating tendon-loaded helicopter blade demonstrator. *Mechanical Systems and Signal Processing,* 178.

WU, J., QIU, Y. & SUN, C. 2022b. Modelling and analysis of coupled vibration of human body in the sagittal and coronal planes exposed to vertical, lateral and roll vibrations and the comparison with modal test. *Mechanical Systems and Signal Processing,* 166.

YACK, J. E. 2004. The structure and function of auditory chordotonal organs in insects. *Microscopy Research and Technique,* 63**,** 315-337.

YAGER, D. D. 1999. Structure, development, and evolution of insect auditory systems. *Microscopy Research and Technique,* 47**,** 380-400.

YOUNG, S. L., CHYASNAVICHYUS, M., BARTH, F. G., ZLOTNIKOV, I., POLITI, Y. & TSUKRUK, V. V. 2016. Micromechanical properties of strain-sensitive lyriform organs of a wandering spider (*Cupiennius salei*). *Acta Biomaterialia,* 41**,** 40-51.

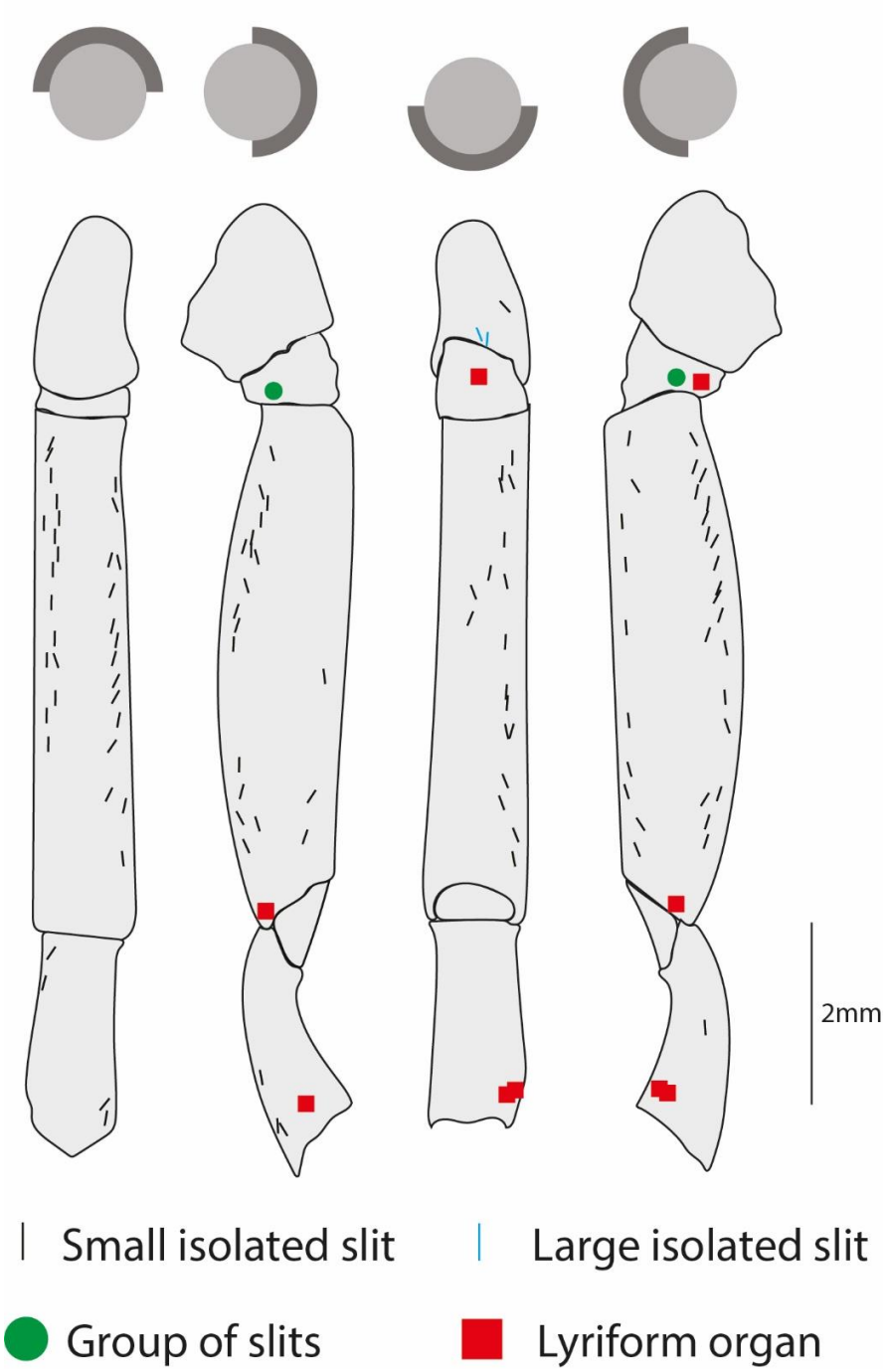
YOUNG, S. L., CHYASNAVICHYUS, M., ERKO, M., BARTH, F. G., FRATZL, P., ZLOTNIKOV, I., POLITI, Y. & TSUKRUK, V. V. 2014. A spider's biological vibration filter: Micromechanical characteristics of a biomaterial surface. *Acta Biomaterialia,* 10**,** 4832-4842.

ZAERA, R., SOLER, A. & TEUS, J. 2014. Uncovering changes in spider orb-web topology owing to aerodynamic effects. *Journal of the Royal Society Interface,* 11.

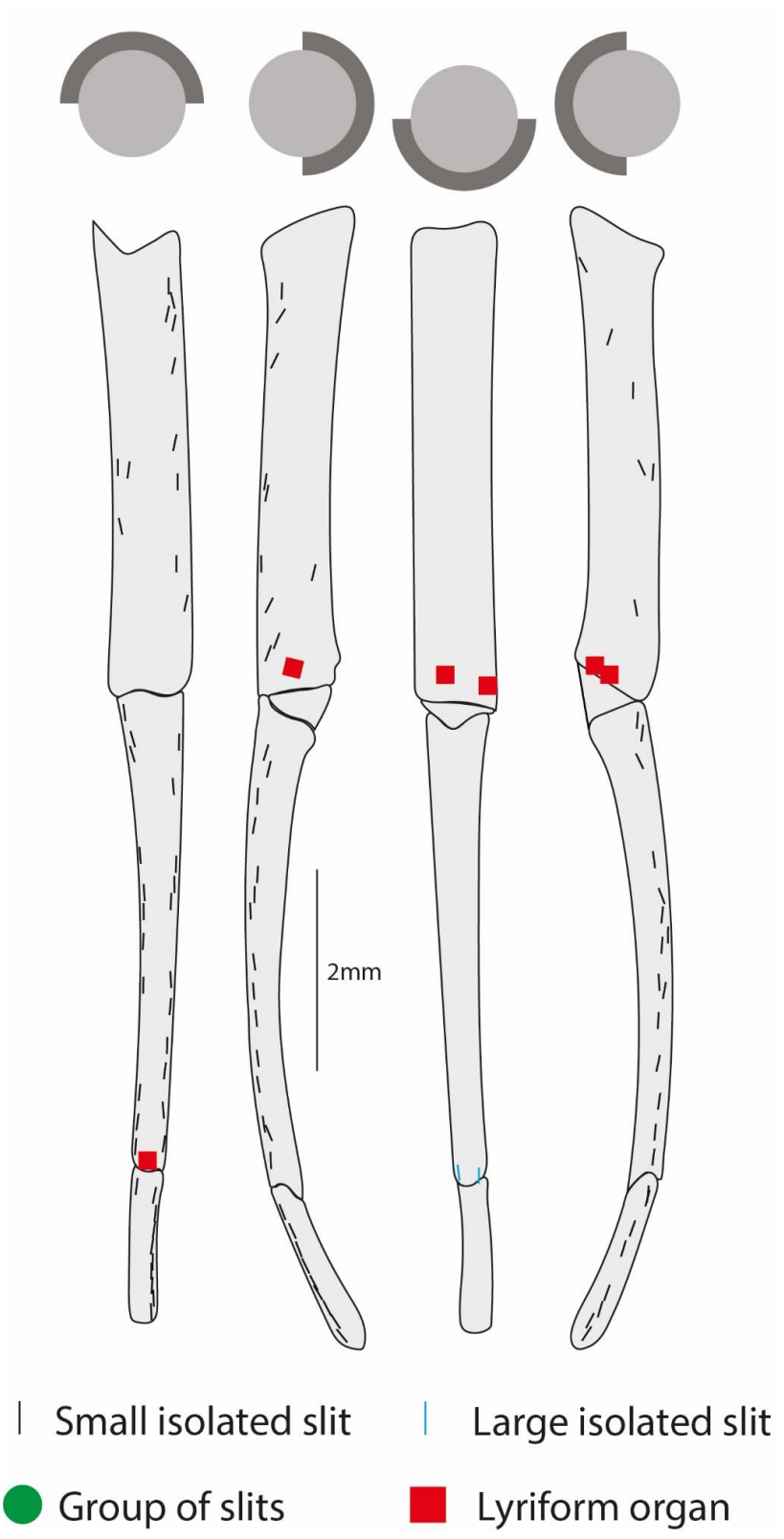
ZENTNER, L. 2013. *Modelling and application of the hydraulic spider leg mechanism.* Book chapter.

Appendix 1

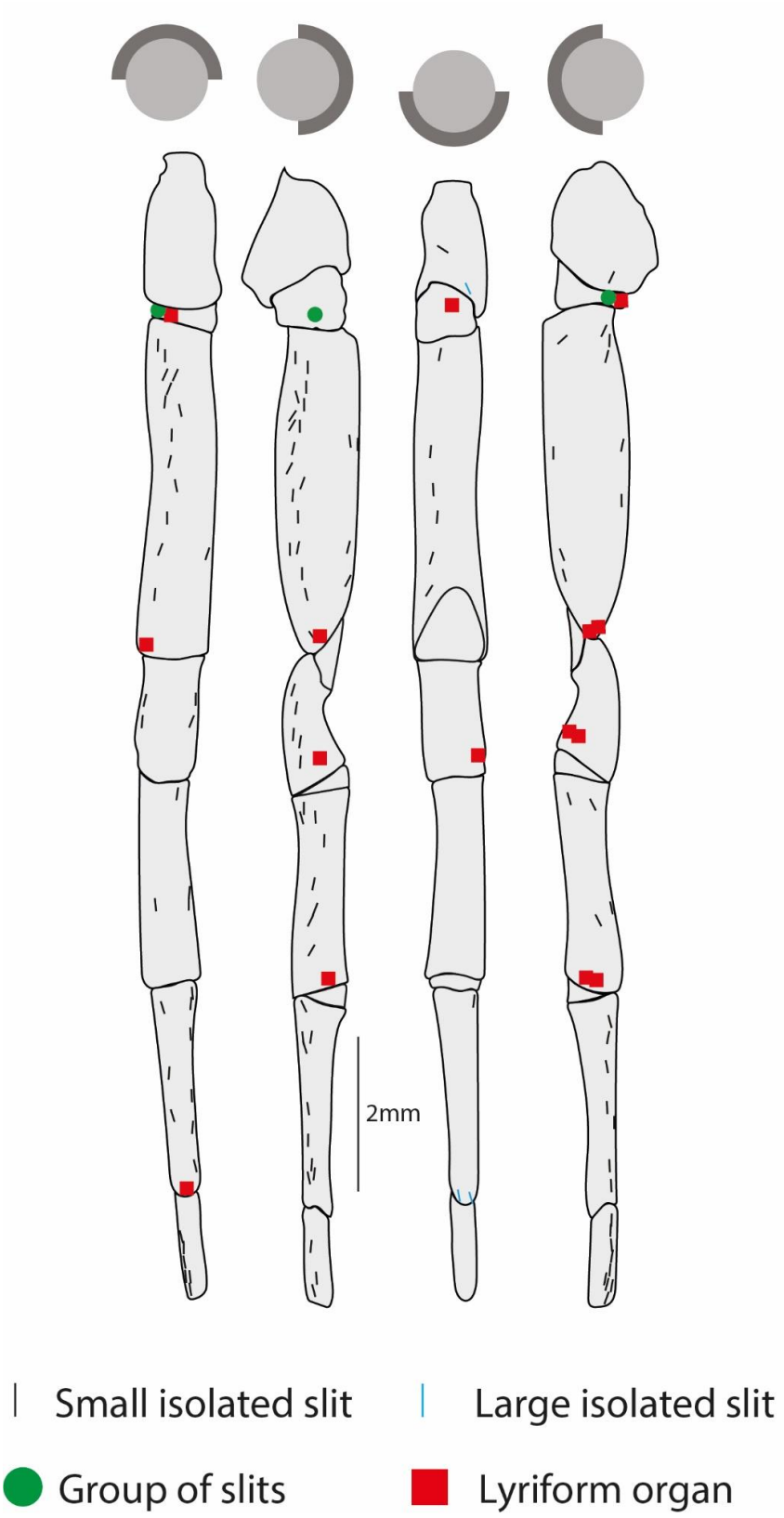
Chapter 2 – Supplementary Material



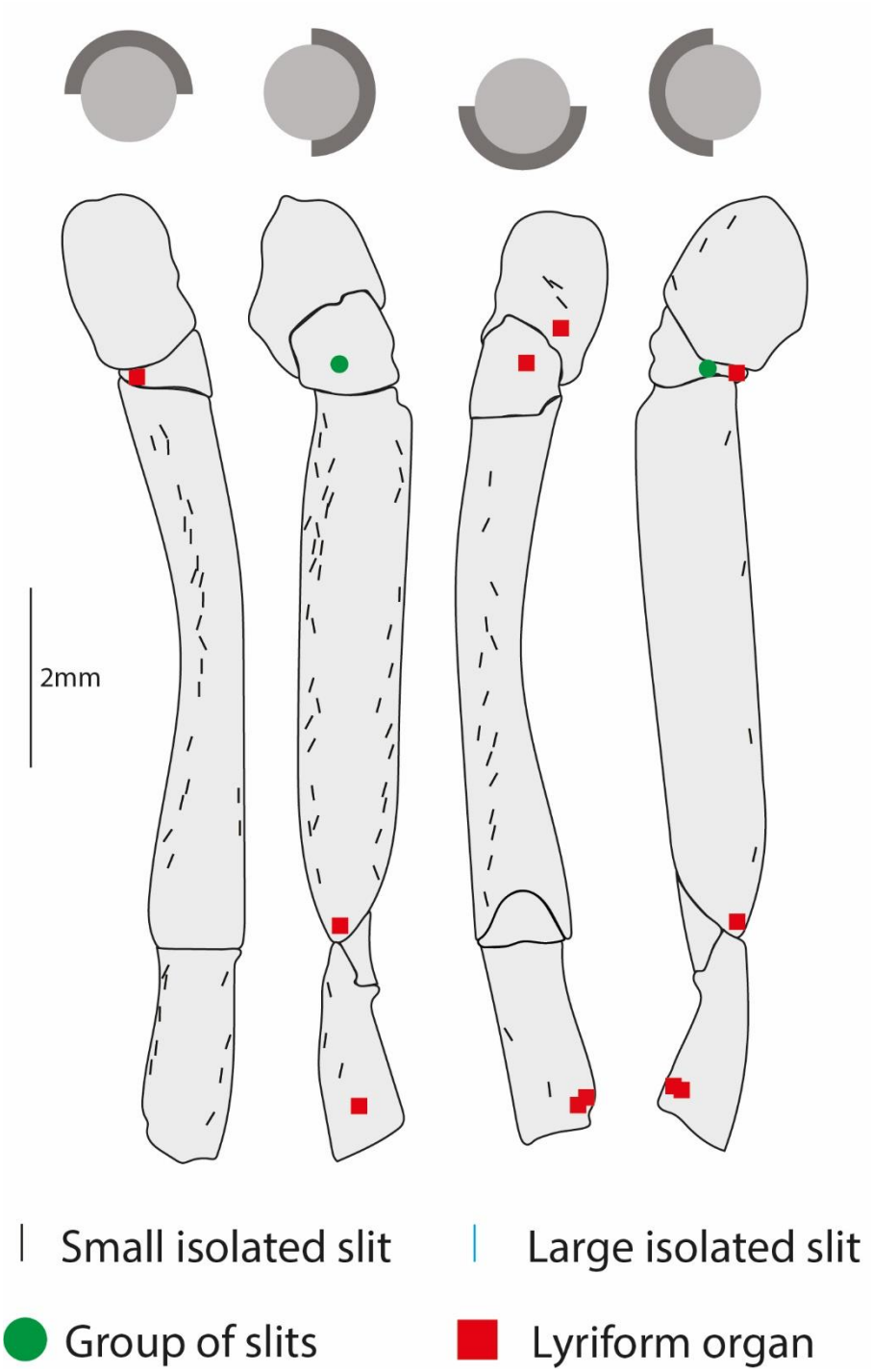
Supplementary figure 1: Schematic map of upper portion of Leg 2 of *Araneus diadematus*. From left to right – dorsal, prolateral, ventral and retrolateral view.



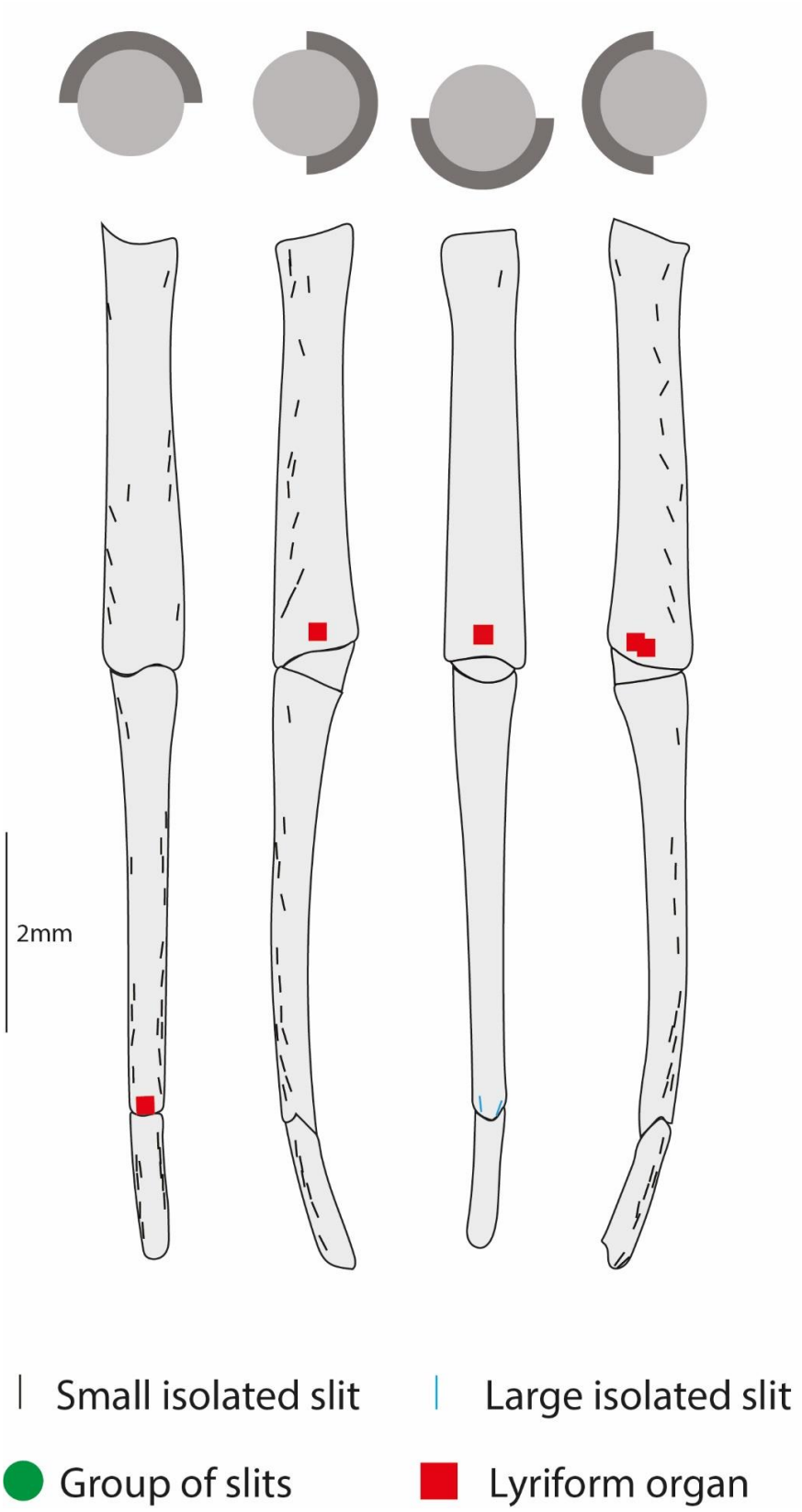
Supplementary figure 2 : Schematic map of lower portion of Leg 2 of *Araneus diadematus*. From left to right – dorsal, prolateral, ventral and retrolateral view.



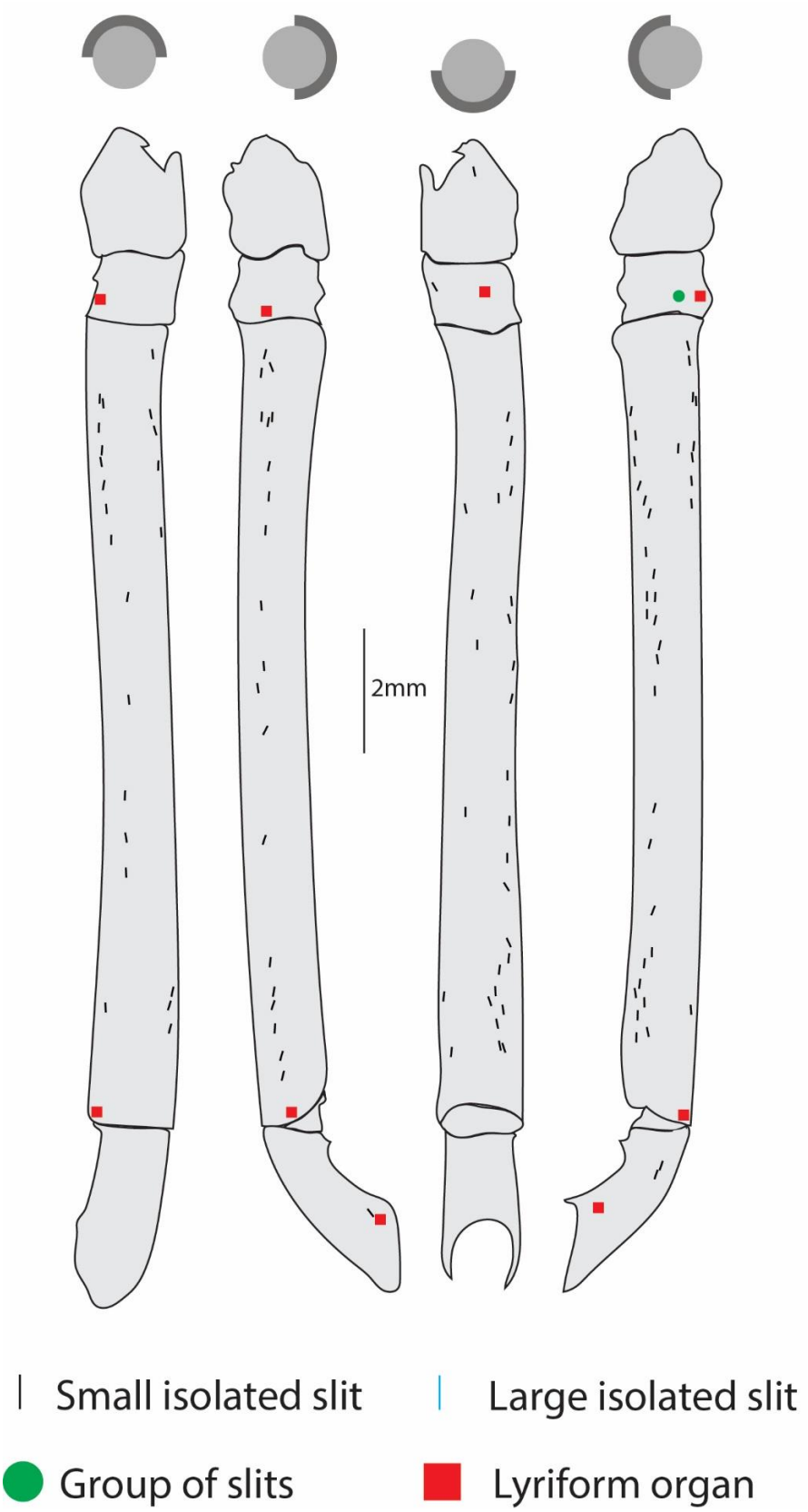
Supplementary figure 3: Schematic map of Leg 3 of *Araneus diadematus*. From left to right – dorsal, prolateral, ventral and retrolateral view.



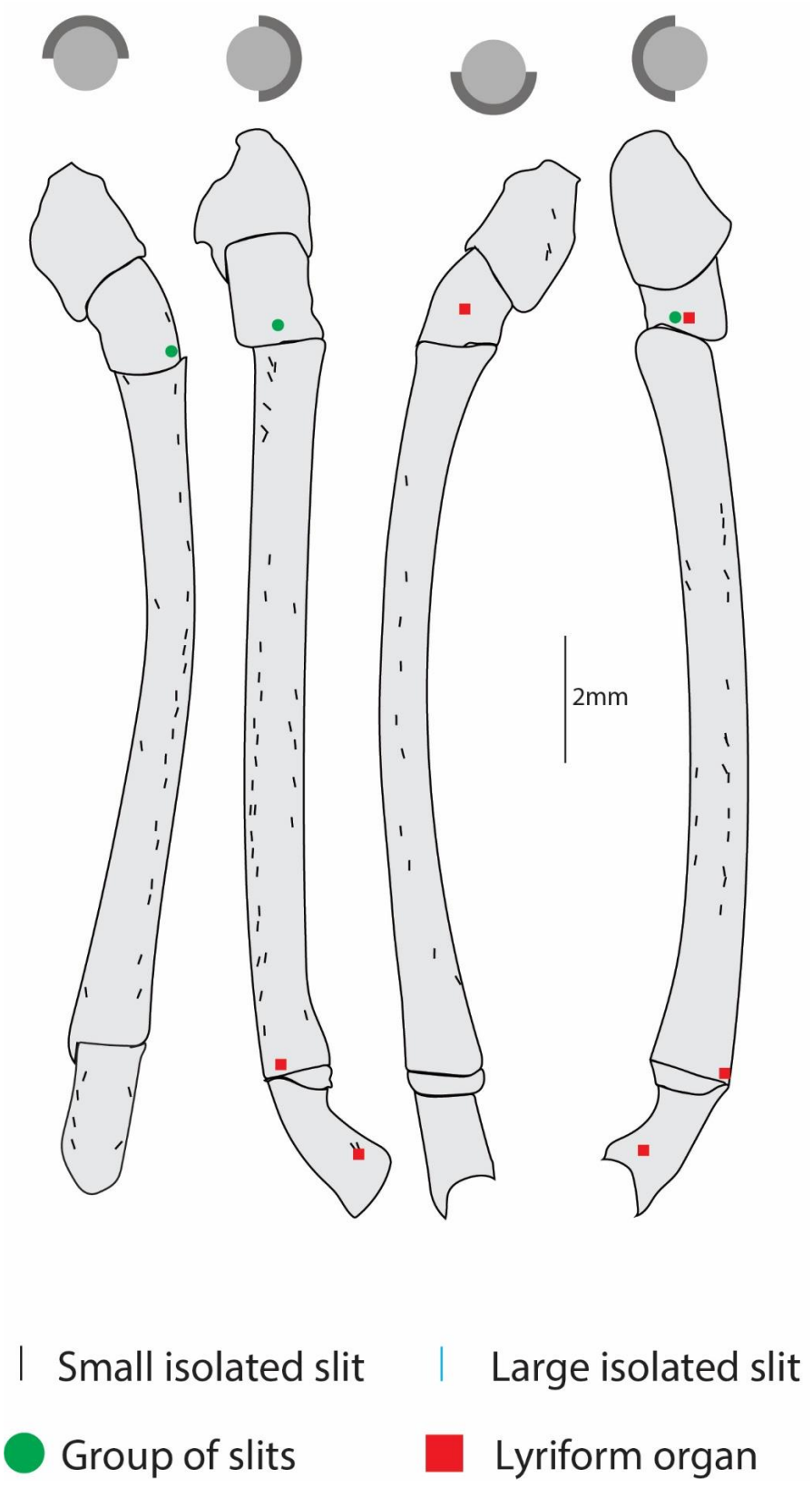
Supplementary figure 4: Schematic map of upper portion of Leg 4 of *Araneus diadematus*. From left to right – dorsal, prolateral, ventral and retrolateral view.



Supplementary figure 5: Schematic map of lower portion of Leg 4 of *Araneus diadematus*. From left to right – dorsal, prolateral, ventral and retrolateral view.

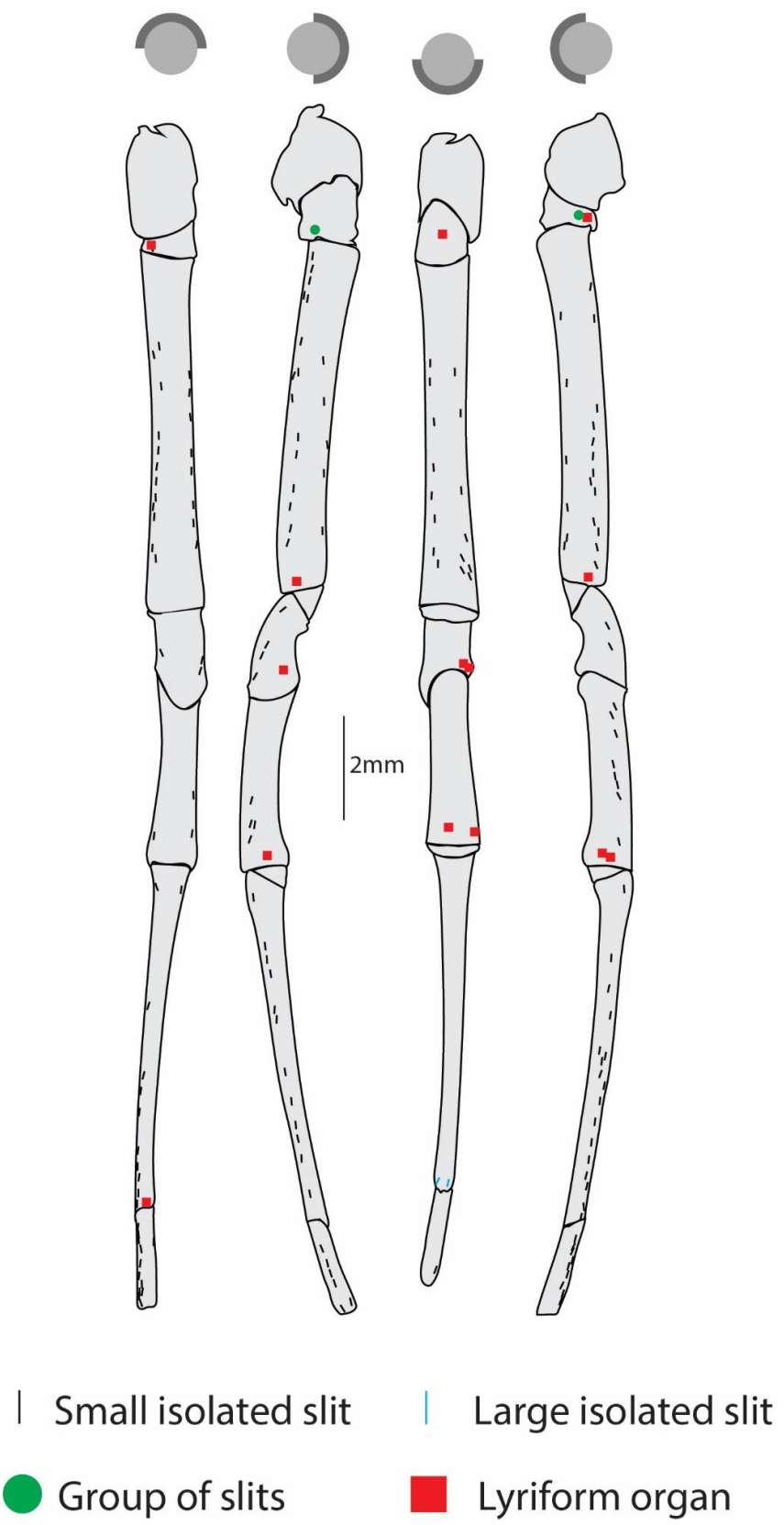


Supplementary figure 6: Schematic map of upper portion of Leg 2 of *Trichonephila edulis*. From left to right – dorsal, prolateral, ventral and retrolateral view.

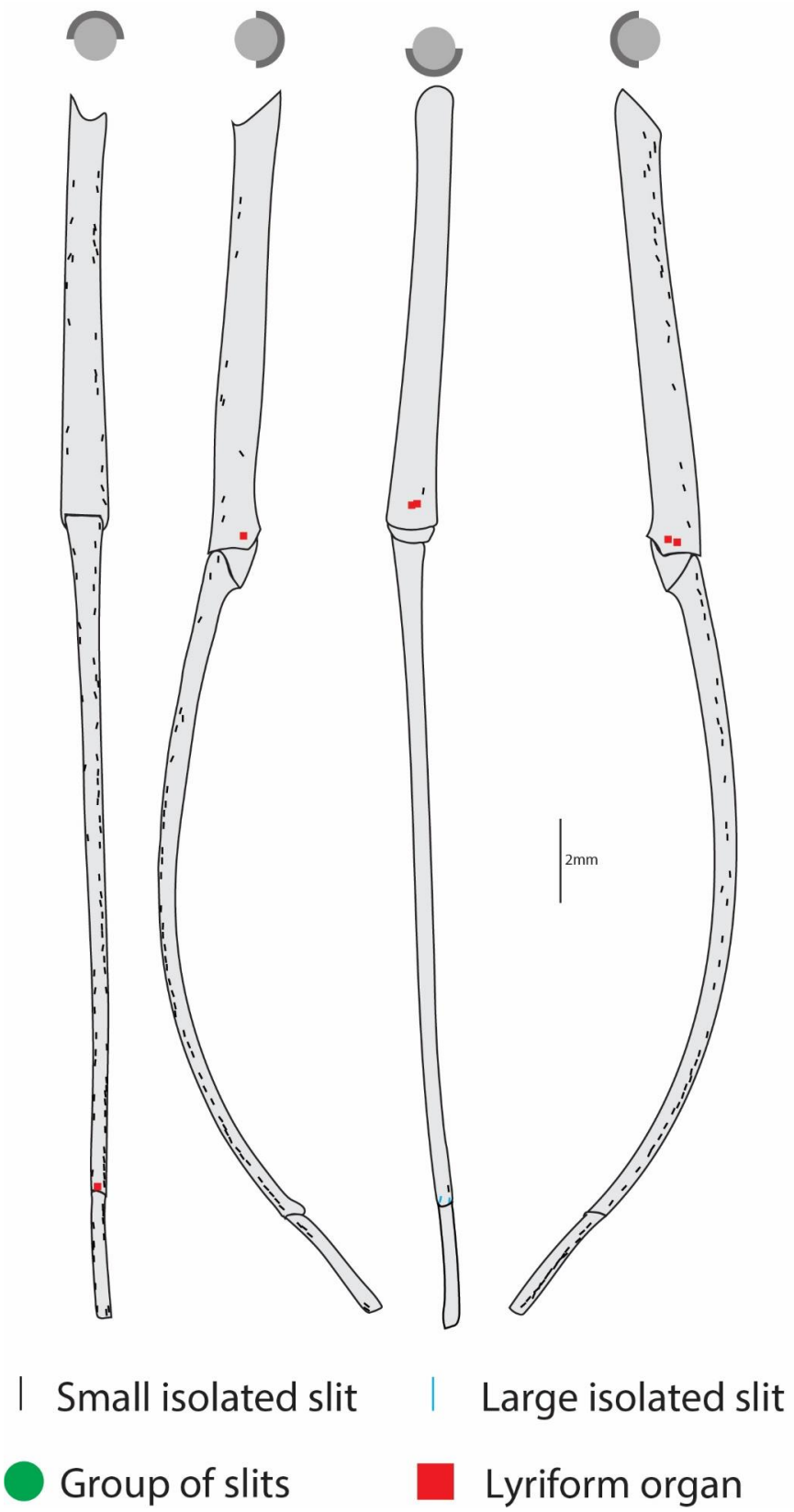


Supplementary figure 7: Schematic map of lower portion of Leg 1 of *Trichonephila edulis*. From left to right – dorsal, prolateral, ventral and retrolateral view.

Appendix 1

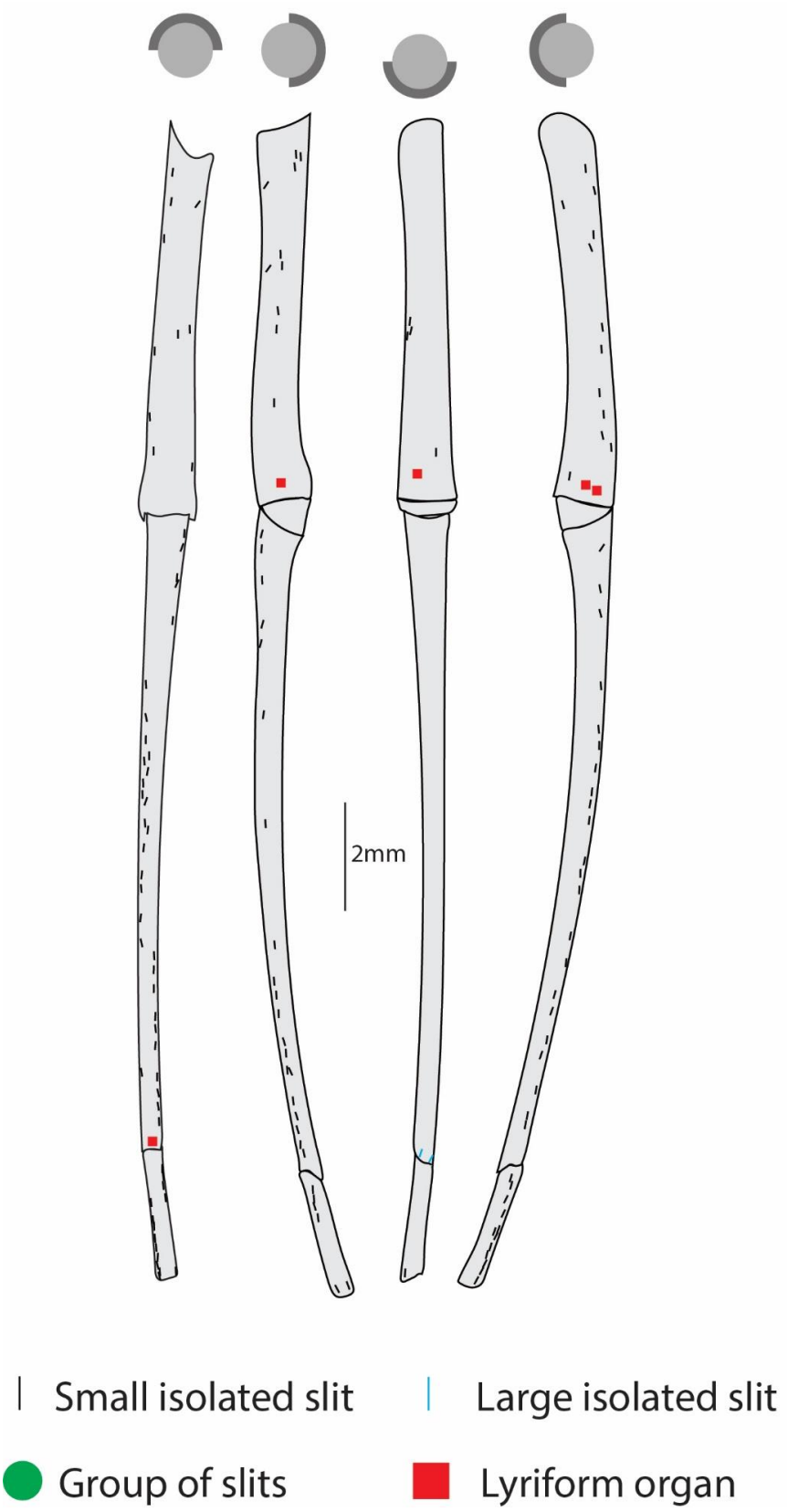


Supplementary figure 8: Schematic map of Leg 3 of *Trichonephila edulis*. From left to right – dorsal, prolateral, ventral and retrolateral view.



Supplementary figure 9: Schematic map of upper portion of Leg 4 of *Trichonephila edulis*. From left to right – dorsal, prolateral, ventral and retrolateral view.

Appendix 1



Supplementary figure 10: Schematic map of lower portion of Leg 1 of *Trichonephila edulis*. From left to right – dorsal, prolateral, ventral and retrolateral view.

Appendix 2

Chapter 3 – Supplementary Material

Supplementary table 1. Location of the centre of mass relative to the edges of the segment. xc, yc, zc: centre of mass coordinates. x1, x2, y1, y2, z1, z2: coordinates of maximum dimensions of each segment. measured along principal axes x, y and z passing through xc, yc, zc. All values given as pixel coordinates relative to reference frame of aligned segment (origin bottom left corner of final slice in stack). x1, x2, y1, y2, z1, z2 not given for pedipalp due to the geometry of this segment.

Segment	xc	yc	zc	x1	x2	y1	y2	z1	z2
Leg 1 coxa	154	185	278	69	274	105	272	127	450
Leg 1 femur	163	233	379	115	238	150	325	123	675
Leg 1 metatarsus	102.5	110	216	60	147	68	154	69	384
Leg 1 patella	145.5	155.5	192	80	215	93	219	58	362
Leg 1 tarsus	107	110	211	63	153	66	156	64	311
Leg 1 tibia	139.5	225	319.5	86	201	164	283	118	542
Leg 1 trochanter	124.5	135.5	153.5	46	207	46	234	87	236
Leg 2 coxa	159.5	190.5	228	39	246	109	271	108	370
Leg 2 femur	153	223.5	378.5	101	226	146	304	158	594
Leg 2 metatarsus	101	107.5	253.5	62	142	70	146	93	387
Leg 2 patella	121	171	194	62	182	106	235	72	346
Leg 2 tarsus	105	114	182.5	64	149	73	158	26	305
Leg 2 tibia	130	208.5	256.5	84	185	154	260	47	441
Leg 2 trochanter	105	105.5	128.5	34	180	38	172	33	208
Leg 3 coxa	136.5	179.5	264.5	57	215	67	275	118	378
Leg 3 femur	187	198.5	413.5	120	260	134	266	199	639
Leg 3 metatarsus	163	186.5	294.5	126	203	151	225	132	478
Leg 3 patella	127	191.5	207.5	78	180	91	320	145	271
Leg 3 tarsus	128	173.5	192.5	91	168	135	215	40	327
Leg 3 tibia	104.5	238.5	255.5	63	158	191	286	89	434
Leg 3 trochanter	115.5	130	164	27	197	66	194	98	236
Abdomen	561.5	562	860	98	1030	44	1078	166	1522
Cephalothorax	390	472	596.5	132	641	258	742	104	1142
Pedipalp	230	292	465	-	-	-	-	-	-

Appendix 3

Chapter 4 – Supplementary Material

S1 Method

S1.1 Equations of motion

The equations of motion (EoM) of the spider model under leg excitations are first derived separately for each degree-of-freedom, and then combined in matrix form. For the bounce of the spider body, the EoM is given by

$$m_b\ddot{w}_b + \sum_{\substack{i=l,r\\ j=f,r\\ n=1,2}} k_{ijn}(w_{ijn} - \mathrm{g}_{ijn}) + c_{ijn}(\dot{w}_{ijn} - \dot{\mathrm{g}}_{ijn}) = 0 \tag{S1}$$

where $w_{ijn} = w_b + \varphi_b y_{jn} - \theta x_{ijn}$ is the displacement of the spider body at the coordinate (x_{ijn}, y_{jn}); $\dot{\square} = \frac{\mathrm{d}\square}{\mathrm{d}t}$, and $\ddot{\square} = \frac{\mathrm{d}^2\square}{\mathrm{d}t^2}$.

For the pitch of the spider body, the EoM is given by

$$I_x\ddot{\varphi}_b + \sum_{\substack{i=l,r\\ j=f,r\\ n=1,2}} \left[k_{ijn}(w_{ijn} - \mathrm{g}_{ijn}) + c_{ijn}(\dot{w}_{ijn} - \dot{\mathrm{g}}_{ijn})\right] y_{jn} = 0 \tag{S2}$$

For the roll of the spider body, the EoM is given by

$$I_y\ddot{\theta}_b + \sum_{\substack{i=l,r\\ j=f,r\\ n=1,2}} \left[k_{ijn}(w_{ijn} - \mathrm{g}_{ijn}) + c_{ijn}(\dot{w}_{ijn} - \dot{\mathrm{g}}_{ijn})\right] x_{ijn}(-1) = 0 \tag{S3}$$

For the bounce of the leg ijn, the EoM is given by

$$m_{ijn}\ddot{\mathrm{g}}_{ijn} + k_{ijn}(\mathrm{g}_{ijn} - w_{ijn}) + c_{ijn}(\dot{\mathrm{g}}_{ijn} - \dot{w}_{ijn}) + k^g_{ijn}(\mathrm{g}_{ijn} - z_{ijn}) + c^g_{ijn}(\dot{\mathrm{g}}_{ijn} - \dot{z}_{ijn}) = 0 \tag{S4}$$

$$i = l, r;\ j = f, r;\ n = 1, 2$$

The above equations of motion are then expressed in matrix form as follows:

$$\mathbf{M}\ddot{\mathbf{q}} + \mathbf{C}\dot{\mathbf{q}} + \mathbf{K}\mathbf{q} = \mathbf{K}_r\mathbf{q}_r + \mathbf{C}_r\dot{\mathbf{q}}_r \tag{S5}$$

where $\mathbf{q}=\begin{bmatrix} w_b & \varphi_b & \theta_b & g_{lf1} & g_{lf2} & g_{lr1} & g_{lr2} & g_{rf1} & g_{rf2} & g_{rr1} & g_{rr2} \end{bmatrix}^{\mathrm{T}}$ is the generalized coordinate vector of the spider model, $\mathbf{q}_r=\begin{bmatrix} z_{lf1} & z_{lf2} & z_{lr1} & z_{lr2} & z_{rf1} & z_{rf2} & z_{rr1} & z_{rr2} \end{bmatrix}^{\mathrm{T}}$ is the vector consisting of the leg inputs. And $\mathbf{M}$, $\mathbf{C}$ and $\mathbf{K}$ are the mass, damping, stiffness matrices of the spider model, respectively; $\mathbf{K}_r$ and $\mathbf{C}_r$ are the stiffness and damping matrices associated with the input, respectively. How these parameters are determined is described in Section S2.

Analyses using the model in the frequency domain are carried out, and the corresponding methods, including modal analysis and the calculation of FRF, are introduced in general in the following Sections S1.2 and S1.3.

S1.2 Modal analysis

To perform modal analysis, $\mathbf{q}=\mathbf{Q}e^{\lambda t}$, where λ is the eigenvalue and $\mathbf{Q}$ is the eigenvector, is substituted into the state-space form of Eq.(S6) in free vibration as follows:

$$\mathbf{A}\dot{\mathbf{y}}+\mathbf{B}\mathbf{y}=\mathbf{0} \tag{S6}$$

where $\mathbf{y}=\begin{bmatrix}\mathbf{q}\\ \dot{\mathbf{q}}\end{bmatrix}$, $\mathbf{A}=\begin{bmatrix}\mathbf{C} & \mathbf{M}\\ \mathbf{M} & \mathbf{O}\end{bmatrix}$, and $\mathbf{B}=\begin{bmatrix}\mathbf{K} & \mathbf{O}\\ \mathbf{O} & -\mathbf{M}\end{bmatrix}$.

After solving the eigenvalue problem, the eigenvalues and the corresponding eigenvectors are obtained. The complex eigenvalues occur in the form of the complex conjugate pairs, where $\lambda_i=a_i+\mathrm{j}\omega_i$ and $\lambda_i^*=a_i-\mathrm{j}\omega_i$ is assumed for the i[th] pair and ω_i is the damped circular frequency. The damped natural frequency is $f_i=\dfrac{\omega_i}{2\pi}$ and the damping ratio is $\zeta_i=\dfrac{-a_i}{\sqrt{a_i^2+\omega_i^2}}$. The corresponding eigenvectors also come in the complex conjugate form, respectively, as $\mathbf{Y}_i=\begin{Bmatrix}\mathbf{Q}_i\\ \lambda_i\mathbf{Q}_i\end{Bmatrix}$ and $\mathbf{Y}_i^*=\begin{Bmatrix}\mathbf{Q}_i^*\\ \lambda_i^*\mathbf{Q}_i^*\end{Bmatrix}$, where $\mathbf{Q}_i=\mathrm{Re}(\mathbf{Q}_i)+\mathrm{j}\,\mathrm{Im}(\mathbf{Q}_i)$. The modal vector $\mathbf{Q}_i$ is used to plot the i[th] mode shape.

S1.3 Frequency response function (FRF)

As from the experimental measurements, we calculate FRFs from our models to inform model calibration (Section S2) and for parametric studies (Section 4). The FRFs matrix from each leg input to the 11 generalized coordinates are derived from Eq.(S5) as follows:

$$\mathbf{H}(f) = (-\mathbf{M}\omega^2 + \mathrm{j}\omega\mathbf{C} + \mathbf{K})^{-1}(\mathbf{K}_r + \mathrm{j}\omega\mathbf{C}_r) \tag{S7}$$

where $\omega = 2\pi f$ (rad/s) is the circular frequency while f (Hz) is the frequency, $\mathrm{j} = \sqrt{-1}$ is the imaginary unit, the i[th] row j[th] column element in the FRF matrix $\mathbf{H}(f)$ is the FRF from j[th] leg input in $\mathbf{q}_r$ to the i[th] generalized coordinate in $\mathbf{q}$. In the following two cases, there is a specific relationship between the 8 leg inputs, which enables the calculation of FRF from one reference leg input to one of the generalized coordinates.

S1.3.1 Equal inputs

To enable comparison of the modal test from experimental data and our model, we used an input where the vibration to all the eight legs are the same (similar to the metal plate where the spider sits), so the input vector $\mathbf{q}_r = \mathbf{I}z$, where $\mathbf{I} = [\underbrace{1 \quad \cdots \quad 1}_{8}]^{\mathrm{T}}$, z is the vertical input from the plate. The FRF vector from the input to the outputs is given by

$$\mathbf{H}_e(f) = \mathbf{H}(f)\mathbf{I} \tag{S8}$$

The FRF $H_{ei}(f)$ from the plate input to the i[th] generalized coordinate of the model in $\mathbf{q}$ is the i[th] element in the vector $\mathbf{H}_e(f)$.

S1.3.2 Different inputs

We also used a different input scenario for the models for our parametric test (Section 4). We used a more realistic circumstance where there is a point vibration source in front of the spider, as shown in Figure2b. The vibration from the source transmits in a speed of V and a decay rate of β. The FRFs are calculated by frequency sweeping, so the vibration source is assumed to be in the following sinusoidal form:

$$y = A\exp\left(-\beta x + \mathrm{j}\left(2\pi x/\lambda - 2\pi ft + \varphi\right)\right) \tag{S9}$$

where A is the amplitude of the sinusoidal vibration, φ is the initial phase, $\lambda = V / f$ is the wavelength, x is the travelling distance from the source, and t is time.

The inputs to all the eight legs are different, dependent on their distance from the vibration source. Thus, the input vector in this case is given by

$$\mathbf{q}_r = \mathbf{Q} z_{lf1} \tag{S10}$$

where z_{lf1} is the input for the leg lf1 (chosen as the reference input), and $\mathbf{Q} = [\underbrace{1 \quad \cdots \quad \exp(-\beta\Delta l_{ijn} + \mathrm{j}2\pi\Delta l_{ijn}/\lambda) \quad \cdots \quad \exp(-\beta\Delta l_{rr2} + \mathrm{j}2\pi\Delta l_{rr2}/\lambda)}_{8}]^{\mathrm{T}}$, $\Delta l_{ijn} = l_{ijn} - l_{lf1}$, and l_{ijn} is the distance from the leg ijn to the vibration source.

The FRF vector from the leg lf1 input (z_{lf1}) to the outputs is given by

$$\mathbf{H}_d(f) = \mathbf{H}(f)\mathbf{Q} \tag{S11}$$

The FRF $H_{di}(f)$ from the reference input z_{lf1} to the ith generalized coordinate of the model in $\mathbf{q}$ is the ith element in the vector $\mathbf{H}_d$. Other leg inputs can also be selected as the reference input, which will change the FRFs consistently, but will not influence the parametric study.

S2 Model Calibration

To make the model have a good consistency with the experiment, model calibration is necessary. The purpose of this section is to introduce the modal parameters to be calibrated, the chosen objectives for calibration and the algorithm used for calibration.

S2.1 Model parameters for calibration

Some parameters are obtained by measurement from the real spider, i.e., the total mass of the spider from weighing it (m), the leg-ground contact coordinates from photographs (x_{ijn}^g, y_{jn}^g). There are in total 31 parameters that need to be calibrated. Among them, 16 parameters are all the stiffness and damping coefficient (k_{ijn}, c_{ijn}, k_{ijn}^g, c_{ijn}^g); 7 parameters are the moments of inertia (I_x, I_y) and the masses for the body (m_b) and all the legs (

m_{ijn}); the other 8 parameters are the coordinates of the connection between the legs and the body (x_{ijn}, y_{jn}). All the parameters for calibration are constrained in a reasonable range. There is a constraint for all the masses, i.e., the summation of all the masses should be equal to the total mass of the spider, given as follows:

$$m_b + \sum_{\substack{i=l,r \\ j=f,r \\ n=1,2}} m_{ijn} = m \tag{S12}$$

S2.2 Objectives of model calibration

The model calibration takes the following four objectives into account:

Objective 1: to minimize the difference of the natural frequencies between the model and experiment, which is evaluated by the weighted root-mean-square (r.m.s) error given as follows:

$$\mathrm{obj}_1 = \sqrt{\frac{1}{N}\sum_{i=1}^{N}\left(\frac{f_i^{exp} - f_i^{m}}{f_i^{exp}} w_i^f\right)^2} \tag{S13}$$

where f means the natural frequency; the superscripts *exp* and *m* represent the values from the experiment and model, respectively; the subscript *i* represents the ith mode; w_i^f is the weighting factor for ith mode; N is the total number of the considered modes.

Objective 2: to minimize the difference of the damping ratios between the model and experiment, which is evaluated by the weighted r.m.s error given as follows:

$$\mathrm{obj}_2 = \sqrt{\frac{1}{N}\sum_{i=1}^{N}\left(\frac{\zeta_i^{exp} - \zeta_i^{m}}{\zeta_i^{exp}} w_i^d\right)^2} \tag{S14}$$

where ζ means the damping ratio; w_i^d is the weighting factor for ith mode.

Objective 3: to maximize the resemblance of the mode shapes between the model and experiment, which is evaluated by the weighted modal assurance criterion (WMAC) value between the mode shapes obtained from the model and experiment [1]. The reason why the WMAC value is used instead of the modal assurance criterion (MAC) value is that the model includes both translational DOFs and rotational DOFs and their weightings are not the same. To this end, the experimental mode shapes are reconstructed according to the model DOFs. The vertical displacement at K0 is selected to correspond to the body bounce

(w_b). The difference between the vertical displacements at L0 and K0 divided by their distance (2 cm) is selected to correspond to the body pitch (φ_b). The difference between the vertical displacements at K3 and K2 divided by their distance (1.1 cm) is selected to correspond to the body roll (θ_b). The vertical displacements at the proximal leg joints (A5, B5, …, H5) (more significant leg vibrations when being close to the body) are selected to correspond to the bounce of the legs in the model (g_{ijn}). Then the WMAC values between the mode shapes obtained from the model and experiment are calculated and the objective function is given as follows:

$$\mathrm{obj}_3 = -\sum_{i=1}^{N} \mathrm{WMAC}_i \cdot w_i^m \tag{S15}$$

where w_i^m is the weighting factor for i[th] mode; minus sign is added because the objective is to maximize the WMAC values; WMAC_i is the WMAC value between i[th] experimental mode shape and i[th] model mode shape, given by

$$\mathrm{WMAC}_i = \frac{\left|\mathbf{Q}_i^{exp\mathrm{H}} \mathbf{W} \mathbf{Q}_i^m\right|^2}{\left(\mathbf{Q}_i^{exp\mathrm{H}} \mathbf{W} \mathbf{Q}_i^{exp}\right)\left(\mathbf{Q}_i^{m\mathrm{H}} \mathbf{W} \mathbf{Q}_i^m\right)} \tag{S16}$$

where $\mathbf{Q}_i^m$ and $\mathbf{Q}_i^{exp}$ represent the i[th] modal vectors from the model and experiment, respectively; $\mathbf{W}$ is the weighting matrix; in this paper, the weighting matrix is the mass matrix $\mathbf{M}$; the superscript H stands for the conjugate transpose.

Objective 4: to minimize the difference of the FRFs between the model and experiment under equal leg inputs. The FRFs from the vertical input of the plate to the 10 DOFs of the model (except the body roll) are calculated according to Eq.(S8). The corresponding experimental FRFs to the displacements/rotational angles reconstructed in the same way as objective 3 are also calculated. Roll DOF is not included because the equal inputs for all the eight legs cannot excite the roll motion of the spider due to the symmetry about the mid-sagittal plane. The objective function is given as follows:

$$\mathrm{obj}_4 = \sum_{\substack{i=1 \\ i\neq 3}}^{11} w_i^h \sum_{j=1}^{N_f} \left\{ \left[\mathrm{Re}\left(H_i^{exp}(f_j)\right) - \mathrm{Re}\left(H_i^m(f_j)\right) \right]^2 + \left[\mathrm{Im}\left(H_i^{exp}(f_j)\right) - \mathrm{Im}\left(H_i^m(f_j)\right) \right]^2 \right\} \tag{S17}$$

where $H_i^{exp}(f_j)$ and $H_i^m(f_j)$ are the experimental FRF and model FRF to ith generalized coordinate at the frequency f_j, respectively; w_i^h is the weighting factor for ith FRF; f_j is the jth frequency point, and the frequency range taken into account in the model calibration is 20-200 Hz and the frequency resolution is 0.7812 Hz; N_f is the total number of frequency points. Taking both the real part and imaginary part of the FRFs into account ensures both the amplitude and phase of the FRFs are accurate.

The objective of the model calibration is to satisfy the objectives 1-4 while satisfying the upper and lower bounds for all parameters and the equality in Eq.(S12), so the total objective function is given by

$$\mathrm{obj} = \sum_{i=1}^{4} \mathrm{obj}_i \cdot w_i \tag{S18}$$

where w_i is the weighting factor for the ith objective function.

S2.3 Calibration algorithm

The model calibration is performed using a combined algorithm introduced in [2]. The procedure is summarized as follows: (1) All the parameters to be calibrated are constrained in a reasonable range; (2) The calibration starts from a global optimization using the genetic algorithm ('ga' function in Matlab) with randomly generated parameters in the constrained ranges; (3) Then the calibration follows with a local optimization using 'fmincon' function in Matlab by setting its initial values as the parameters obtained in the last step; (4) The steps 2-3 are repeated for a number of times and the optimal set of parameters among them are chosen as the final calibration result.

Appendix 3

Table S1 The parameters of the calibrated model. The superscript 1 means the parameters that were obtained by calibration. The superscript 2 means the parameters were obtained from measurement of the spider.

Parameters	Values	Parameters	Values
m [2]	7.7 g	c^g_{lr2}, c^g_{rr2} [1]	0.01 Ns/m
I_x [1]	6.18x10^{-7} kgm^2	x_{lf1} [1]	0.003 m
I_y [1]	3.03x10^{-7} kgm^2	y_{f1} [1]	-0.0046 m
m_b [1]	7.06 g	x_{lf2} [1]	0.0037 m
m_{lf1}, m_{rf1} [1]	0.08 g	y_{f2} [1]	-0.0035 m
m_{lf2}, m_{rf2} [1]	0.08 g	x_{lr2} [1]	0.0033 m
m_{lr1}, m_{rr1} [1]	0.08 g	y_{r2} [1]	0.003 m
m_{lr2}, m_{rr2} [1]	0.08 g	x_{lr1} [1]	0.003 m
k_{lf1}, k_{rf1} [1]	0.0123 N/m	y_{r1} [1]	0.0056 m
k_{lf2}, k_{rf2} [1]	33.78 N/m	x^g_{lf1} [2]	1.23 cm
k_{lr1}, k_{rr1} [1]	1000 N/m	y^g_{f1} [2]	-3.2 cm
k_{lr2}, k_{rr2} [1]	23.89 N/m	x^g_{lf2} [2]	2.34 cm
c_{lf1}, c_{rf1} [1]	4.64 Ns/m	y^g_{f2} [2]	-1.65 cm
c_{lf2}, c_{rf2} [1]	0.0116 Ns/m	x^g_{lr2} [2]	2.3 cm
c_{lr1}, c_{rr1} [1]	0	y^g_{r2} [2]	0.89 cm
c_{lr2}, c_{rr2} [1]	0	x^g_{lr1} [2]	1.41 cm
k^g_{lf1}, k^g_{rf1} [1]	565.56 N/m	y^g_{r1} [2]	3.17 cm
k^g_{lf2}, k^g_{rf2} [1]	28.52 N/m	$w^f_1 / w^f_2 / w^f_3 / w^f_4 / w^f_5$	3/3/2/2/2
k^g_{lr1}, k^g_{rr1} [1]	297.95 N/m	w^d_i $(i = 1, 2 \cdots 5)$	$w^f_i / 3$
k^g_{lr2}, k^g_{rr2} [1]	15.58 N/m	$w^m_1 / w^m_2 / w^m_3 / w^m_4 / w^m_5$	1/3/6/1/1
c^g_{lf1}, c^g_{rf1} [1]	0.44 Ns/m	w^h_i $(i = 1, 2 \cdots 11, i \neq 3)$	0.005, if $i = 2$; 1, others
c^g_{lf2}, c^g_{rf2} [1]	0.005 Ns/m	$w_1 / w_2 / w_3 / w_4$	3/3/1/1x10^{-3}
c^g_{lr1}, c^g_{rr1} [1]	0		

The stiffness and damping for different legs in Table S1 vary, which can be explained by the fact that the considered stiffness and damping are the vertical components of the

total leg stiffness and damping, which are dependent on the orientation of each leg, and also on hydrostatic pressure [3] or muscle action [4].

S3 Sensitivity analysis

Sensitivity analysis is conducted to show the sensitivity of the four objective functions (Section S2.2) to all the calibrated parameters. It is conducted by increasing one of the parameters by γ and keeping all the others unchanged, and the sensitivity is defined as follows:

$$S = \frac{\left|\mathrm{obj}_{new} - \mathrm{obj}_0\right| / \mathrm{obj}_0}{\gamma} \tag{S19}$$

where obj_0 and obj_{new} are the original value of the objective function and the value after parameter change. In this paper, γ is chosen as 20%.

Appendix 3

Table S2 Sensitivity analysis for the calibrated parameters. Please refer to Section S2.2 for objectives.

Parameters	Obj1	Obj2	Obj3	Obj4	Parameters	Obj1	Obj2	Obj3
I_x	7.91	0.27	0.21	0.88	I_y	6.83	0.008	0.007
k_{lf1}	0	0	0	0	k_{rf1}	0	0	0
k_{lf2}	0	0.003	0	0	k_{rf2}	0	0.003	0.012
k_{lr1}	0.5	0.05	0.014	0.048	k_{rr1}	0.5	0.05	0.01
k_{lr2}	0.03	0.002	0.01	0.0076	k_{rr2}	0.03	0.002	0.01
c_{lf1}	0.026	0.11	0	0.05	c_{rf1}	0.026	0.11	0.025
c_{lf2}	0	0.003	0	0.001	c_{rf2}	0	0.003	0.01
k^g_{lf1}	1.33	0.19	0.14	0.007	k^g_{rf1}	1.33	0.19	0.05
k^g_{lf2}	0.05	0	0.009	0.004	k^g_{rf2}	0.05	0	0.009
k^g_{lr1}	0.93	0.21	0.06	0.36	k^g_{rr1}	0.93	0.21	0.03
k^g_{lr2}	0.03	0.01	0	0.02	k^g_{rr2}	0.03	0.01	0.009
c^g_{lf1}	0.45	0.32	0.02	0.07	c^g_{rf1}	0.45	0.32	0.02
c^g_{lf2}	0	0.02	0.008	0.004	c^g_{rf2}	0	0.02	0.006
c^g_{lr2}	0.02	0.11	0.01	0.01	c^g_{rr2}	0.02	0.11	0.007
x_{lf1}	4.66	0.007	0.09	0	y_{f1}	0.94	0.57	0.42
x_{lf2}	0.04	0	0.002	0	y_{f2}	0.07	0.01	0
x_{lr2}	0.02	0	0	0	y_{r2}	0.08	0.003	0.01
x_{lr1}	1.3	0.02	0.009	0.001	y_{r1}	6.59	0.07	0.03
m_{lf1}	0.05	0.01	0.01	0.005	m_{rf1}	0.05	0.01	0.01
m_{lf2}	0.03	0.006	0.006	0.03	m_{rf2}	0.03	0.006	0.01
m_{lr1}	0.05	0.009	0.002	0.007	m_{rr1}	0.05	0.009	0.003
m_{lr2}	0.11	0.002	0.04	0.02	m_{rr2}	0.11	0.002	0.02
m_b	5.45	0.22	0.18	0.03				

The sensitivity analysis results are shown in Table S2. Results show that the natural frequencies (objective 1) are most sensitive to I_x, then I_y, y_{r1}, m_b, x_{lf1}, y_{f1}, k^g_{lf1}, k^g_{rf1}, x_{lr1}, k^g_{lr1}, k^g_{rr1}, k_{lr1}, k_{rr1}, c^g_{lf1}, c^g_{rf1} in descending order. The damping ratios (objective 2) are most sensitive to y_{f1}, then c^g_{lf1}, c^g_{rf1}, I_x, m_b, k^g_{lr1}, k^g_{rr1}, c_{lf1}, c_{rf1}, c^g_{lr2}, c^g_{rr2} in descending order. The mode shapes (objective 3) are most sensitive to y_{f1}, then I_x, m_b, k^g_{lf1}, x_{lf1}, k^g_{lr1}, k^g_{rf1}, k^g_{rr1}, m_{lr2}, y_{r1} in descending order. The FRFs (objective 4) are most sensitive to y_{r1}, then I_x, y_{f1}, k^g_{rr1}, k^g_{lr1}, c^g_{lf1}, c^g_{rf1}, m_{rf2}, c_{lf1}, c_{rf1} in descending order. It should be noted that the sensitivities are dependent on the weighting factors in the objective functions. Higher absolute sensitivity indicates that we can have more

confidence in the correctness of the parameter, and vice versa. They are not a measure of which parameters explain more of the dynamic motion of the spider model, this is investigated using a parametric test (Section 4).

S4 Modal identification results

The FRFs were reconstructed according to the PolyMAX theory (called 'modal FRF') and are compared with the measured FRFs, as shown in Figure S2 and Figure S3. In the measured FRFs, the peaks at 50 Hz and its multiples are not the genuine peaks but result from the alternating current mains noise. Because the distal joints of each leg (A1-H1) were in direct contact with the plate, their amplitudes were close to 1 in the whole frequency range. As the measurement joints get closer to the body, the resonances become clearer and the resonance amplitudes become higher.

By comparing the measured FRFs from vibrometry with the modal FRFs from PolyMAX theory, it can be seen the modal FRFs show good consistency with the measured FRFs, and all the resonances are reconstructed quite well, which means the modal identification is successful and the identified modal properties are reliable.

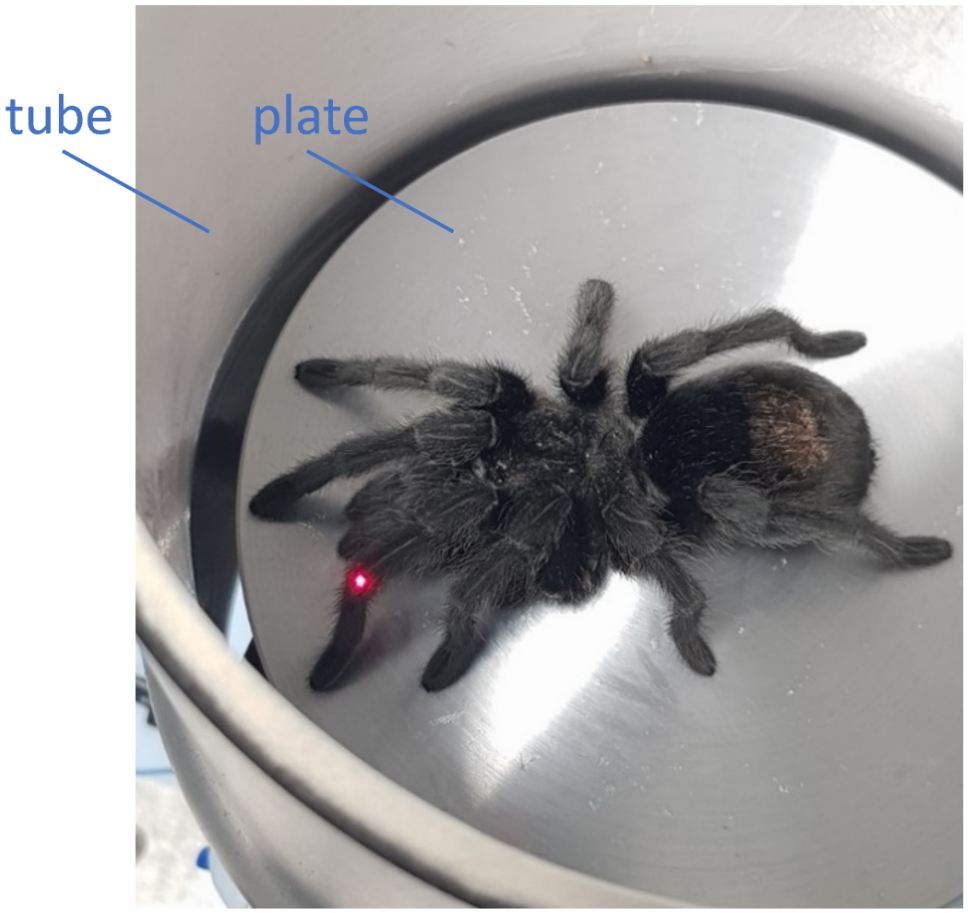


Figure S1 The posture of the real spider in the modal test.

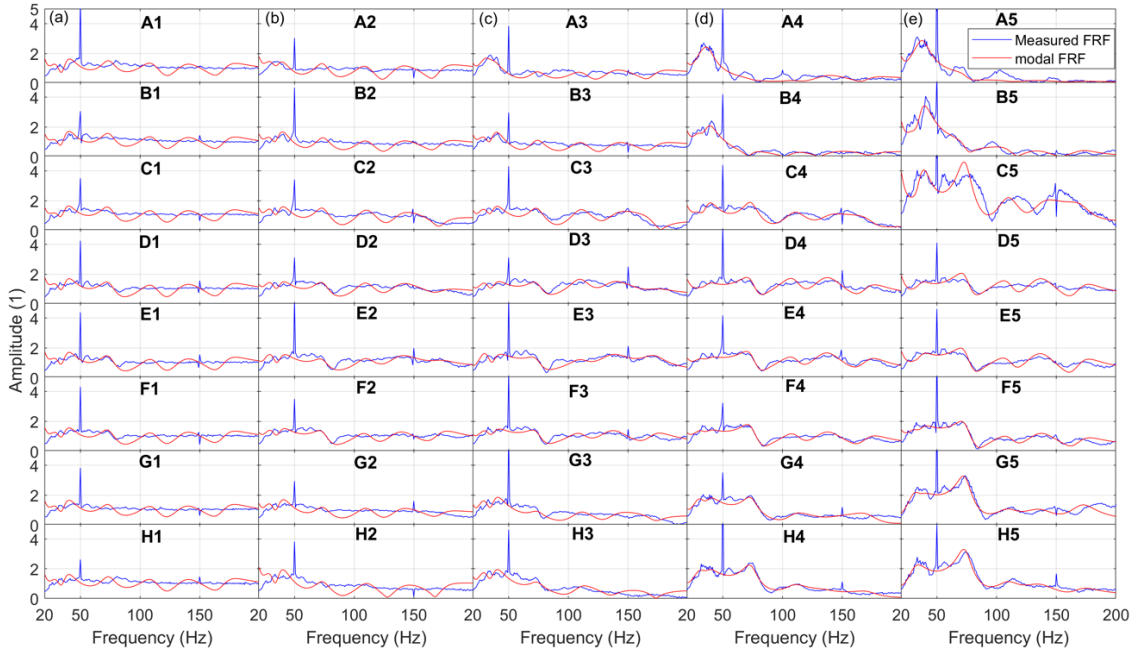


Figure S2 The comparison between the measured FRFs and the modal FRFs on the legs at (a) joints 1; (b) joints 2; (c) joints 3; (d) joints 4; (e) joints 5.

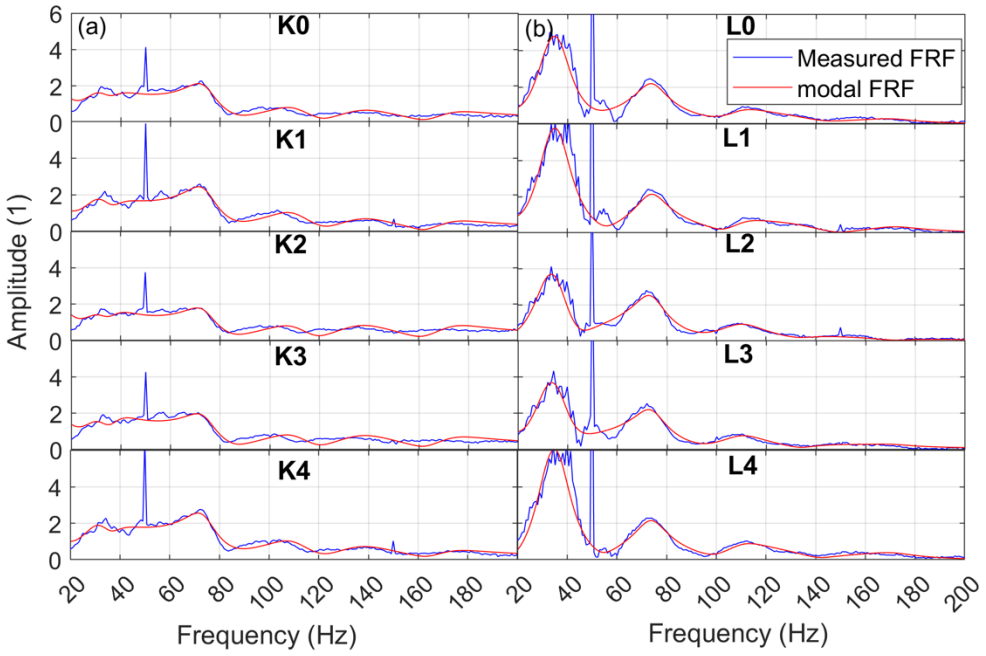


Figure S3 The comparison between the measured FRFs and the modal FRFs on the body at (a) cephalothorax; (b) abdomen.

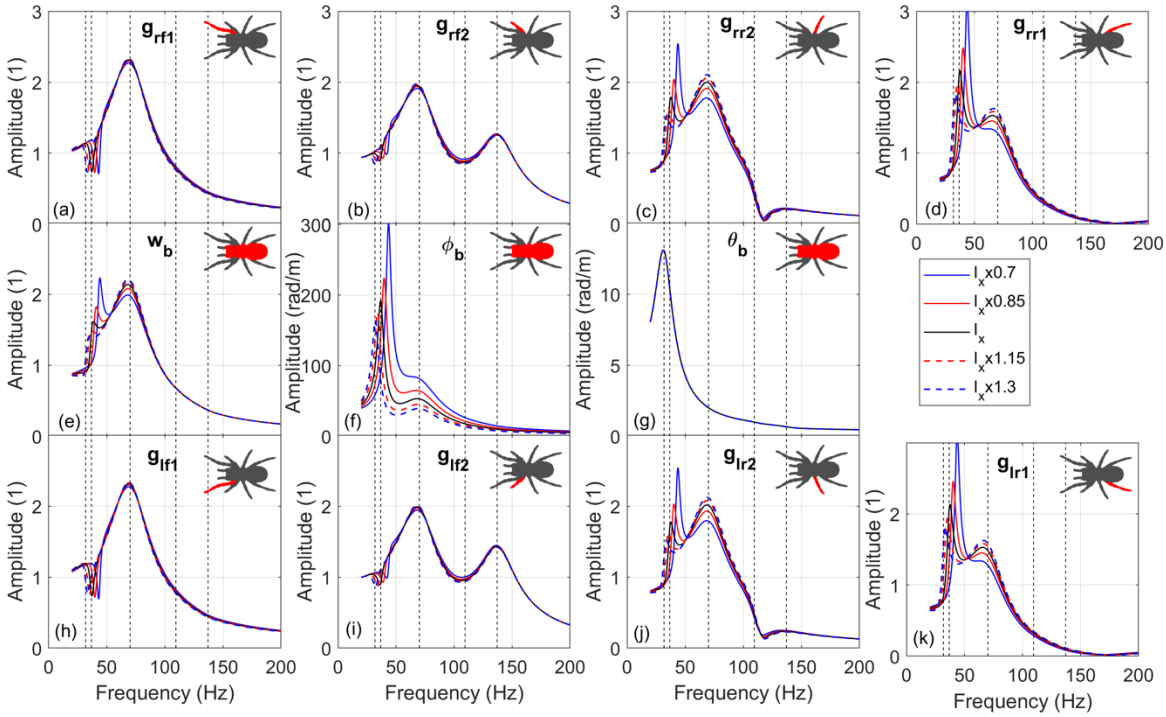


Figure S4 The influence of moment of inertia in pitch direction I_x on the FRFs to (a) leg rf1 bounce; (b) leg rf2 bounce; (c) leg rr2 bounce; (d) leg rr1 bounce; (e) body bounce; (f) body pitch; (g) body roll; (h) leg lf1 bounce; (i) leg lf2 bounce; (j) leg lr2 bounce; (k) leg lr1 bounce. The vertical dashed lines represent the natural frequencies of the original system.

Supplementary Videos

Available at https://doi.org/10.6084/m9.figshare.c.6823914.

Supplementary Video 1: animation of the first experimental mode shape

Supplementary Video 2: animation of the second experimental mode shape

Supplementary Video 3: animation of the third experimental mode shape

Supplementary Video 4: animation of the fourth experimental mode shape

Supplementary Video 5: animation of the fifth experimental mode shape

Supplementary Video 6: animation of the second model mode shape

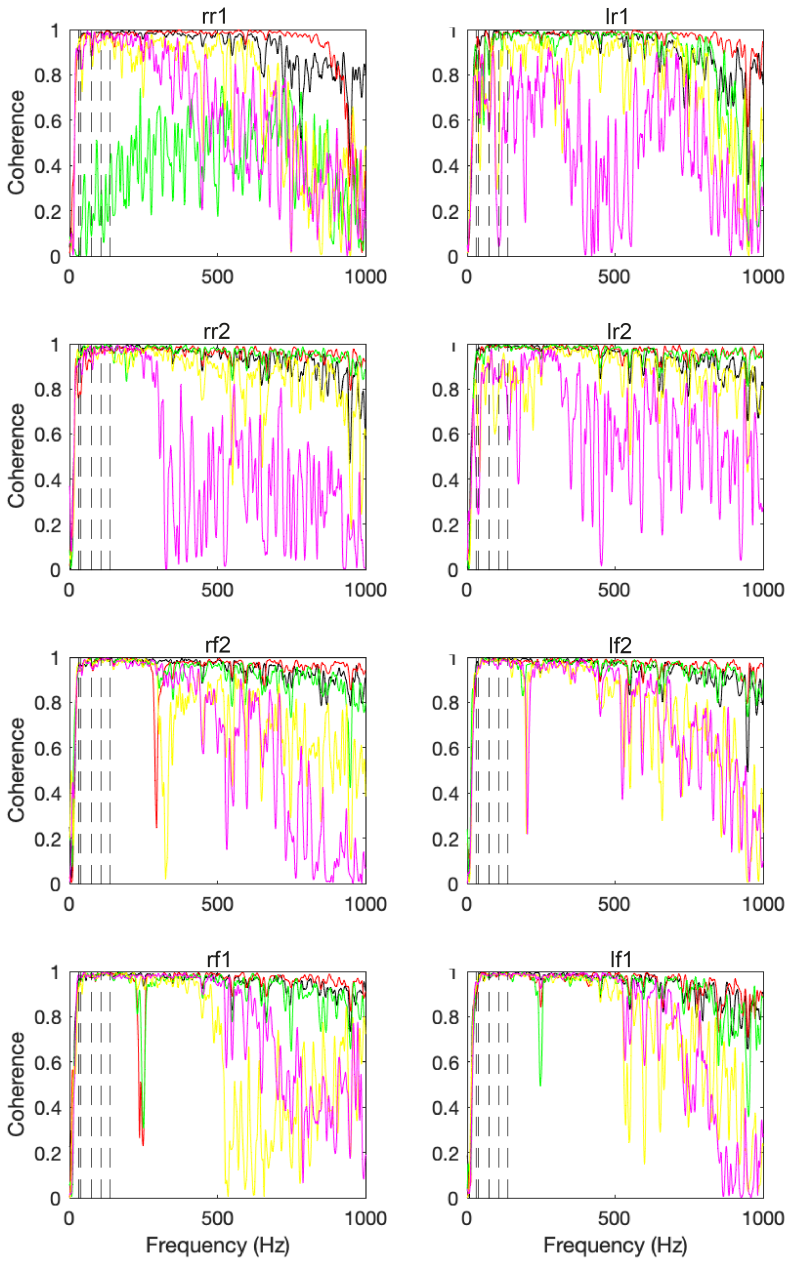
Supplementary Video 7: animation of the third model mode shape

Bibliography

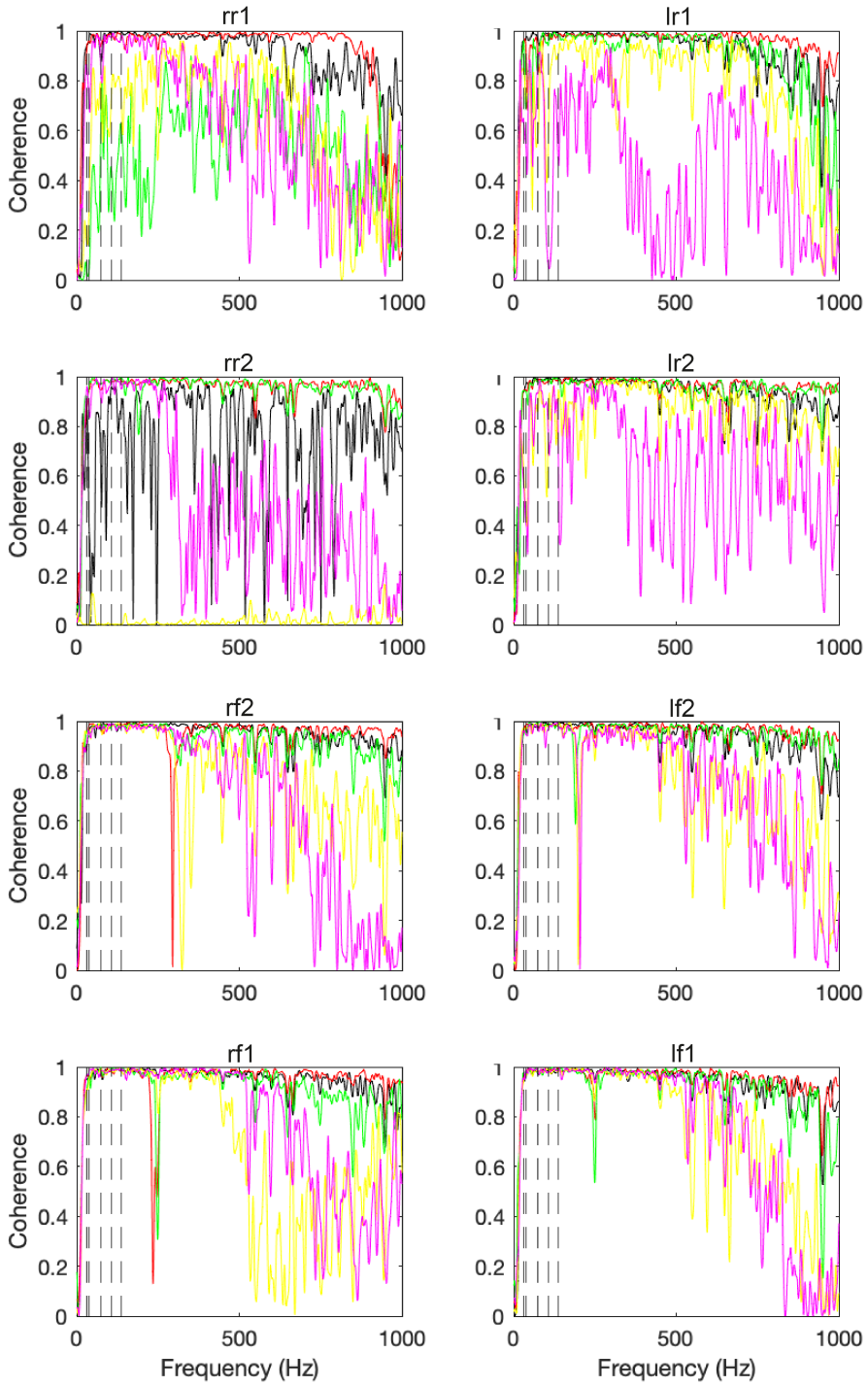
1 Allemang, R. J. 2003 The modal assurance criterion–twenty years of use and abuse. *Sound and vibration*. **37**, 14-23.
2 Wu, J., Qiu, Y. 2020 Modelling of seated human body exposed to vertical, lateral and roll vibration. *J Sound Vib*. **485**, (10.1016/j.jsv.2020.115509)
3 Wilson, R. S. 1970 Some comments on the hydrostatic system of spiders (Chelicerata, Araneae). *Zeitschrift für Morphologie der Tiere*. **68**, 308-322.
4 Blickhan, R. 1986 Stiffness of an arthropod leg joint. *Journal of biomechanics*. **19**, 375-384.

Appendix 4

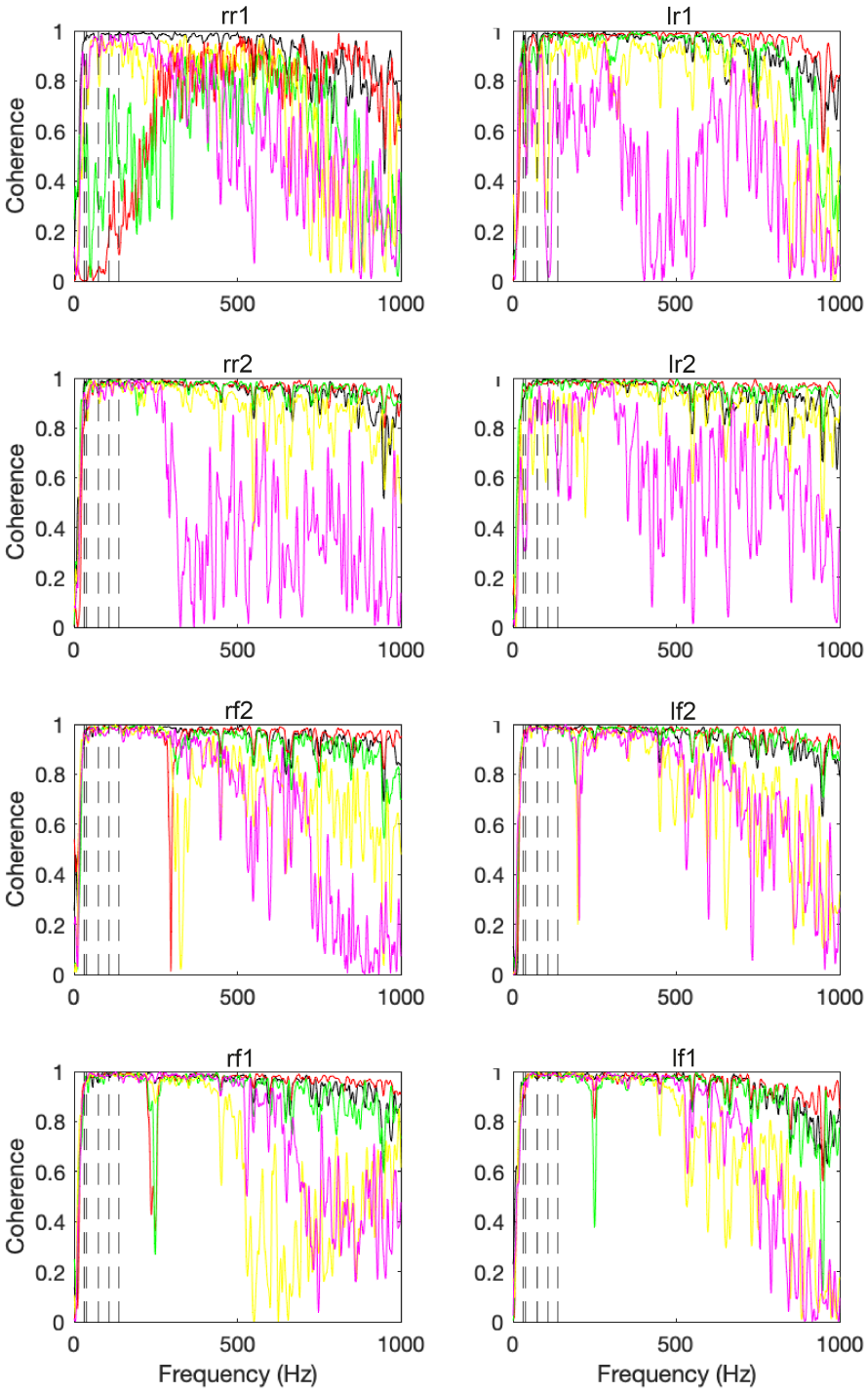
Chapter 5 – Supplementary Material



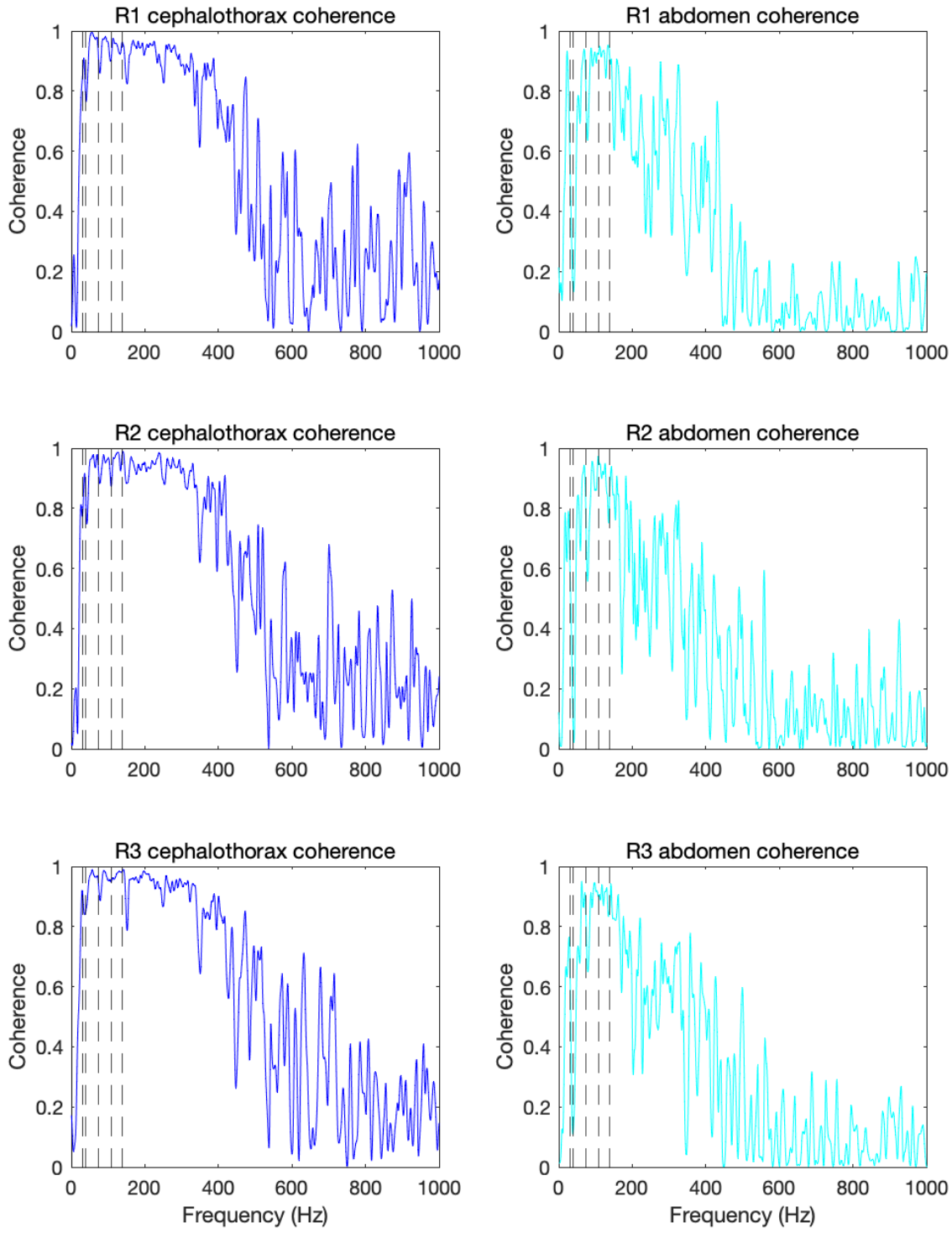
Supplementary figure 1. Coherence of each measurement point from the first repeat of the modal test in the range 0-1000 Hz. Vertical dashed lines indicate the five modes of the spider body in the frequency range of interest. Colours of each leg segment as for legend in Figures 3 and 4.



Supplementary figure 2. Coherence of each measurement point from the second repeat of the modal test in the range 0-1000 Hz. Vertical dashed lines indicate the five modes of the spider body in the frequency range of interest. Colours of each leg segment as for legend in Figures 3 and 4.



Supplementary figure 3. Coherence of each measurement point from the third repeat of the modal test in the range 0-1000 Hz. Vertical dashed lines indicate the five modes of the spider body in the frequency range of interest. Colours of each leg segment as for legend in Figures 3 and 4.



Supplementary figure 4. Coherence of each measurement point from the cephalothorax and abdomen of the modal test in the range 0-1000 Hz. Vertical dashed lines indicate the five modes of the spider body in the frequency range of interest.

Supplementary table 1. MSE between average FRFs of leg segments. Column 1 – left/right leg segment pair comparison; columns 2 and 3 – comparison between cephalothorax and all other segments in each leg; columns 4 and 5 – comparison between tarsus and all other segments in each leg; columns 6 and 7 – comparison between adjacent segments in each leg.

	lr1/rr1	**lr1(6)**	**rr1(6)**	**lr1(1)**	**rr1(1)**	**lr1i+1**	**rr1i+1**
Tarsus	0.005	0.311	0.33	0	0	0.044	0.032
Metatarsus	0.047	0.244	0.12	0.044	0.032	0.056	0.012
Tibia	0.422	0.218	0.345	0.172	0.07	0.112	0.23
Patella	0.295	0.256	0.049	0.484	0.513	0.066	0.185
Femur	0.687	0.248	0.229	0.628	0.631	0.248	0.292
Cephalothorax	0	0	0	0.311	0.297	0.543	0.543
Abdomen	0	0.543	0.543	0.983	0.969	0	0

	lr2/rr2	**lr2(6)**	**rr2(6)**	**lr2(1)**	**rr2(1)**	**lr2i+1**	**rr2i+1**
Tarsus	0.005	0.297	0.327	0	0	0.032	0.05
Metatarsus	0.017	0.216	0.194	0.032	0.05	0.012	0.068
Tibia	0.076	0.21	0.092	0.07	0.208	0.23	0.098
Patella	0.299	0.293	0.032	0.513	0.223	0.185	0.27
Femur	0.829	0.292	0.392	0.631	0.334	0.292	0.392
Cephalothorax	0	0	0	0.297	0.327	0.543	0.543
Abdomen	0	0.543	0.543	0.969	1.006	0	0

	lf2/rf2	lf2(6)	rf2(6)	lf2(1)	rf2(1)	lf2i+1	rf2i+1
Tarsus	0.006	0.325	0.281	0	0	0.079	0.009
Metatarsus	0.07	0.174	0.261	0.079	0.009	0.016	0.011
Tibia	0.092	0.188	0.23	0.138	0.024	0.035	0.02
Patella	0.085	0.196	0.136	0.128	0.056	0.21	0.018
Femur	0.358	0.54	0.076	0.354	0.115	0.54	0.076
Cephalothorax	0	0	0	0.325	0.281	0.543	0.543
Abdomen	0	0.543	0.543	1.018	0.965	0	0

	lf1/rf1	lf1(6)	rf1(6)	lf1(1)	rf1(1)	lf1i+1	rf1i+1
Tarsus	0.003	0.296	0.286	0	0	0.027	0.038
Metatarsus	0.018	0.262	0.35	0.027	0.038	0.021	0.01
Tibia	0.035	0.385	0.407	0.06	0.063	0.015	0.016
Patella	0.022	0.405	0.308	0.052	0.046	0.013	0.016
Femur	0.032	0.339	0.215	0.037	0.05	0.339	0.215
Cephalothorax	0	0	0	0.296	0.286	0.543	0.543
Abdomen	0	0.543	0.543	0.982	0.97	0	0